NASA Technical Memorandum 109151

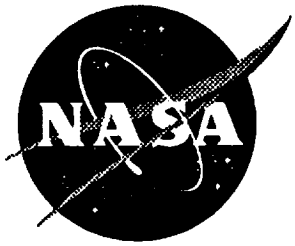

Modelling and Simulation of Space Station Freedom Berthing Dynamics and Control

Paul A. Cooper, James L. Garrison, Jr., and Raymond C. Montgomery
Langley Research Center, Hampton, Virginia

Shih-Chin Wu and Alan E. Stockwell
Lockheed Engineering & Sciences Company, Hampton, Virginia

Martha E. Demeo
ViGYAN, Inc., Hampton, Virginia

August 1994

National Aeronautics and
Space Administration
Langley Research Center
Hampton, Virginia 23681-0001

CONTENTS

LIST OF FIGURES

LIST OF TABLES

FOREWORD

This document presents the final results of a 14-month study of the Space Station Freedom (SSF) Assembly Dynamics and Control. This study was conducted under the technical direction of Paul Cooper with management support from the NASA Langley Research Center Controls-Structures Integration (CSI) Office.

The study was initiated in response to a request from the NASA Johnson Space Center (JSC) for an independent analysis of the dynamic interaction studies underway at JSC to support SSF assembly. Langley was asked to assess multi-body models and provide an independent analysis of the SSF assembly process. Langley agreed to this opportunity to apply CSI technology and to provide help in understanding and controlling the SSF assembly process.

The authors gratefully acknowledge the assistance of John Sunkel and T. Hua of the NASA Johnson Space Flight Center in Houston, Texas, for facilitating LaRC's participation in the dynamic interaction analysis of the SSF berthing process. We also acknowledge the assistance of Thomas P. Russell of McDonnell Douglas Space Systems Company, Houston, Texas, in the SSF ACS modeling effort.

It is also appropriate to acknowledge Ralph Edlow of Analytical Services and Materials, Inc., Hampton, VA, for his role as computer system manager and Christopher Sontag of George Washington University, Hampton, VA, for his assistance in the finite element modelling effort.

ABSTRACT

A large-angle, flexible, multi-body, dynamic modelling capability has been developed to help validate numerical simulations of the dynamic motion and control forces which occur during berthing of Space Station Freedom to the Shuttle Orbiter in the early assembly flights. This paper outlines the dynamics and control of the station, the attached Shuttle Remote Manipulator System, and the Orbiter. The simulation tool developed for the analysis is described and the results of two simulations are presented. The first is a maneuver from a gravity-gradient attitude to a torque equilibrium attitude using the station reaction control jets. The second simulation is the berthing of the station to the Orbiter with the station control moment gyros actively maintaining an estimated torque equilibrium attitude. The influence of the elastic dynamic behavior of the station and of the Remote Manipulator System on the attitude control of the station/Orbiter system during each maneuver was investigated. The flexibility of the station and the arm were found to have only a minor influence on the attitude control of the system during the maneuvers.

ACRONYMS

ACS	Attitude Control System
ADS	Attitude Determination System
ASAD	All Singing, All Dancing
CM	Center of Mass
CMG	Control Moment Gyro
CPU	Central Processing Unit
DADS	Dynamic Analysis and Design System
DOF	Degrees of Freedom
DRS	Draper RMS Simulation
EEOP	End Effector Operating Frame
ELP	Elbow Pitch
EPS	Electrical Power System
FEM	Finite-Element Model
FRF	Frequency Response Function
GG	Gravity Gradient
GPC	General Purpose Computer
HRS	Heat Rejection System
ISA	Integrated Sensor Assembly
LaRC	Langley Research Center
LVLH	Local Vertical - Local Horizontal
MB	Mission Build
MCIU	Manipulator Control Interface Unit
MDSSC	McDonnell Douglas Space Systems Company
MTS	Module to Truss Structure
OBAS	Orbiter Body-Axis System
OSR	Orbiter Structural Reference
PAS	Payload Axis System
PDA	Pressurized Docking Adapter
PDR	Preliminary Design Review
PLOP	Payload Operating System
PMAS	Propulsion Module Attach Structure
POHS	Position-Orientation-Hold-Submode
POR	Point of Resolution
PV	Photo-Voltaic
RCS	Reaction Control System

SARJ	Solar Array Alpha Joint
SC	Spacecraft
SGI	Silicon Graphics Incorporated
SHP	Shoulder Pitch
SHY	Shoulder Yaw
SPA	Servo Power Amplifier
SRMS	Shuttle Remote Manipulator System
SSF	Space Station Freedom
SSSRF	Space Station Structural Reference Frame
ST	Star Trackers
STS	Space Transportation System
TCS	Thermal Control System
TEA	Torque Equilibrium Attitude
WRP	Wrist Pitch
WRR	Wrist Roll
WRY	Wrist Yaw

1.0 OVERVIEW

1.1 Introduction

Berthing of the Space Station Freedom (SSF) to the Orbiter was once considered as the primary method of mating the station to the Orbiter during initial assembly flights. The berthing procedure uses the Shuttle Remote Manipulator System (SRMS) to grapple the station and draw the station and Orbiter together. This operational scenario presents a number of potential dynamic interaction issues among the Orbiter, SRMS, SSF and their respective control systems. NASA is involved in research programs to address this challenging set of problems and to establish hardware, software, and operational requirements for safe and timely berthing operations in space. The activity that is the focus of this paper is the development of a large-angle, flexible, multi-body spacecraft simulation which supports the dynamic interaction analysis of the SSF berthing process.

Simulation of this berthing operation is fairly complex because it involves the interaction of large, highly-flexible components during a large-motion maneuver while in orbit. The components are subject to active control forces and moments, as well as to the mechanics of an orbiting spacecraft. These complexities motivated the independent development of comparable simulators for validation purposes. Hence, both the NASA Johnson Space Center (ref. 1-1, 1-2) and the NASA Langley Research Center independently developed simulators for analysis of the berthing process. This paper describes the simulator developed at Langley.

During the early assembly flights, the Orbiter attitude control systems maintain attitude of the coupled spacecraft system consisting of the Orbiter, SRMS, and SSF (herein referred to as the 'stack'). The sixth assembly flight was the first flight that would use the station attitude control systems rather than the Orbiter digital autopilot to maintain the attitude of the stack. Berthing during this flight was selected for the study scenario because the control systems of both the station and the SRMS are active and the dynamic interaction of the combined system may be investigated.

The salient features of the simulated system components, including the control systems for both the SSF and the SRMS, the orbital mechanics, and the structural dynamic representation are described herein. Also, the procedure used to combine and integrate the equations governing the rigid-body dynamics, flexible-body modes, and control dynamics is presented. Simulation results for two maneuvers, which between them exercise the SSF Attitude Control System (ACS) and the SRMS control system, are presented. The first simulation is a maneuver from a gravity-gradient (GG) attitude to a Torque Equilibrium Attitude (TEA) using station Reaction Control System (RCS) jets with the brakes applied at each SRMS joint. The second simulation is of the berthing maneuver where the SRMS

joint servo motors are used to draw the station to the Orbiter while the station Control Moment Gyros (CMGs) actively maintain attitude of the stack. In both cases, the Space Shuttle is treated as a rigid body while the SSF and SRMS are modelled as flexible bodies.

1.2 Description of Simulation Scenarios

The following is an overview of the berthing scenario simulation which highlights many of the features of the assembly operation that have been incorporated into the multi-body simulation. The simulations focus on the berthing maneuver during the sixth assembly flight after the SRMS has grappled the SC-5 (spacecraft 5) station. The SC-5 station configuration is shown in figure 1-1. The solar alpha rotary joint permits a relative rotation of the photo-voltaic (PV) arrays with respect to the core body so that the attitude of the station core body can be held constant with respect to the nadir axis during an orbit while the PV arrays track the sun and provide electrical power. Before the berthing maneuver begins, the arrays are rotated to an orientation to minimize plume impingement loads from the Orbiter jets during the final approach of the Orbiter prior to grappling by the SRMS. The PV joints are then locked and remain locked during the entire berthing maneuver. Figure 1-1 also indicates the location of the avionics platform containing sensors which provide attitude and attitude-rate information. The attitude can be controlled by firing jets, located on the top and bottom of the inboard station framework, at a constant force level of 25 lbs per jet, or by a set of four double-gimbaled CMG's, each with a capacity of 3500 ft-lb-sec, located on a platform close to the avionics platform.

As indicated in figure 1-2, the Orbiter approaches the station along the direction opposite the orbital velocity vector and flies in tandem with the station maintaining a distance of about 30 feet between the V guides in the Shuttle cargo bay and the trunnion pins on the SSF docking adapter. The SRMS moves from its stowed configuration on the port side of the cargo bay toward the station and grapples the station by snaring the grapple fixture located on the resource node, a pressurized shell attached to the station framework inboard of the alpha joint.

The simulations performed in the current study begin after the SRMS has grappled the resource node and attitude control has been handed over to the station. For the first simulation, the brakes are applied to each of the SRMS joints and the RCS jets are fired to move the station from a GG attitude to a computed TEA. The torque equilibrium attitude is the average attitude which must be held so that no net angular momentum would be accumulated over one orbit by a perfect control system in the presence of gravity-gradient, aerodynamic, and orbital gyroscopic disturbances. Figure 1-3 contains a schematic drawing of the stack configuration before and after the TEA maneuver. For the second simulation, the brakes on the SRMS are released and the station RCS jets are inhibited from firing. The attitude of the stack is now maintained by the station CMG momentum management system, and berthing begins as the

joint motors on the SRMS are used to draw the station and the Orbiter together. The TEA changes during the berthing process since the inertia of the stack changes. Thus, a real-time estimate of the TEA is computed at each controller time-step. The change in the commanded pitch angle during the berthing maneuver is shown in figure 1-3.

The three point trajectory followed in berthing SC-5 to the Orbiter is depicted in Figure G-1. The first point is representative of a nominal capture configuration and the third point is two feet from a fully berthed configuration (i.e., the pressurized berthing adapter trunnion pins are two feet from the bottom of the V-guides). The second point is an intermediate point which is directly above the third position. The corresponding joint angles, end effector positions and attitudes are given in Appendix G. These configuration definitions are consistent with a grapple fixture mounted on the SSF resource node.

1.3 Dimensions, Masses, and Component Locations

Figure 1-4 shows the relative size and location of the stage 5 station, the Orbiter, and the extended SRMS at the beginning of the simulation. The SSF has a weight of 145,000 lbs and the Orbiter, with the lab module in the cargo bay, has a weight of 250,000 lbs. The 50-foot long SRMS has a weight of only 900 lbs.

The mass properties for the Orbiter, SRMS and SSF are listed in Appendices C-1, C-2 and C-3. The Orbiter properties were selected from the SSFP Preliminary Design Review (PDR) Loads Data Book (ref. 1-3). This Orbiter definition was selected because it accounts for the 35,000 pound lab module in the payload bay on the sixth Mission Build (MB-6) flight. The mass properties for the SC-5 SSF were derived from the MSC/NASTRAN model discussed in part 2. This model is consistent with having the SSF PV arrays feathered to reduce Orbiter plume impingement (alpha=38°, beta=-34° (starboard-inboard-upper), -38° (starboard-inboard-lower), gamma=0°).

The SSF sensor, jet and CMG component locations are listed in Appendices C-4, C-5 and C-6.

1.4 Description of Models

Nine bodies are used to model the complete multi-body system as shown in figure 1-5. The nine bodies include the Orbiter, the seven links of the SRMS, and the SSF. Three components, the two long booms of the SRMS and the SSF, were modeled as flexible bodies. All other links between joints were treated as rigid bodies. Eight joints are defined to connect each of the bodies of the system. The swing-out joint at the base of the SRMS and the connection between the end-effector and payload are modeled

as rigid joints. The remaining six joints are modeled as single degree-of-freedom (DOF) joints which accommodate the six DOF of the SRMS. There are 12 rigid-body DOF and 40 flexible-modal DOFs in the overall system definition.

The following is a brief overview of the relevant models used in the multi-body simulation. These models include the SSF structural dynamics, SSF ACS, SRMS structural dynamics and control system, and the orbital environmental disturbances. Each of these models is described in greater detail in the subsequent sections of this report.

1.4.1 Space Station Freedom

The Space Station structural dynamics are represented during the TEA simulation by a set of 36 natural modes which range in frequency from 0.1 Hz to approximately 5 Hz. For the berthing maneuver, 13 natural modes were used in the same frequency range. A conservative critical proportional modal damping level of 0.2 percent was assumed for each SSF mode. The modes were selected to provide an accurate representation of the flexible response at the station sensor location caused by forces applied at the RCS jet locations for the TEA maneuver, and caused by forces applied at the grapple fixture and moments applied at the CMG location for the berthing maneuver. The modes were obtained using a detailed Finite-Element Model (FEM) called the PDR model (ref. 1-3) shown in figure 1-6. The modes were obtained for the model fixed at the grapple fixture point. A detailed description of the selection of the reduced mode set is provided in section 2, and the procedure for incorporating the modes in the multi-body simulation is given in reference 1-4.

A simplified block diagram of the RCS and CMG control system logic is shown in figure 1-7. The Attitude Determination System (ADS), which measures the attitude and feeds this information back to the controller, was assumed to be perfect. Thus, a transfer function of unity was assumed for the ADS in the current simulations. The control system is designed for use in all configurations of the station covering a large range of inertias during the 3-year assembly process. To accommodate this wide range of system parameters, the control system uses a mass estimator to predict the on-orbit inertias and to adjust the control gains to provide acceptable performance. Normally, the gains will not change significantly for a given flight configuration, since the inertia matrix will remain nearly constant until the next assembly flight; however, during the berthing process, the system inertia matrix is continuously changing. Hence, the gains would also have to be continuously updated. A mass estimation algorithm, based upon knowledge of the SRMS end effector position and orientation, is employed to provide an updated system inertia matrix to the SSF attitude control system throughout the berthing process. This computation assumes the existence of a communication link, e.g., radio frequency, between the SSF and the orbiter control systems. There are two low-pass bending filters in the control system which are

designed to remove high frequency components of the feedback signals (torque output and rate error). The filter blocks are not shown in the simplified block diagram of figure 1-7.

The functional representation of the SSF ACS used in the multi-body simulation is equivalent to the Honeywell critical design review proposed attitude controller (ref. 1-5). Several modifications were made to the SSF ACS to facilitate simulation of the study scenarios. First, the gain scaling was changed so that the full inertia tensor is used to scale the proportional gains. Second, bending filters were inserted to filter the torque output and the rate error feedback. For the CMG controller, a mass estimator was added to predict the inertia tensor of the stack as it changes during the berthing maneuver. In addition, a TEA estimator was added to compute the commanded attitude as a function of the alignment of the nearest spacecraft principal axes with an orbital reference frame. A more extensive discussion of the SSF-ACS modelling effort in the multi-body simulation is presented in reference 1-6 and section 5.0 of this report.

1.4.2 Shuttle Remote Manipulator System

The SRMS is the six-joint anthropomorphic arm used for on-orbit maneuvering, deployment and retrieval of payloads (ref. 1-7). As shown in figure 1-8, the arm is composed of two single DOF shoulder joints, a 21-foot long upper boom, a single DOF elbow joint, a 23-foot long lower boom, three single DOF wrist joints, and a snare-type end effector capable of mating with a payload mounted grapple fixture. Each of the six arm joints consists of a reversible motor, a mechanical joint brake, a tachometer, a joint gear train, a position encoder, and servo compensation as shown in figure 1-9. The arm is telerobotically operated from the aft flight deck of the Orbiter using rotational and translational hand controllers and control panel inputs. Structural flexibility of the long booms, the joint housings, and the gear trains contribute to the overall structural flexibility of the SRMS.

For simulation of the arm dynamics, the upper and lower long booms of the SRMS were treated as flexible cantilevered beams and the structural dynamic behavior of the components was represented by natural modes computed from finite-element models of these members. For these two cantilever modes, a modal damping of 2.2 percent was assumed. The other arm segments, which are much stiffer, were treated as rigid bodies. The mass and stiffness properties were taken from the SRMS database (ref. 1-7). The components of the SRMS control system include the SRMS joint servo drive mechanisms, the software command algorithms resident in the Orbiter General Purpose Computer (GPC), and the Manipulator Control Interface Unit (MCIU) that links the arm electronics to the GPC. Detailed models of these components were extracted from the Draper RMS Simulation (DRS), a high-fidelity non-real-time simulation of the SRMS (ref. 1-8). They were incorporated into the multi-body simulation as self-contained FORTRAN routines and informally validated against the performance predicted by the DRS.

A detailed description of the SRMS control system modelling in the multi-body simulation is presented in reference 1-9.

1.4.3 Orbital Mechanics

The orbital environmental disturbances, including the gravity-gradient moments and the aerodynamic moments, were computed as external loads. The aerodynamic torques were computed for the system modeled as three flat plates. A Jacchia 1970 atmosphere model was used to compute the atmospheric density. The computed gravity-gradient moment was applied as a rigid-body moment about the stack center of mass. The TEA was computed for the given configuration by minimizing the secular momentum which must be absorbed by a perfect controller to maintain a constant attitude through one complete orbit. An available code, called IDEAS**2, was used to compute the TEA (ref. 1-10).

1.5 Simulator Description

The computational tool developed at LaRC is built around a general purpose multi-body dynamics code called DADS (Dynamic Analysis and Design System, ref. 1-11). The detailed architecture of the tool consists of four major parts: the multi-body dynamics code DADS, the SRMS controller, the SSF ACS, and the MAIN program as shown in figure 1-10. The DADS code is used to generate equations of motion of the system, including the SRMS arm, the Orbiter, and SSF. Each of these modules has its own integration routine and integrates its state equations at its own integration step size. Several routines in the DADS code were modified to accommodate this inherently multi-rate system. In addition, a MAIN routine was added to control the timing and program execution flow.

For the SRMS controller, joint angles and rates from DADS, along with simulated operator command inputs, are fed into the SRMS command algorithm to compute joint rate commands. The SRMS controller model calculates driving torques, based on the joint rate commands, which are then applied back to DADS through DADS control elements. The DADS code provides the attitude and attitude rate of the stack to the ACS. Along with the commanded attitude, the ACS computes attitude errors and rate errors that are used to compute commanded torques to be applied to the system. At the same time, the mass property estimator is used to estimate the inertia of the composite system. This estimated information is used to compute the appropriate gain scheduling in the ACS and to update the commanded attitude to track the changing TEA. Depending on the type of actuator used, the commanded torques are converted to either RCS forces or to CMG torques which are fed back to DADS using DADS control elements. Environmental disturbances from aerodynamic moments and gravity

gradient torques, recomputed based on the changes in system geometry, are also applied to the system through the DADS control elements.

1.6 Simulation of Maneuvers

The following sections, 2.0 through 5.0, provide detailed descriptions of the finite element models of both the Stage 5 station and the SRMS links used in the simulation, a detailed description of the Remote Manipulator System and its control system including operational constraints, a description of the environmental disturbances assumed including aerodynamic drag and gravity gradient moments, and a detailed description of the space station attitude control systems including the reaction control system and the control moment gyro momentum management system. In section 6, the procedure followed to perform the numerical simulations is discussed. Sections 7 and 8 present specific results from the TEA maneuver and berthing maneuver simulations, respectively. The dynamic response and selected structural loads were also evaluated and presented. Supporting configuration data, coordinate definitions, and input parameters are provided in the attached appendices.

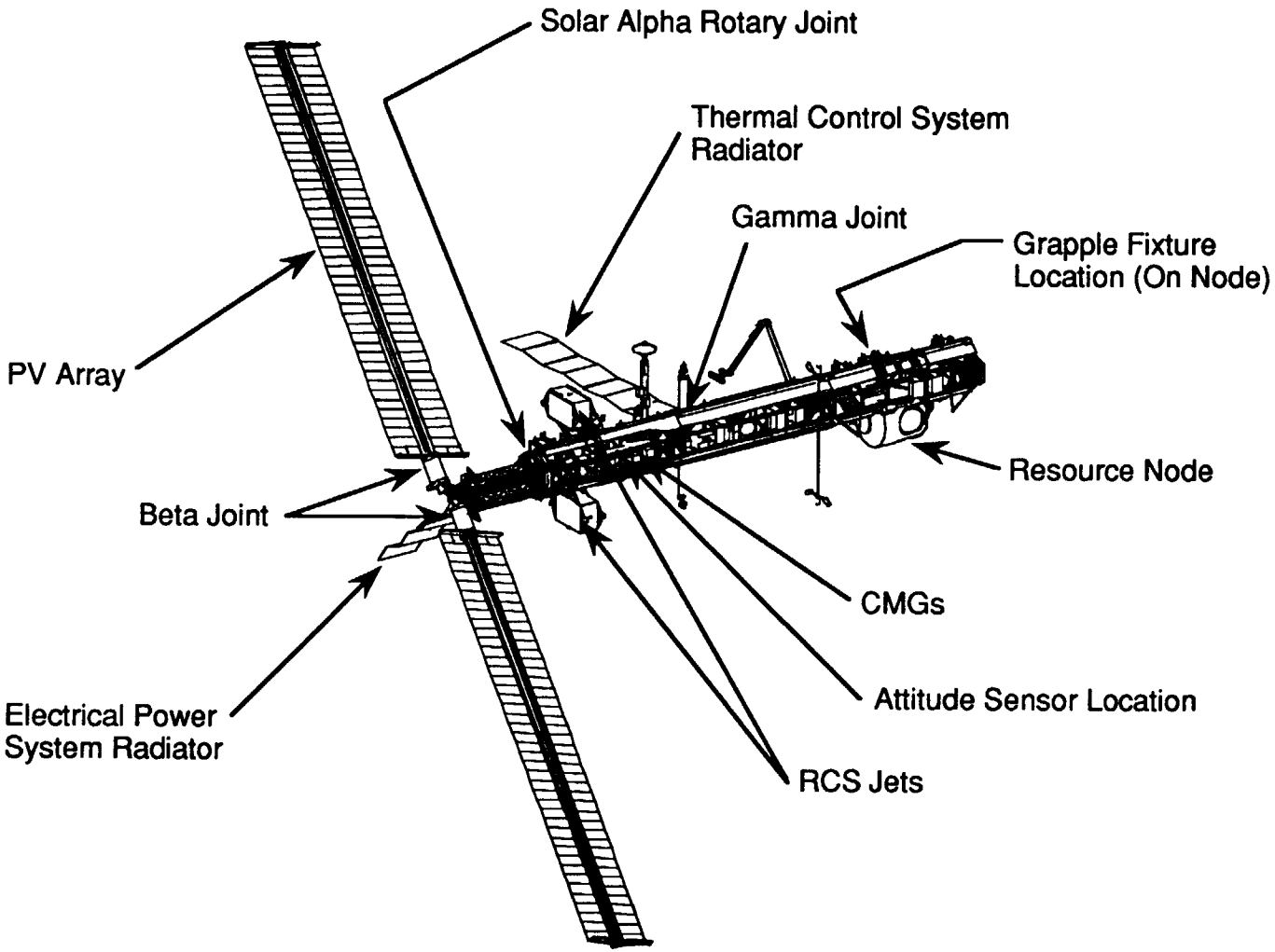

Figure 1-1.- Stage 5 Space Station configuration

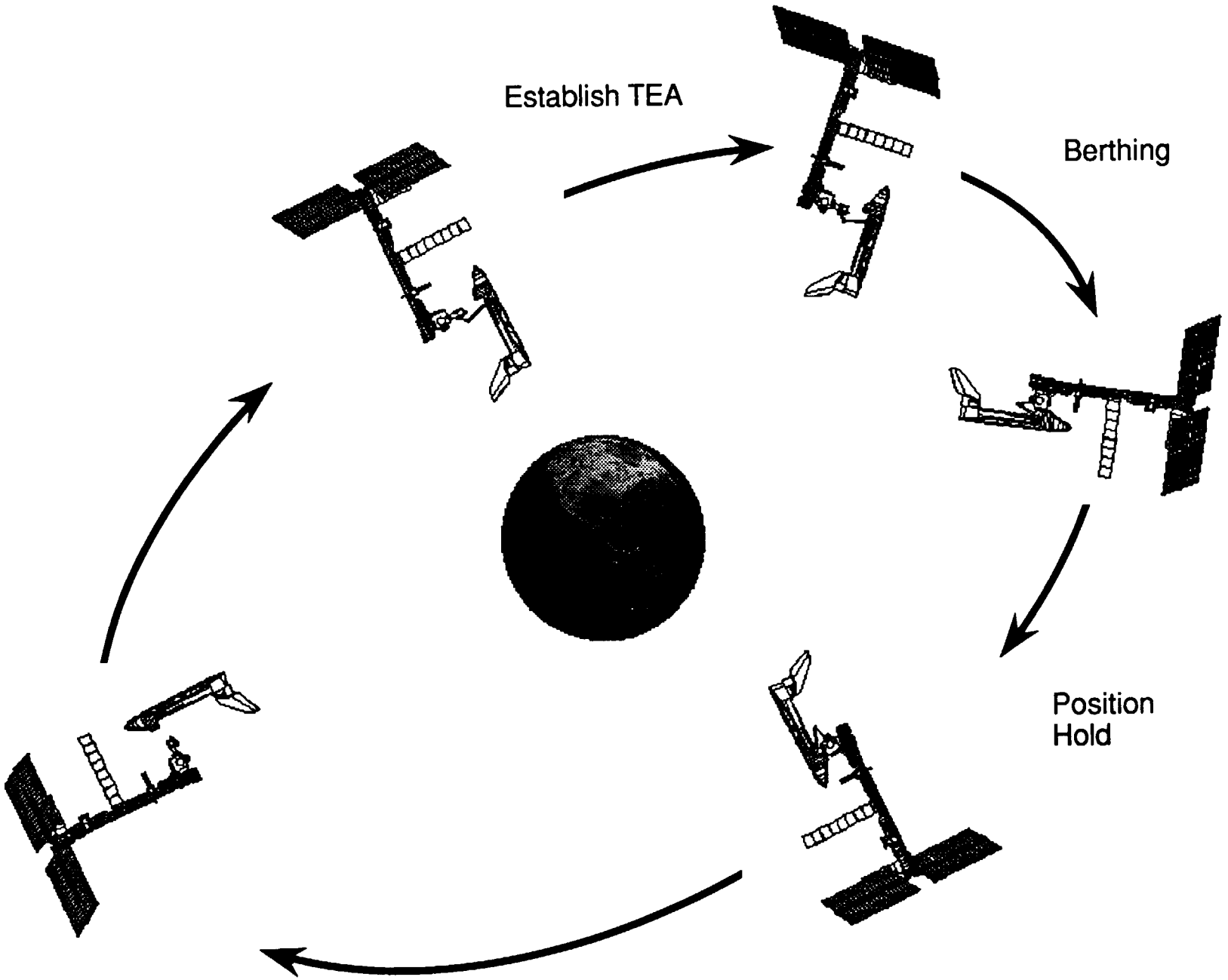

Figure 1-2.- Simulation scenario

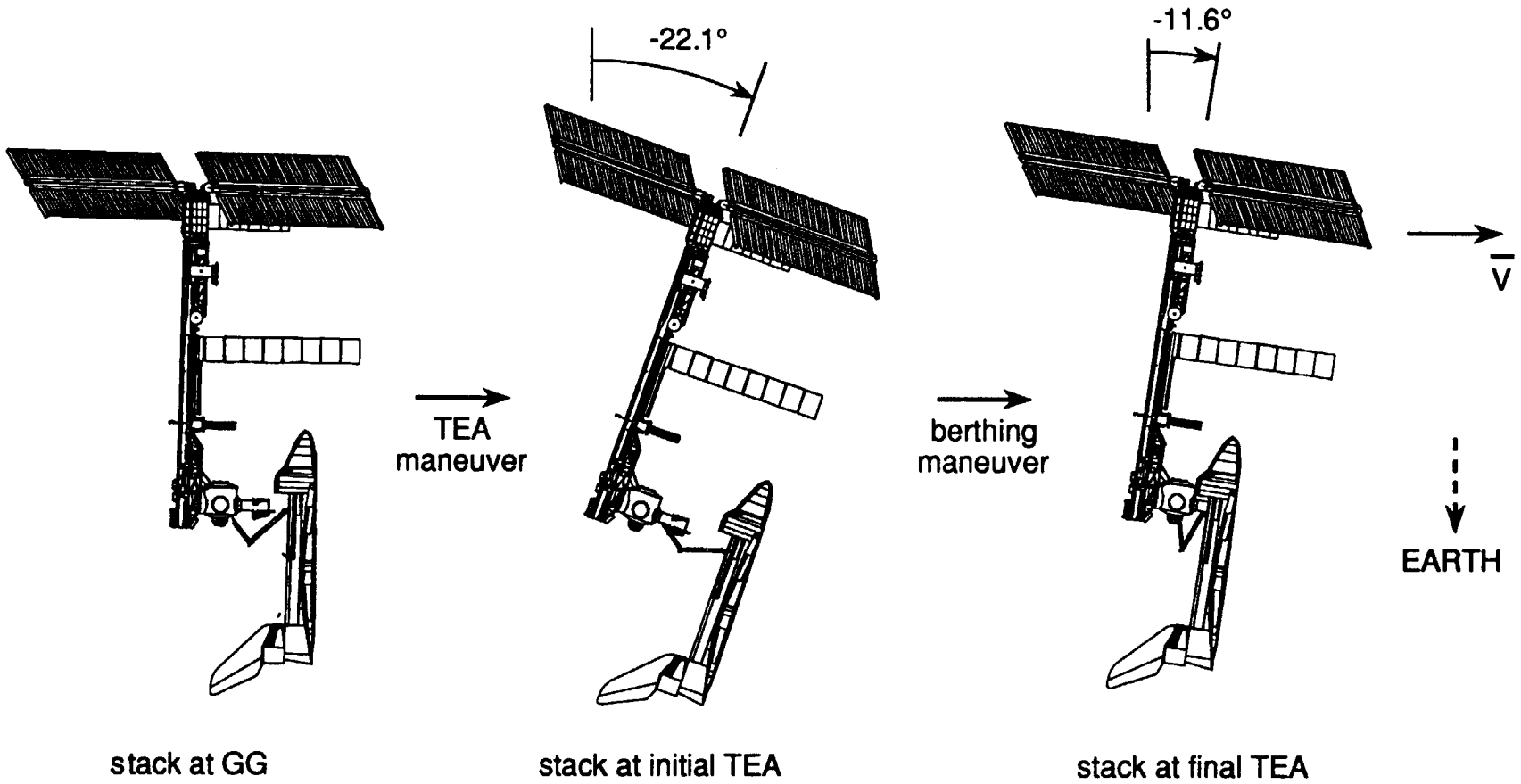

Figure 1-3.- Change in attitude (pitch) of stack during maneuvers

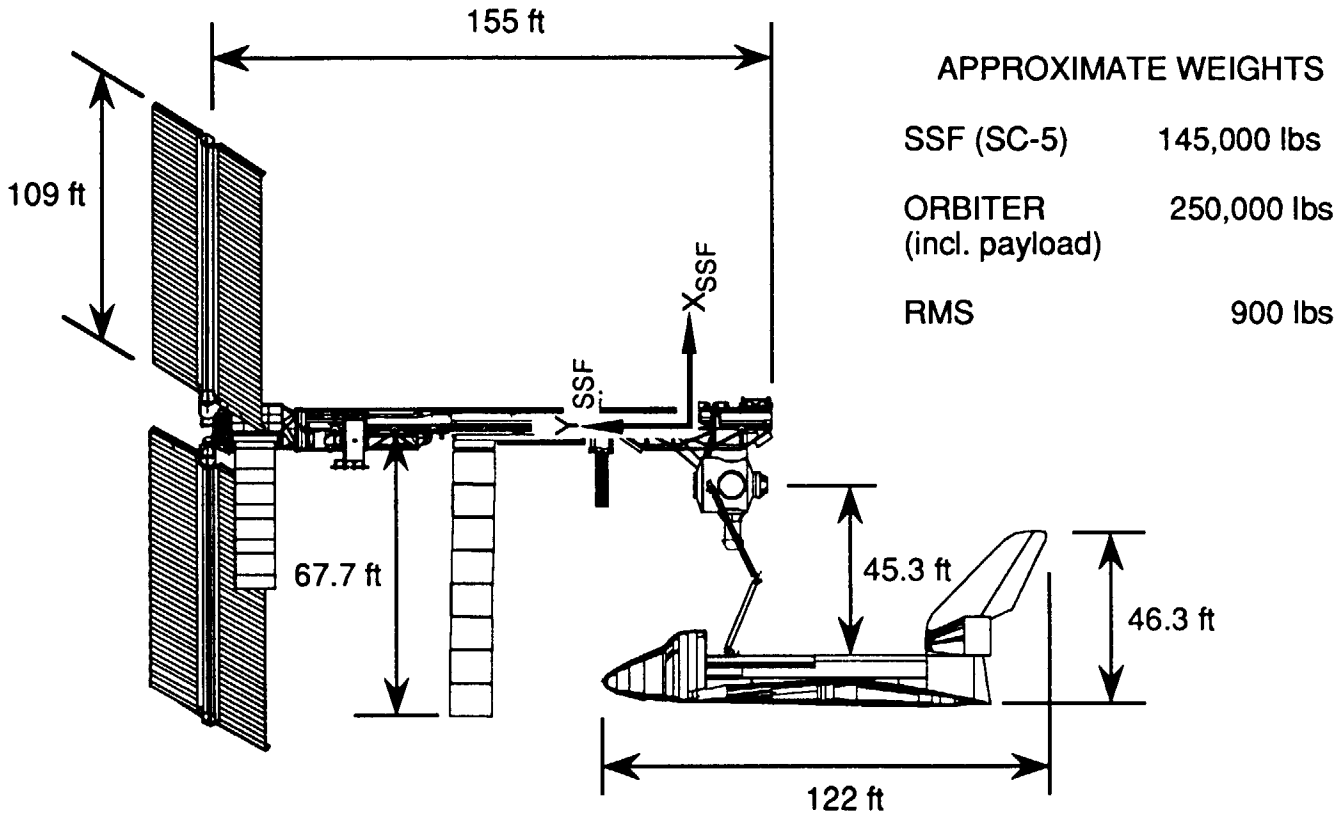

Figure 1-4.- SSF/Orbiter approximate dimensions, flight MB-6, orbiter berthed to SC-5 station

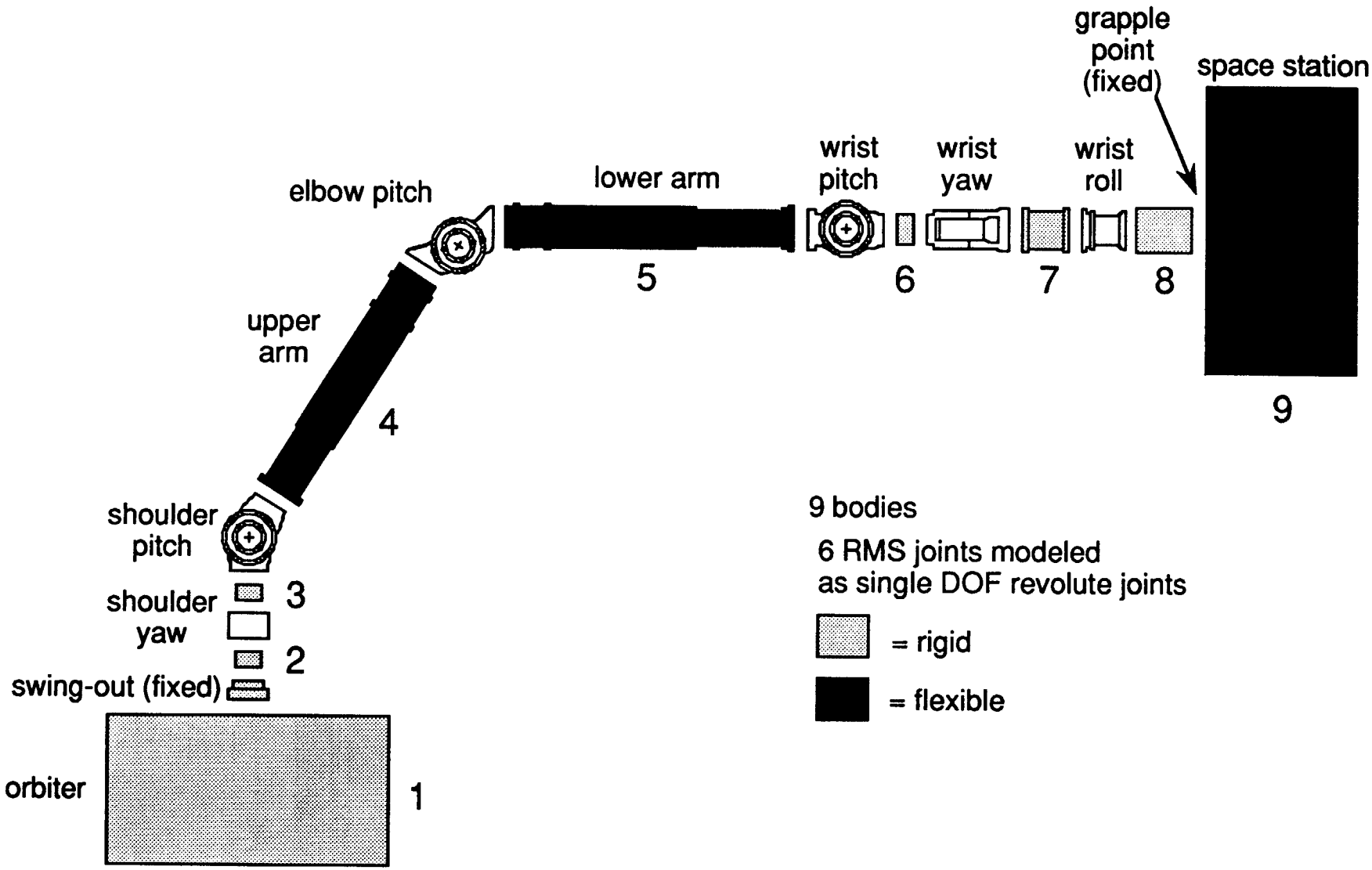

Figure 1-5.- Multibody representation

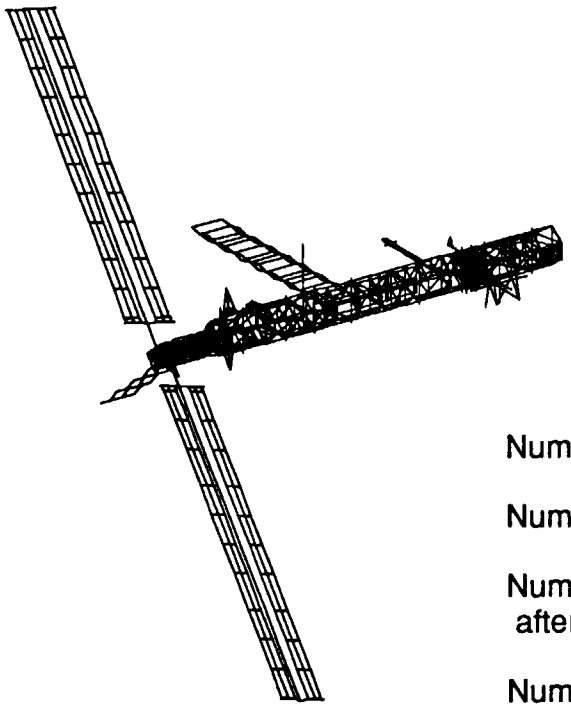

Number of Grid Points	= 2442
Number of Elements	= 2851
Number of Dynamic DOF after component mode reduction	= 781
Number of Modes < 5 Hz	= 181
Number of key modes selected for simulation	= 36 TEA
	13 Berthing

Figure1-6.- PDR finite element model of Stage 5 SSF

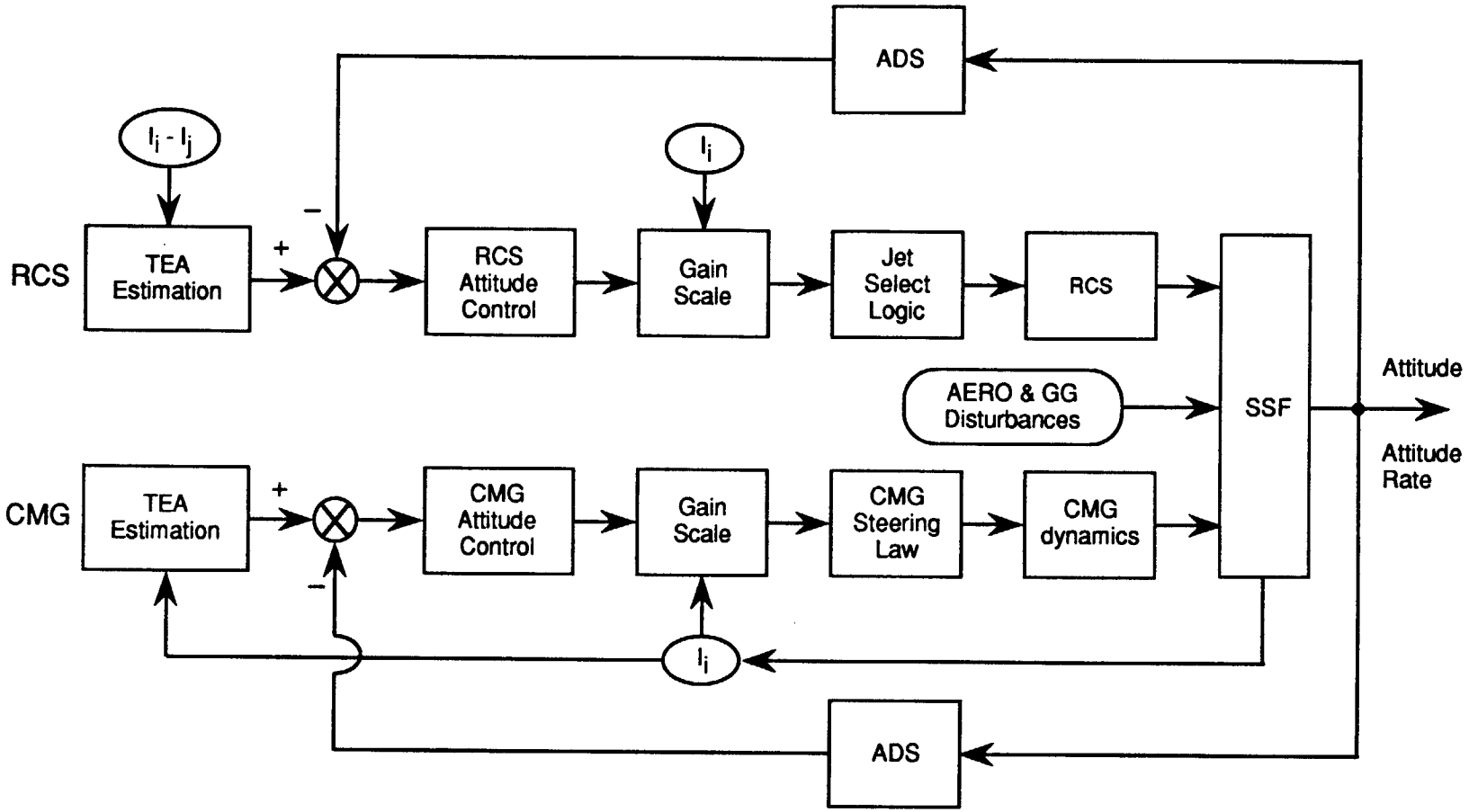

Figure 1-7-. SSF attitude controller system

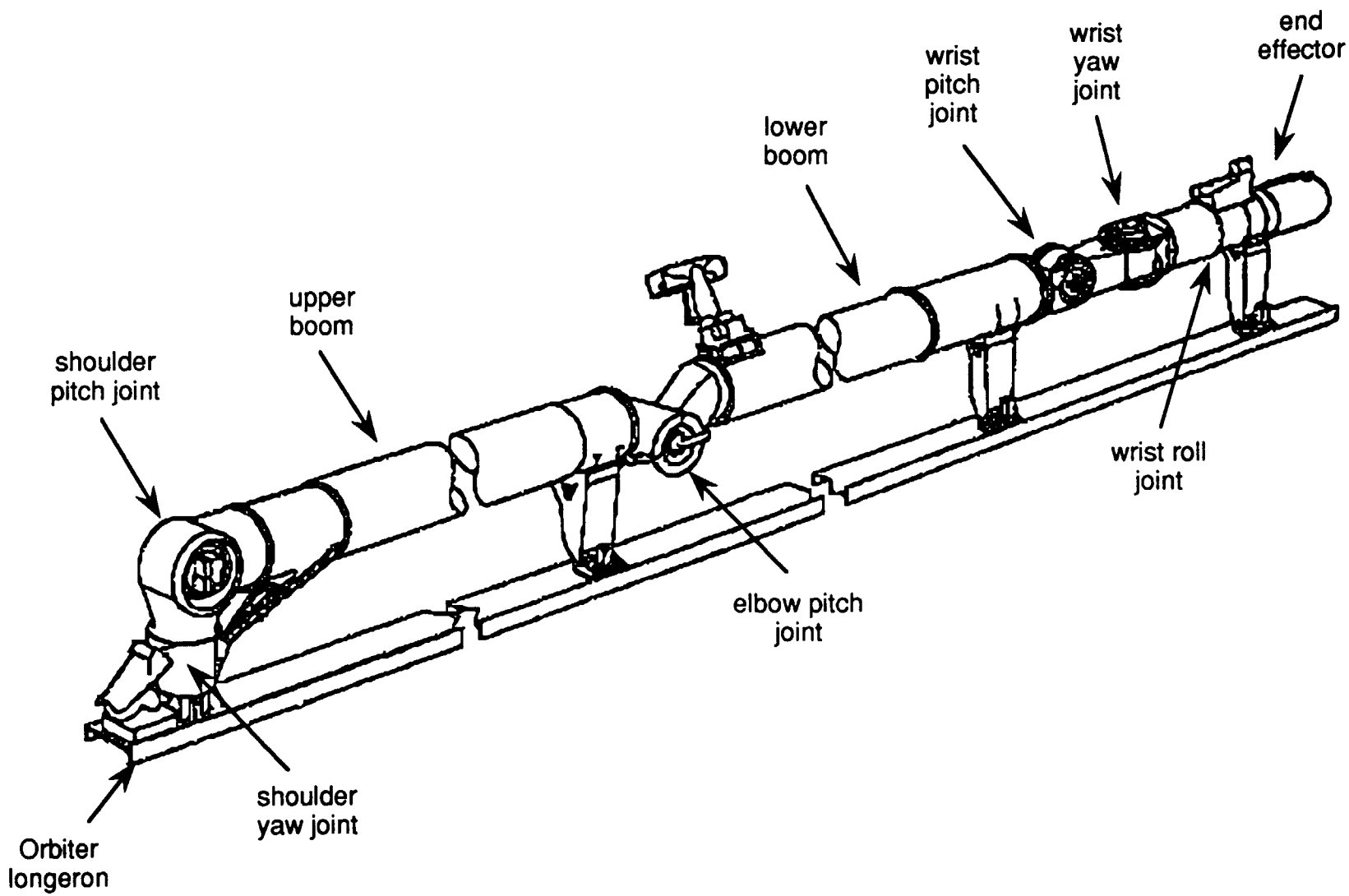

Figure 1-8.- Shuttle Remote Manipulator System

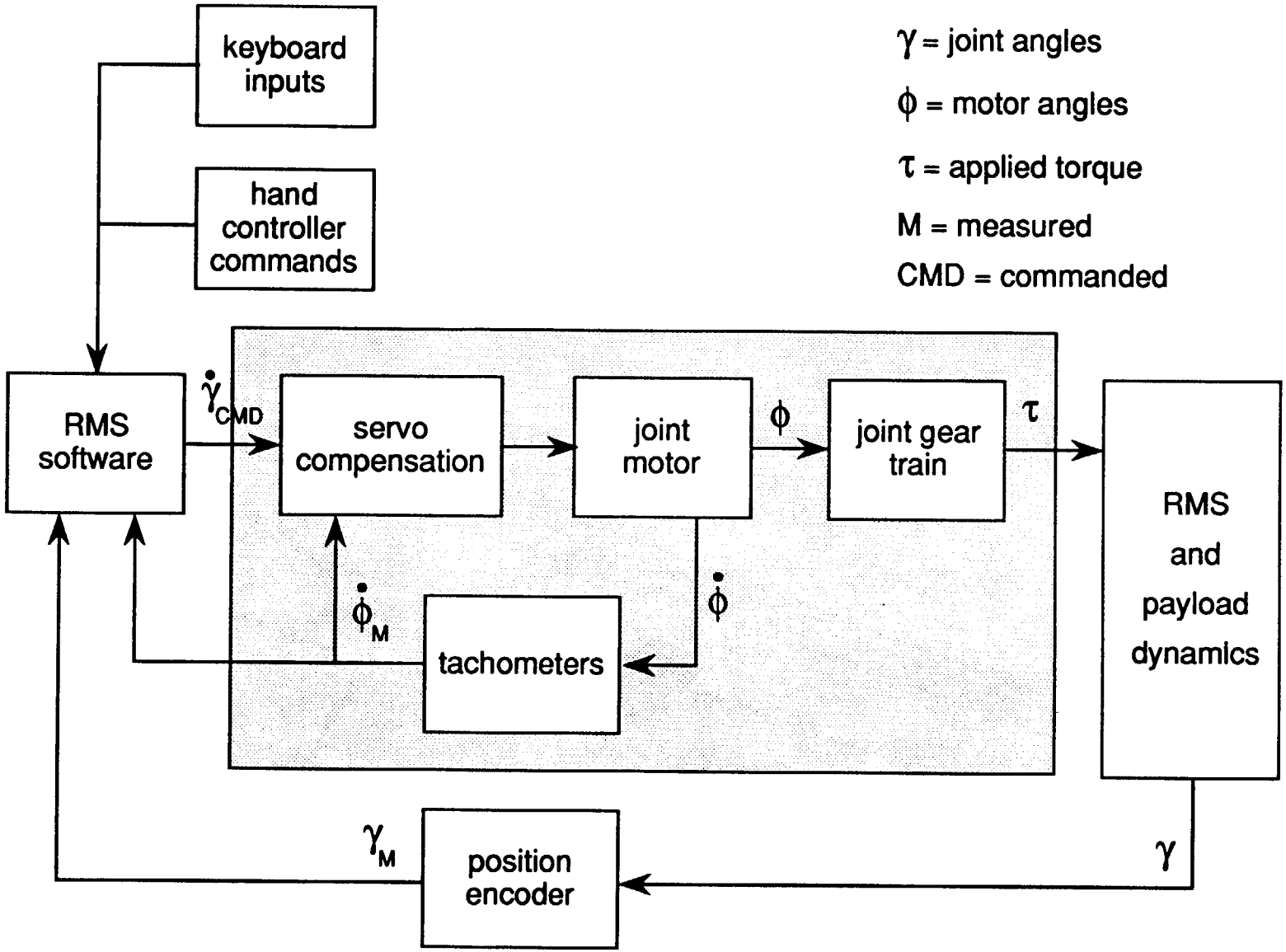

Figure 1-9.- Motor servo controller for each SRMS joint

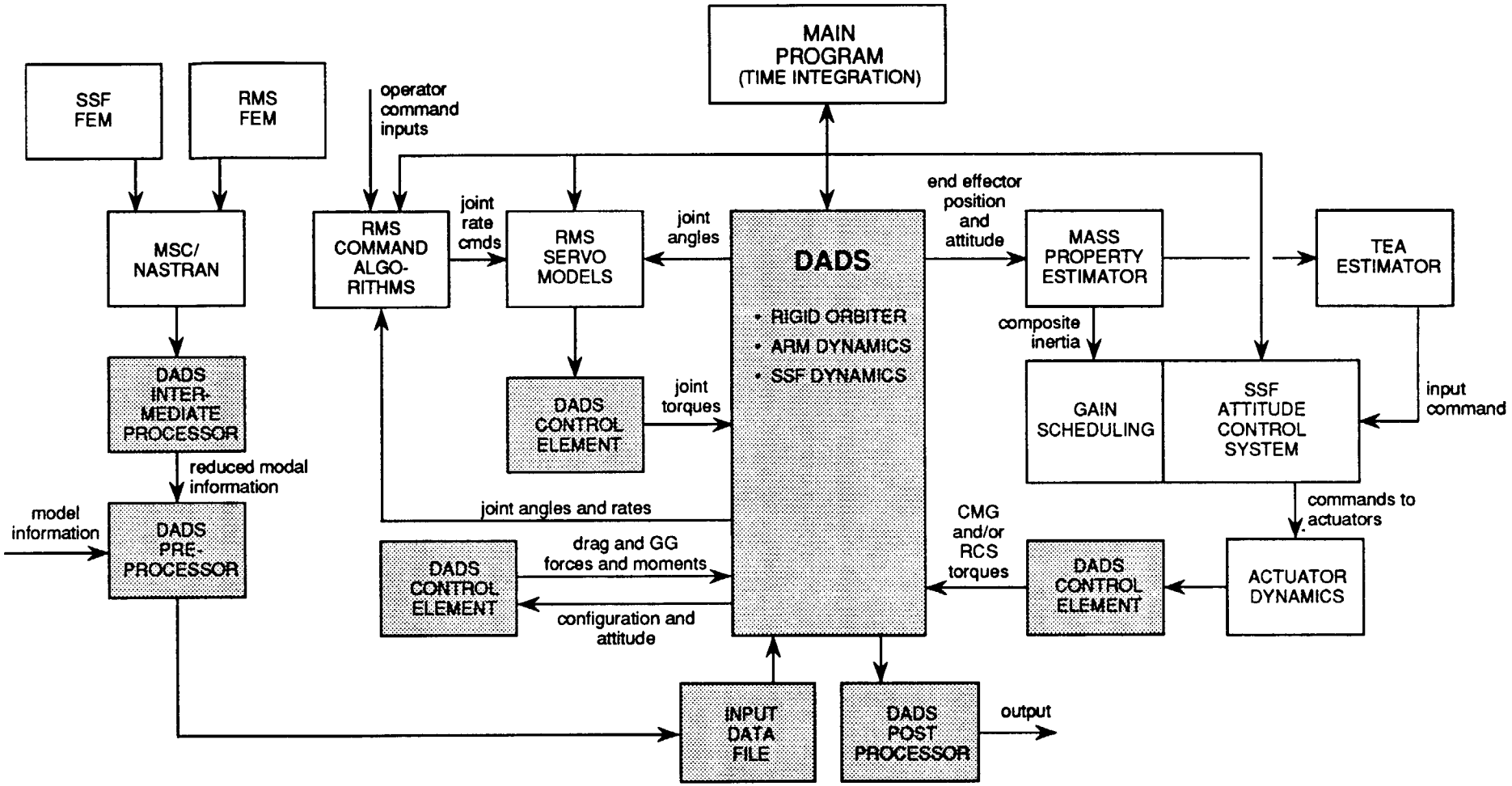

Figure 1-10.- Simulation architecture

2.0 FINITE ELEMENT MODELS

2.1 Stage 5 Finite Element Model

The SSF Stage 5 finite element model, provided by McDonnell Douglas Space Systems Company (MDSSC), is described in the SSF PDR Loads Data Book (ref. 2-1). The "perfectly feathered" configuration was chosen to account for the feathering of the PV arrays to minimize plume impingement from the Orbiter jets during the Orbiter's approach to the station. It was assumed that the arrays would remain in this position during the berthing scenario. A plot of the model showing the location of critical control system components is shown in figure 2-1. The only modification made to the model was the addition of a grid point representing the grapple fixture location. The grid point was added by attaching a "very stiff beam" to the beam elements used in the simplified equivalent beam model of the resource node. The new beam references the same beam properties as the existing resource node beam elements. The grapple fixture location is shown in figure 2-2. Weight properties are listed in Appendix C.

The superelement modal analysis was performed following the same method used by MDSSC to calculate the PDR loads. Minor modifications were made to update the procedures from Version 66b of MSC/NASTRAN (ref. 2-2) to Version 67, and a grid point was added at the grapple fixture location. The model was fixed in all six degrees of freedom at the grapple fixture. The analysis produced 181 modes below 5 Hz, and the first mode had a frequency of 0.099 Hz. The frequencies are plotted in figure 2-3 and listed in table 2-1. Modal kinetic energy was calculated for each of the super elements to help characterize the modes. Figure 2-4, which shows a plot of percent kinetic energy in the PV arrays, indicates that the structural dynamics are dominated by the arrays. The plot in figure 2-5 shows the percent kinetic energy in the truss segments which support the RCS, CMGs, and the avionics platform. This plot was used to help verify the selection of modes which affect motion near the sensor locations.

A reduced number of modes was chosen to represent the flexibility of the station in the DADS multibody simulation. First, frequency response functions (FRFs) plotted from 0 to 5 Hz were computed for all possible input/output pairs. The input loads included forces at the RCS locations, moments at the CMG location and forces and moments at the grapple point and the output responses included elastic rotations and rotation rates at the sensor location. A typical FRF is shown in figure 2-6. The natural modes whose frequencies were within a 10 dB region of the maximum response for each FRF were selected. Unit impulse responses were computed and compared with similar responses computed using the full set of 181 modes below 5 Hz. In the few cases where impulse response comparisons were unacceptable, additional modes were added to the reduced set. A small number of modes were removed when their kinetic energy contribution proved to be near zero in the region of the sensors. Impulse

results using the final reduced set of modes were compared with results using the full set of modes. The response vector lengths and angles were compared as shown in figure 2-7. The reduced mode sets used in the multibody simulations are given in tables 2-2 and 2-3, and the ten most important modes for the TEA simulation are plotted in appendix B.

The procedure for adding flexible bodies to a DADS model was modified to allow processing of the external superelements (photovoltaic arrays and electrical power system radiator). The standard DADS procedure requires making a single NASTRAN run to generate the geometry, mass and stiffness matrices, and mode shapes and frequencies of a flexible body. The DADS Intermediate Processor converts this information into standard DADS flexible-body input data.

The DADS program assumes a lumped mass formulation for the flexible body and requires each grid point in the body to have a mass associated with it. The lumped mass matrix is then used to calculate the nonlinear coupling terms in the equations of motion. An approximate mass representation was generated for the grid points which were used to graphically represent the geometry of the PV arrays and Electrical Power System (EPS) radiator in the assembled finite element model. The approximate external super element mass data was combined with the mass data for the physical portions of the SC-5 model to produce a single mass matrix for the SSF. The super element mode shapes calculated using the MDSSC approach were combined into "system" mode shapes, and the data was combined with the mass and geometry data using a customized MSC/NASTRAN Direct Matrix Abstraction Procedure to format the data for the DADS Intermediate Processor.

2.2 SRMS Finite Element Model

In order to incorporate the flexibility of the SRMS into the simulations, segments of the arm were modeled using finite elements. Only the two very long sections of the arm, Links 3 (upper arm) and 4 (lower arm), were modeled as flexible bodies. The other segments, which are much stiffer, were represented as rigid bodies. MSC/NASTRAN CBAR elements were used to model the links. Mass and stiffness properties were taken from reference 2-3. A total of nine elements were used to model each link. This discretization was adequate to provide a good approximation of the overall mass properties of each link. The models are summarized in figures 2-8 and 2-9. There is some significant flexibility at the SRMS attachment region on the Orbiter port longeron; however, the corresponding lowest frequency for a mode which contains motion in this region is well above the frequency range of interest and this region was not modelled as a flexible structure.

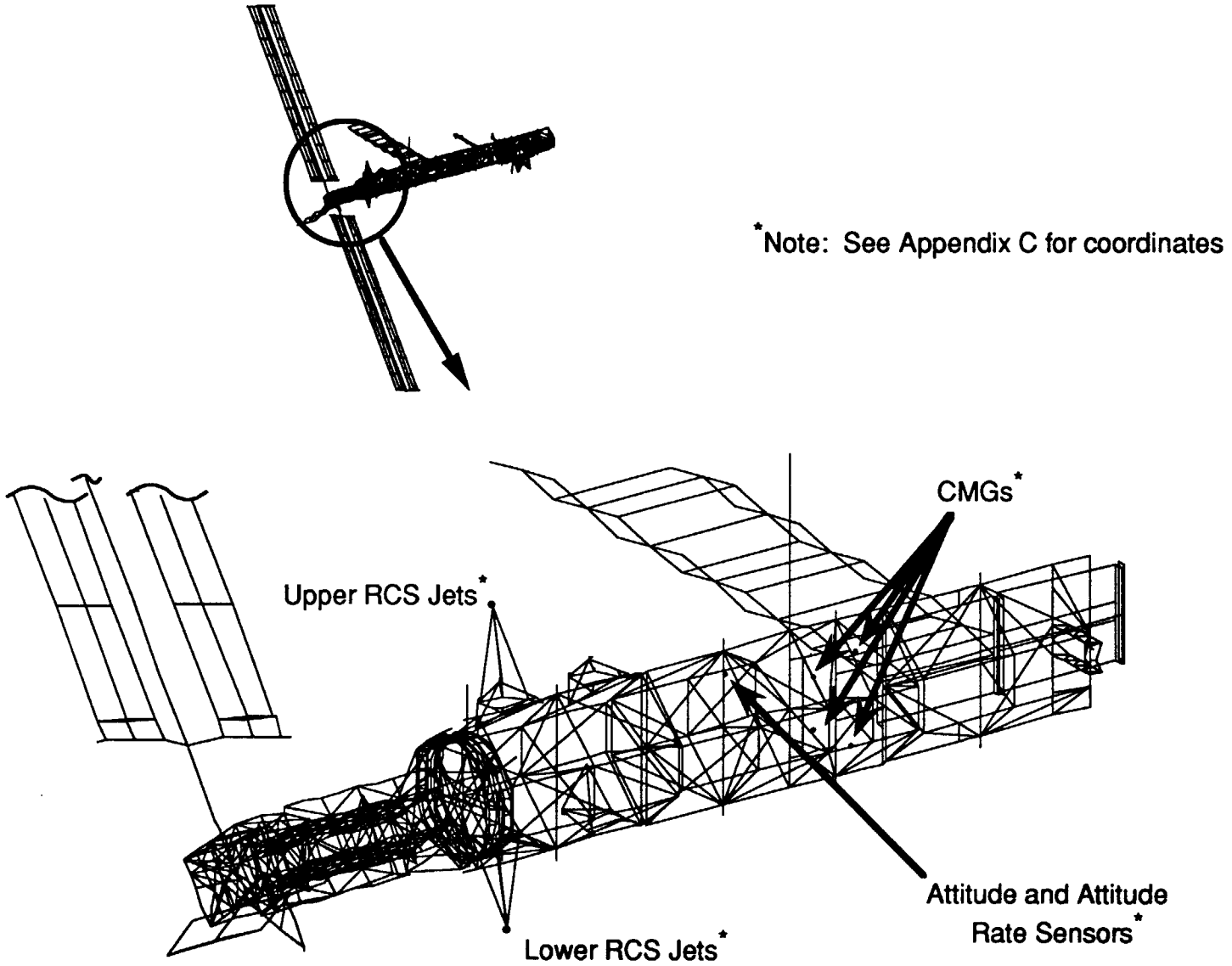

Figure 2-1.- Propulsion module, sensor and CMG locations.

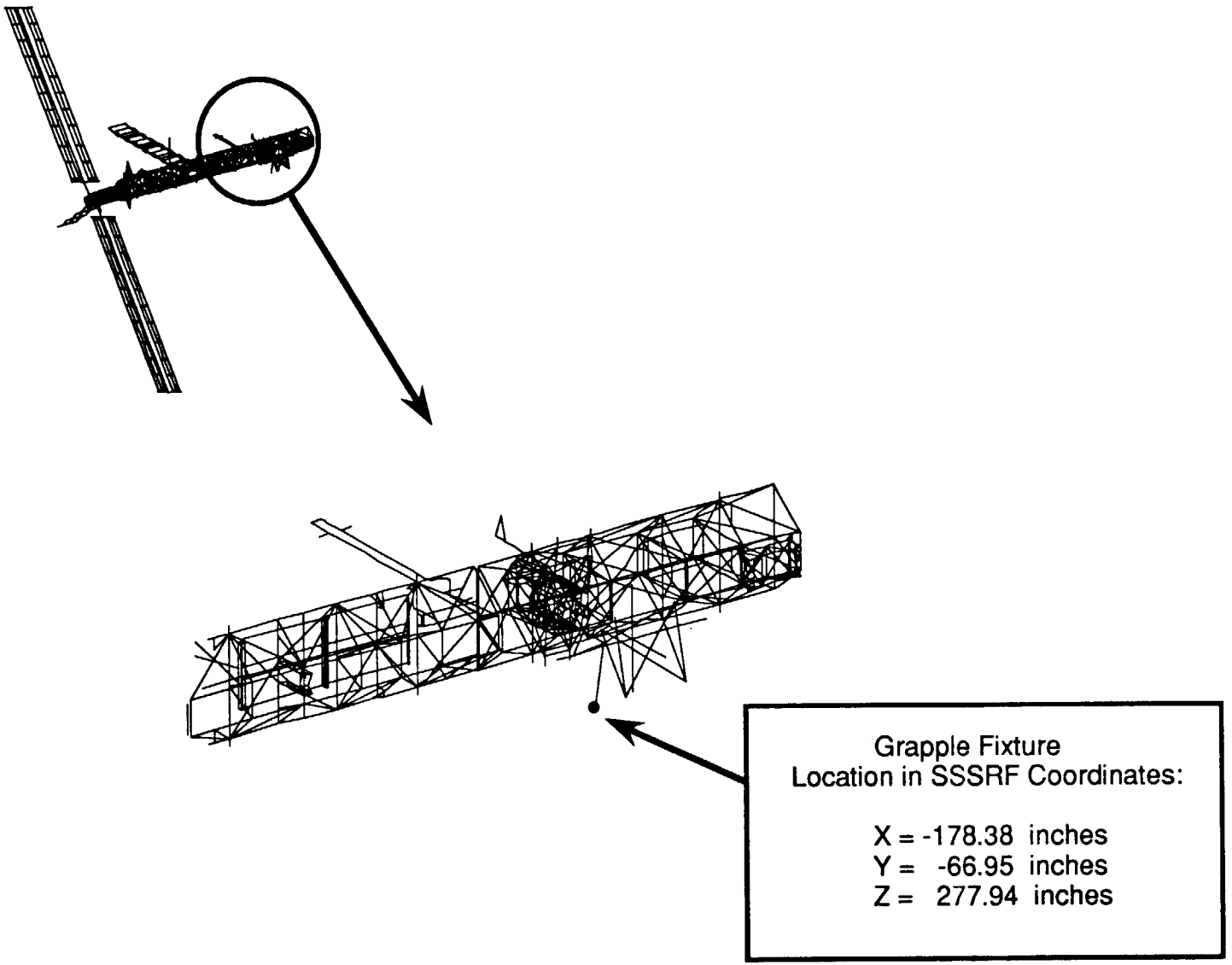

Figure 2-2.- Grapple fixture location.

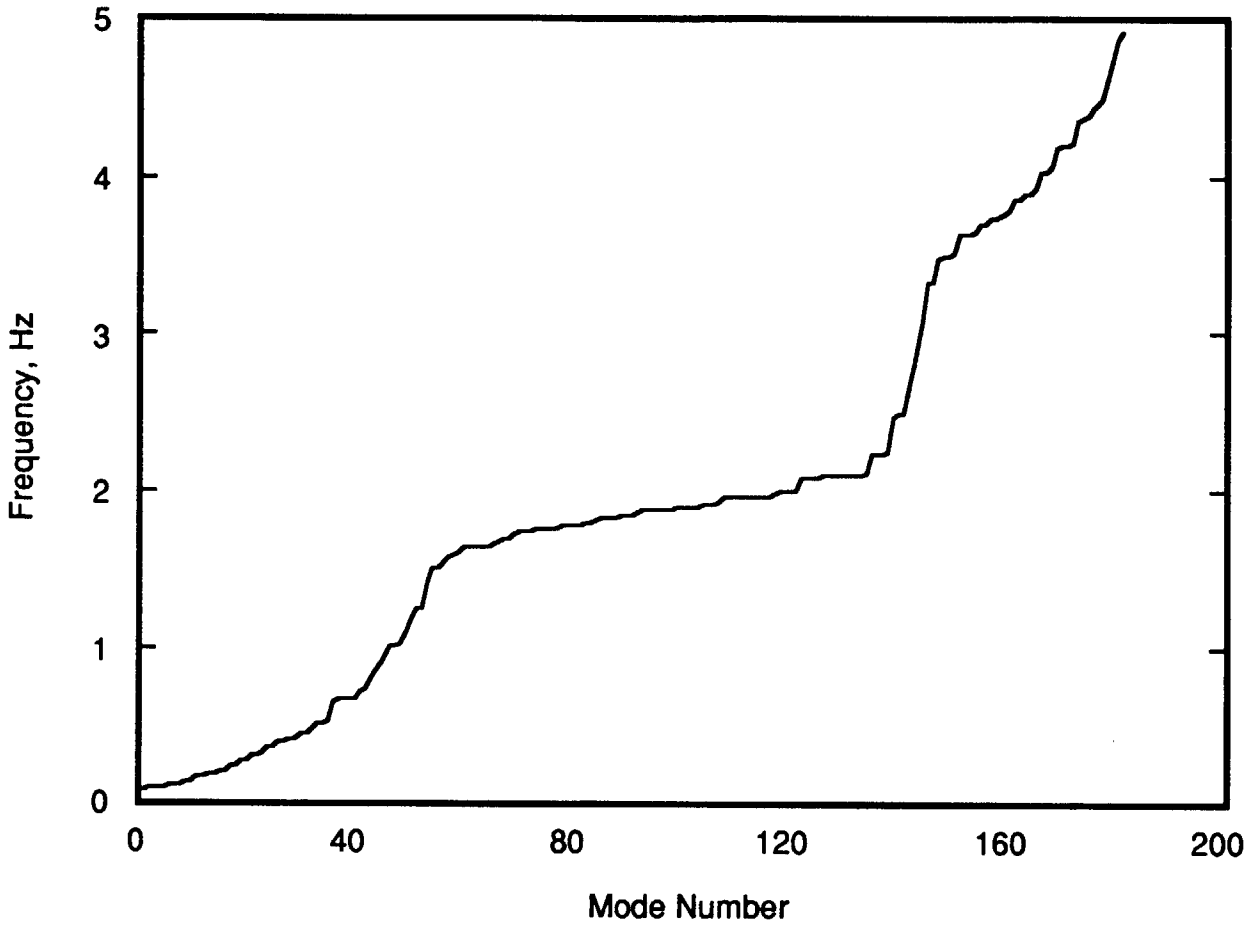

Figure 2-3.- Frequencies of SC5 finite element model below 5 Hz.
(PV Arrays Feathered; Fixed at Grapple Fixture)

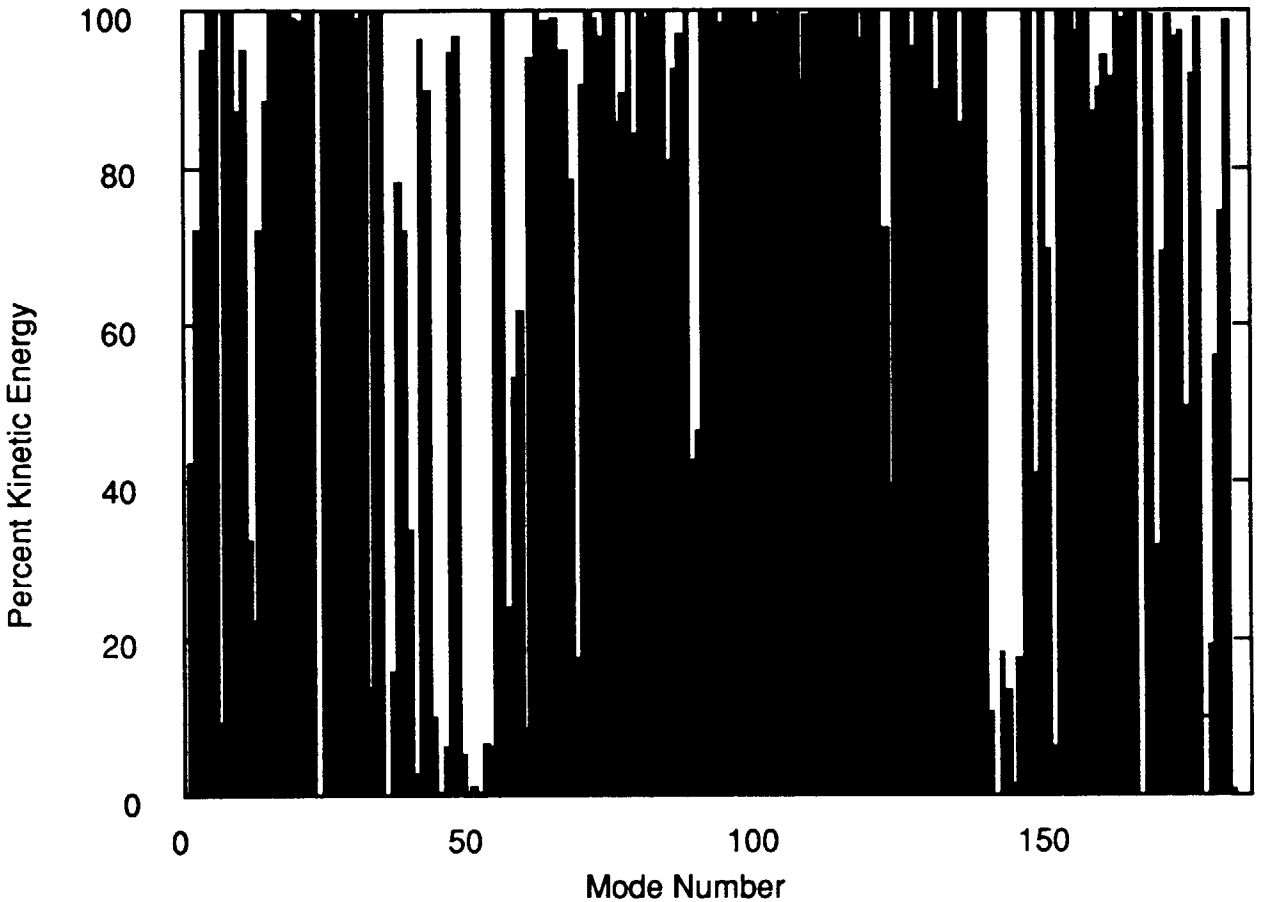

Note: SC-5 with PVs feathered; fixed at grapple fixture

Figure 2-4.- Modal kinetic energy in PV Arrays.

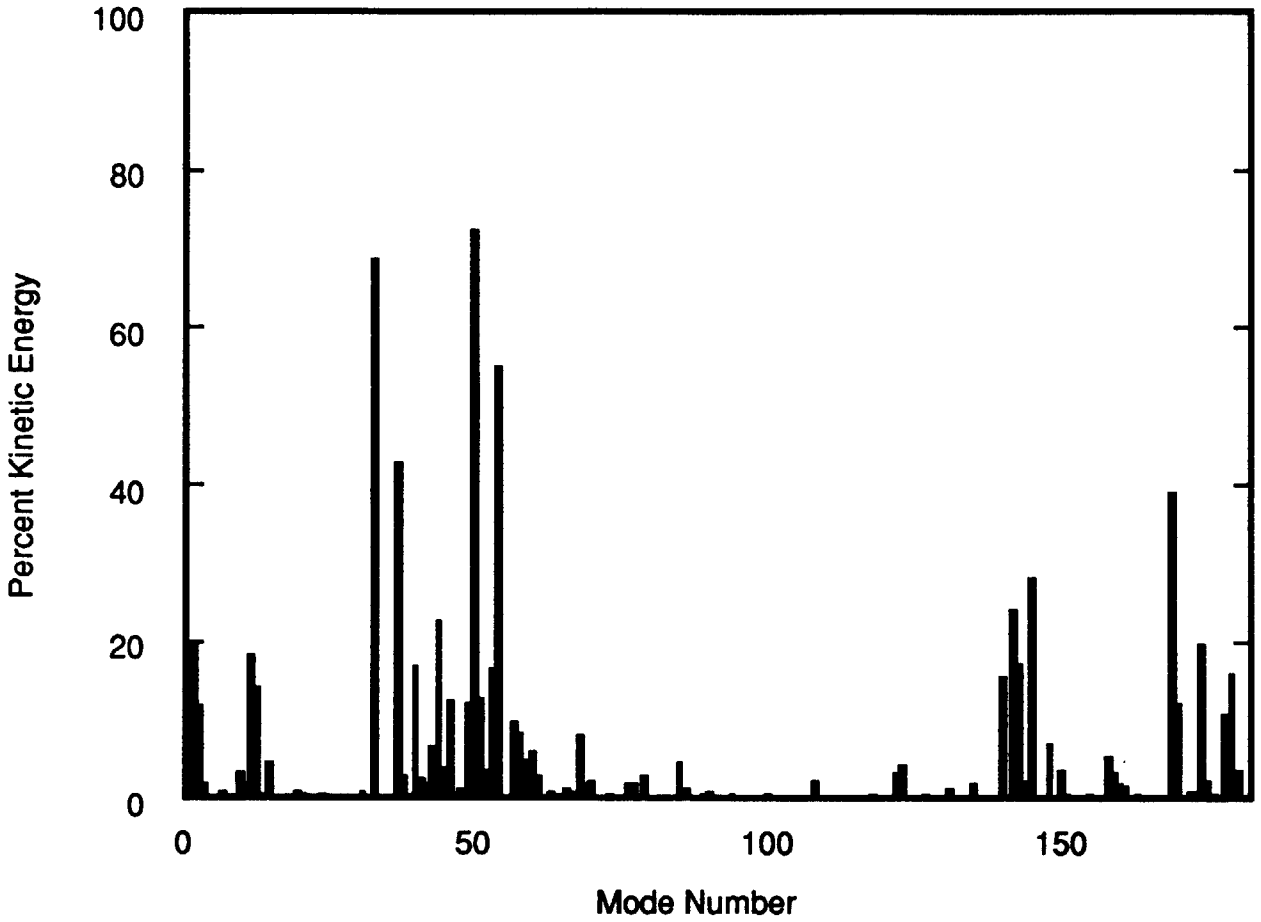

Figure 2-5.- Modal kinetic energy in truss segments near sensors.

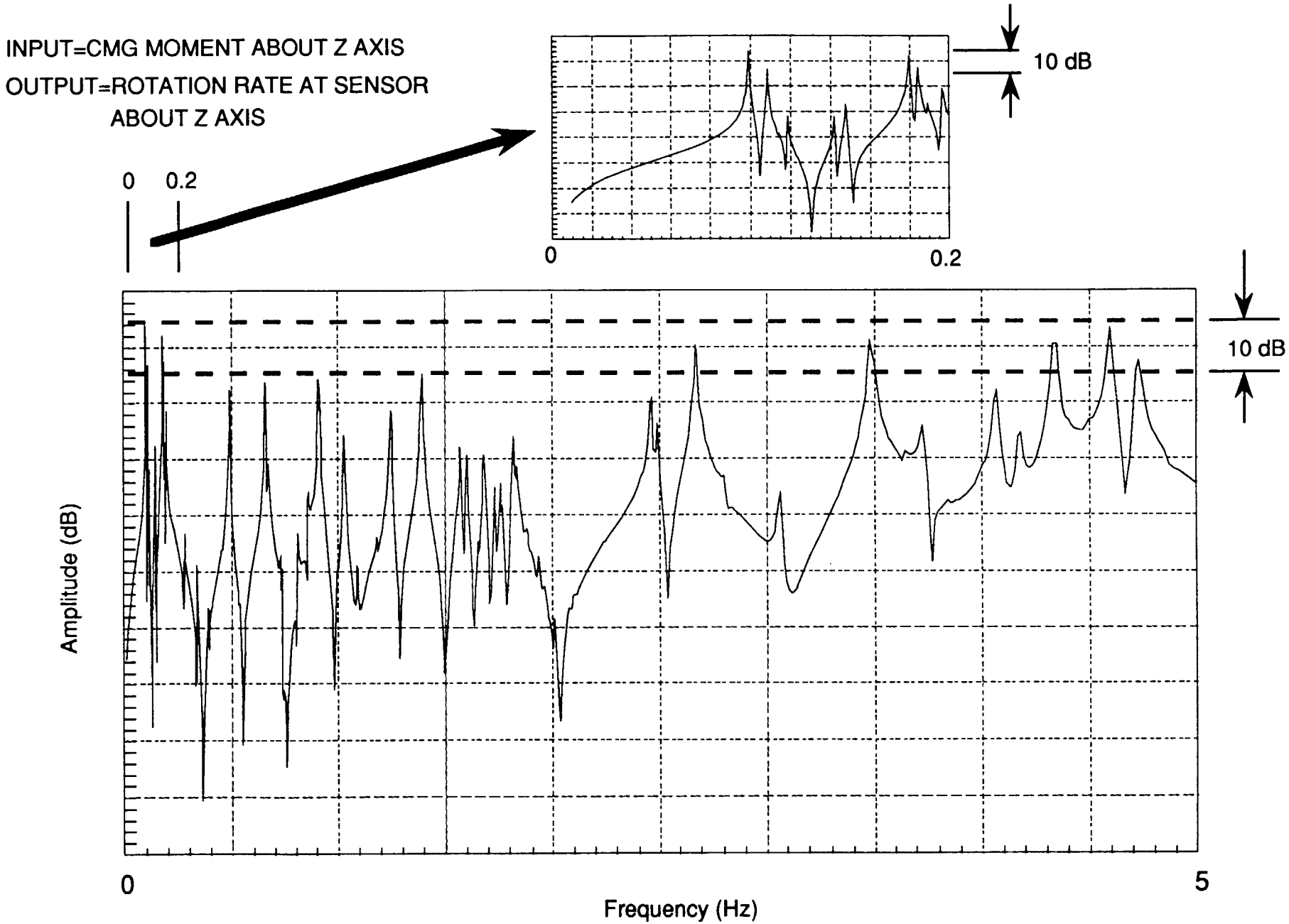

Figure 2-6.- Typical FRF used to select modes for a reduced modal set.

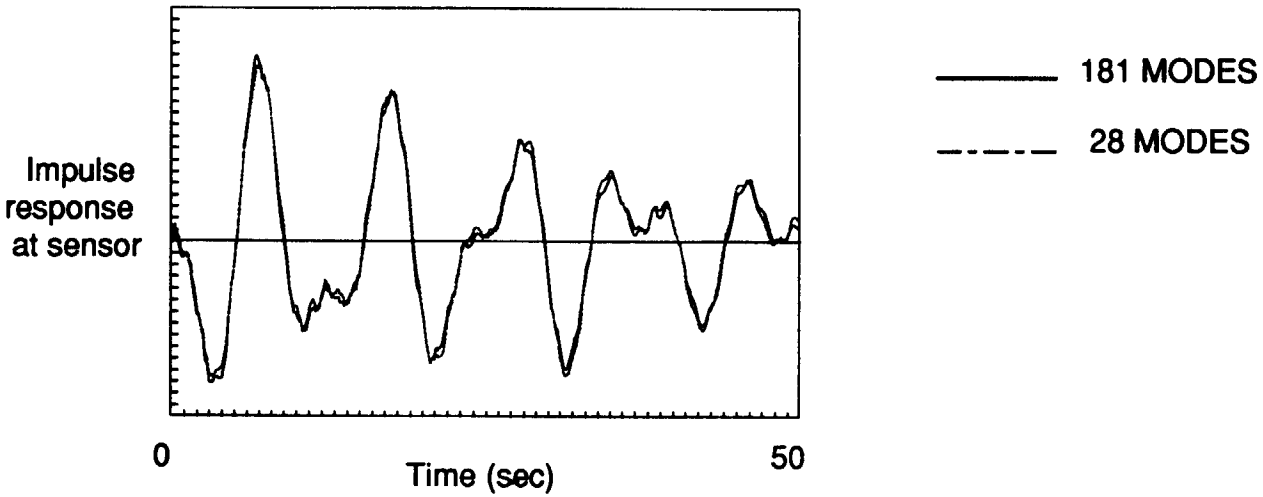

	AVERAGE COS $^{2}\theta$ / % DIFF IN VECTOR NORM	
	ANGULAR DISPLACEMENT	ROTATION RATE
RCS ONLY (28 MODES)	0.99 / 0.70	0.93 / 3.99
GRAPPLE FIXTURE AND CMG (33 MODES)	0.99 / 0.54	0.95 / 2.30

Figure 2-7.- Validation of reduced modal description of SSF for each scenario.

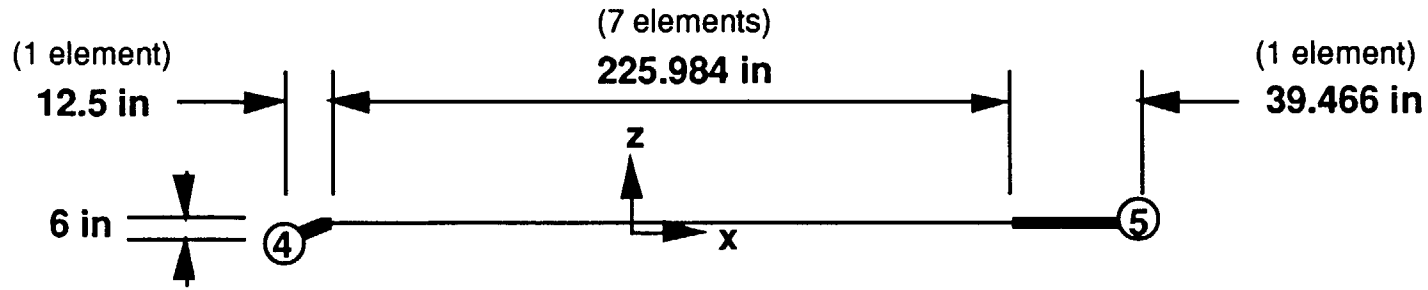

MASS PROPERTIES

	PDRS	FEM
Mass, slugs	5.9901	5.9902
Inertia Tensor (from ASAD model), slug-ft^2		
Ixx	1.7596	1.7594
Iyy	267.8036	277.5304
Izz	267.8036	277.4941
Ixy	0.0	0.0
Ixz	0.0	-0.85694
Iyz	0.0	0.0

FREQUENCIES

Mode	Frequency (Hz)	Description
1*	4.54	1st Z bending
2*	4.86	1st Y bending
3	29.0	2nd Z bending
4	30.2	2nd Y bending
5	73.5	1st torsion
6	74.4	3rd Z bend+1st tors
7	77.3	3rd Y bending
8	132	4th Z bending
9	133	1st ax+4th y bend

* = used in flexible DADS component

Figure 2-8.- RMS Lower Arm (Link 4) finite element model.

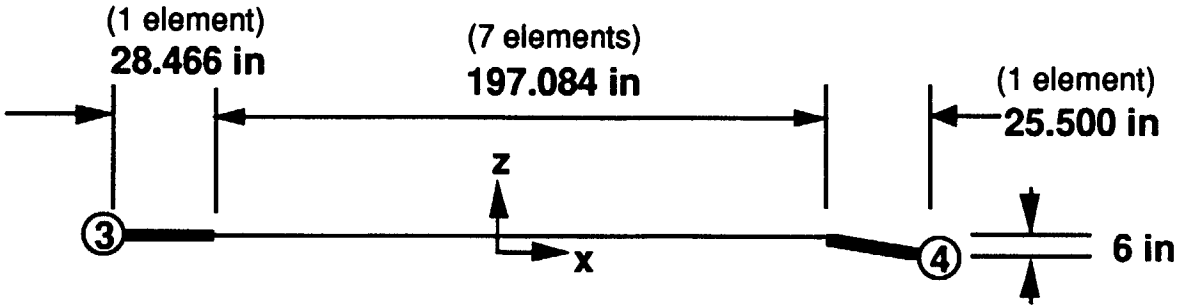

MASS PROPERTIES

	PDRS	FEM
Mass, slugs	9.5485	9.5485
Inertia Tensor (from ASAD model), slug-ft^2		
Ixx	2.8025	2.8025
Iyy	347.955	358.3754
Izz	347.955	358.2576
Ixy	0.0	0.0
Ixz	0.0	2.5919
Iyz	0.0	0.0

FREQUENCIES

Mode	Frequency (Hz)	Description
1*	5.12	1st Z bending
2*	5.23	1st Y bending
3	34.1	2nd Z bending
4	34.5	2nd Y bending
5	65.7	1st torsion
6	97.2	3rd Y bending
7	98.0	3rd Z bending
8	137	1st axial

* = used in flexible DADS component

Figure 2-9.- RMS Upper Arm (Link 3) finite element model.

Mode	Freq (Hz)	Mode	Freq (Hz)	Mode	Freq (Hz)	Mode	Freq (Hz)
1	0.099	47	1.006	93	1.876	139	2.471
2	0.109	48	1.031	94	1.879	140	2.487
3	0.112	49	1.094	95	1.882	141	2.494
4	0.114	50	1.188	96	1.883	142	2.678
5	0.114	51	1.246	97	1.883	143	2.817
6	0.119	52	1.252	98	1.884	144	3.069
7	0.124	53	1.396	99	1.901	145	3.326
8	0.124	54	1.504	100	1.904	146	3.326
9	0.142	55	1.504	101	1.904	147	3.484
10	0.148	56	1.549	102	1.905	148	3.493
11	0.180	57	1.574	103	1.907	149	3.498
12	0.184	58	1.598	104	1.909	150	3.523
13	0.189	59	1.603	105	1.910	151	3.637
14	0.197	60	1.639	106	1.910	152	3.641
15	0.219	61	1.642	107	1.932	153	3.642
16	0.219	62	1.643	108	1.961	154	3.647
17	0.245	63	1.646	109	1.964	155	3.703
18	0.245	64	1.647	110	1.964	156	3.705
19	0.277	65	1.657	111	1.967	157	3.733
20	0.282	66	1.684	112	1.967	158	3.742
21	0.311	67	1.687	113	1.973	159	3.752
22	0.311	68	1.691	114	1.974	160	3.787
23	0.338	69	1.736	115	1.974	161	3.857
24	0.364	70	1.740	116	1.974	162	3.859
25	0.364	71	1.740	117	1.991	163	3.891
26	0.395	72	1.753	118	1.994	164	3.892
27	0.395	73	1.754	119	1.994	165	3.925
28	0.412	74	1.755	120	1.994	166	4.021
29	0.412	75	1.760	121	2.008	167	4.022
30	0.455	76	1.769	122	2.083	168	4.071
31	0.455	77	1.770	123	2.093	169	4.185
32	0.491	78	1.771	124	2.093	170	4.192
33	0.521	79	1.781	125	2.093	171	4.193
34	0.521	80	1.781	126	2.095	172	4.216
35	0.535	81	1.782	127	2.098	173	4.345
36	0.657	82	1.795	128	2.098	174	4.374
37	0.664	83	1.795	129	2.098	175	4.393
38	0.666	84	1.811	130	2.102	176	4.441
39	0.670	85	1.823	131	2.108	177	4.490
40	0.674	86	1.834	132	2.108	178	4.606
41	0.730	87	1.835	133	2.108	179	4.731
42	0.736	88	1.837	134	2.113	180	4.862
43	0.813	89	1.839	135	2.246	181	4.916
44	0.861	90	1.850	136	2.248		
45	0.915	91	1.851	137	2.248		
46	1.004	92	1.867	138	2.248		

Table 2-1.- Frequencies of stage 5 FE model fixed at grapple fixture, PV arrays feathered

Mode Number	Frequency (Hz)
1	0.099
2	0.109
3	0.112
9	0.142
10	0.148
11	0.180
12	0.184
14	0.197
32	0.491
36	0.657
39	0.670
42	0.736
43	0.813
45	0.915
48	1.031
49	1.094
50	1.188
52	1.252
53	1.396
76	1.769
78	1.771
139	2.471
141	2.494
142	2.678
144	3.069
147	3.484
149	3.498
157	3.733
158	3.742
159	3.752
168	4.071
169	4.185
173	4.345
174	4.374
178	4.606
179	4.731

Note: Mode Numbers refer to modes in un-reduced 181-mode model.

Table 2-2.- 36 mode reduced set for TEA maneuver

Mode Number	Frequency (Hz)
1	0.099
2	0.109
3	0.112
9	0.142
10	0.148
11	0.180
12	0.184
32	0.491
36	0.657
39	0.670
43	0.813
49	1.094
53	1.396

Note: Mode Numbers refer to modes in un-reduced 181-mode model.

Table 2-3.- Reduced mode set for berthing simulation

3.0 DESCRIPTION OF THE REMOTE MANIPULATOR SYSTEM

3.1 System Description

The SRMS is a six-joint anthropomorphic arm which was originally designed to deploy payloads weighing up to 65,000 pounds and retrieve payloads weighing up to 35,000 pounds. The 50-foot arm is mounted to the port longeron of the Orbiter cargo bay by means of a manipulator positioning mechanism. This is the, so-called, swing-out joint which is used to rotate and lock the arm (19.48°) outboard for adequate clearance during arm/payload operations. From this attachment point, the arm is comprised of two single DOF shoulder joints, a 21-foot long upper boom, a single DOF elbow joint, a 23-foot long lower boom, 3 single DOF wrist joints and a snare-type end effector capable of mating with a payload mounted grapple fixture. A simplified sketch of the SRMS is presented in figure 1-8.

Each of the six arm joints consists of a reversible dc drive motor, a mechanical joint brake, an inductosyn tachometer, an epicyclical gear train and an electro-optical encoder. The encoder is physically mounted on the joint side of the gearbox and the tachometer is mounted on the motor side of the gearbox. The encoder and tachometer measure joint position and joint rate, respectively. Structural flexibility of the long booms, the joint housings, and the gear trains contribute to the overall structural flexibility of the SRMS. Significant dynamic coupling between joints is also introduced when the joints are back-driven.

The arm is telerobotically controlled from the aft cockpit of the Orbiter by way of translational and rotational hand controllers and control panel command inputs. Joint rate commands are sent from software algorithms resident in the Orbiter GPC to the joint servos by way of the MCIU. The joint rate commands that are generated in the GPC depend on the selected operational mode, i.e., single joint mode, manual mode or automatic mode. The rate commands output which are limited according to arm loading conditions, i.e., payload mass. When not being commanded to move, the arm is held in place by either "position hold", "zero-rate command hold", or "brakes on".

The SRMS has several operational modes. The modes exercised during the berthing simulation are the automatic mode, the manual mode, and the position hold mode. The automatic mode uses an inverse kinematic analysis to provide rate commands to each joint so that a selected point of resolution (POR) will move in a straight line from a given position and orientation to a new given position and orientation. In the berthing simulation, the end effector was selected as the POR. In manual mode, translational and rotational hand controller inputs are resolved into joint rate commands applied to each servo motor so that the requested motion is realized. The position-hold mode uses feedback of the joint angles to generate commands to the joint servos to maintain the commanded position of the arm. For the

TEA simulation, the joint brake system is engaged to maintain the arm position and orientation. These brakes are designed to slip to prevent overloading the arm when the applied brake torque exceeds the permissible level. (ref. 3-1)

Modeling of the SRMS is broken down into two parts: 1) SRMS Control System and 2) Arm Dynamics. The arm dynamics modeled using FEM and DADS are discussed in Part 2.0 and Part 6.0, respectively. A description of the SRMS control system modeling is presented in the following section.

3.2 SRMS Control System

The SRMS control system module includes models of the SRMS joint servo drive mechanisms, the software command algorithms in the GPC and the MCIU that links the arm electronics to the GPC. These models were extracted from the DRS, a high fidelity model of the SRMS developed by The Charles Stark Draper Laboratory, Inc., Cambridge, MA. They were incorporated into DADS as self-contained FORTRAN routines and validated against the performance predicted by the DRS.

There are several SRMS upgrades which are being made to support SSF assembly operations. These upgrades include the Position-Orientation-Hold-Submode (POHS), the Position Hold upgrade and the Servo Power Amplifier (SPA) upgrade. The POHS upgrade corrects for unwanted motion encountered while operating in manual mode. The Position Hold Upgrade improves RMS stability margins when handling very heavy payloads. The SPA upgrade stiffens the wrist joint servo loops to reduce inertial cross-coupling when handling heavy payloads. Based on schedule constraints and the maturity of these upgrades, they were not incorporated into the current assembly simulation.

3.2.1 Command Algorithms

The SRMS command algorithms were implemented in DADS as self contained FORTRAN routines which were adapted from the DRS. This software is consistent with the SRMS functional subsystem software requirements definition document (ref. 3-2). As such, it simulates each of the principal functions which perform the required mathematical and logical operations to support the SRMS.

3.2.2 Servo Model

The math model for the joint servo is shown in figure 3-1. This model is essentially equivalent to the model described in reference 3-3. The servo configuration is identical for each of the six joints, although joint-dependent parameters vary. The specific servo parameter values used are given in Appendix D-1. As shown in the figure 3-1, a digital joint rate command (in counts) is received from the GPC by way of the MCIU. This input rate command is compared with the actual motor rate from a digital tachometer feedback to form an error signal. This error is then converted to an analog voltage signal and processed in a set of continuous electronics consisting of an integrator and a low pass filter. The purpose of the integrator is to provide a high gain at low frequencies needed to break motor and gear train static friction (stiction) and to overcome small errors. The output of these electronics are summed with negative feedback of the analog tachometer signal. This continuous part of the tachometer is run through a high pass filter which serves to provide stability. In contrast, the purpose of the digital tachometer is to improve tracking accuracy. The analog voltage signal is then sent to the motor drive amplifier and a current limiter which results in attenuation of the voltage applied to the joint motor. The resulting motor rate is then passed to the gearbox to generate the required output torque.

As shown in the servo diagram, nonlinear friction losses are modeled on both the motor or input side of the gearbox and on the output or joint side of the gearbox. The output friction models include both the joint friction and the gearbox friction. Details of the models used are described briefly in the following sections.

3.2.3 Motor/brake friction/stiction

Motor/brake friction/stiction is modeled as shown in figure 3-2a where τ_C and τ_S are the coulomb and stiction torque levels, respectively, τ_{fi} is the motor friction torque, and τ_n is the applied torque. If the joint is moving, the friction torque is equal to the coulomb (sliding) friction value. If the joint is not moving and the torque is larger than the stiction level, the friction torque is set to the stiction level. If the torque is less than the stiction level, just enough stiction is applied to the joint to make the net torque output zero.

3.2.4 Gearbox stiffness

The nonlinear gearbox model is represented by an asymptotic linear compliance and a quadratic stiffness relation at low torque levels as described in reference 3-2. This stiffness is computed as a function of the backlash angle of the gearbox as shown in figure 3-2b where B_L is the backlash half

angle as seen on the joint side of the gearbox, T_Δ is the torque at the backlash half angle as seen on the joint side, and K_G is the linear stiffness as seen on the joint side.

3.2.5 Joint stiction/friction

In this friction model, the joint friction torque, τ_f, is computed as a function of the joint angle as shown in figure 3-2c where $\Delta\gamma$ is the difference in the actual joint angle, γ, and a friction reference angle, γ_f, τ_C is the coulomb torque level, and τ_S is the stiction torque level. This is the so-called "old hair-brush" friction model. When $\Delta\gamma$ is less than a stiction reference angle, $\pm \Delta\gamma_S$, the friction torque acts like a spring restraint. In this region, a steady torque produces a small rotational displacement. When an applied torque is removed, the joint returns to an equilibrium position at $\Delta\gamma = 0$. If the displacement exceeds $\Delta\gamma_S$, the friction torque drops to a coulomb torque level, τ_C. While joint rate remains positive, the friction torque is constant. If the rate becomes negative, the friction reference angle is reset and the model reverts to its spring-like behavior about the new reference point (ref. 3-4).

3.3 Point of Resolution Location

The Point of Resolution for the SRMS berthing operations was selected to be at the end effector aligned with the End Effector Operating Frame (ref. 3-2). The specific vector definitions and transformations used in the simulation to designate this POR location are given in Appendix C-7.

3.4 SRMS Rate Limits

The payload dependent joint rate and effector translational and rotational rate limits used in the assembly simulation are listed in Appendix D-2.

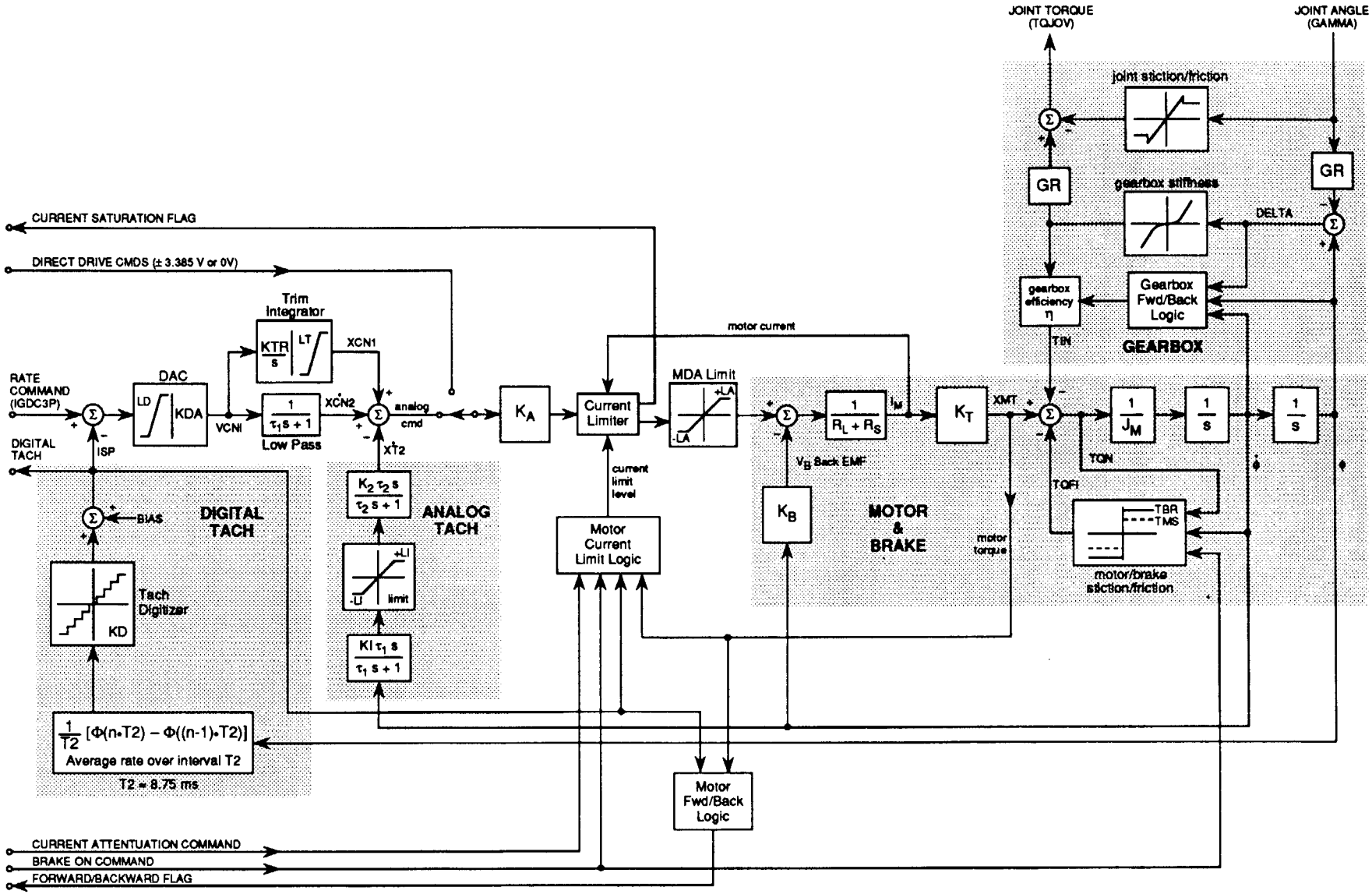

Figure 3-1.- DRS servo block diagram

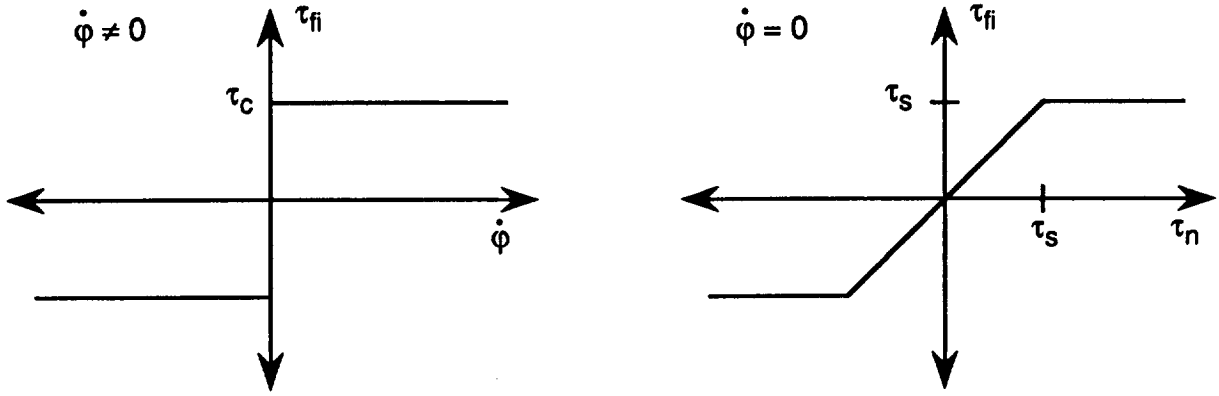

where,
$\dot{\varphi}$ = motor rate (rad/sec)
τ_C = coulomb torque level (ft-lbs)
τ_S = stiction torque level (ft-lbs)

a.- Motor/brake friction/stiction

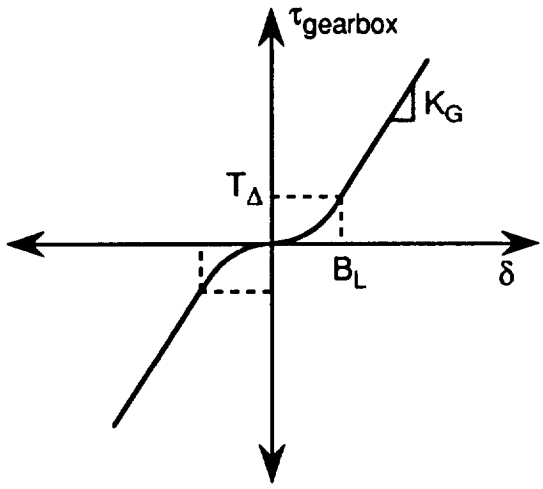

where,
T_Δ = gearbox transition torque (ft-lbs)
B_L = gearbox transition angle (rad)
K_G = gearbox linear stiffness (ft-lbs / rad)

b.- Gearbox stiffness

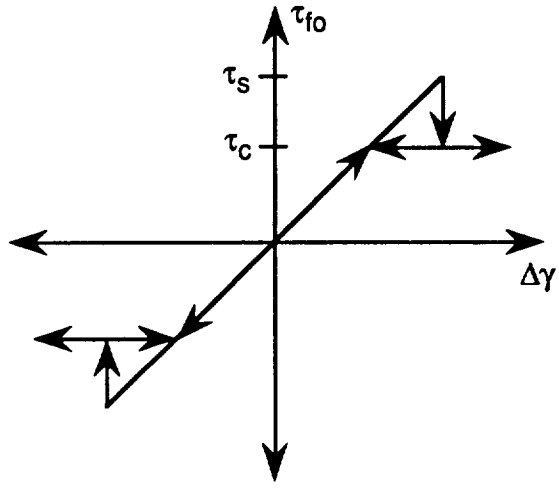

where,
$\Delta\gamma$ = difference in actual joint angle (deg)
τ_C = coulomb torque level (ft-lbs)
τ_S = stiction torque level (ft-lbs)

c.- Joint stiction/friction

Figure 3-2.- Nonlinear servo models

4.0 ORBITAL MECHANICS AND ENVIRONMENTAL DISTURBANCES

4.1 TEA Maneuver

In the RCS maneuver, it is assumed that the forces applied to the spacecraft body from the jet firings are much larger than the external moments resulting from gravity gradient and aerodynamic drag of the rarefied upper atmosphere. These moments were included in the dynamics primarily for determining the final steady state attitude of the stack following the maneuver to an estimated TEA. For this reason, a simplified model for the orbital disturbances on the Space Station and Shuttle system was derived by considering the stack as possessing a single set of mass and aerodynamic properties. Data assumed for these models is given in appendix E. Only gravity gradient and aerodynamic moments are included in these simulations.

Aerodynamic torques are computed for the spacecraft modeled as three orthogonal flat plates each with a projected area vector, A_i, and a center of pressure to center of gravity offsets, r_{CPi}, from the vector equation:

$$M_{aero} = -\sum_{i=1}^{3} r_{CPi} \times \rho \, | A_i \cdot V_{S/C} | \, V_{S/C} \qquad (4\text{-}1)$$

in which VS/C is the velocity vector of the spacecraft relative to the Earth's atmosphere. The projected areas and center of pressure to center of gravity offsets were computed from an I-DEAS solid model of the stack using the MODGEN software. This software takes into account the shadowing of one component by another. At the time that these data were computed, the exact RMS retraction trajectory was not determined, so the stack geometry in figure 4-1, representing the "capture" configuration was assumed.

A Jacchia 1970 atmosphere model (ref. 4-1) is used to compute the atmospheric density. In this model, the density at a specific time and point in the orbit is a function of: altitude of spacecraft; latitude of sub-satellite point; day of the year; solar hour angle; geomagnetic index; and the 10.7-cm solar flux. A circular orbit was assumed in computing orbital position. Numerical data for the aerodynamic model is also summarized in appendix E.

The gravity gradient, assuming a circular orbit in a pointing mass field, is computed for a single rigid body spacecraft from:

$$M_{gg} = 3\omega_o^2 \begin{bmatrix} 0 & -u_3 & u_2 \\ u_3 & 0 & -u_1 \\ -u_2 & u_1 & 0 \end{bmatrix} [I]\, u \qquad (4\text{-}2)$$

in which u is the local vertical unit vector. The moment of inertia, I, for the combined stack was assumed to remain constant throughout the simulation and the same numerical data as used in the controller gain scaling was used in the gravity gradient equation.

The aerodynamic and gravity gradient moments were resolved into equivalent torque couples applied at the center of mass of the Space Station body and the Orbiter body.

The TEA was estimated for this configuration by minimizing the secular momentum which must be absorbed by a "perfect" controller in order to maintain a constant attitude of the stack configuration described above through one complete orbit. The IDEAS**2 software (ref. 4-2) provided this function. Expressed as a Pitch-Yaw-Roll (2-3-1) Euler angle sequence describing the relative orientation of the Space Station Structural Reference Frame (SSSRF) with respect to Local Vertical Local Horizontal (LVLH), the TEA is {158°, -7°, 93°}.

4.2 Berthing Maneuver

When the berthing is performed under CMG control, computation of the external disturbances must be done differently because of the changing mass properties. The multibody dynamics code only allows external forces and torques to be applied to a fixed point defined in a rigid body, i.e., they cannot be applied at the combined system center of mass (which is moving). The resultant of these disturbances was best represented within the simulation as moments and forces (couples) located at the centers of mass of the Orbiter and the Space Station bodies.

The gravity gradient was implemented by breaking the net gravity gradient moment into two components. The first results from the gravity gradient of each extended body about its own center of mass and the second results from the "dumbbell" effect of both bodies, represented as point masses, connected to each other. The individual body's gravity gradient moments are computed from

$$M_{gg}SSF = 3\omega_o^2 \begin{bmatrix} 0 & -u_3 & u_2 \\ u_3 & 0 & -u_1 \\ -u_2 & u_1 & 0 \end{bmatrix} [I_{SSF}]\, u \qquad (4\text{-}3)$$

$$M_{gg}STS = 3\omega_o^2 \begin{bmatrix} 0 & -u_3 & u_2 \\ u_3 & 0 & -u_1 \\ -u_2 & u_1 & 0 \end{bmatrix} [I_{STS}]\, u \qquad (4\text{-}4)$$

These moments are applied as external torques at the centers of gravity of the Space Station and the Space Shuttle bodies appropriately.

The "dumbbell" gravity-gradient moment resulting from the relative location of the Station and Shuttle, represented as point masses (M_{SSF} and M_{STS}) located at the center of gravity of each body, can be expressed in vector form by the equation

$$M_{gg}(DB) = 3\omega_o^2\left(\frac{M_{SSF}\,M_{STS}}{M_{SSF}+M_{STS}}\right)[(\rho \cdot u)\,(\rho \times u)] \tag{4-5}$$

In which ρ is the position vector from the center of mass of the Space Station to the center of mass of the Space Shuttle. This moment applied about the combined stack center of mass is equivalent to the couple expressed as the force applied at the center of mass of each body computed from

$$F_{gg}(DB) = \pm 3\omega_o^2\left(\frac{M_{SSF}\,M_{STS}}{M_{SSF}+M_{STS}}\right)[(\rho \cdot u)\,u] \tag{4-6}$$

In each of these equations, the unit vertical vector, u, is the same for both bodies and for the complete system. This assumes that the difference in rigid body attitude of the two bodies is not large compared to the net attitude change of the whole stack. This assumption was made for two reasons. First, the RMS arm is only commanded to make translational moves in this scenario. Second, the attitude dynamics equations are not sensitive to changes in net system properties of the magnitude that would be expected to result from flexibility of the arm. Figure 4-2 illustrates this system of forces and moments.

The magnitude of the aerodynamic disturbances would be of a lower magnitude than the gravity gradient. For this reason, the same method used for the RCS maneuver (which inherently assumed constant aerodynamic properties) was applied for the CMG maneuver. Several runs of the ray-trace software MODGEN were performed at different Shuttle positions representing a straight line translation in the Orbiter Body Axis System (OBAS) Z-direction. In comparing the changes in the aerodynamic properties in translating the Shuttle, it was determined that this change was of a lower order of magnitude than the uncertainty inherent in any model of upper atmosphere aerodynamic drag.

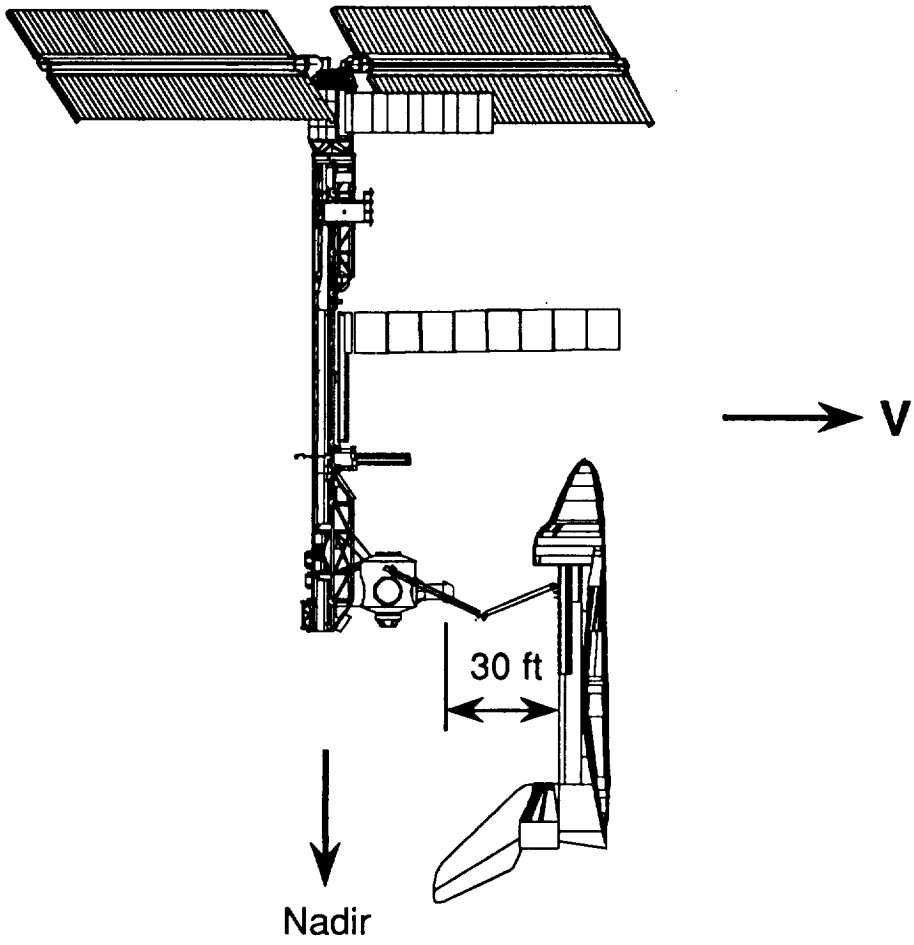

Figure 4-1.- Spacecraft geometry for aerodynamic model

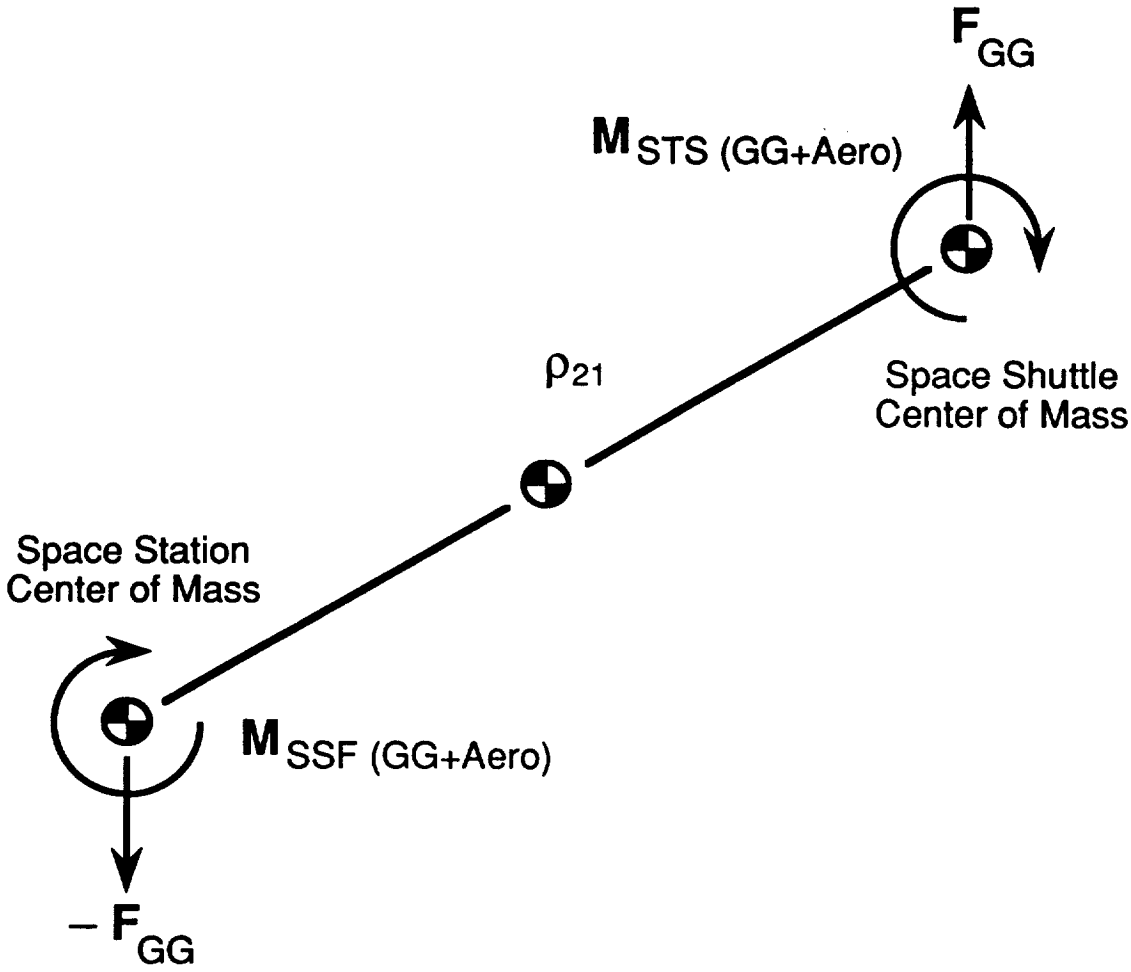

Figure 4-2.- External disturbance model for CMG control

5.0 SPACE STATION ATTITUDE DETERMINATION AND CONTROL SYSTEM

In the two scenarios considered in this study, the maneuver of the stack to an estimated TEA using RCS jets and the berthing of the Orbiter under CMG control, the Space Station Attitude Determination and Control System (ADCS) alone is responsible for attitude control. As shown in Figure 5-1, the ADCS consists of an Attitude Determination System (ADS) and an Attitude Control System (ACS). In the scenario simulations, the ADS is assumed to provide perfect information on the attitude and attitude rates of the coupled SSF/Orbiter configuration. The ACS that was implemented in this study was derived from FORTRAN code delivered at the SSF GN&C technical exchange meeting on March 19, 1992. Several modifications were made to this software in order for it to work properly with the study configurations and to make it consistent with the control system description in the Interim Design Review #6 (reference 5-1). References 5-1, 5-2, and 5-3 were used as sources for the control theory and definition of the specific controller algorithm.

The SSF ACS is based around an inner loop proportional-derivative controller for both the RCS and CMG functions. Commanded attitude and the measured attitude quaternion from the ADS are the inputs to the inner loop and the control torque required at each time step is the output. Attitude error is computed from the difference between the commanded and measured quaternions, with a limit imposed on the total maneuver angle allowed during each time step. The output torque is then fed to either the RCS jet selection logic, or the CMG steering law. The inner loop is operated with a time step of one second.

The following describes each of the ACS subsystems, the ADS, RCS, and CMG, as they were simulated for the study scenarios.

5.1 Attitude Determination System

The ADS provides attitude with respect to the LVLH coordinate system and inertial attitude rate in body coordinates for the ACS. As shown in figure 5-1, the sensor hardware consists of the Integrated Sensor Assembly (ISA) and the Star Trackers (ST). The ISA keeps track of the angular velocity and quaternion of the body by local digital processing of incremental attitude from a set of three ring laser gyros. This is done at extremely high digital sampling rates (> 2000 Hz). The angular rate data are then processed at approximately 600 Hz through anti-aliasing filters to remove frequencies above twice the sample frequency. A direct integration of the filtered angular velocity vector, using quaternion algebra, determines the quaternion describing the rigid body attitude with respect to an inertial reference. This data is then transformed into LVLH coordinates using reference information provided by NAV

processing and is then digitally filtered using a low pass, type 0 filter with a breakpoint at 0.45 Hz. ST data are only used to identify and adjust for bias errors in the ISA data Kalman filter which is not used by the ACS. Design requirements on the system output dictate an attitude measurement accuracy of 0.1 deg. with respect to inertial and an attitude rate estimate accuracy of 0.0008 deg/s, (3 σ value). Based on analysis and tests reported at the Space Station Freedom Guidance, Navigation, and Control System Detailed Design Review, it is expected that the ADS will meet these requirements with ample margin [ref. 5-3] and, for the purpose of evaluation of the performance of the ACS in maneuvering the stack in simulation, the ADS could be considered to provide perfect information. A preliminary investigation into the compatibility of the ADS and the ACS in closed-loop operation was conducted as a separate study and reported in ref. 5-4.

5.2 Reaction Control System Controller

An initialization subroutine was called once at the start of the simulation to set all of the parameters listed in appendix F-1. A main subroutine was written to sequence the calling of each of the individual subroutines in the controller and pass the appropriate internal signals and data between them. This subroutine was called by the multibody simulator at the ACS execution frequency of 1 Hz.

The inputs to the complete RCS controller are the quaternion, defining the attitude of the space station core body with respect to LVLH as sensed by the ADS, and the angular velocity of the core body, in inertial space expressed in body (SSSRF) coordinates as sensed by the ADS. The output is the vector of commanded on-times for each of the jets which is updated once during each jet selection period of 33 sec. The input-output structure of the control subroutine is of the form:

$$[t_{on}] = f(q_{ADS}, [\theta_{CMD}], [\omega_{ADS}])$$

where t_{on} is the jet on time, q_{ADS} is the attitude quaternion, θ_{CMD} is the commanded attitude, and ω_{ADS} is the angular velocity. These parameters are the only interfaces between the software inside of the ACS code and the multibody dynamics code and hence, are the only variables which the simulator sees as changing at every time the ACS is called. State variables are stored from one time step to the next in common blocks internal to the control subroutine. For the RCS maneuver to TEA, the mass properties of the stack are assumed not to vary significantly, so that no on-line mass estimation was performed. The gains were scaled from an inertia tensor calculated external to the simulation software from system geometry data alone. A detailed block diagram of the RCS control system is given in figure 5-2.

A perfect ADS was assumed, so the body attitude quaternion and angular velocity were taken from the rigid body attitude and angular velocity computed for the SSF core body at the actual ADS

sensor location in SSSRF coordinates. The jet on-times were updated once during every jet execution period of 33 sec. For each jet which had an on-time greater than zero, an external control force of 25 lb, the maximum jet thrust, was applied at the jet location on the SSF body for the commanded time. A complete listing of the jet locations and directions used in the simulation of the MB-6 mission is summarized in appendix F-2.

The initial attitude of the stack, following grapple by the SRMS arm and locking of the joint brakes, was {Pitch = 180°, Yaw = 0°, Roll = 90°}. This orientation is referred to as the "gravity gradient" attitude. The commanded attitude, which is the estimated TEA of the combined stack was {Pitch = 157.4°, Yaw = -7.4°, Roll = 92.0°} and was given as a step input attitude command.

5.3 Control Moment Gyroscope Controller

The aforementioned changes for the RCS controller in the gain scaling and bending filters were also applied to the CMG controller. Again, a perfect ADS was assumed. Reference frames, attitudes, and Euler angle sequences defined for the RCS controller are also applicable for the CMG controller. Four CMG's, each with a momentum capacity of 3500 ft-lb-sec were used.

An initialization subroutine was called once at the start of the simulation to set all of the parameters listed in Appendix F-3. As in the RCS controller, a main subroutine was written to sequence the calling of each of the individual subroutines and pass the appropriate internal signals between them. It has an execution frequency of 1 Hz.

The inputs to this subroutine are a quaternion giving the attitude of the space station core body with respect to LVLH as sensed by the ADS, the angular velocity of the core body in inertial space expressed in body (SSSRF) coordinates as sensed by the ADS, and the SRMS geometry (end effector position and attitude) to be used to estimate the system mass properties. The output is the commanded inner and outer gimbal rates of the CMG's. Conceptually, the input and output structure of the CMG controller in the simulator can be represented as a subroutine:

$$[\alpha_{CMG}] = f(q_{ADS}, [\theta_{CMD}], [\omega_{ADS}], [RMSDATA])$$

where α_{CMG} is the gimbal rate command, q_{ADS} is the attitude quaternion, θ_{CMD} is the commanded attitude, ω_{ADS} is the angular velocity, and RMSDATA is the end effector position and attitude.

A mass estimator was created to compute the estimated inertia tensor, the principal moments of inertia (eigenvalues), and the transformation from principal axes to body coordinates (eigenvectors) of

the stack at each 1 sec time step. These signals are used to scale the controller gains and to compute a new estimated TEA at each time step.

The second modification was the introduction of a TEA estimator. This section of the controller computes, at each time step, the commanded attitude which represents the alignment of the nearest spacecraft principal axes with the LVLH frame.

A detailed block diagram of the complete CMG controller as realized in the berthing studies, including the TEA estimator is given in figure 5-3.

5.4 Mass Property Estimator

As described above, the mass property estimation algorithm was developed to calculate the composite inertia of the SSF/SRMS/Orbiter stack for use in gain scheduling of the SSF control system. This FORTRAN routine calculates the relative orientation of the Orbiter and SSF masses as a function of the SRMS configuration and applies the parallel axis theorem to find the stack inertia about the combined center of mass. The SRMS configuration is described by the position and attitude of the SRMS POR. In this study, the location of the POR was selected to be at the end effector. The orientation of the payload operating system (whose origin is the POR) was assumed to be aligned with the end effector operating frame as described in Appendix C-7. FORTRAN common blocks are used to pass POR information from the kinematic data generator module of the SRMS command algorithms to the mass property estimation algorithm and to supply the estimated composite inertia to the SSF control system. This procedure assumes the existence of a data transmission link between the station and the Orbiter, i.e., radio frequency communication. The following provides a detailed description of the algorithm.

Inputs to the mass property estimation algorithm are a position vector, **PORPST**, and a transformation matrix, **PORSTR**, which describe the position and orientation of the POR with respect to the Orbiter structural reference frame, respectively. From this point, the position of the SSF Center of Mass (CM) and the orientation of the SSSRF (also referred to herein as the Payload Axis System or PAS) are derived. First, the transformation matrix of the SSSRF to the Orbiter Structural Reference (OSR) frame, **T**, is found:

$$\mathbf{T = PORSTR * PAS2PL}$$

where **PAS2PL** is the known transformation matrix from the Payload Axis System (PAS) to the Payload Operating Frame (PLOP) frame. This transformation matrix is then used to determine the position of the SSF CM in OSR coordinates as follows:

$$\mathbf{CM_{SSF} = PORPST + T * VPASCG - T * VPASOP}$$

where **VPASCG** is the known vector which describes the SSF CM in PAS (equivalent to SSSRF) and **VPASOP** is the known location of the PLOP (or POR) in PAS coordinates as shown in Figure 5-4. Next, the vector between the CM of the Space Shuttle and the CM of the SSF in the OSR coordinates can be found:

$$\mathbf{R = CM_{STS} + CM_{SSF}} = r_1 * \mathbf{i} + r_2 * \mathbf{j} + r_3 * \mathbf{k}$$

where $\mathbf{CM_{STS}}$ is the known CM of the Space Shuttle in OSR (refer to figure 5-5). This vector is then transformed to the SSF reference frame to describe the composite inertia with respect to this frame. Likewise, the Shuttle inertia which is known with respect to OSR, I_{STS}, is also transformed to the SSF reference frame using the following similarity transformation:

$$I_{STS} = T^T * I_{STS} * T$$

Now, the combined body (CB) inertia may be found by applying the parallel axis theorem:

$$I_{CB} = I_{SSF} + I_{STS} + h * \mathbf{RXRX}$$

where h is the defined as

$$h = \frac{m_{SSF} * m_{STS}}{m_{SSF} + m_{STS}}$$

and m_{SSF} and m_{STS} are the mass of the space station and of the space shuttle, respectively.

RXRX is the double vector cross product of **R** defined as:

$$\mathbf{RXRX} = \begin{bmatrix} r_2^2 + r_3^2 & -r_1 r_2 & -r_1 r_3 \\ -r_1 r_2 & r_1^2 r_3^2 & -r_{23} \\ -r_1 r_3 & -r_2 r_3 & r_1^2 + r_2^2 \end{bmatrix}$$

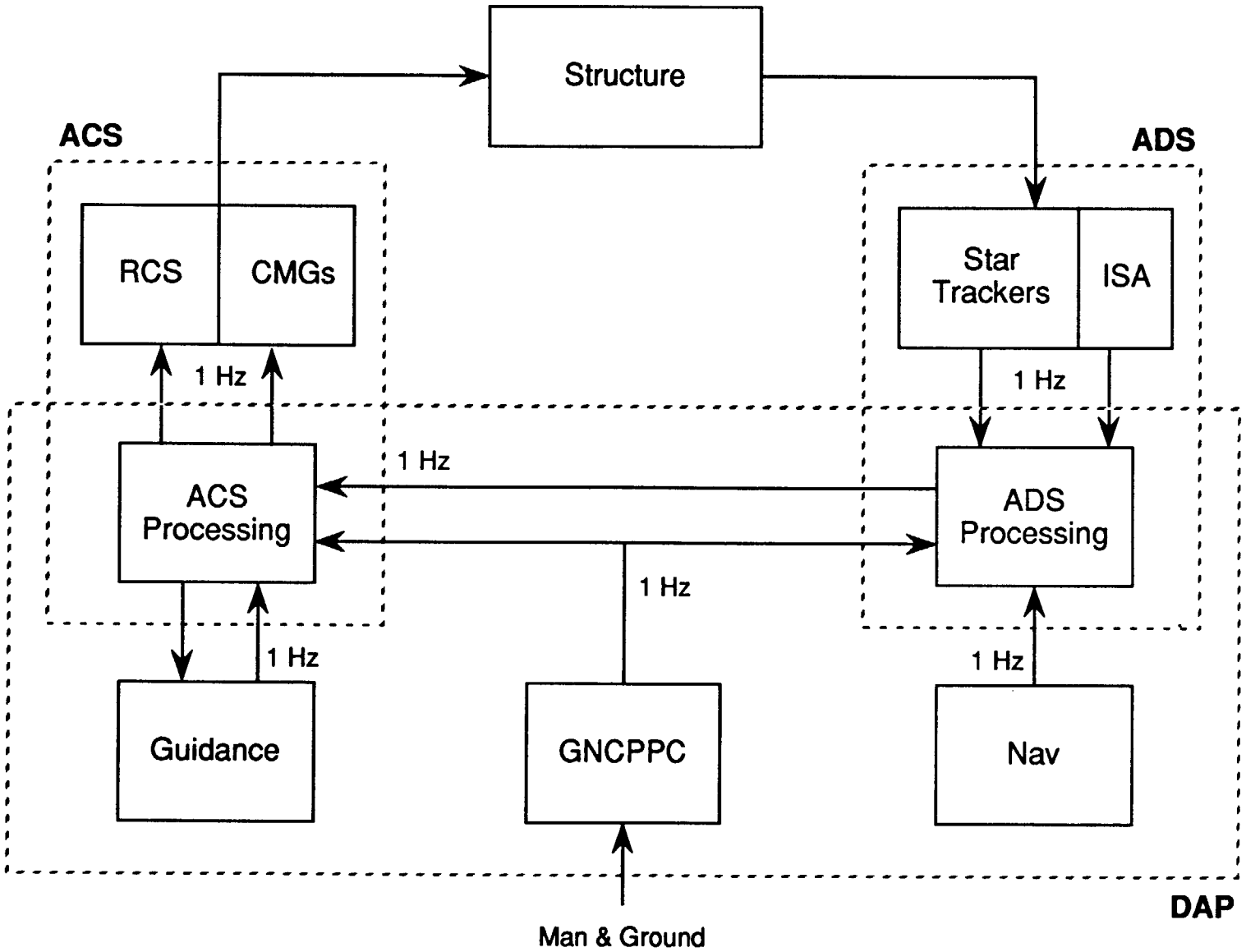

Figure 5.1.- Block diagram of the Attitude Determination and Control System

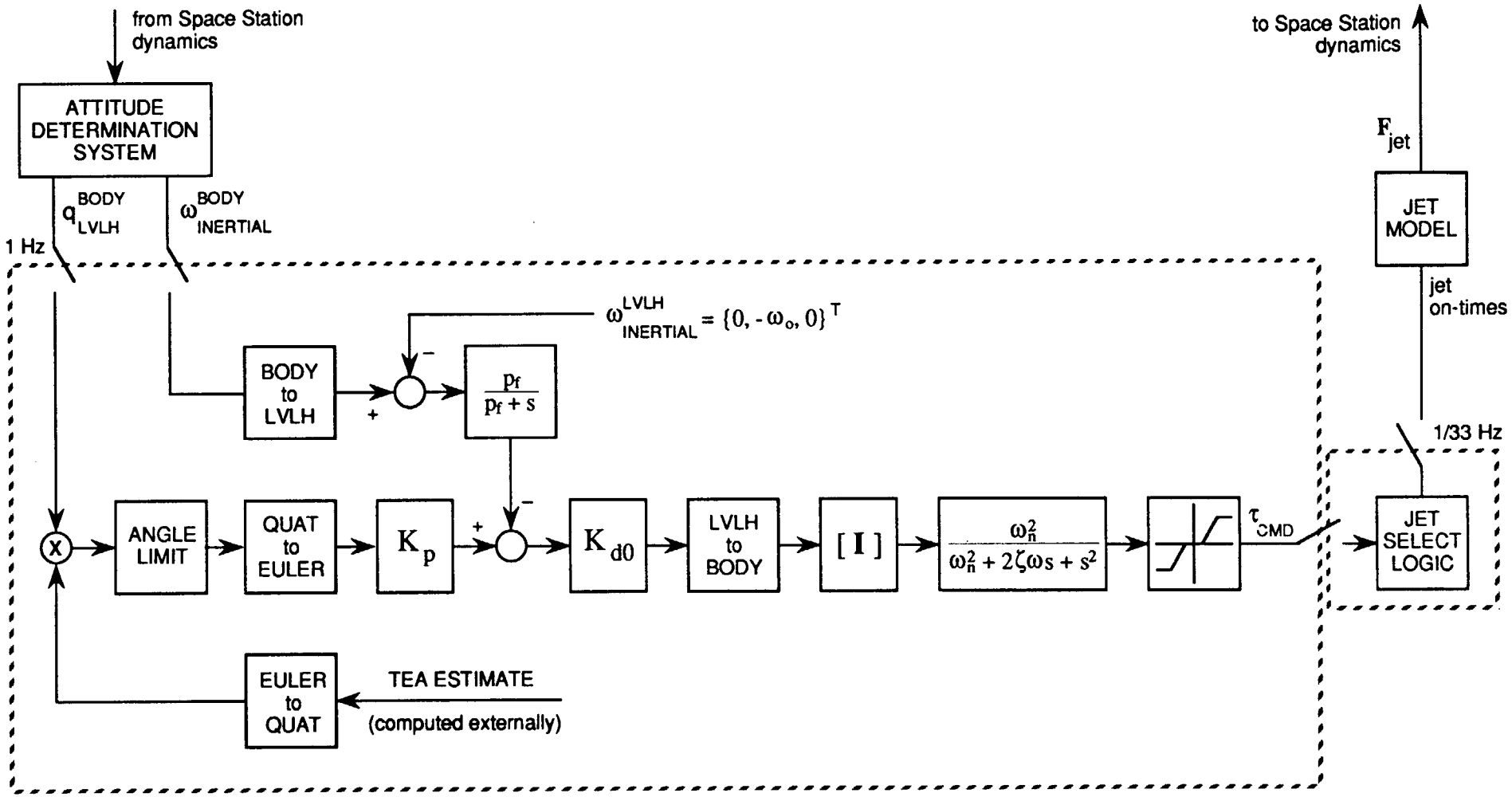

Figure 5-2.- RCS control block diagram

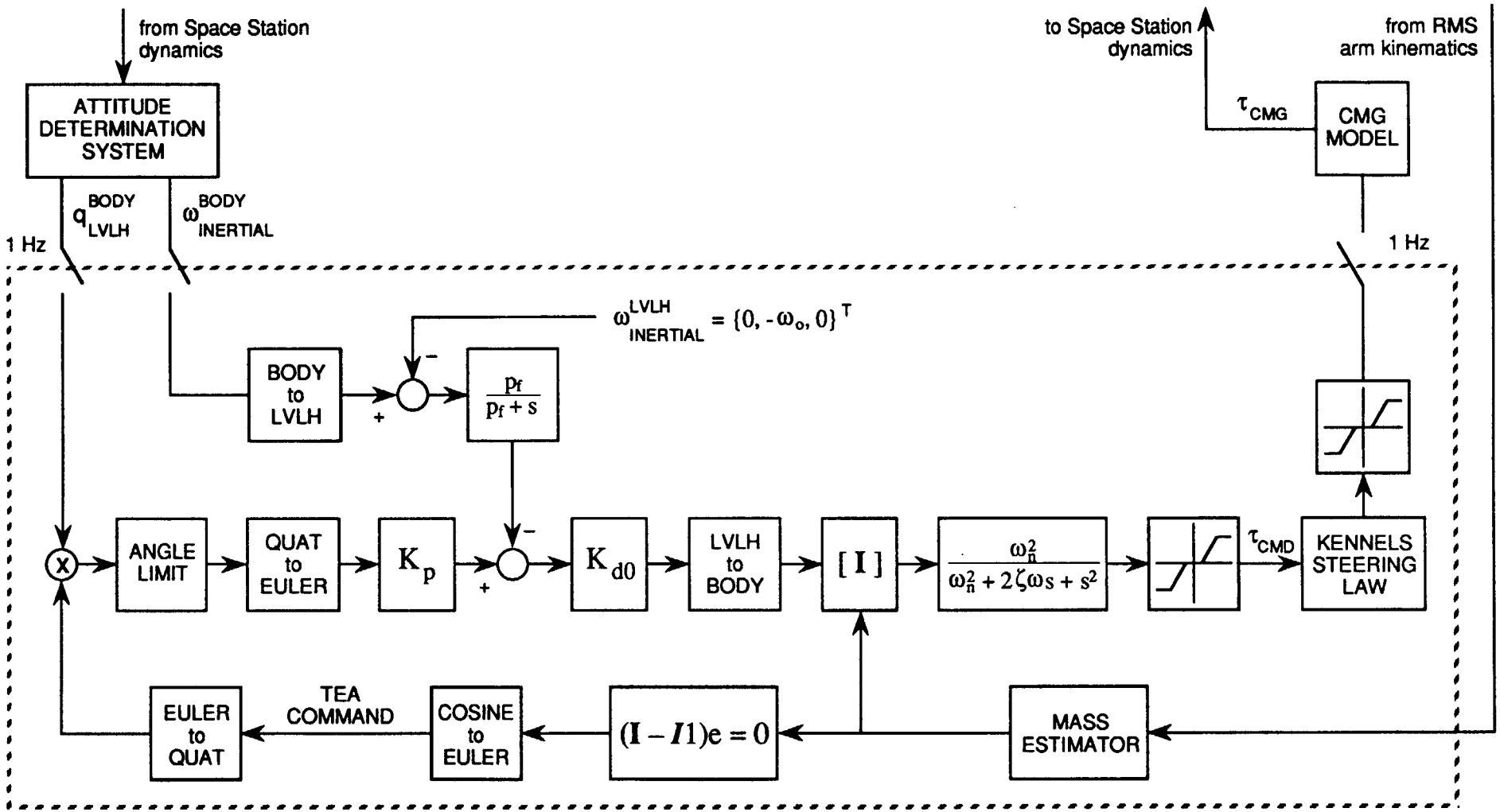

Figure 5-3.- CMG control block diagram

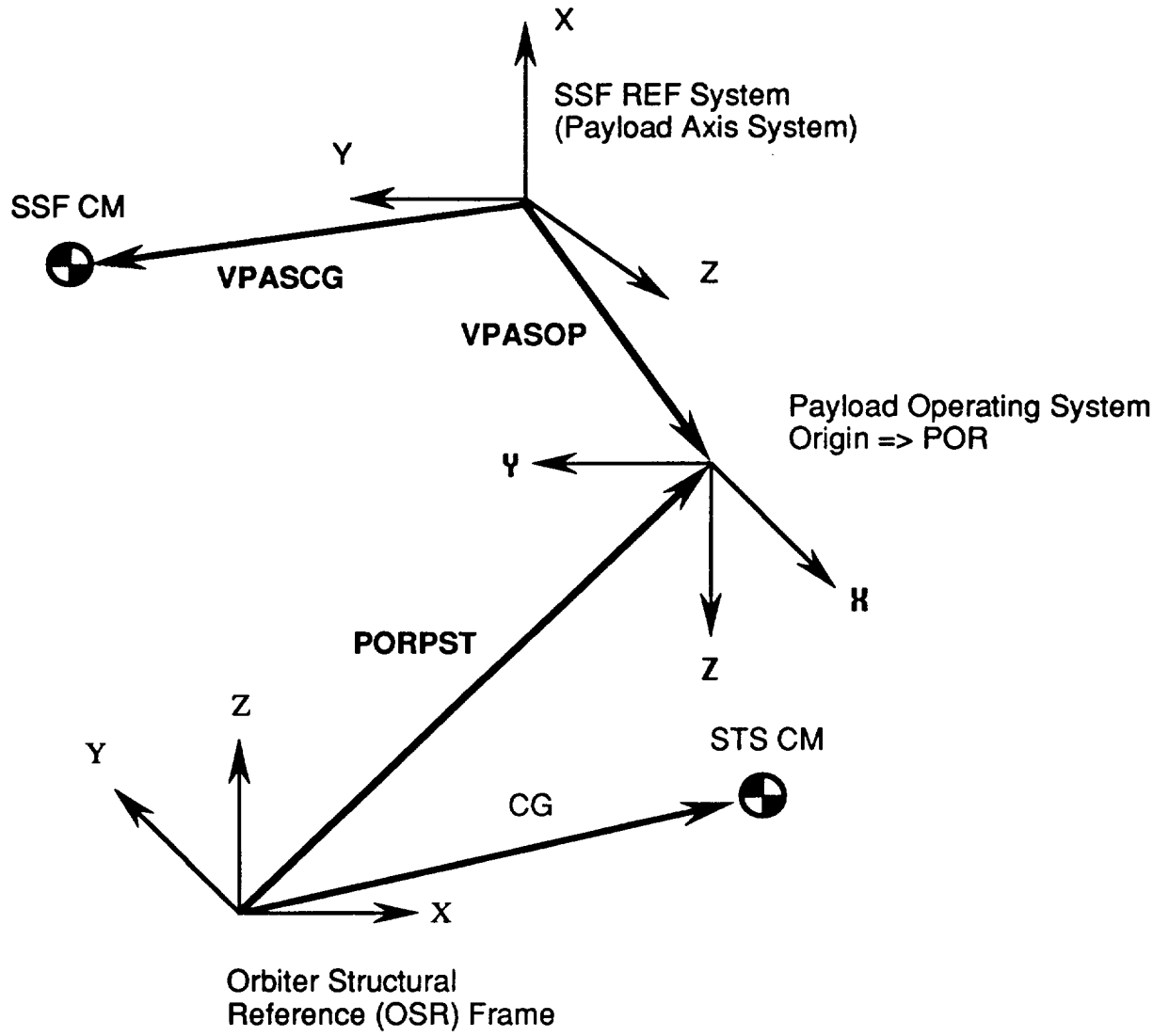

Figure 5-4.- SSF CM location in OSR frame

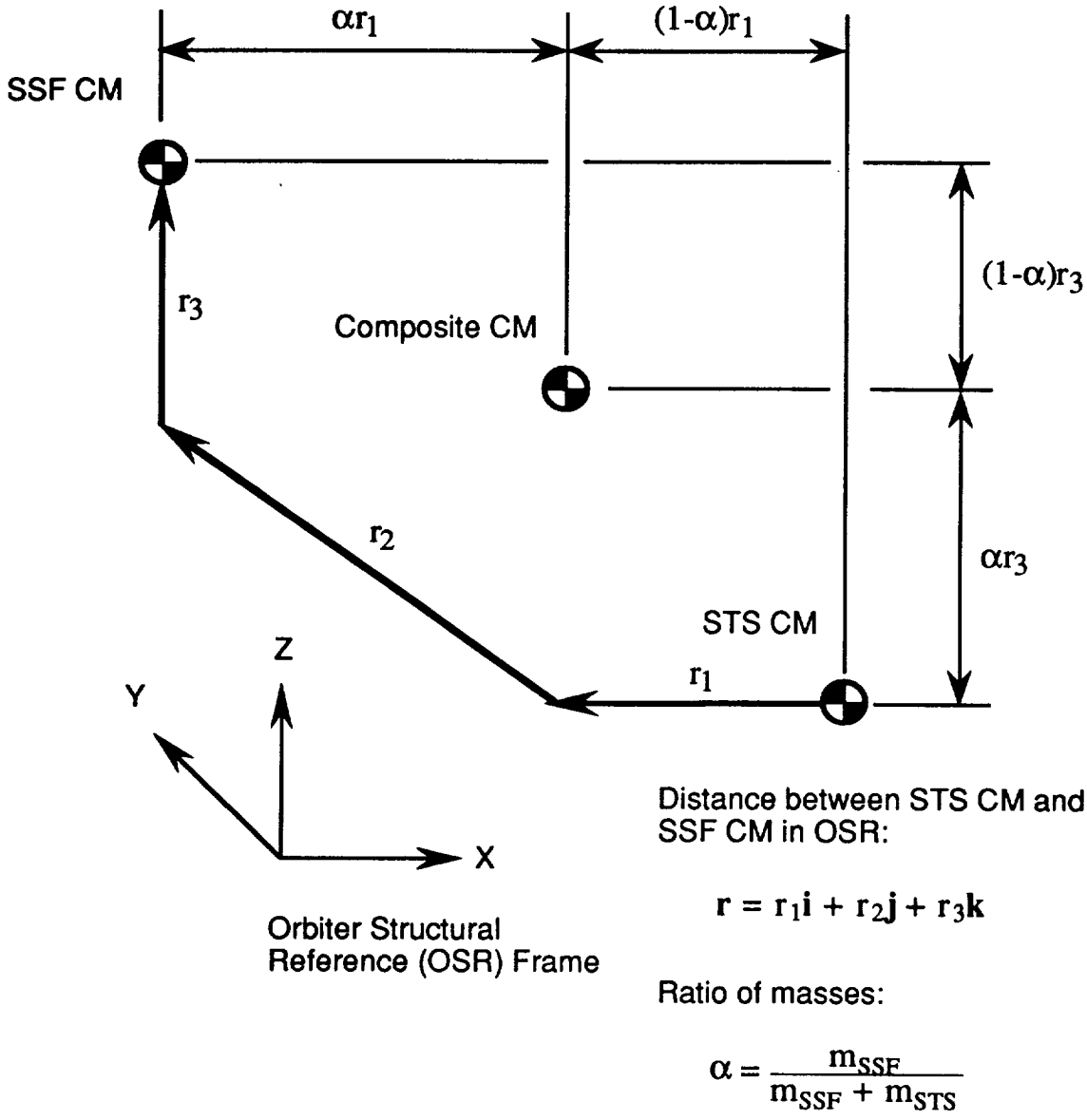

Figure 5-5.- Vector between Orbiter CM and SSF CM in OSR frame

6.0 SIMULATION PROCEDURES

The computational tool for the analysis of SSF assembly dynamics and control is built around a general purpose multibody dynamics code named DADS (Dynamic Analysis and Design System, ref. 6-1). DADS has the capability of modeling both rigid and flexible bodies, as well as detailed control systems. The integration algorithms in DADS are limited to either a single sampling rate or multi-rate systems where the rates are multiples of a single rate. Thus, the integration step size is limited to the greatest common divider of all sampling periods. For the inherently multi-rate assembly simulation, this constraint would result in impractically long computational times. To solve the problem, a modified numerical integration procedure was developed and subsequently established the framework for the assembly dynamics computational tool.

6.1 DADS Model

To set up a DADS model, four essential parts are required. They are: (1) body definition; (2) joint definition; (3) forcing functions; and (4) initial conditions. Each part of the model for the system under investigation is described in the following sections.

6.1.1 Body Definition

Nine bodies are used to model the complete Orbiter/SRMS/SSF system using DADS. They are the Orbiter, the seven links of the SRMS, and the SSF. A multibody representation of the system is shown in figure 6-1. On each body, a body-fixed reference frame located at its center of mass is used to locate and orient the body with respect to the inertial frame. The exact values of the locations and orientations of all the reference frames must be computed to define the system properly. The three components which are modeled as flexible bodies are the lower and upper long booms of the SRMS, and the SSF. Structural deformation of flexible components in DADS is represented by a linear combination of assumed deformation modes. These modes were obtained from the finite element program MSC/NASTRAN (ref. 6-2). Two cantilever modes were used to represent structural flexibility for both link 3 and link 4. Each mode used in link 3 and link 4 is assumed to have a 2.2% of critical proportional modal damping. Thirty-six modes are used for the SSF in the TEA maneuver and 13 modes for the berthing maneuver with an assumed 0.2% of critical modal damping for each mode. The finite element model for the SRMS and SSF are described in detail in section 2.0.

6.1.2 Joint Definition

Joints are used to define geometric constraints between bodies in DADS. Eight joints are defined to connect the nine bodies in the system. Link 1 is connected to the Orbiter by a bracket joint, which models the swing-out joint at the base of the SRMS. Although a bracket joint in DADS does not have any DOF, the use of such a joint makes it easier to prepare the DADS input data. The six joints that connect link 1 through link 7 are single DOF revolute joints. A bracket joint is used to model the connection between link 7 and SSF. Joint angles, required in the simulation, are normally not part of the generalized coordinate vector in DADS. Generalized coordinates normally include the position and orientation of each body in the system. In order to obtain joint angles, a rotational-spring-damper-actuator force element with zero spring constant, zero damping coefficient, and zero actuating force is used for each joint. This scheme forces DADS to compute the joint angle position and rate.

6.1.3 Forcing Functions

All of the control forces and external forces/torques are computed external to DADS. These forces include control torques at six SRMS joints, RCS forces and CMG torques applied to the SSF, and drag forces and gravity gradient torques applied to the center of mass of the system. The latter are resolved into forces and torques and applied to the Orbiter and SSF, respectively. These forces and torques are brought into DADS by the control input element with the user input option. To apply the forces and moments to the correct body, control output elements are used. Control output elements take the scalar values from control input elements, convert them to generalized force form and add them to a generalized force vector.

6.1.4 Initial Conditions

There are a total of 12 rigid body DOF and 40 flexible modal DOF in the defined system. DADS INIT elements are used to define the initial conditions. Only independent generalized coordinates required an initial value and initial rate. All the flexible modal DOF are given an initial value of zero. The twelve rigid body DOF, chosen as independent generalized coordinates, are the six joint angles, and positions and orientation of SSF.

6.2 Basic Structure of the Computational Tool

Figure 6-2 shows the basic structure of the computational tool that was developed at NASA Langley. The tool consists of four major parts; the multibody dynamics code DADS, the SRMS controller, the ACS of SSF and the MAIN program. The DADS code is used to generate equations of motion of the system, including the SRMS arm, the Orbiter, and the station. The SRMS controller is comprised of SRMS maneuver command logic and individual joint servo models which generate the respective joint driving torques. The ACS computes RCS forces and/or CMG torques to control the SSF attitude. Note that all three modules described above have their own integration routines and integrate their state equations at their own integration step sizes. In order to synchronize the simulation process of different sampling rates, a MAIN routine was built to control the timing and program execution flow.

Several unrelated sampling rates were used in the coupled SSF/SRMS/Shuttle system. Some of them are listed below to illustrate the scheme used in the timing control in the MAIN program.

Sampling rate of SRMS servo system	0.001 sec
Sampling rate of Digital Tachometer	0.00875 sec
Sampling rate of General Purpose Computer	0.080 sec
Sampling rate of ACS	1.0 sec

Since the greatest common divider of the above sampling rate is 0.00025 sec, defined as a 'tic', the main loop in the MAIN program is executed at this rate. Therefore, the servo system will be called every 0.001/0.00025 = 4 tics, the Digital Tachometer will be called every 0.00875/0.00025 = 35 tics, and the GPC will be called every 320 tics.

Several routines in DADS were modified to accommodate this multi-sampling rate simulation capability. Figure 6-3 shows the original DADS execution flow and the new execution flow. Instead of calling the initial set-up routine from DADS_MAIN, the new approach calls it from MAIN to set up the mathematic model, which includes reading in the input data and setting up pointers for dynamic arrays. A change is made at the end of the initial set-up routines to make sure the program flow will return back to the MAIN routine. After the first call, the MAIN routine calls DADS' dynamic analysis routine from its own integrator directly. The integrator uses a third order Adams-Bashforth algorithm. The modified system allows the selection of all the DADS generalized coordinates to be integrated, or one can select only independent generalized coordinates to be integrated.

The main purpose for calling the dynamic analysis routine is to compute the acceleration vector of the system generalized coordinates for the current time step with the known generalized coordinates and its time derivatives. A detailed algorithm of the dynamic analysis solution scheme is shown in

figure 6-4. Note that the generalized coordinates from the integrator may not satisfy all the nonlinear constraint equations. A Newton-Raphson method is used to correct the dependent generalized coordinates so that the nonlinear constraint equations are not violated. After the correct generalized coordinates are obtained, the velocity equation is used to compute dependent generalized velocities. The generalized coordinates and velocities are then used to form the equations of motion of the system which are solved for the acceleration vector. The velocity and acceleration vectors of the current time step are integrated for the position and velocity vectors of the next time step.

6.3 Detailed Architecture of Simulation Tool

Figure 1-10 shows the detailed architecture of the computational tool. For the SRMS controller, joint angles and rates from the multibody dynamics code DADS, along with operator command inputs, are fed into the SRMS command algorithm to compute joint rate commands. The SRMS servo model calculates driving torques, based on the joint rate commands. The torques are then applied back to DADS through control elements. For the ACS, the DADS code provides the attitude and attitude rate of the SSF to the ACS. Along with the commanded attitude, the ACS computes attitude errors and rate errors that are used to compute commanded torques that, theoretically, have to be applied to the system. At the same time, the mass property estimator is used to estimate the inertia of the composite system. The estimated information is used to compute proper gain scheduling in the ACS. Depending on the type of actuator used, the commanded torques are converted to either RCS forces or to CMG torques which are fed back to DADS using control elements. The environmental disturbances from aerodynamics moments and gravity gradient torques are applied to the system through control elements.

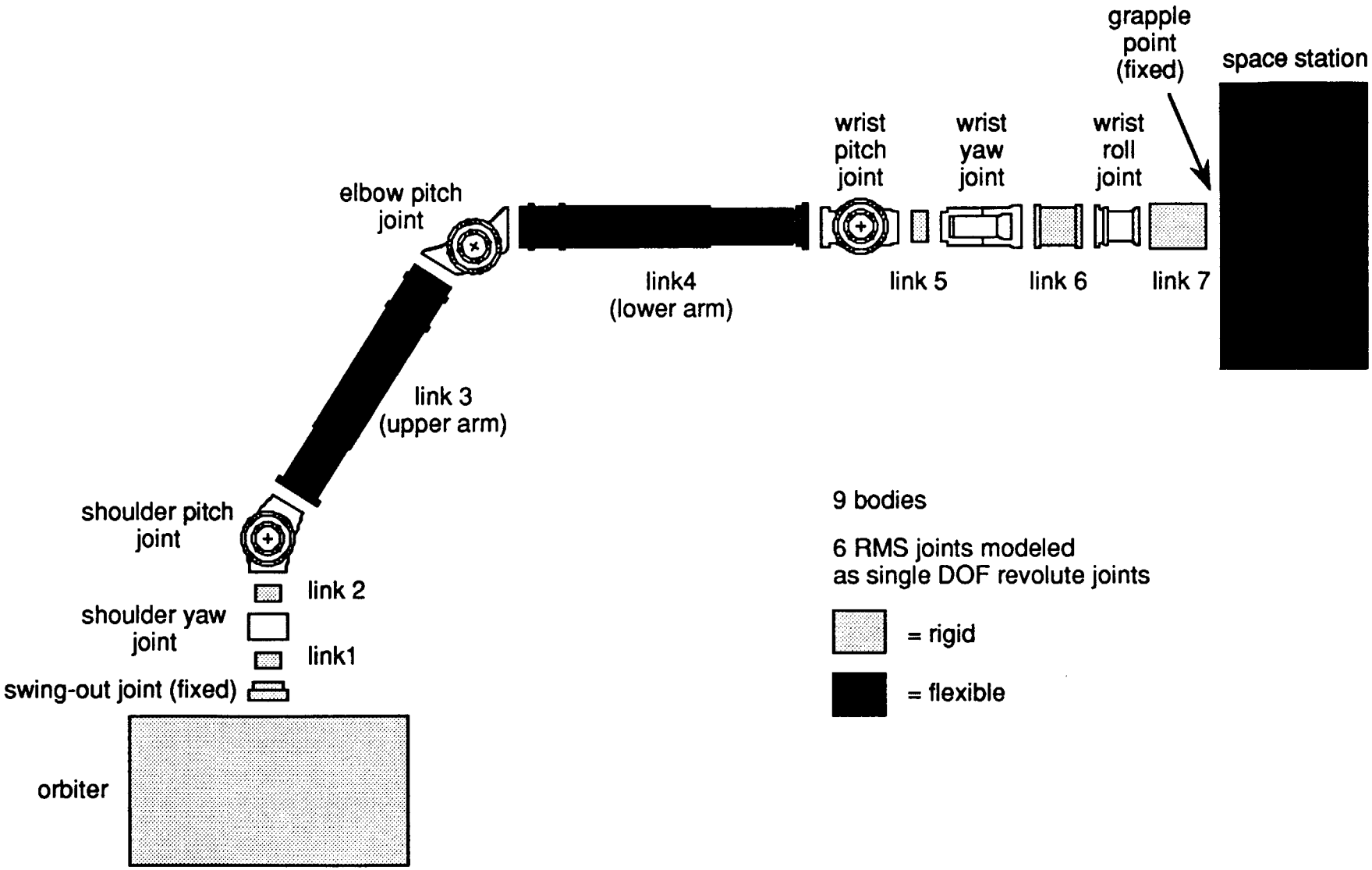

Figure 6-1.- DADS body definition

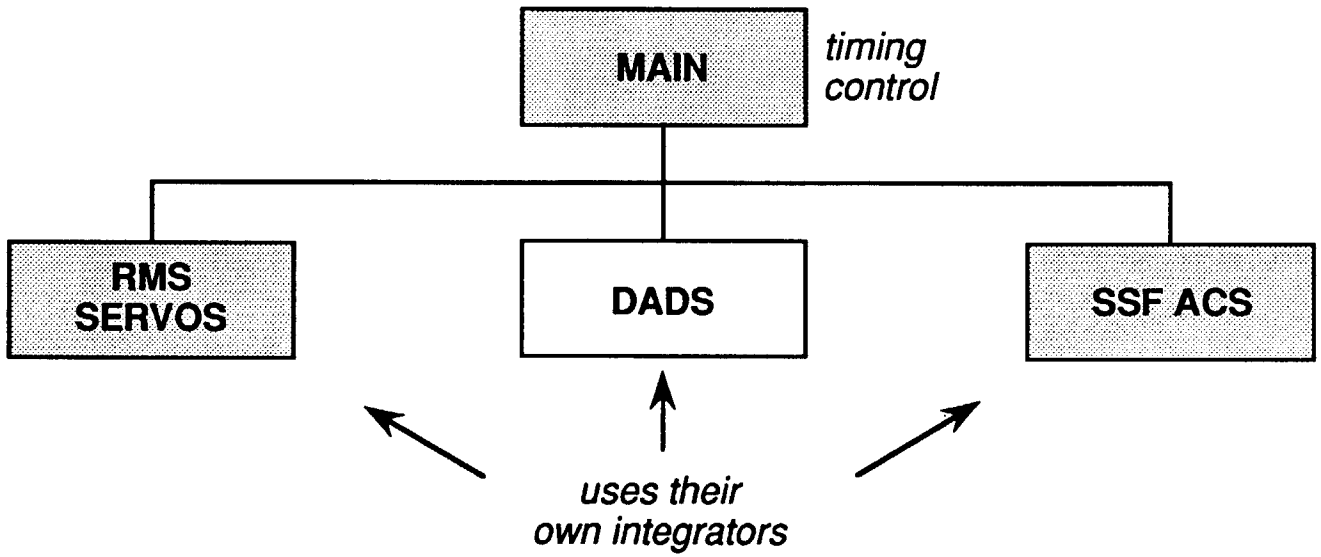

Figure 6-2.- Basic structure of the computational tool

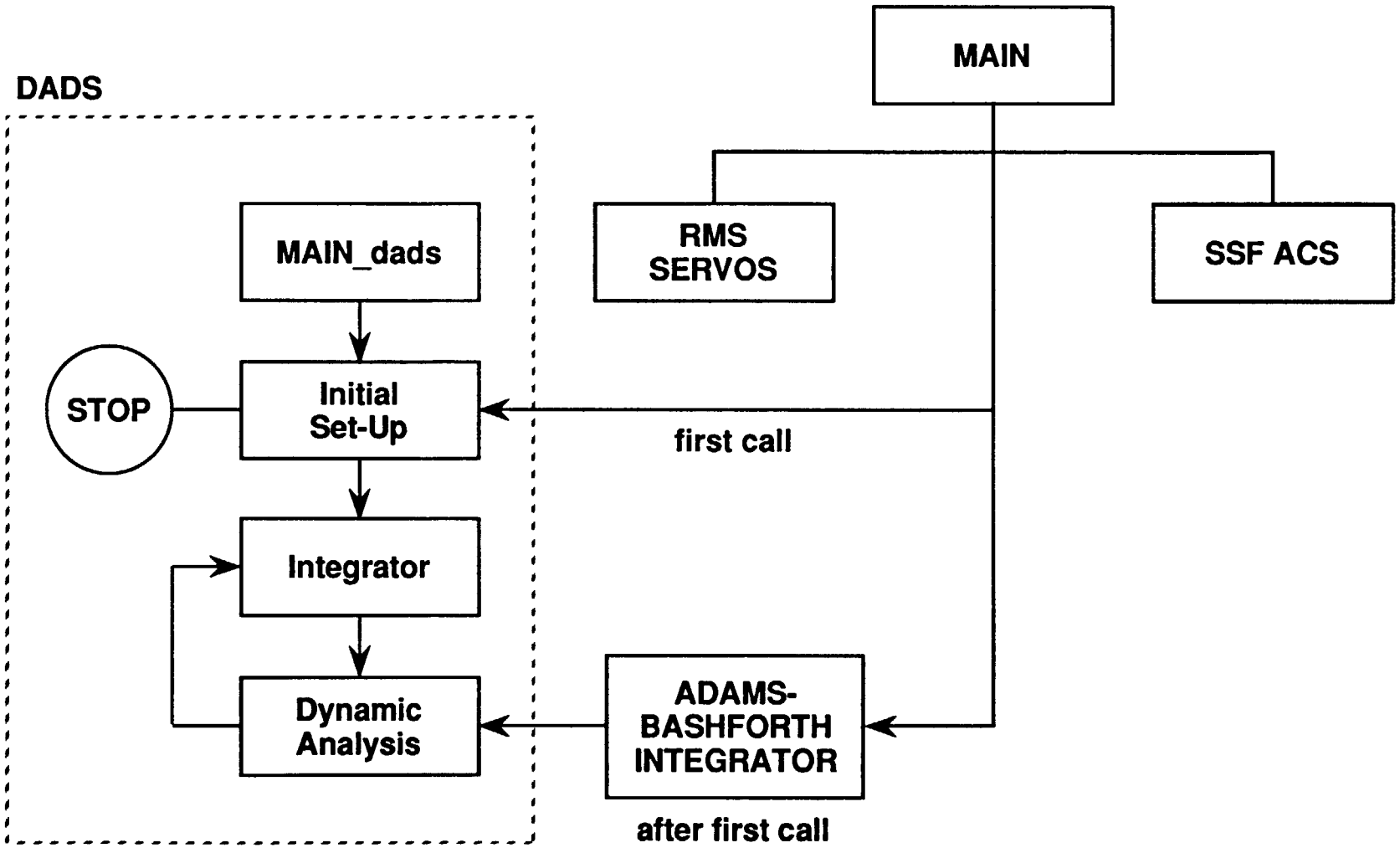

Figure 6-3.- New DADS execution flow

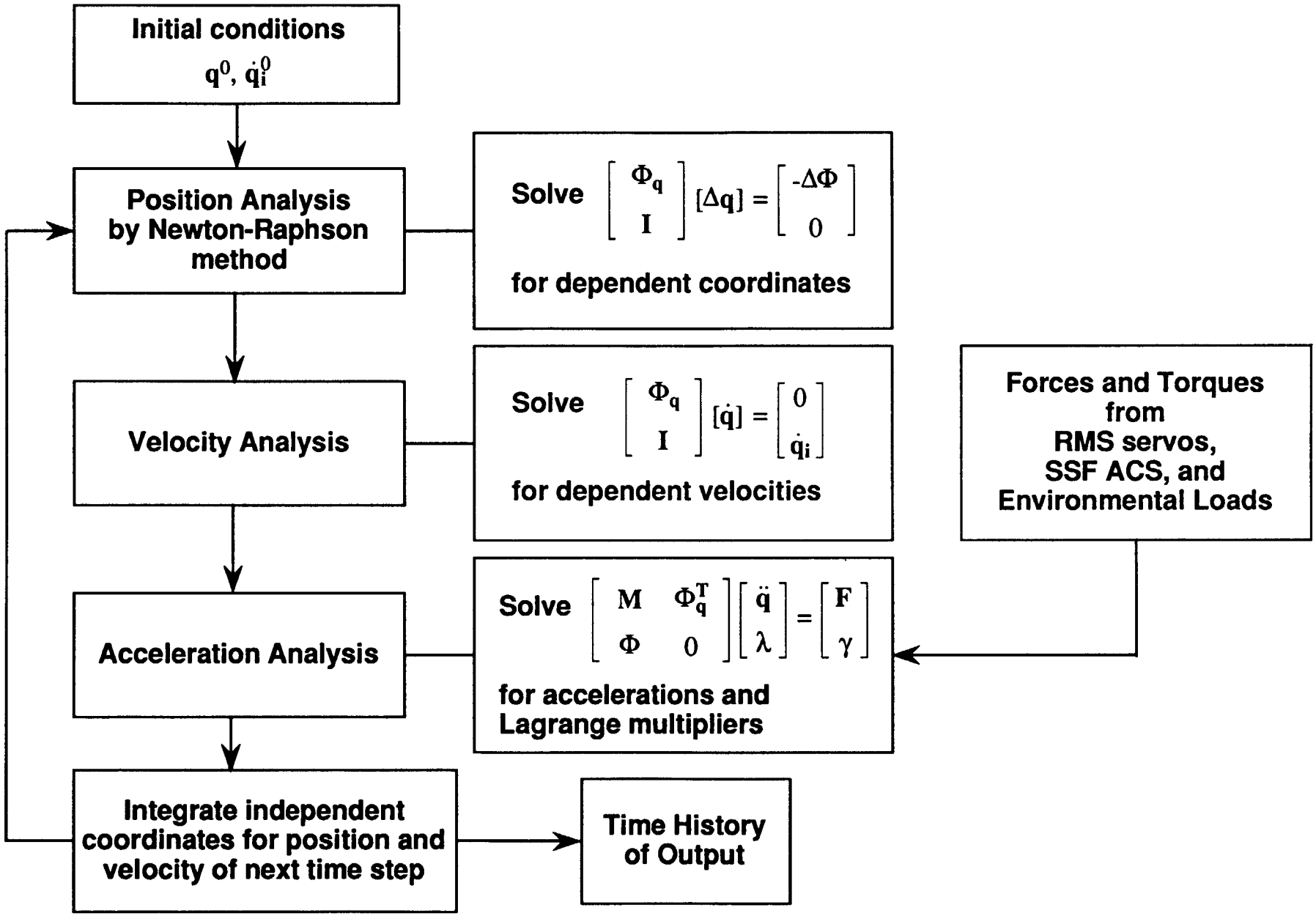

Figure 6-4.- Algorithm of dynamic analysis

7.0 RESULTS OF TORQUE EQUILIBRIUM ATTITUDE MANEUVER

The TEA maneuver consisted of an attitude change, expressed as a pitch-yaw-roll Euler sequence describing the relative orientation of the SSSRF with respect to LVLH, to 157.9°, -7.4°, 93°. Results of the simulation are presented in figures 7-1 through 7-38. Time histories of parameters are plotted for 2500 seconds. The TEA of the stack was successfully established within 1200 seconds, and for the remaining simulation time, the RCS system performs a station hold maneuver. The time integration was calculated using a time step of 0.001 seconds and the computations took approximately 72 hours of dedicated Central Processing Unit (CPU) time on a Silicon Graphics Incorporated (SGI) 4D/440 workstation.

The resulting attitude-time history is plotted in figures 7-1 through 7-3. The attitude and attitude-rate errors input to the controller are shown in figures 7-4 through 7-9 and the commanded torques delivered from the controller are plotted in figures 7-10 through 7-12. An approximation to the commanded torques is realized through the jet selection logic by the selection of jet firings and firing times. The resulting jet firings are plotted in figures 7-13 through 7-15. The occasional firings after the first 1000 seconds provide station keeping.

The RCS commanded torque is realized through the jet selection logic as firing pulses of between approximately 0.2 and 2 seconds in duration. The jet firing times, i.e., the total time that the jets were firing during the simulation time, were compared for the simulation with flexible components (SRMS and SSF) and a corresponding simulation where all components were assumed to be rigid. The firing time was 3 percent greater for the simulation with a flexible SSF and SRMS. This amounted to an increase of about four seconds of firing during the 2500-second simulation. When the bending filter in the SSF control system (with a breakpoint of 140 x orbit rate) was removed for the simulation with flexible components, the amount of firing time only increased by an additional two seconds. Thus, the flexible modes of the SRMS and the SSF were found to have very little influence on the RCS attitude control system.

Figures 7-16 through 7-21 show the time history of application of forces and moments on the SRMS at the grapple point. A force of no greater than 45 lbs and a moment no greater than 440 ft-lbs were applied during the jet firings. With the brakes on at each of the six joints, the servo torques required to resist the force application are plotted in figures 7-22 through 7-27. The SRMS brakes on the two wrist joints were overloaded when the jets were fired, and the joints exhibited a small amount of brake slip during the first 750 seconds of the simulation. This slip is indicated by the non-zero motor shaft rates for the wrist pitch and roll joints as shown in figures 7-28 and 7-29. A time history of the angular motion at each joint is given in figures 7-30 through 7-35. All joint angles, with the exception

of the wrist pitch and the wrist roll joints, had a total change of angle after completion of the maneuver of less than 0.01°. Even the joints which slipped showed a total change of angle of less than 0.1°. The small angle changes which occur in the joints during the jet firings are caused by the elastic response of the joint drive-train and by the elastic response of the long SRMS booms.

Figures 7-36 through 7-38 are plots of the variation in POR position during the maneuver. The largest change in position of the POR, occurring during the jet firings, was less than one inch and the resultant slip after the jet firings were completed was less than 0.2 inches. The POR magnitude change plotted during the jet firings is a combination of brake slip, motion due to arm flexibility, and motion due to joint flexibility in the six joint drive-trains.

Selected displacements and element forces were calculated to evaluate the effect of the control forces on the SSF structure during the TEA simulation. As an example, the motion of the tip of a PV array during the simulation is plotted in figure 7-39. The RCS control system inhibits the jets from firing more than once every 33 seconds to reduce structural dynamic response of the station. However, this frequency is close to the natural response frequency of the stack and a build-up of motion does occur during the first 500 seconds of the simulation. Results show the displacement of the PV tip increases to 2.8 inches. This is a minor displacement considering that the PV array is over 100 feet long. The maximum bending moment at the base of the PV array mast was 5200 in-lb and the maximum transverse shear force was 5 lb. Both values are well below the design capabilities of the mast (ref. 1-3), and no excessive structural loads were computed at the other locations inspected.

Data recovery was performed for the TEA simulation by running an open-loop transient analysis using the MSC/NASTRAN finite element model. Force-time histories were extracted from the DADS simulation and applied as open-loop disturbances at the RCS jet and grapple fixture locations. Element forces were calculated for selected components, and the results, listed in table 7-1, indicate that the structural loads on the SC5 SSF are well below the limit loads calculated by MDSSC for the PDR Loads Data Book. PV array tip displacements were also recovered and are listed in table 7-2. Modal damping of 0.2% of critical damping was assumed for all structural modes.

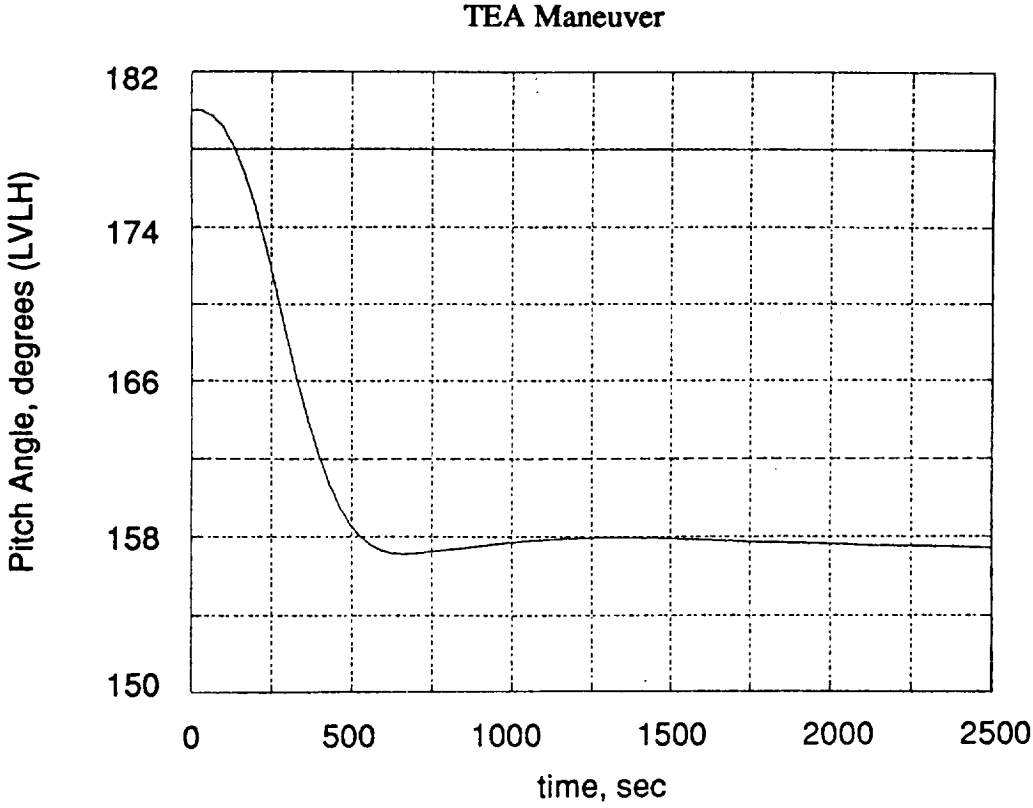

Figure 7-1.- Pitch Angle, SSF.

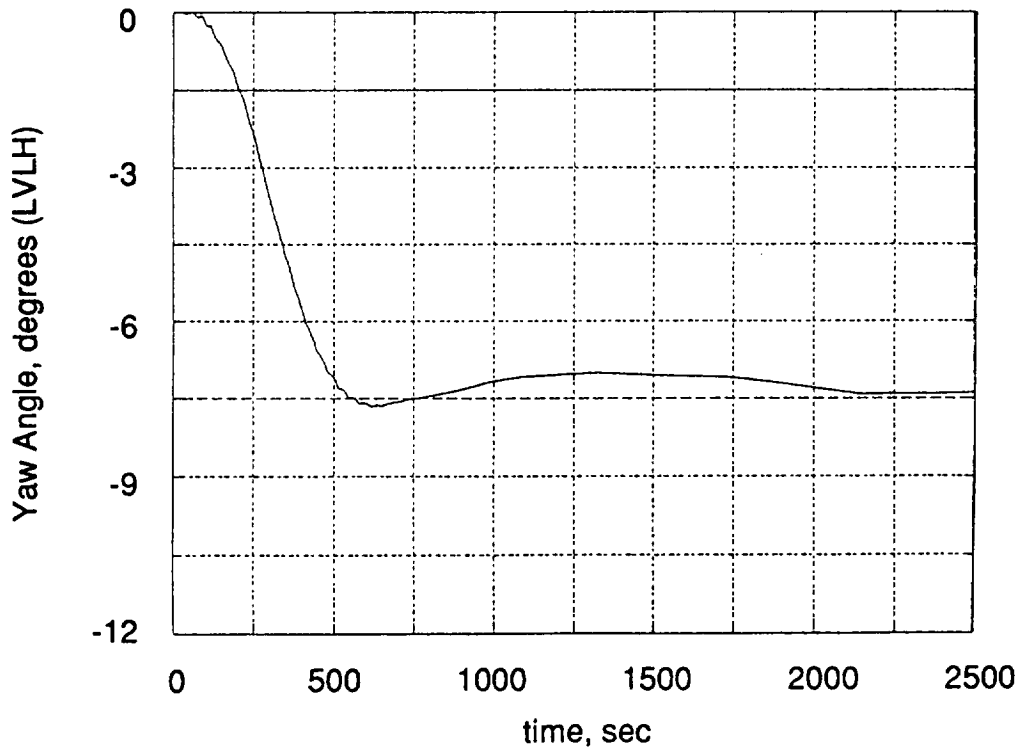

Figure 7-2.- Yaw Angle, SSF.

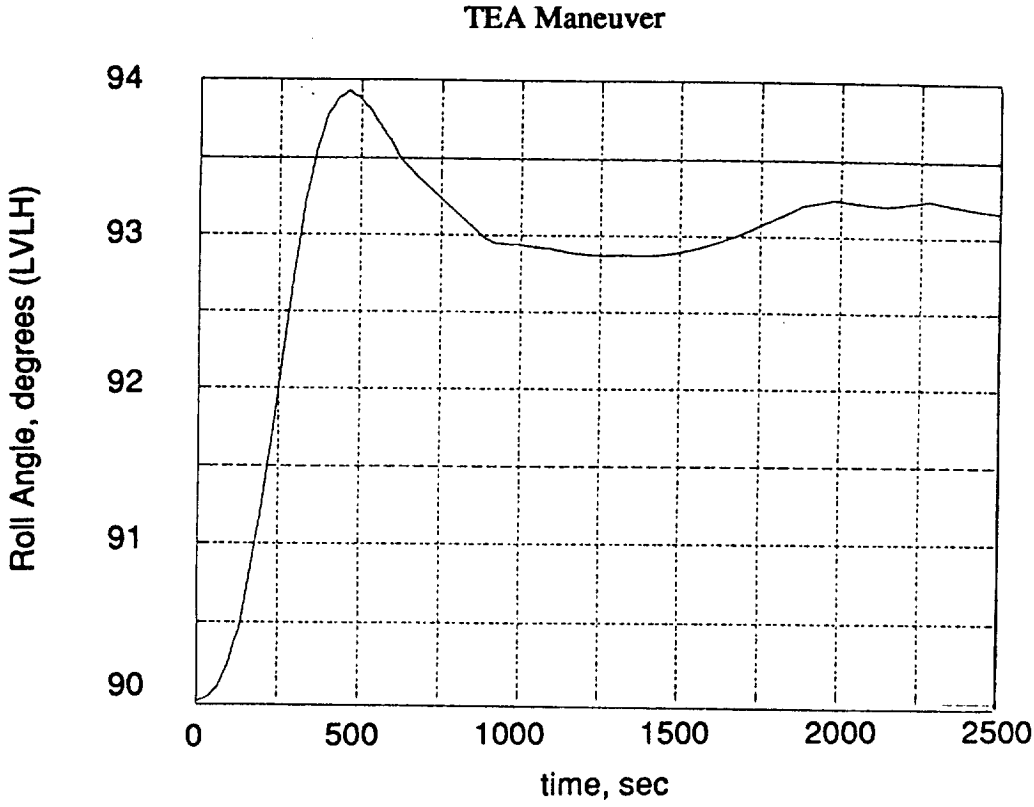

Figure 7-3.- Roll angle, SSF.

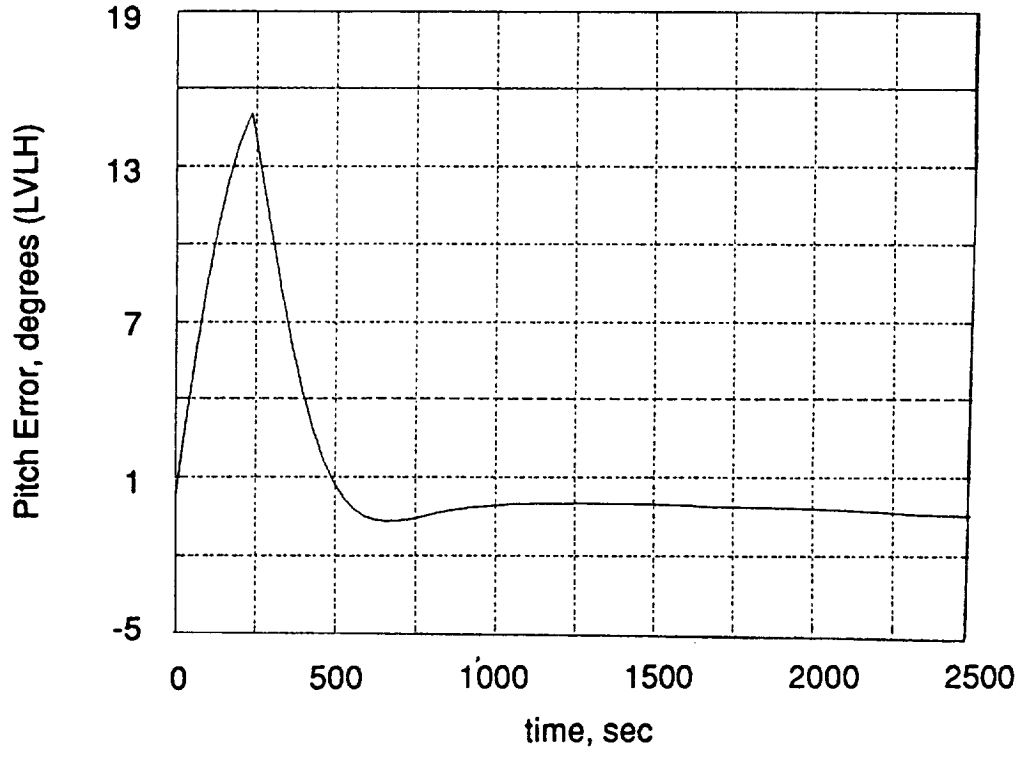

Figure 7-4.- Pitch error, SSF.

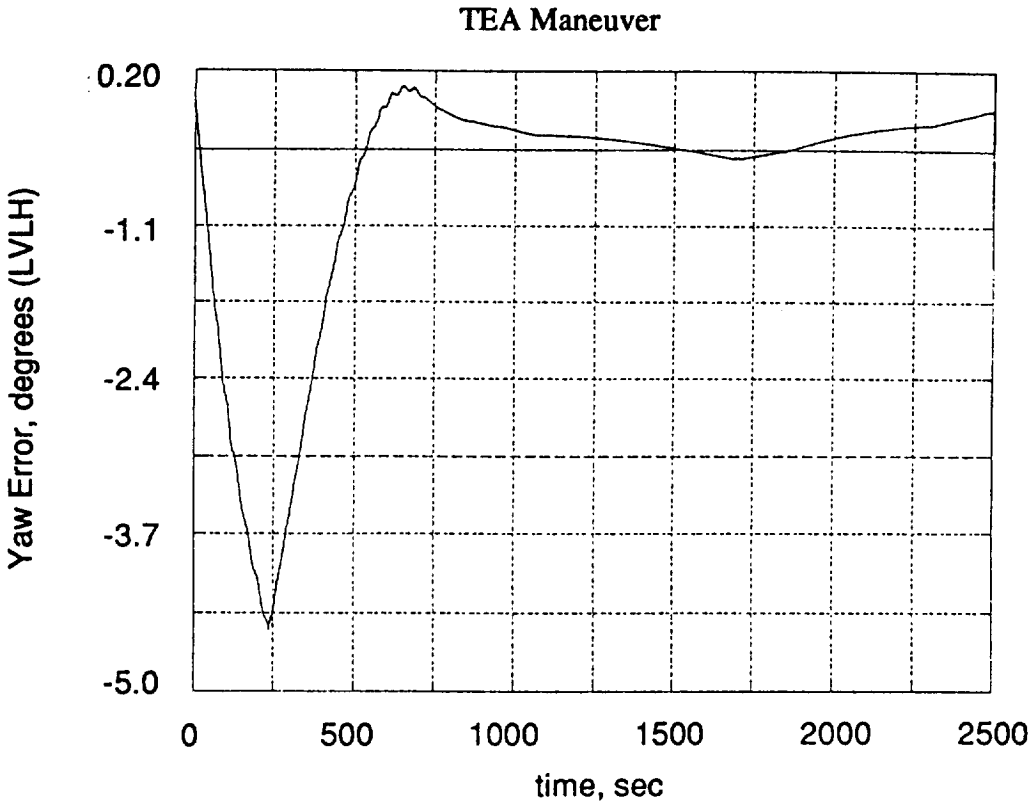

Figure 7-5.- Yaw error, SSF.

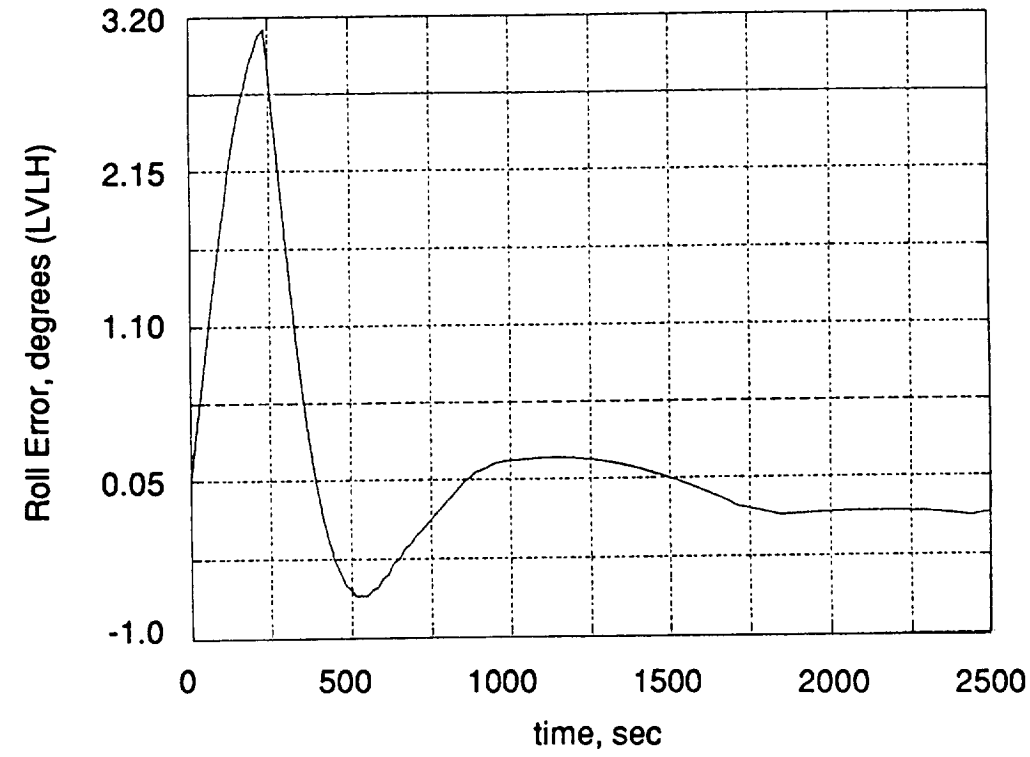

Figure 7-6.- Roll error, SSF.

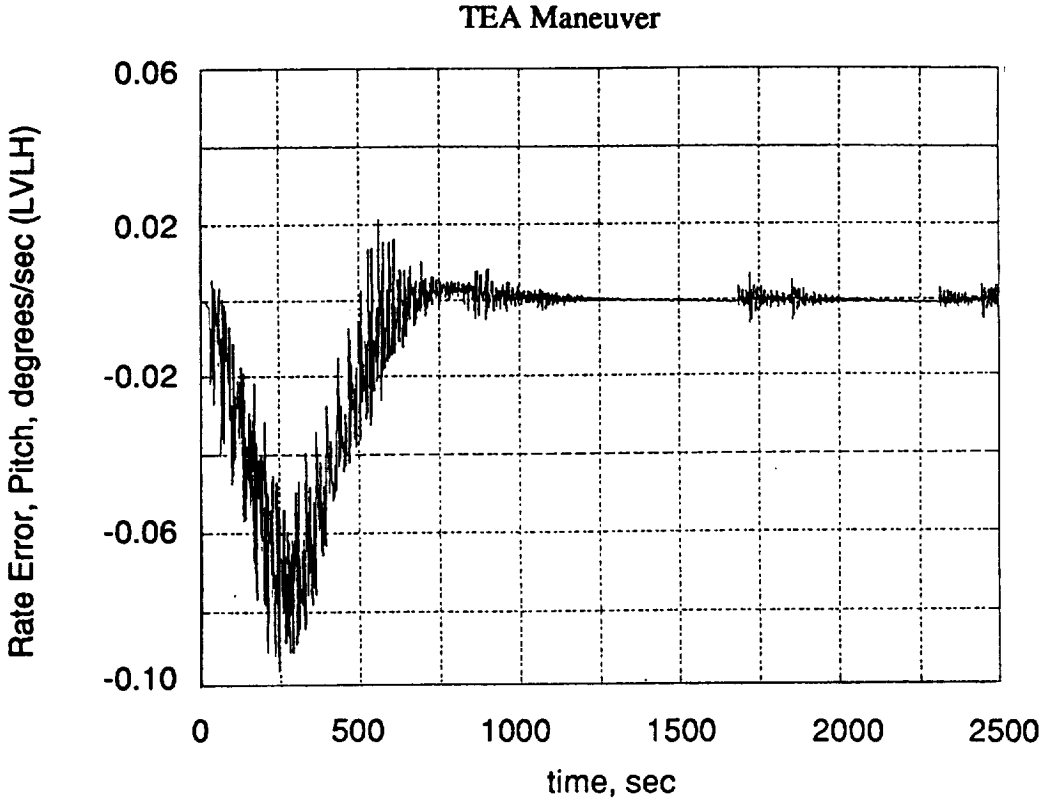

Figure 7-7.- Rate error, pitch, SSF.

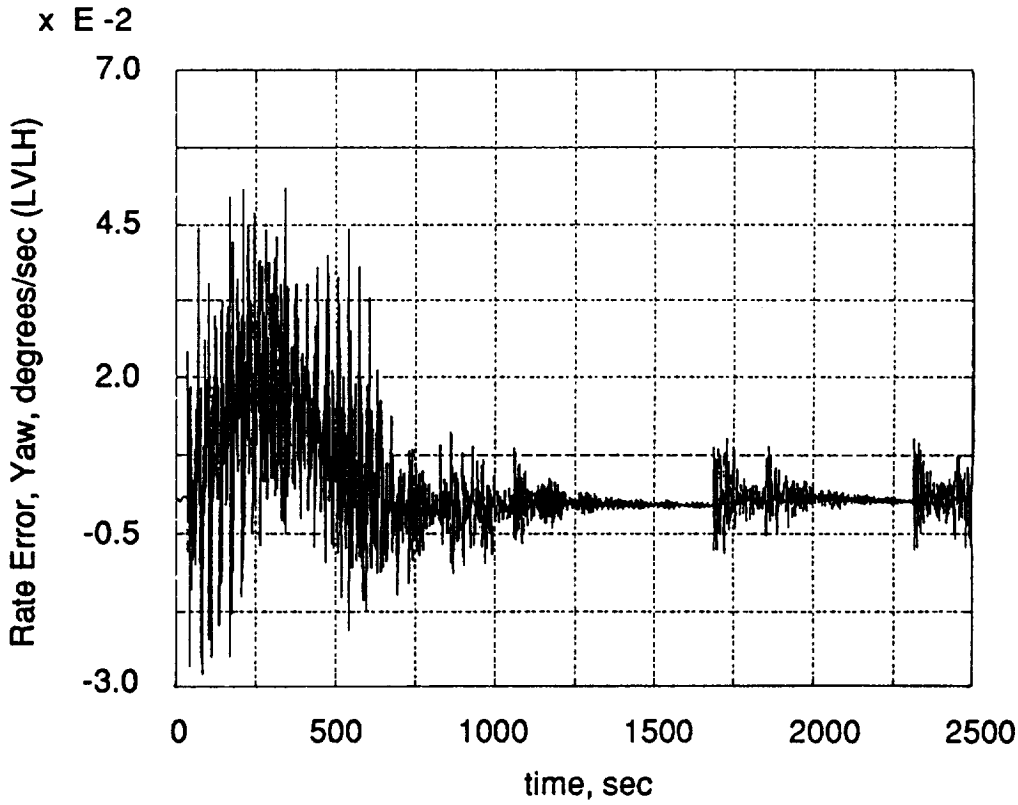

Figure 7-8.- Rate error, yaw, SSF.

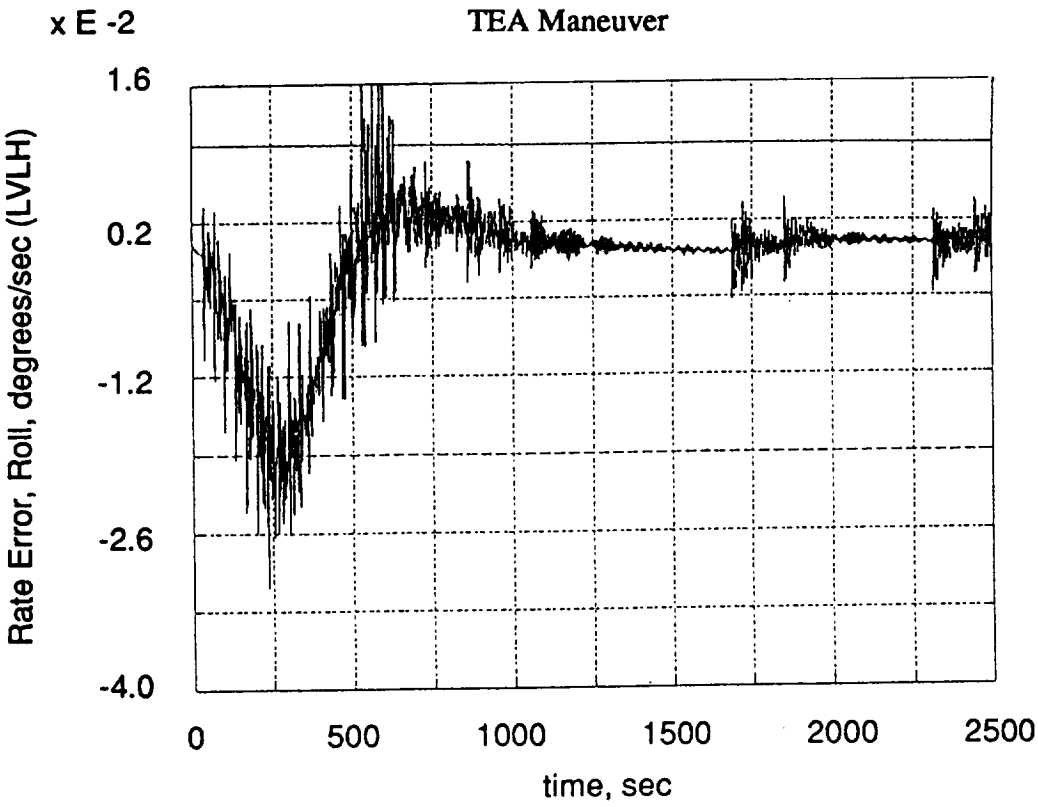

Figure 7-9.- Rate error, roll, SSF.

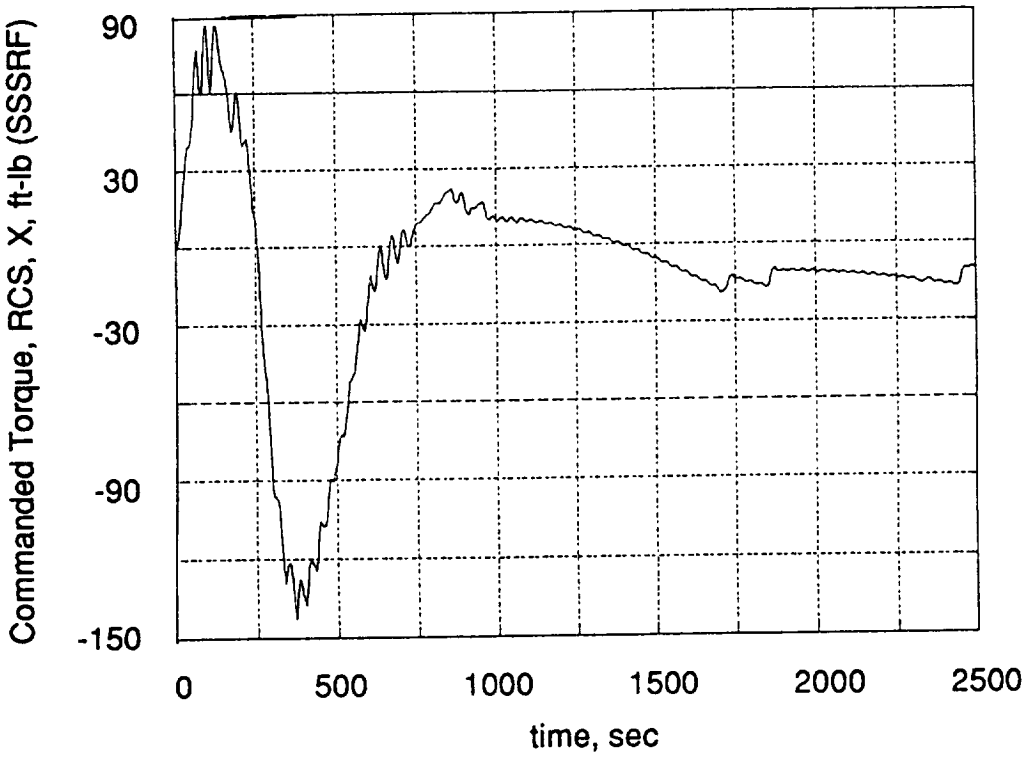

Figure 7-10.- Commanded torque, RCS, x.

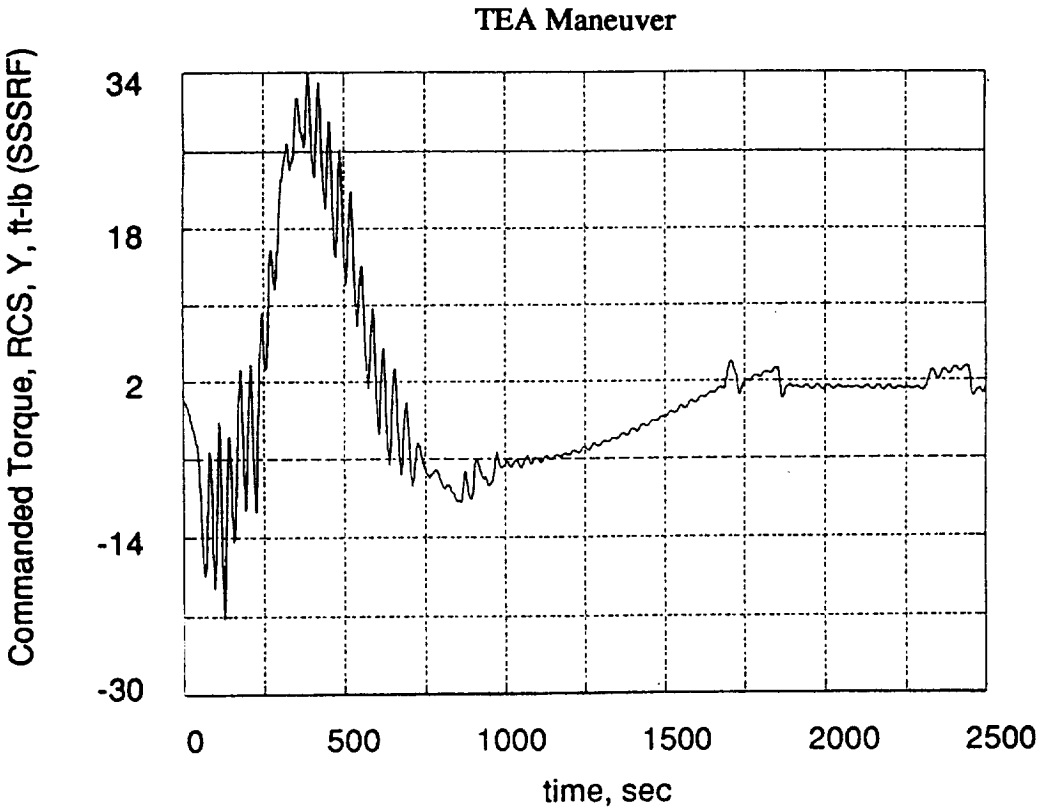

Figure 7-11.- Commanded torque, RCS, y.

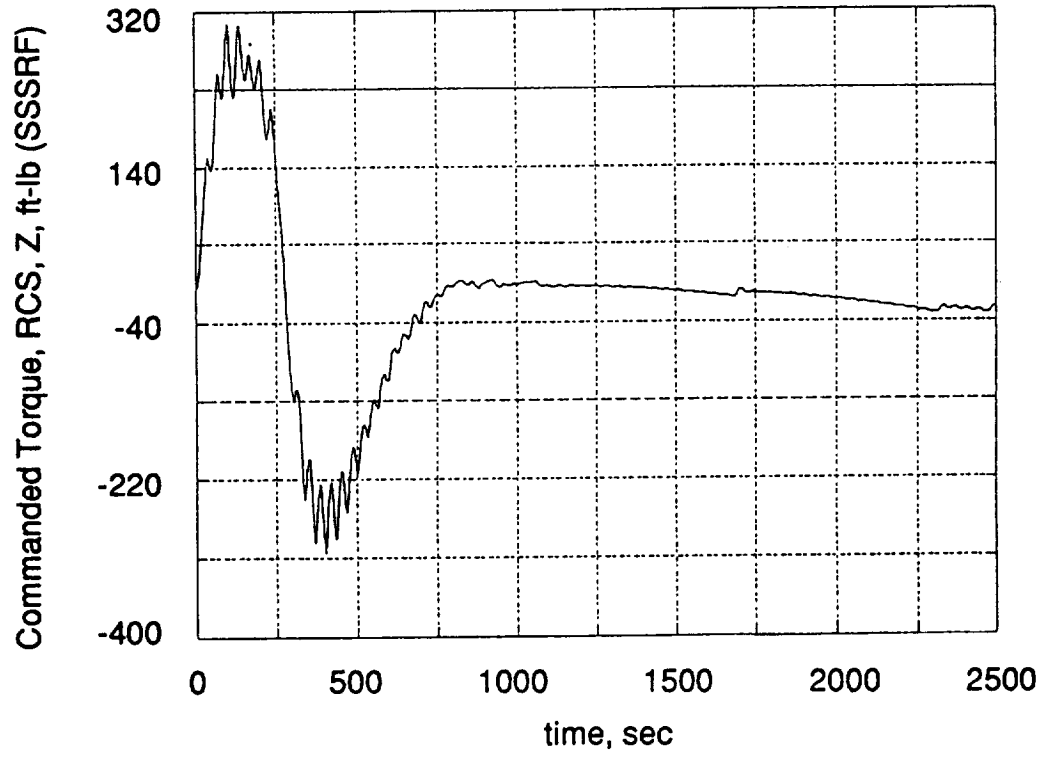

Figure 7-12.- Commanded torque, RCS, z.

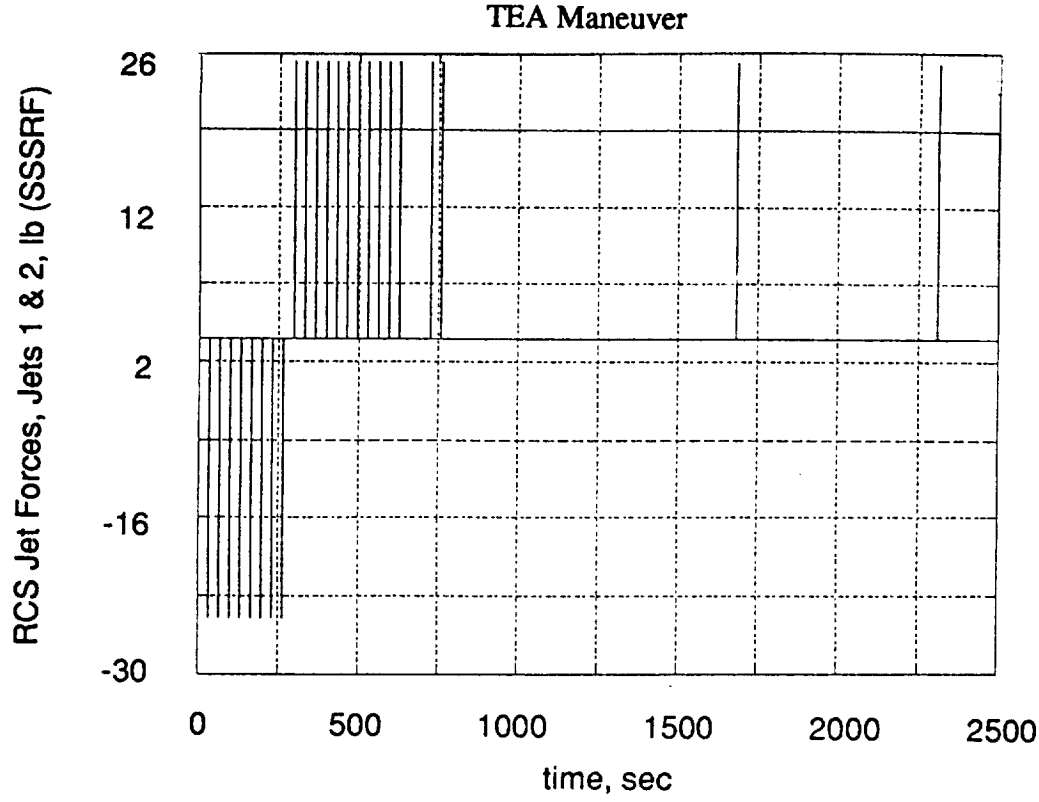

Figure 7-13.- RCS Jet Forces, Jets 1 & 2.

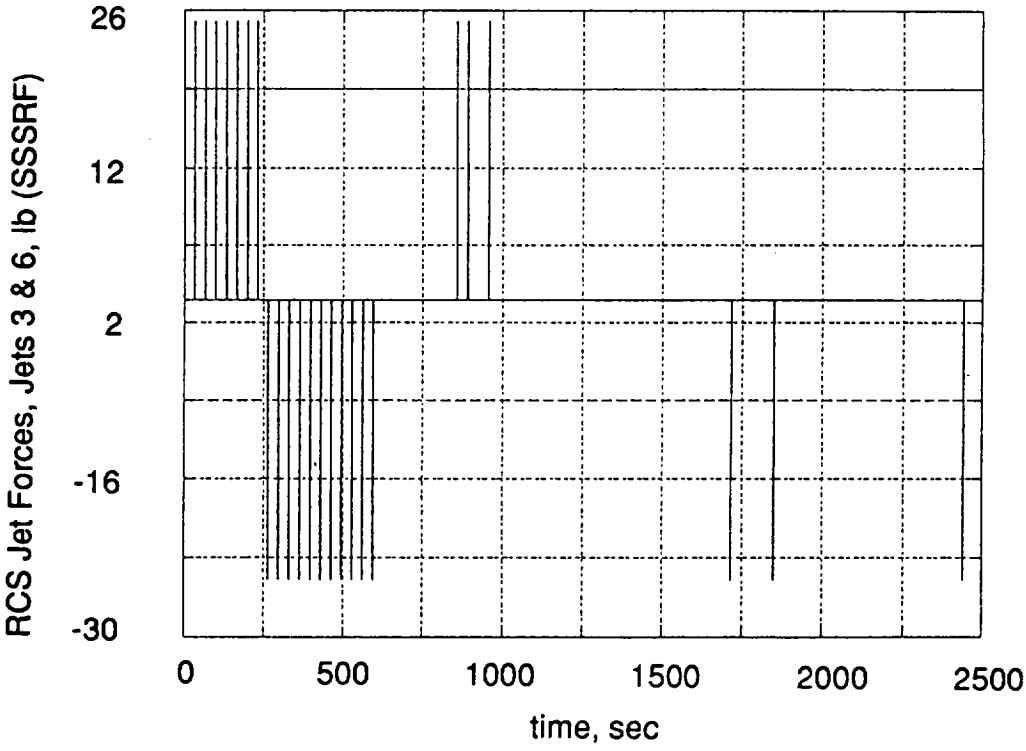

Figure 7-14.- RCS Jet Forces, Jets 3 & 6.

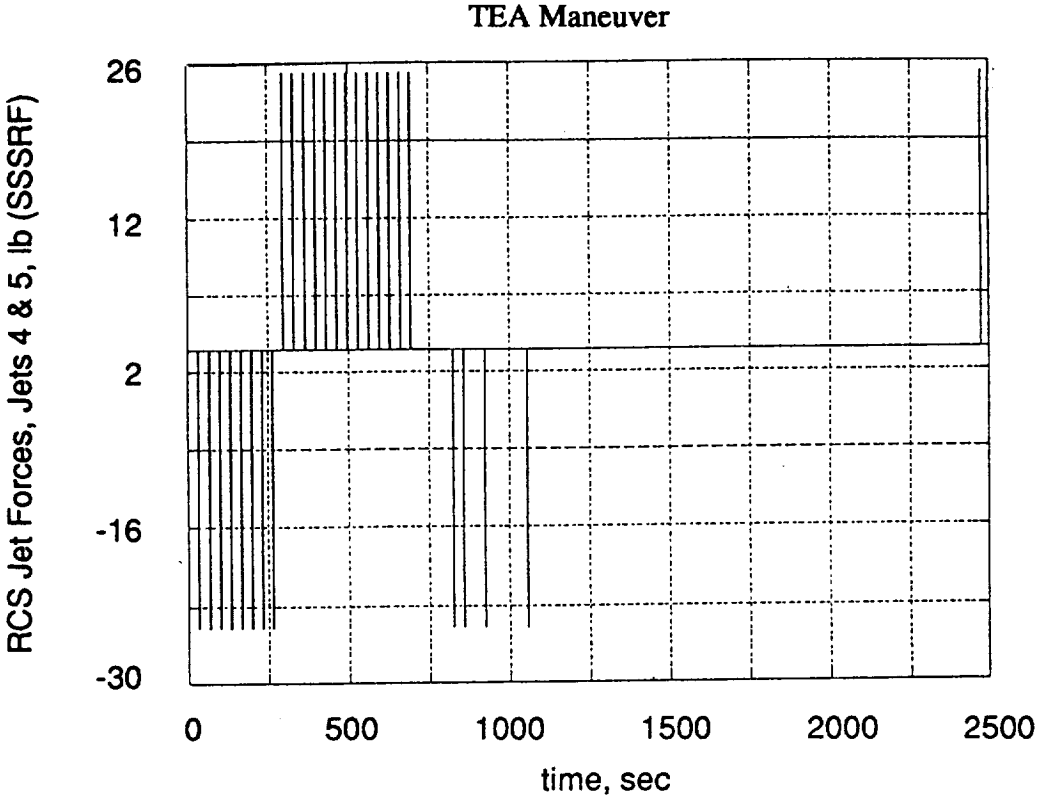

Figure 7-15.- RCS Jet Forces, Jets 4 & 5.

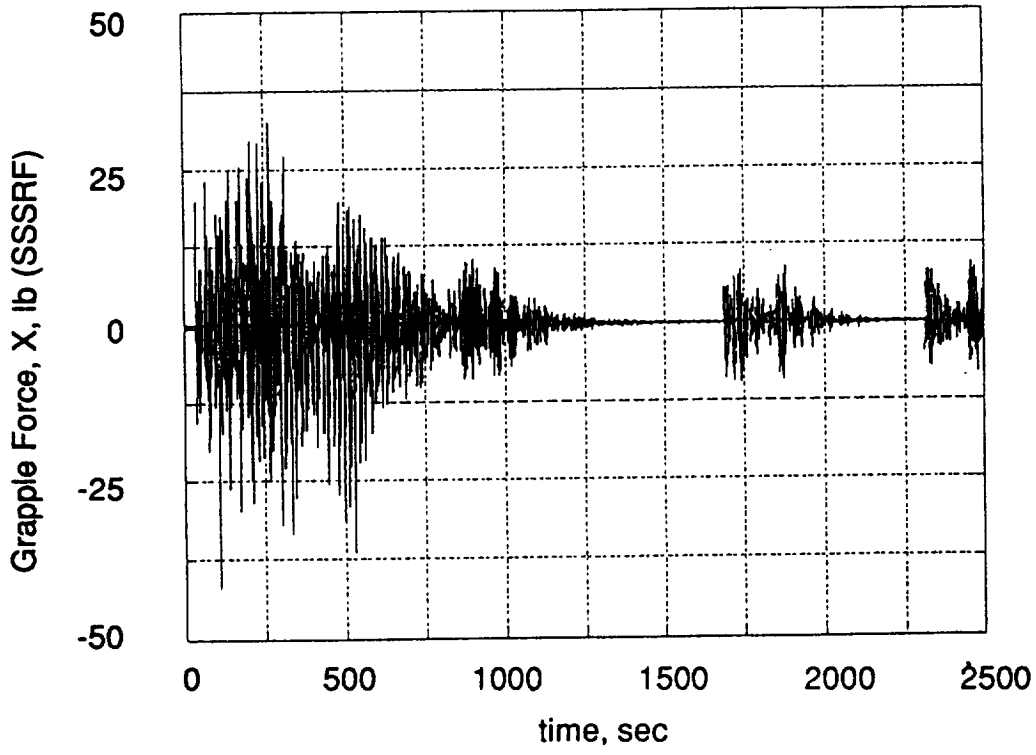

Figure 7-16.- Force at grapple point, x.

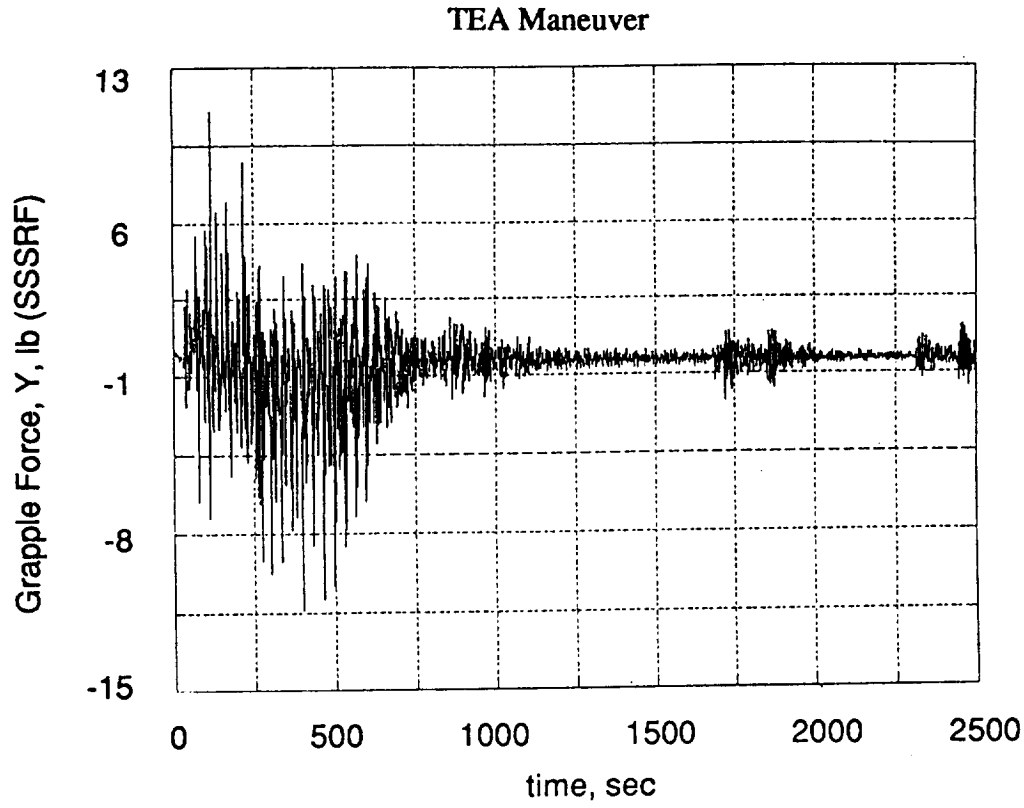

Figure 7-17.- Force at grapple point, y.

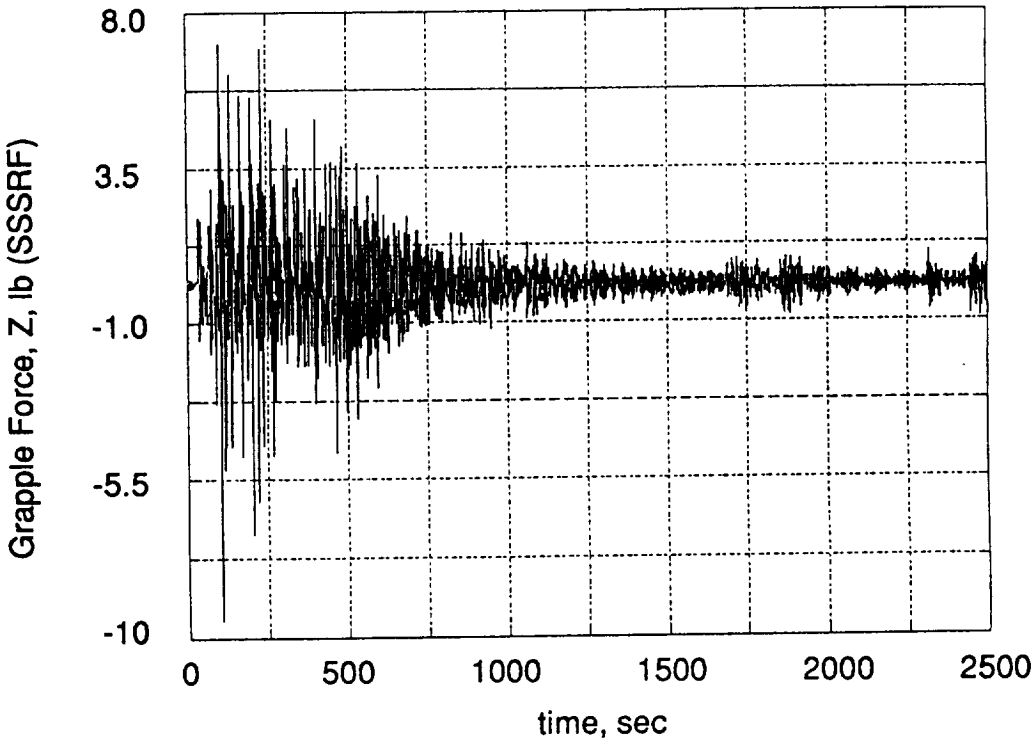

Figure 7-18.- Force at grapple point, z.

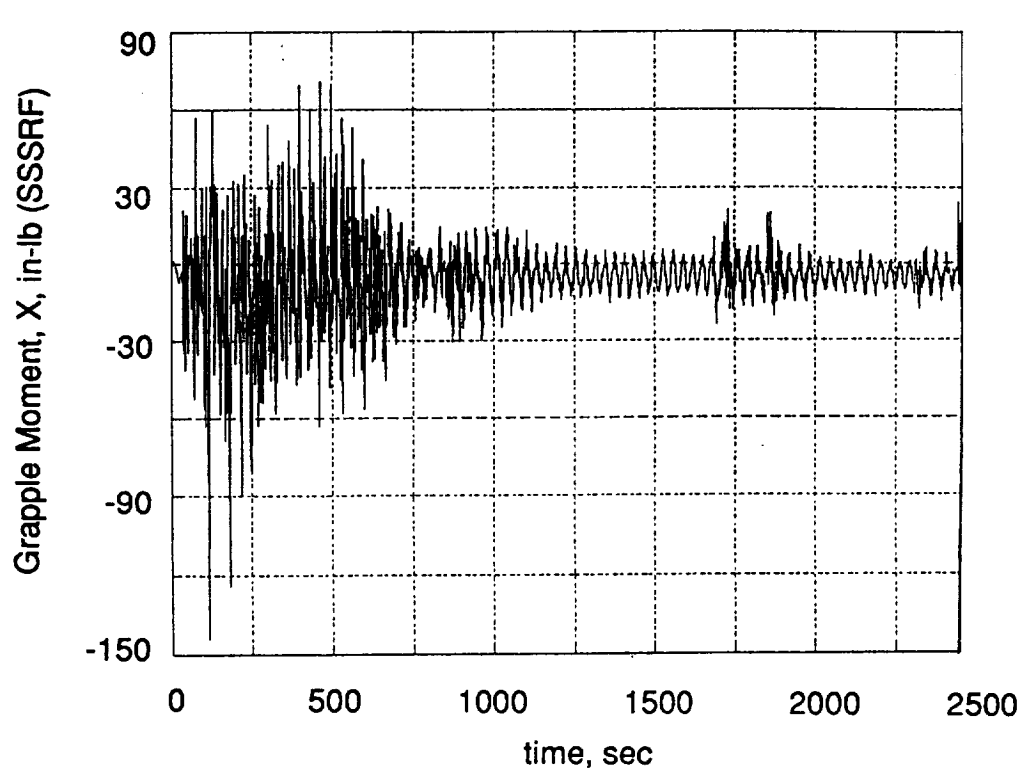

Figure 7-19.- Moment at grapple point, x.

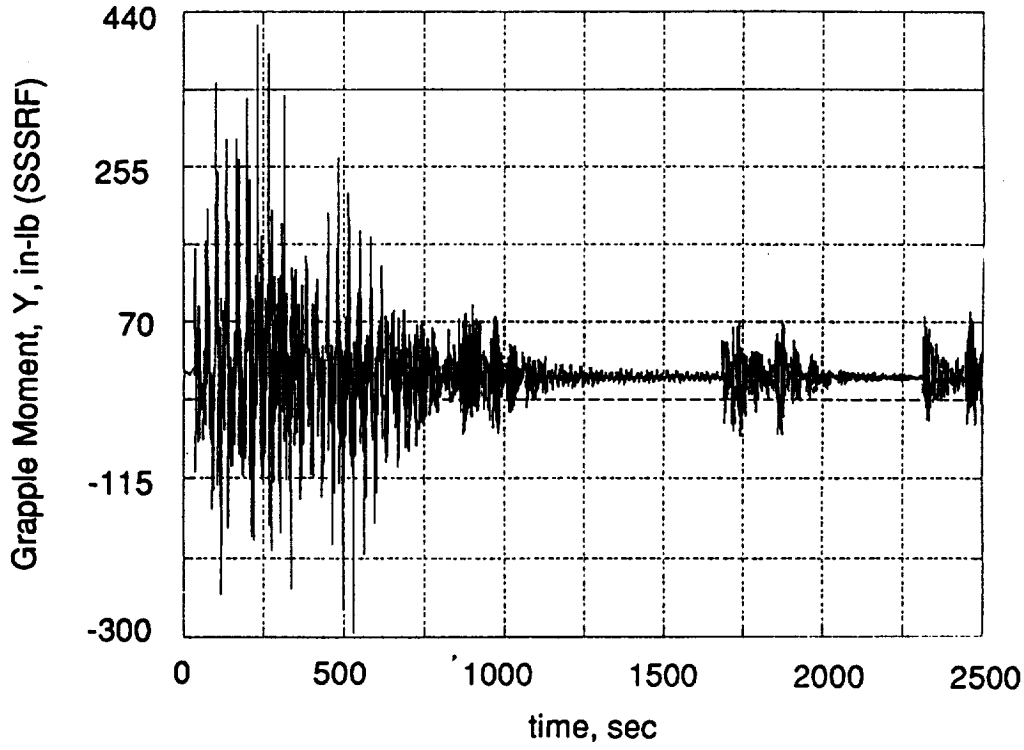

Figure 7-20.- Moment at grapple point, y.

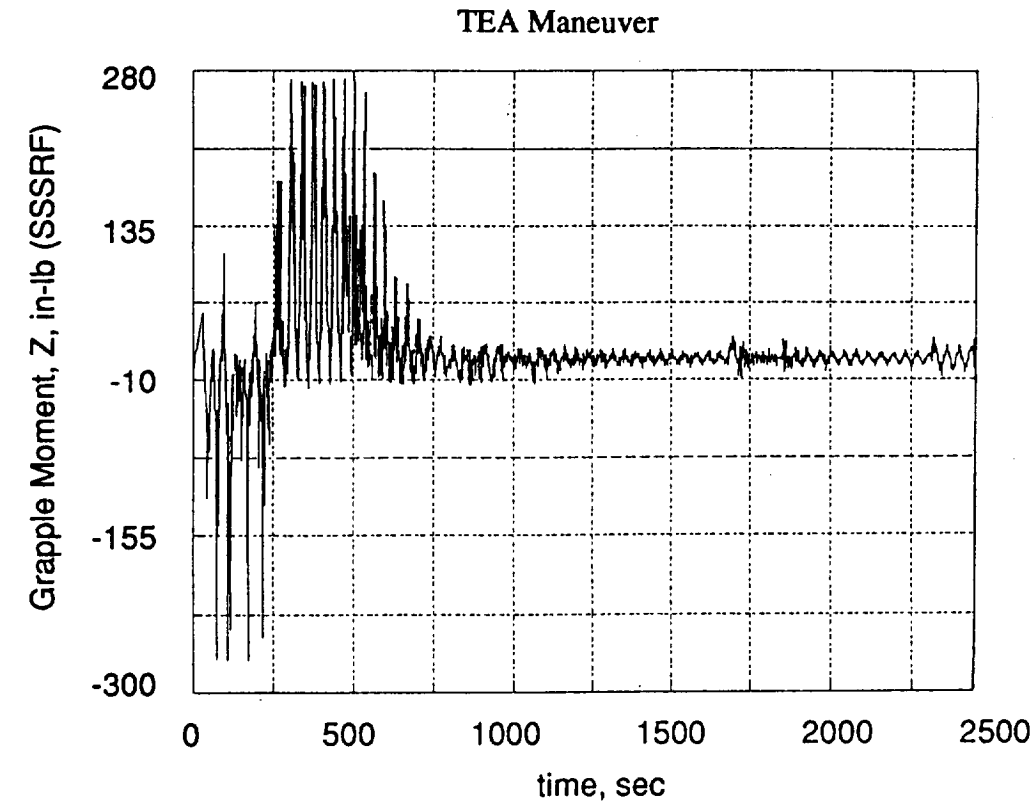

Figure 7-21.- Moment at grapple point, Z.

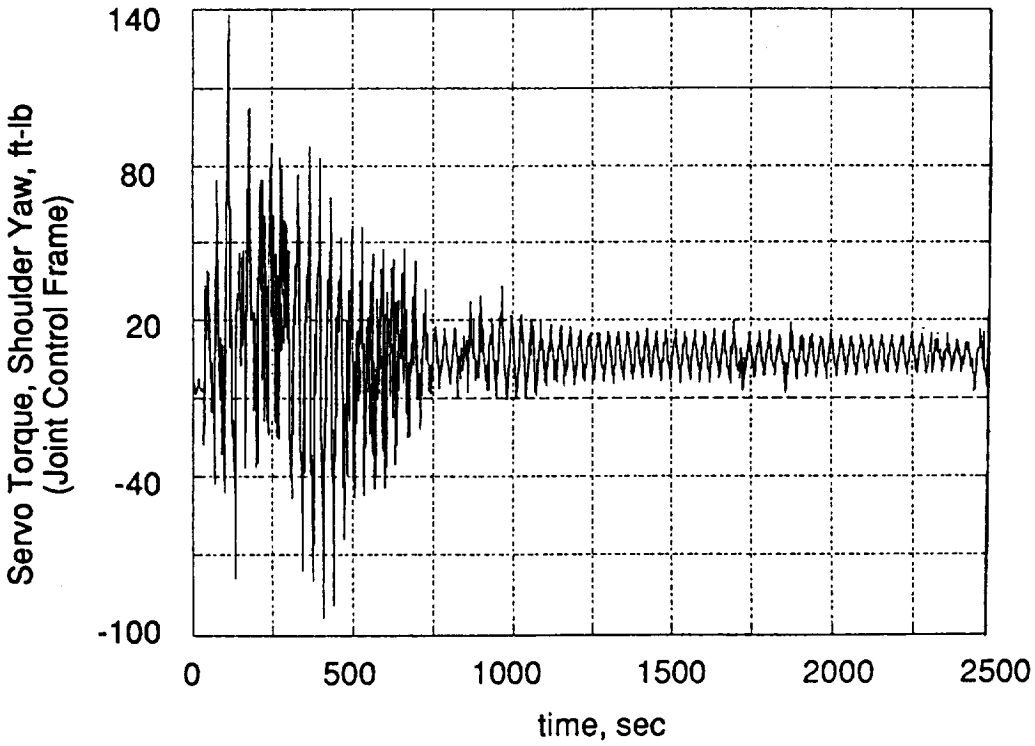

Figure 7-22.- Servo torque, shoulder yaw.

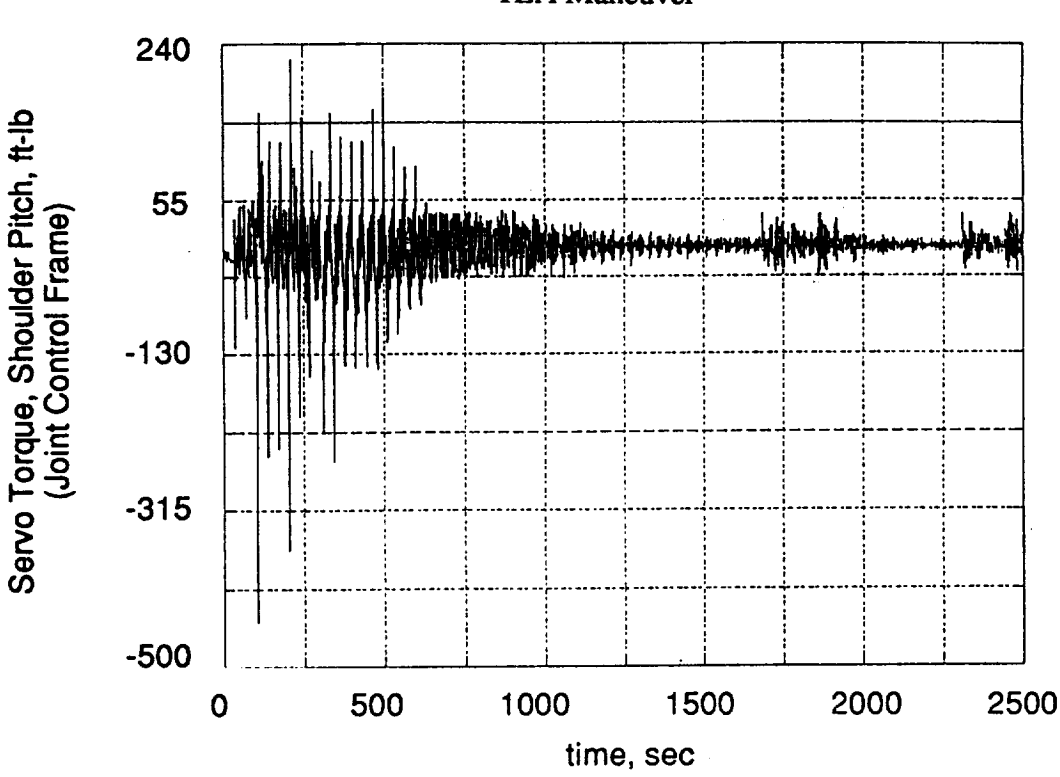

Figure 7-23.- Servo torque, shoulder pitch.

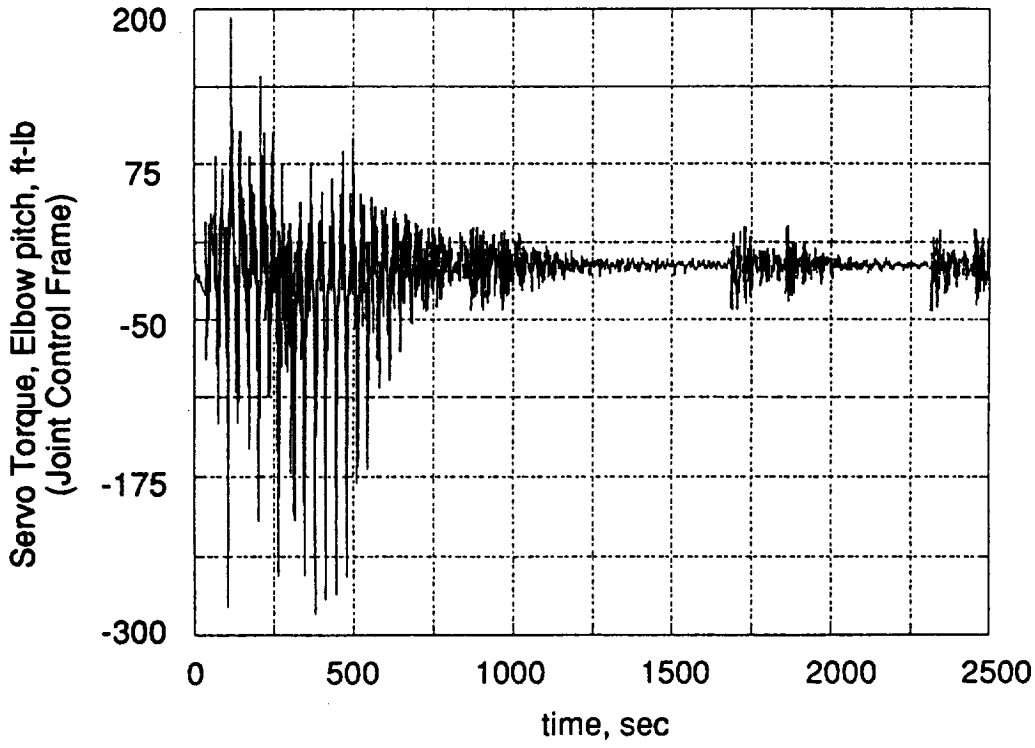

Figure 7-24.- Servo torque, elbow pitch.

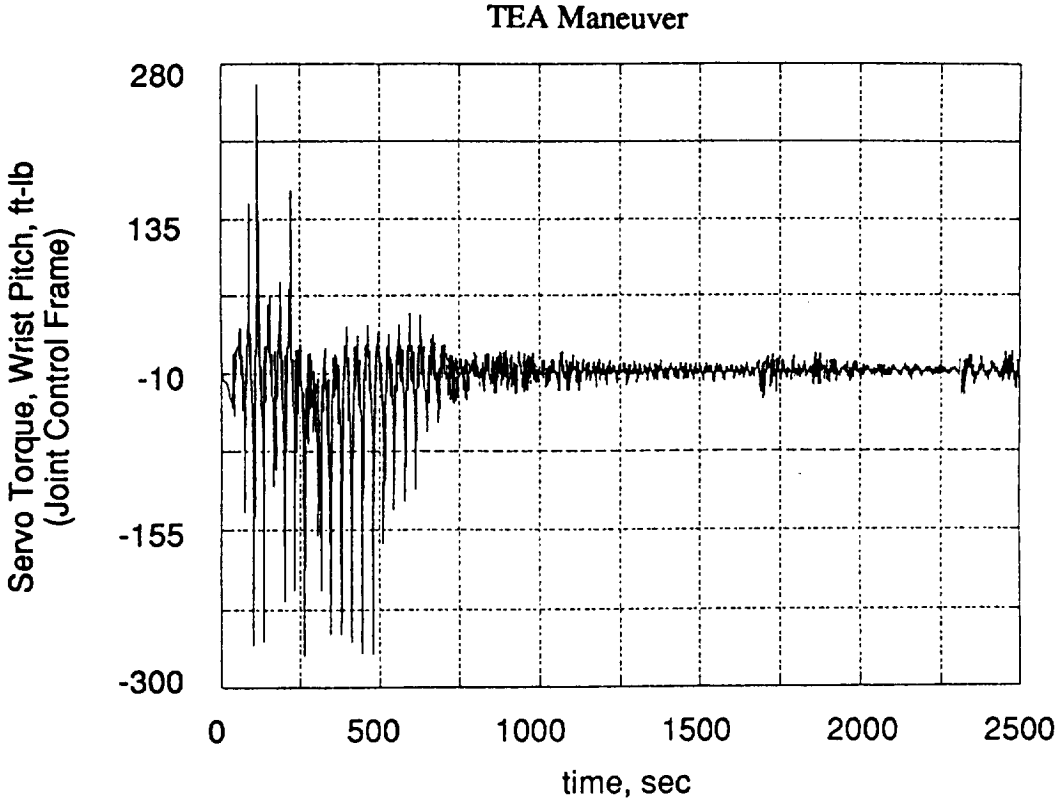

Figure 7-25.- Servo torque, wrist pitch.

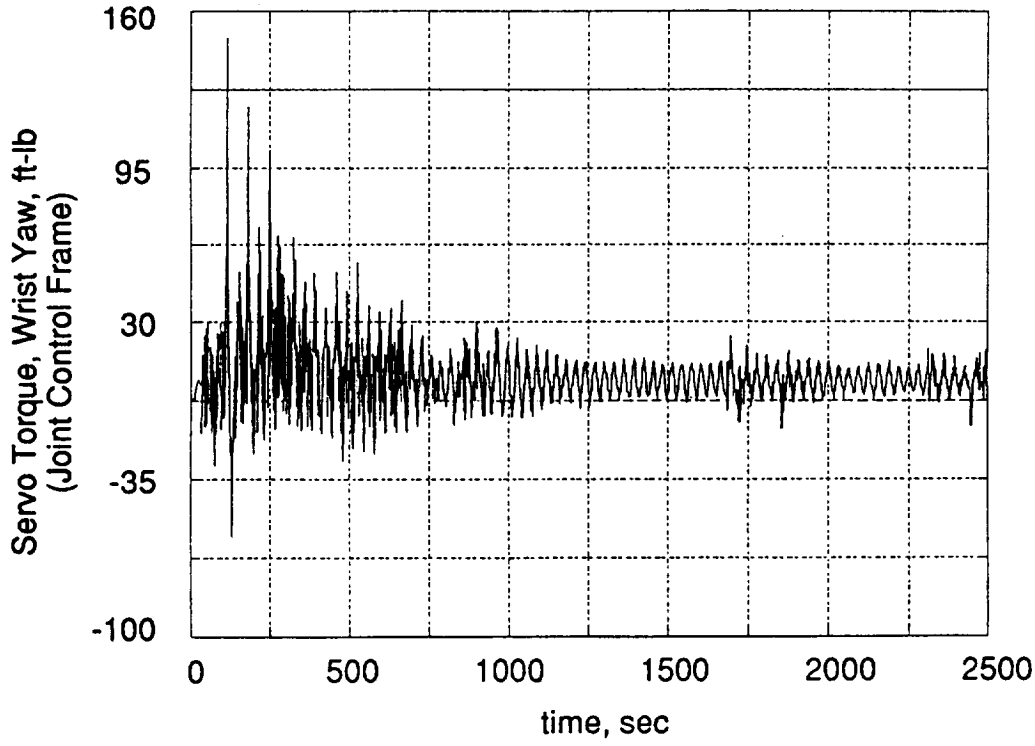

Figure 7-26.- Servo torque, wrist yaw.

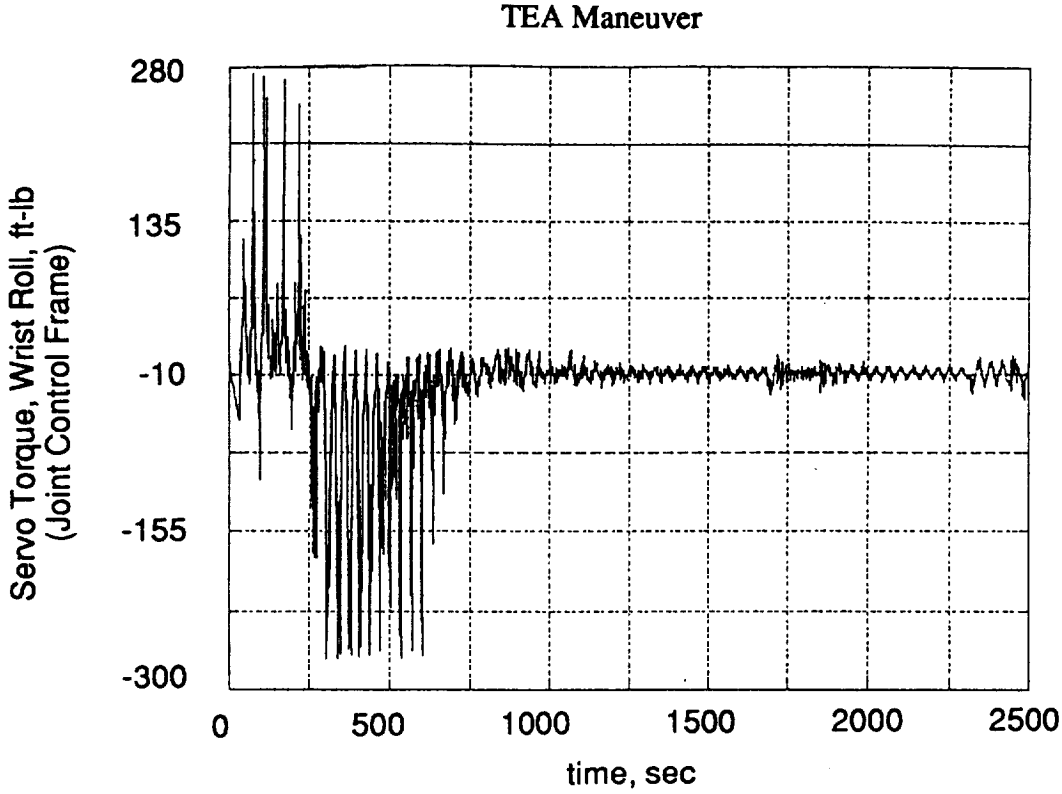

Figure 7-27.- Servo torque, wrist roll.

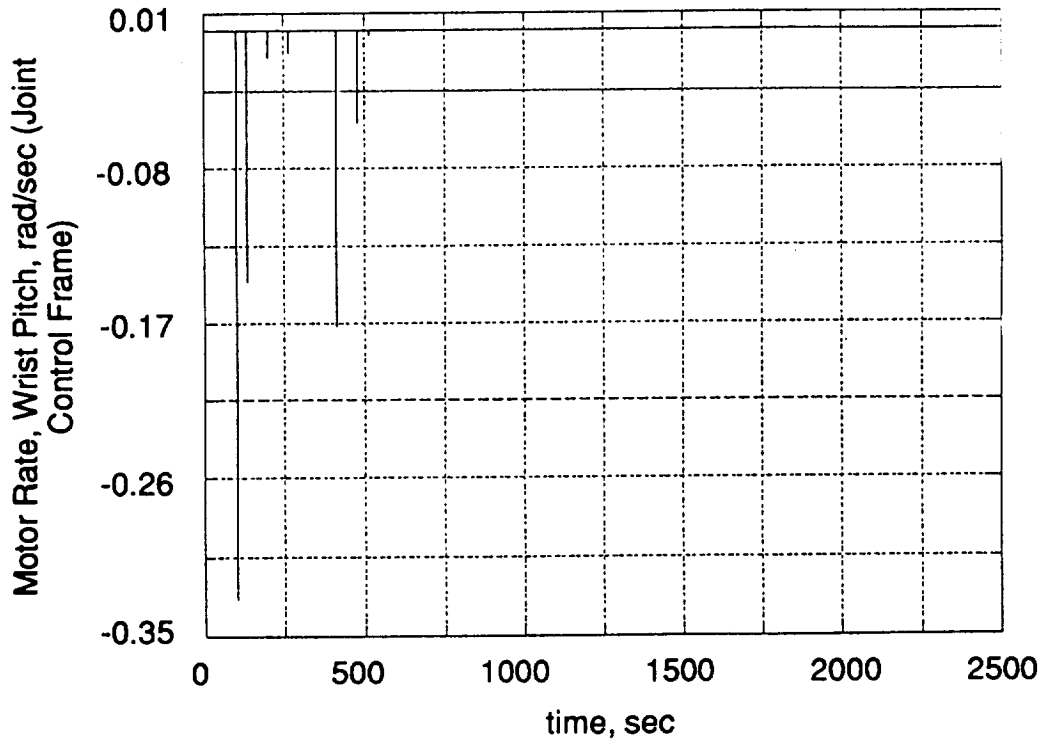

Figure 7-28.- Motor rate, wrist pitch.

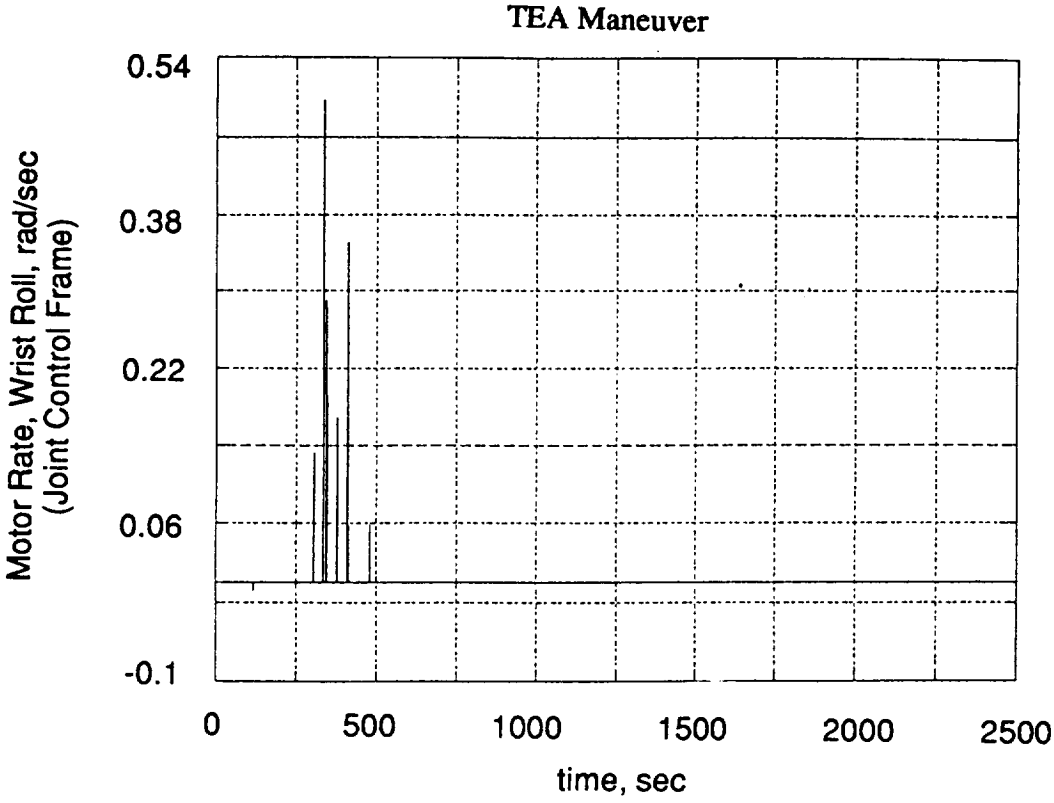

Figure 7-29.- Motor rate, wrist roll.

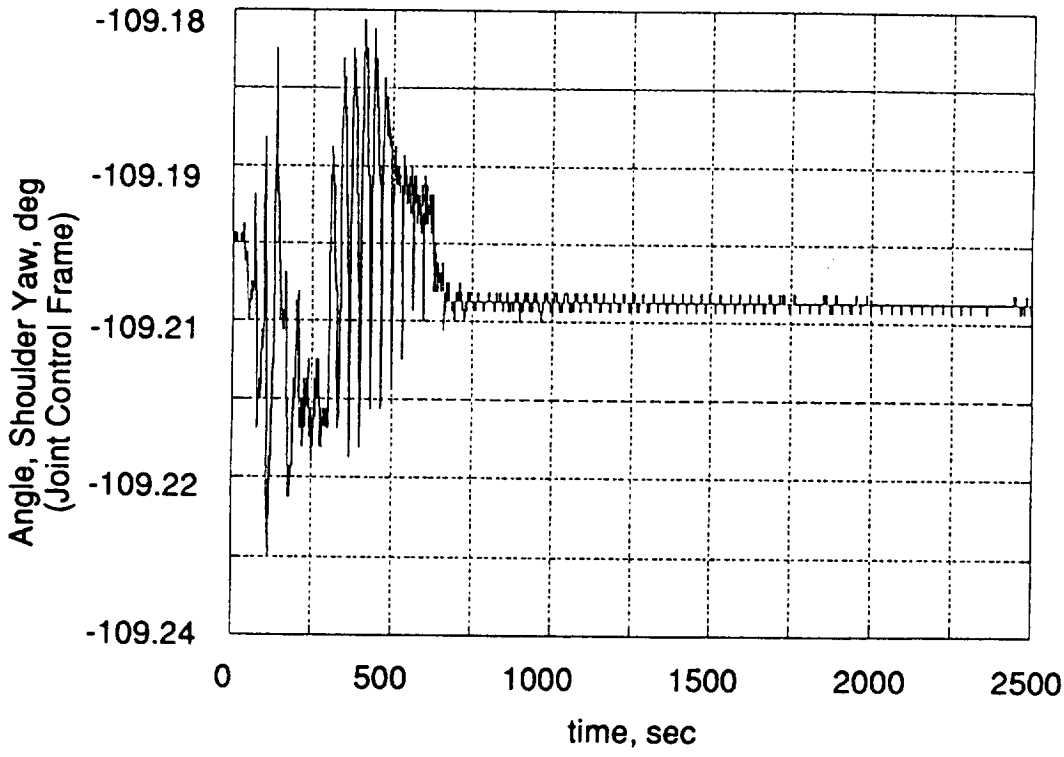

Figure 7-30.- Angle, shoulder yaw.

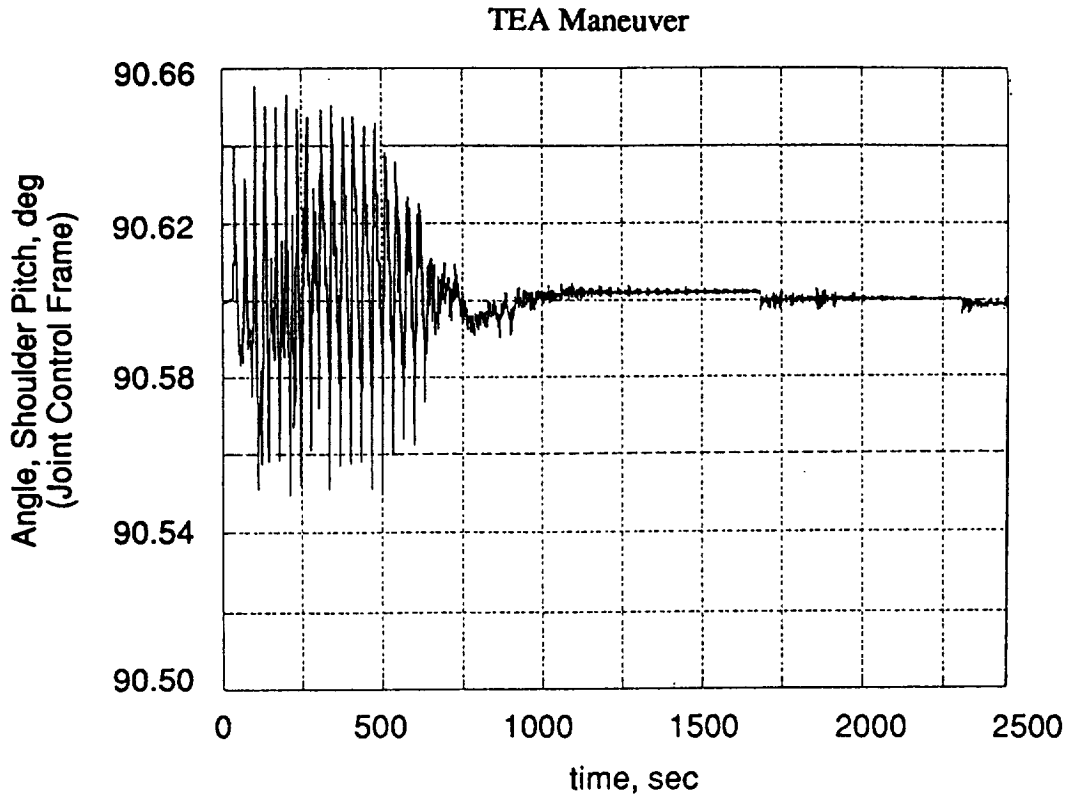

Figure 7-31.- Angle, shoulder pitch.

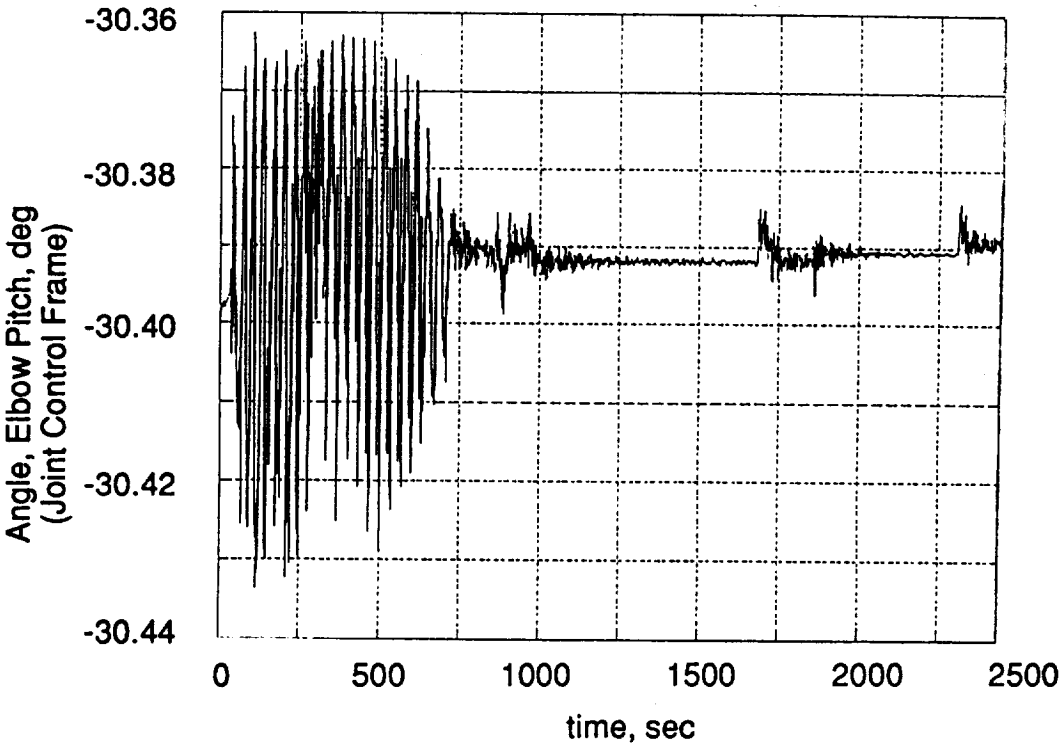

Figure 7-32.- Angle, elbow pitch.

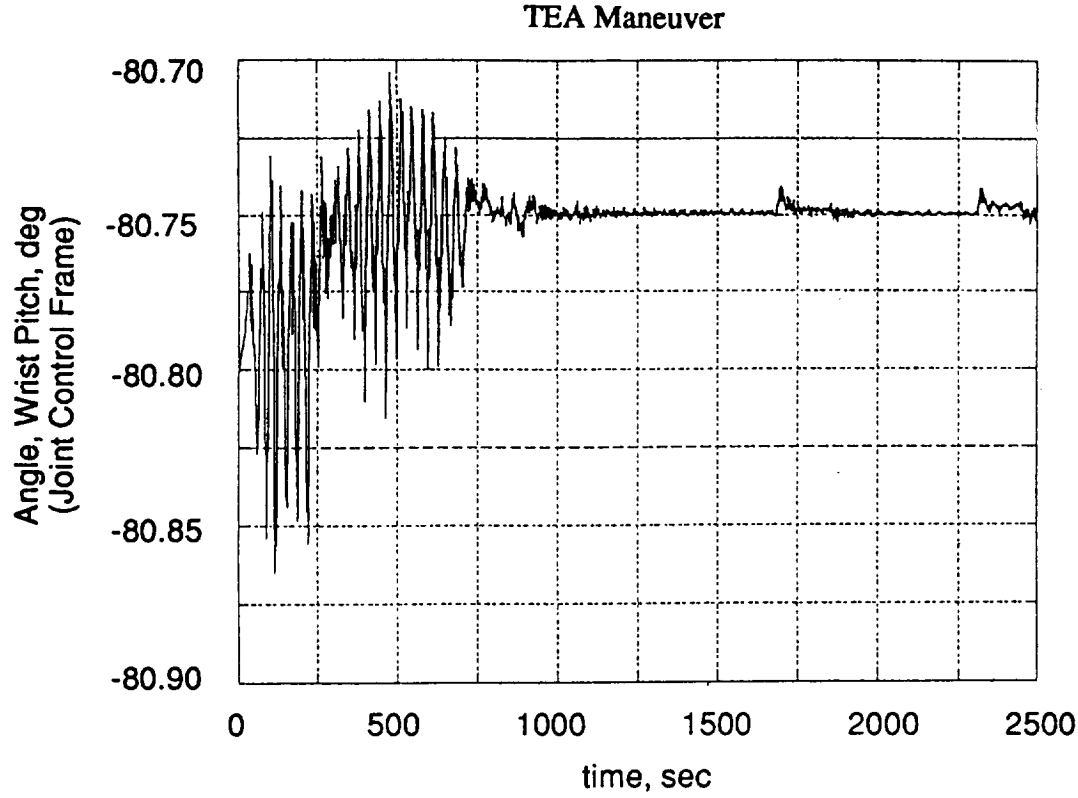

Figure 7-33.- Angle, wrist pitch.

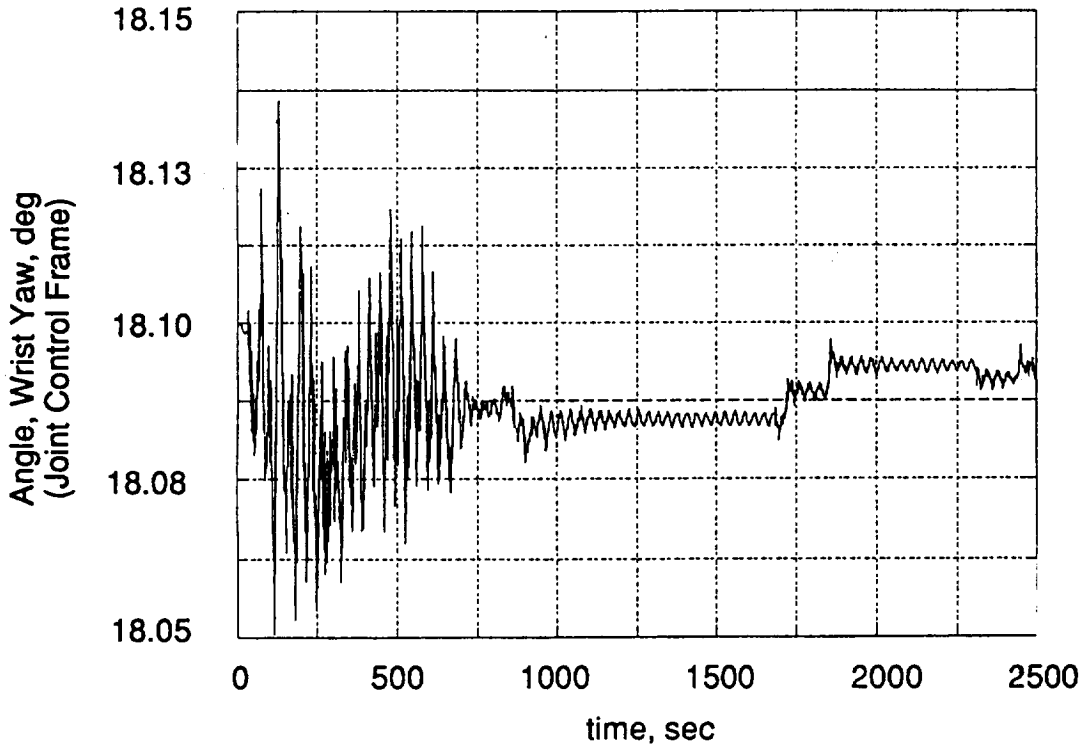

Figure 7-34.- Angle, wrist yaw.

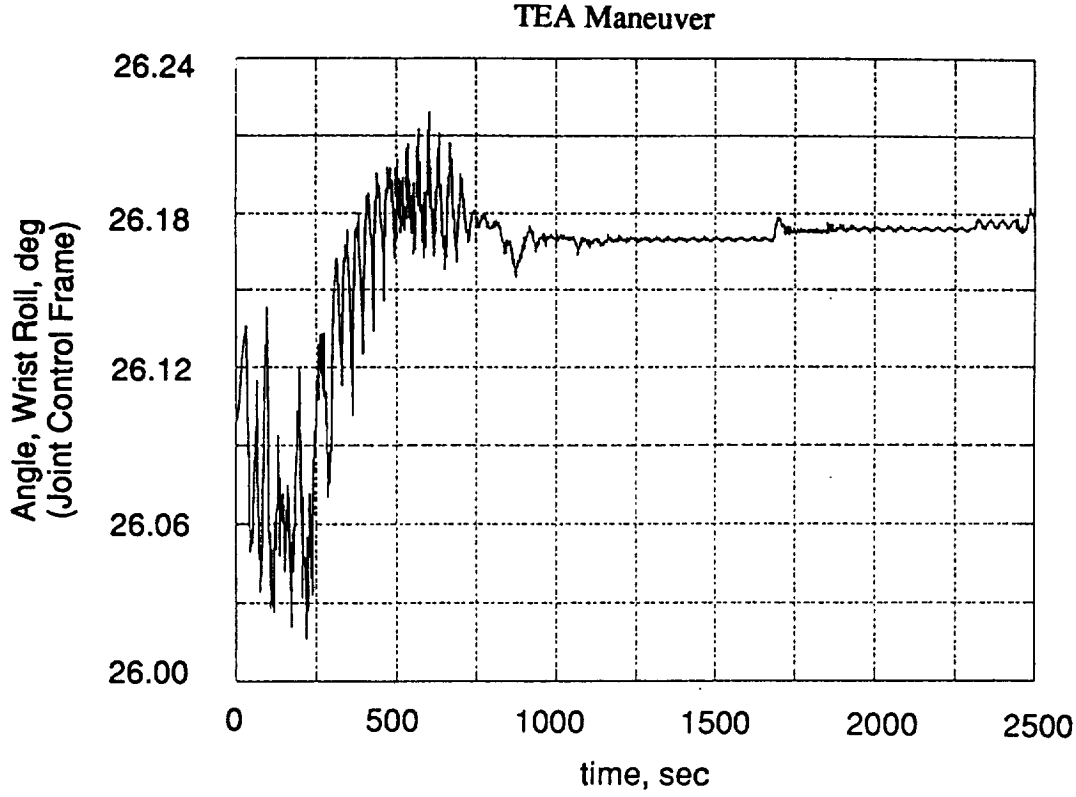

Figure 7-35.- Angle, wrist roll.

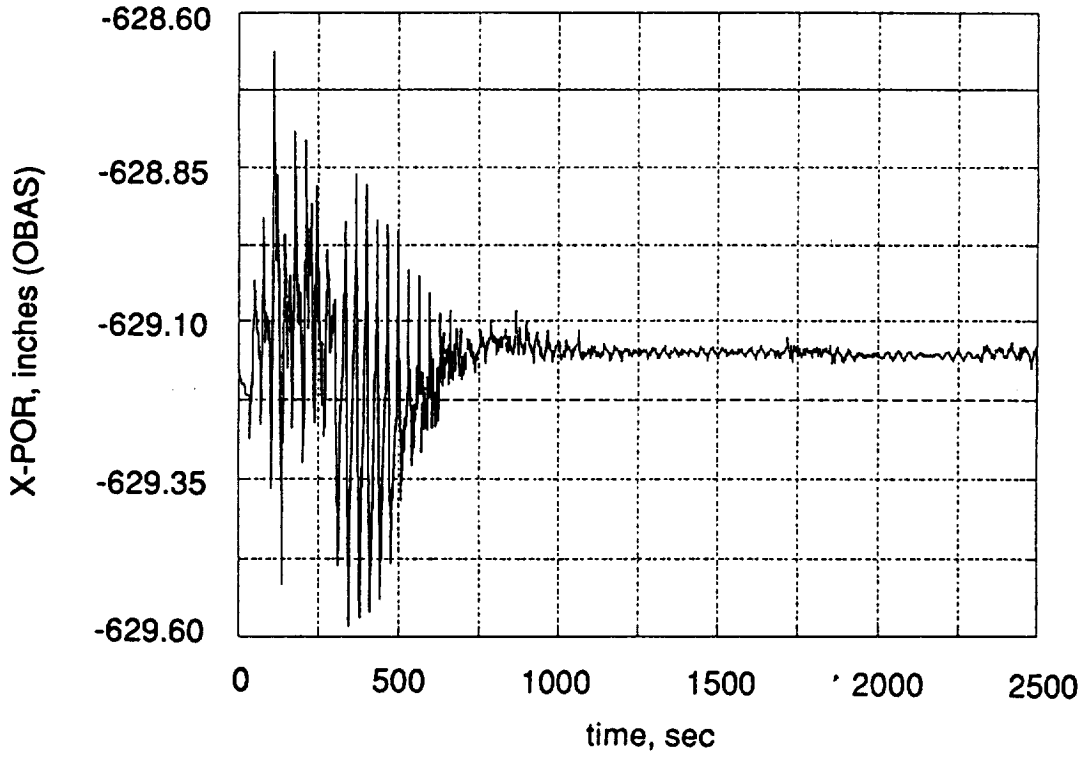

Figure 7-36.- POR, x-direction.

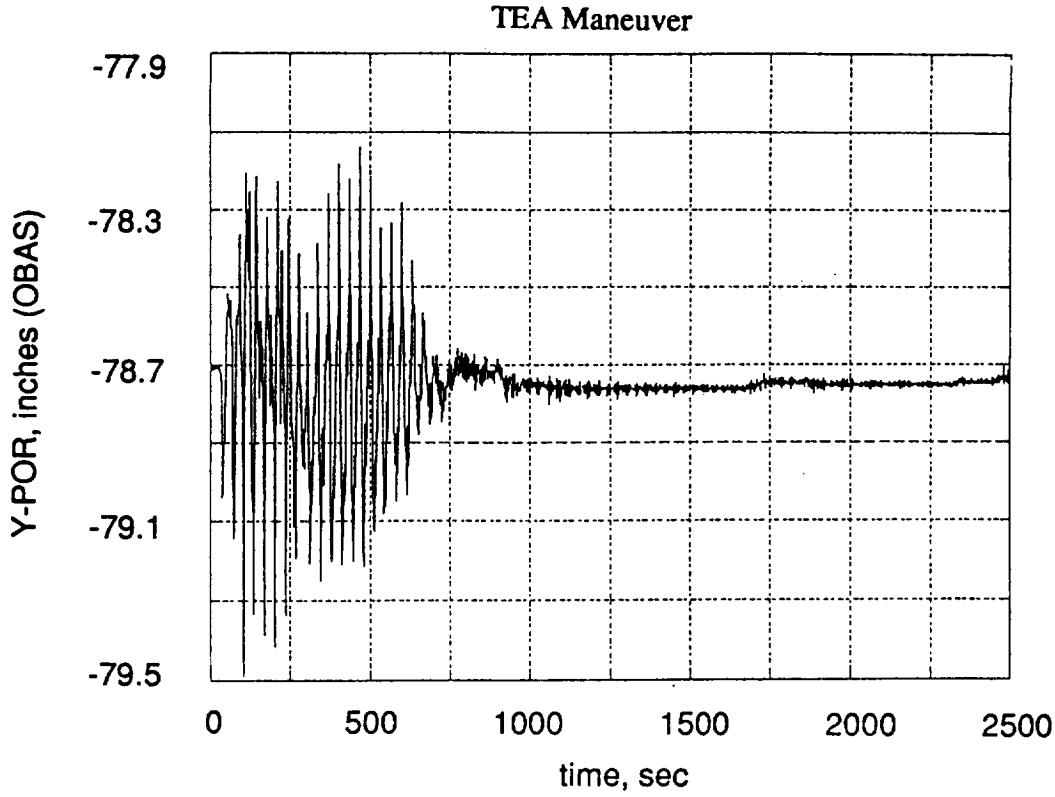

Figure 7-37.- POR, y-direction.

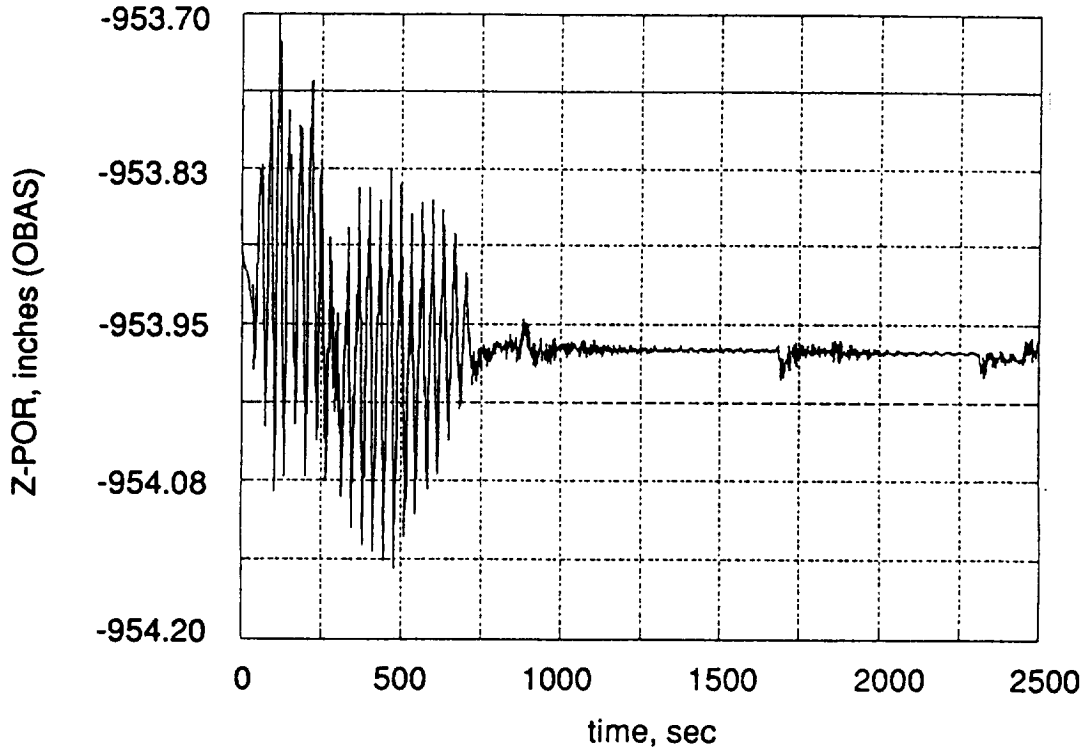

Figure 7-38.- POR, z-direction.

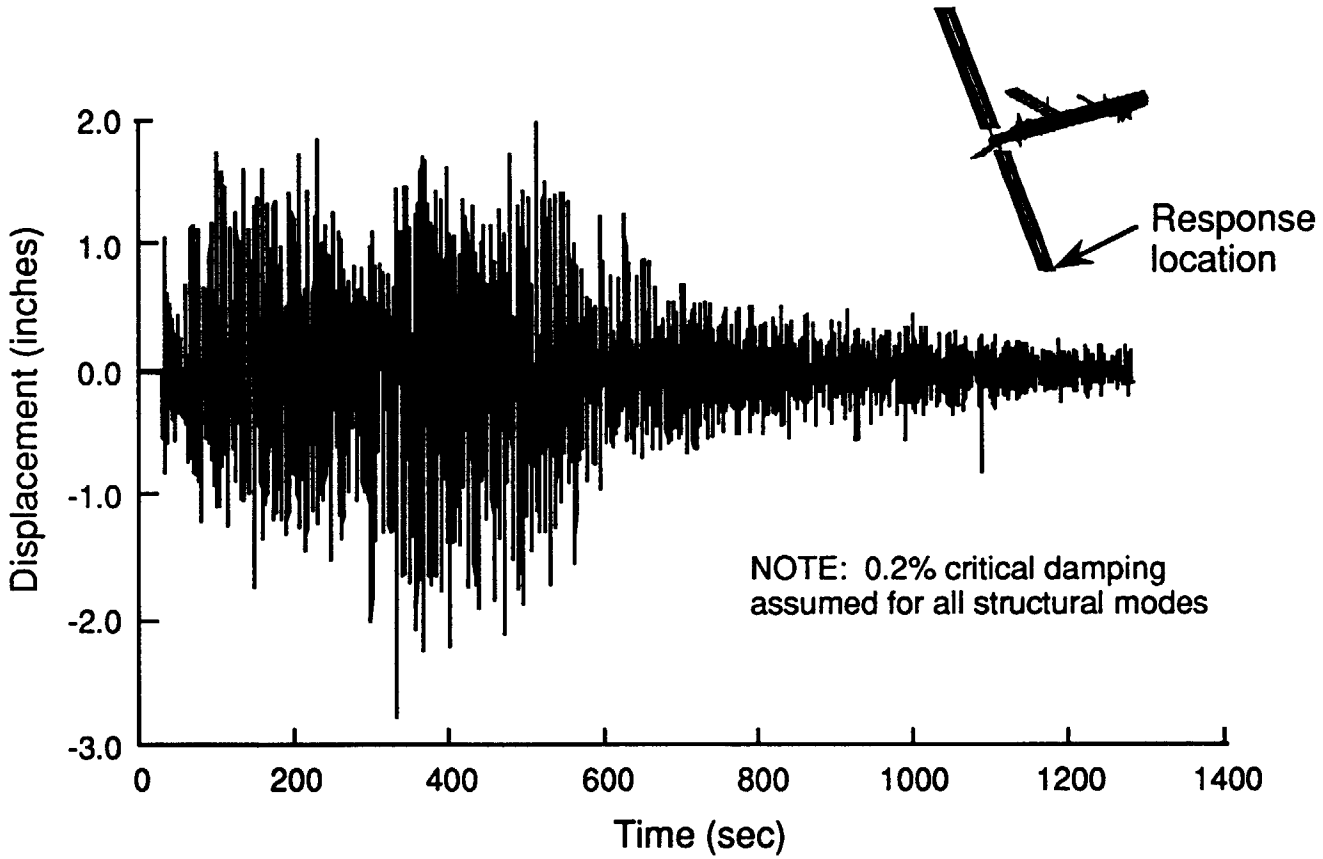

Figure 7-39.- Response of tip of PV array during TEA maneuver

COMPONENT	TEA Load (lb, in-lb)	SC5 Limit Load[a] (lb, in-lb)	SSF Limit Load[b] (lb, in-lb)
NODE2/PDA INTERFACE			
Bending Moment	2,757	134,094	—
Shear Force	13	1,598	—
Axial Force	6	4,550	—
Torsional Moment	304	121,376	—
MB3-MB4 BOLTS			
Axial Force	465	2,862[c]	7,700[c]
MB4 TRUSS			
Bending Moment	1,331	27,918	36,351[d]
Shear Force	44	—	—
Axial Force	-80	2,604	7,436[d]
Torsional Moment	7	—	—
PMAS SUPPORT BRACING			
Bending Moment	1,060	1,563	7,754
Shear Force	99	—	—
Axial Force	225	665	3,252
Torsional Moment	66	—	—
MTS/NODE2 INTERFACE			
Axial Force	-164	-4,458	-17,725
STBD HRS SCISSOR BEAMS			
Bending Moment	444	6,449	7,059
Shear Force	10	131	—
Axial Force	65	828	1,352
Torsional Moment	0	3	—
SARJ TRANSITION			
Bending Moment	238	—	—
Shear Force	7	—	—
Axial Force	-73	—	—
Torsional Moment	22	—	—

Table 7-1.- Maximum structural loads for selected components during TEA maneuver

COMPONENT	TEA Load (lb, in-lb)	SC5 Limit Load[a] (lb, in-lb)	SSF Limit Load[b] (lb, in-lb)
PV ARRAY MAST BASE			
Bending Moment	5,206	16,526	30,667[e]
Shear Force	5	33	53[e]
Axial Force	7	42	3,133[e]
Torsional Moment	38	120	1,600[e]
EPS RAD. SCISSOR BEAMS			
Bending Moment	834	1,677	6,165
Shear Force	—	—	—
Axial Force	179	360	807
Torsional Moment	—	—	—

NOTES:

a. SC5 Limit Loads are equal to the maximum scaled response for all PDR load cases applied to the SC5 configuration. (Scale factors are discussed in Ref. 2-1)

b. SSF Limit Loads are equal to the maximum scaled response for all PDR load cases and all stage configurations analyzed for the PDR Loads analysis.

c. Maximum for all truss segment interfaces.

d. Maximum for all PIT truss segments.

e. Current design capability (See Ref. 2-1).

f. Modal damping = 0.2% critical for all modes.

Table 7-1 (concluded).- Maximum structural loads for selected components during TEA maneuver

DISPLACEMENTS:

TIP OF PV ARRAY	2.8 INCHES (NORMAL TO PLANE OF BLANKET) 2.7 INCHES (IN PLANE OF BLANKET)
BASE OF PV	0.09 INCHES (NORMAL TO PLANE OF BLANKET) 0.06 INCHES (IN PLANE OF BLANKET)

Table 7-2.- Maximum displacement of PV array

8.0 RESULTS OF BERTHING MANEUVER

It was determined during the TEA simulation that a reduction in number of SSF modes and an increase in the integration time-step could be made while maintaining sufficient accuracy. For the berthing maneuver, the integration was performed at a time-step of 0.002 seconds. The station structural dynamics were represented using 13 natural modes and the SRMS structural dynamics were represented using 2 modes for each of the long booms. Results of the simulation are presented in figures 8-1 through 8-42.

The SRMS POR is commanded to move along the three-point berthing trajectory described in section 1.2 and depicted in Figure G-1. The resulting motion of the POR is plotted in figures 8-1 through 8-3. From the initial grapple point, position 1, the SRMS is commanded to move 54 inches in the x and z-axis directions and two inches in the y-axis direction using an operator commanded auto sequence maneuver (where x, y, and z refer to the Orbiter Body-Axis System shown in appendix A-7). From position 2, the SRMS is immediately commanded to move 300 inches vertically to position 3 using the manual mode z-axis translational hand controller input. When position 3 (two feet from a full berthed position) is reached, the hand controller commands are removed and the position hold mode is automatically enabled by the SRMS command algorithms to maintain its commanded position and attitude. The berthing simulation was conducted with the SRMS in coarse mode operation, i.e., the respective translational and rotational end-effector rate limits of 0.14 ft/sec and 0.14 °/sec were used. These rates, together with the described combination of automatic and manual mode maneuvers, allowed the berthing to be aggressively completed in 15 minutes. As shown in 8-1 through 8-3, very little vibratory motion was observed following completion of the berthing maneuver. The time history for each joint angle is plotted in figures 8-4 through 8-9. The largest angular travel of 107° occurred at the elbow pitch joint. The position hold mode was quite effective as can be seen by the constant value of each joint angle after completion of the berthing motion. The servo torque time history for each joint is given in figures 8-10 through 8-15. The maximum torques occurred during SRMS control mode transfer from automatic to manual (at approximately t = 200 sec) and from manual to position hold (at approximately t = 800 sec). The maximum torque of 420 ft-lbs was applied at the elbow pitch joint at the transition from automatic to manual mode.

The time history of forces and moments at the grapple point are given in figures 8-16 through 8-21 and reflect the force and moment transfer provided by the SSRMS joint motors to change the relative location of the SSF and the Orbiter, and the moment transfer provided by the CMGs to move the entire stack to the latest computed TEA. The maximum forces and moments at the grapple fixture occurred at transition from automatic to manual and manual to position hold mode.

The change in attitude of the stack during the berthing maneuver is shown in figures 8-22 through 8-24. The final attitude of the stack is achieved in approximately 1700 seconds. The attitude and attitude-rate errors are plotted in figures 8-25 through 8-30, resulting in the commanded CMG torques plotted in figures 8-31 through 8-33. The momentum transfer provided by the CMGs about each axis is plotted in figures 8-34 through 8-36. The variation in moment of inertia of the stack during the berthing process is plotted in figures 8-37 through 8-39. The required momentum exchange exceeded the available momentum, that is, the CMGs saturated during the berthing maneuver when initiated from a zero setting. This saturation may be avoided by using the RCS to give the CMGs an initial bias of approximately 1400 ft-lb-sec or approximately 10 percent of the combined capacity of the CMGs before beginning the berthing maneuver. Adverse effects of flexible dynamics were not observed in this simulation.

The external disturbances which include both the drag moments and gravity gradient moments vary during the berthing maneuver and are plotted in figures 8-40 through 8-43

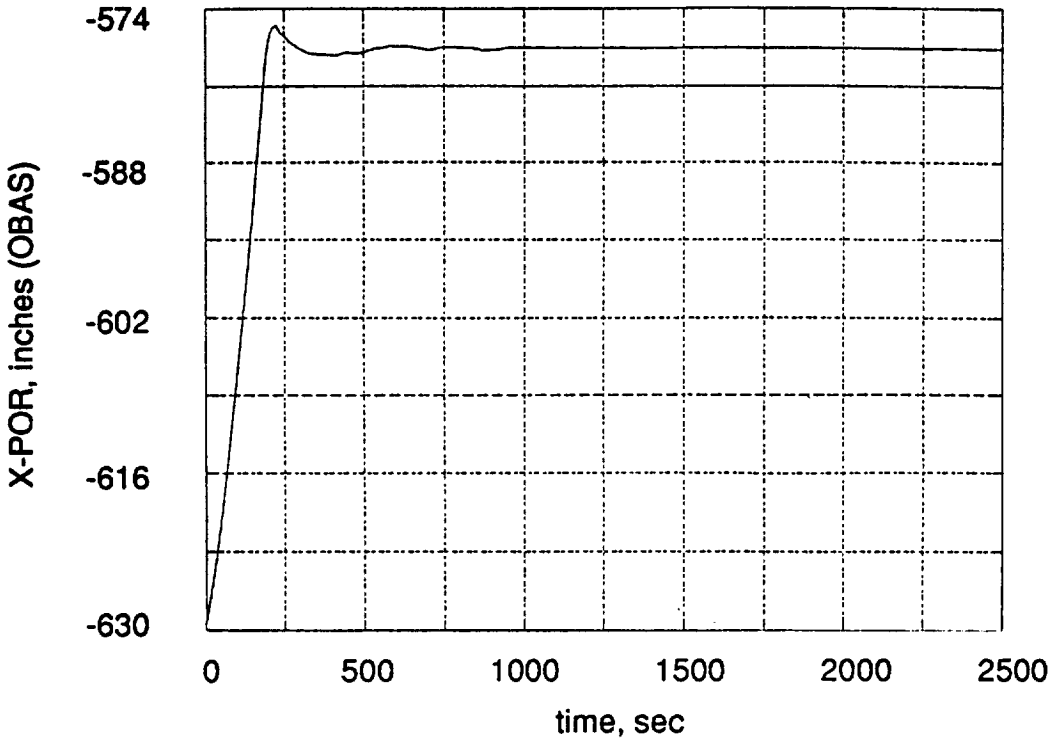

Figure 8-1.- POR, x-direction.

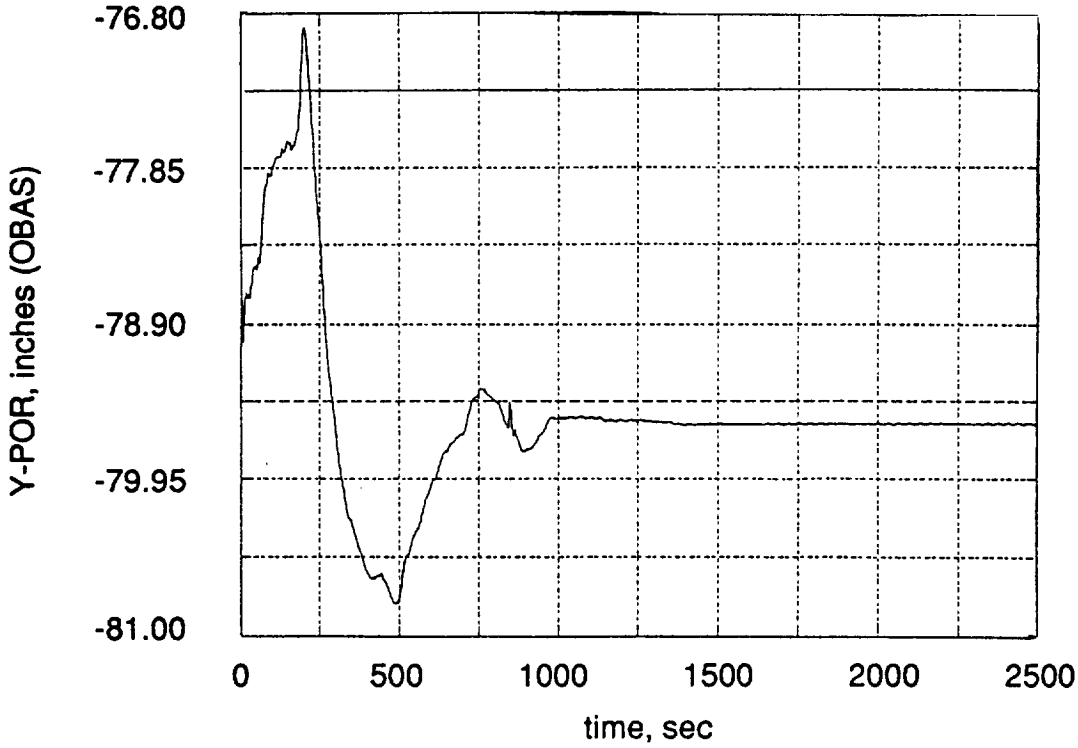

Figure 8-2.- POR, y-direction.

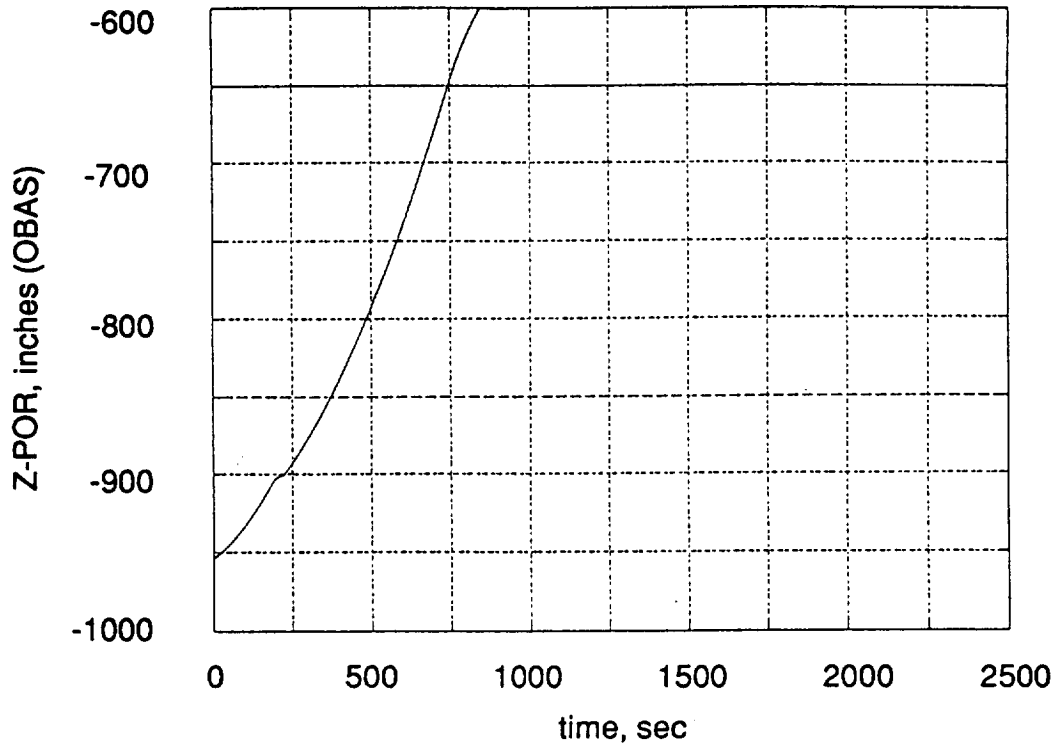

Figure 8-3.- POR, z-direction.

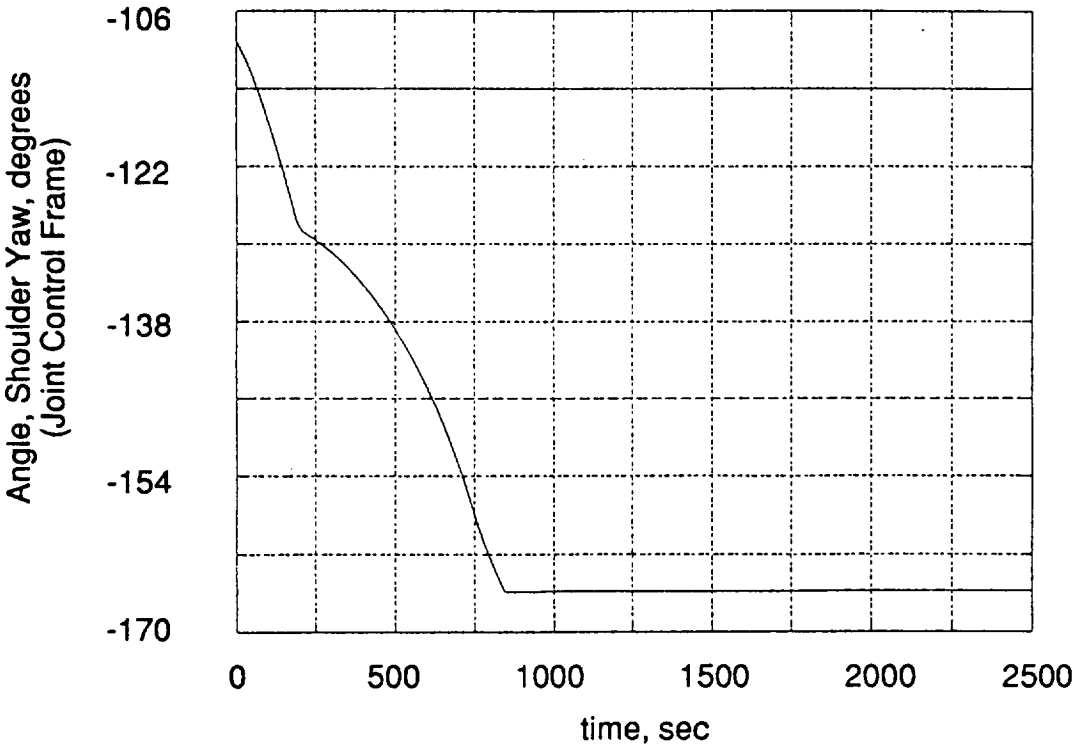

Figure 8-4.- Angle, shoulder yaw.

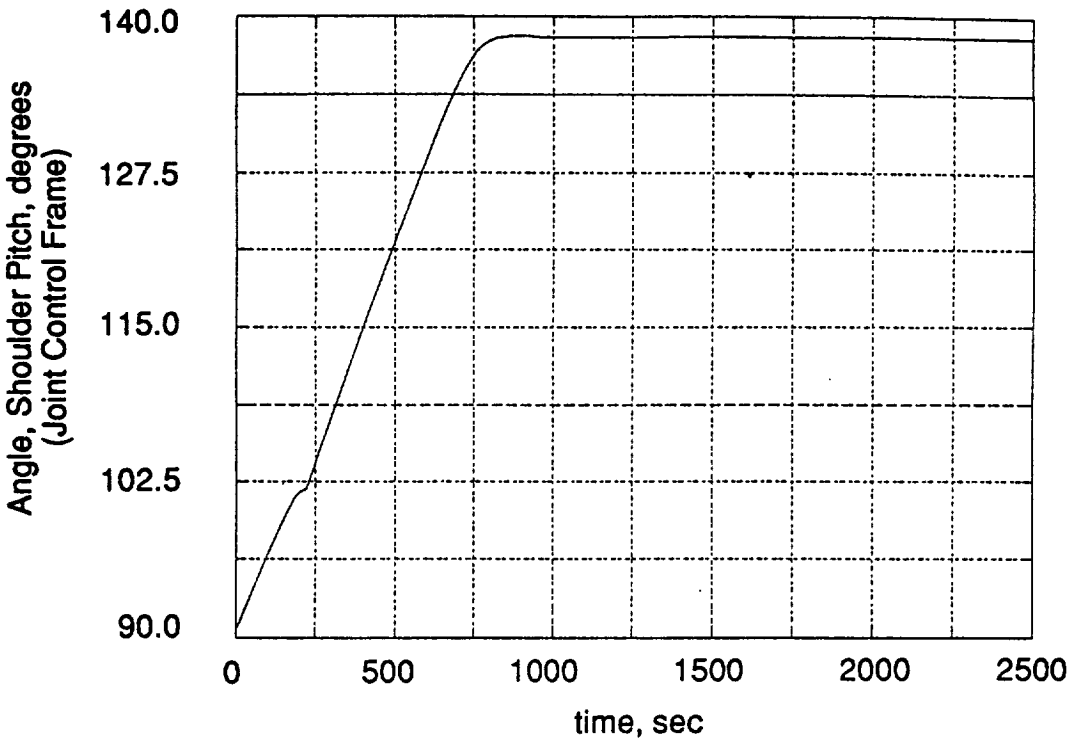

Figure 8-5.- Angle, shoulder pitch.

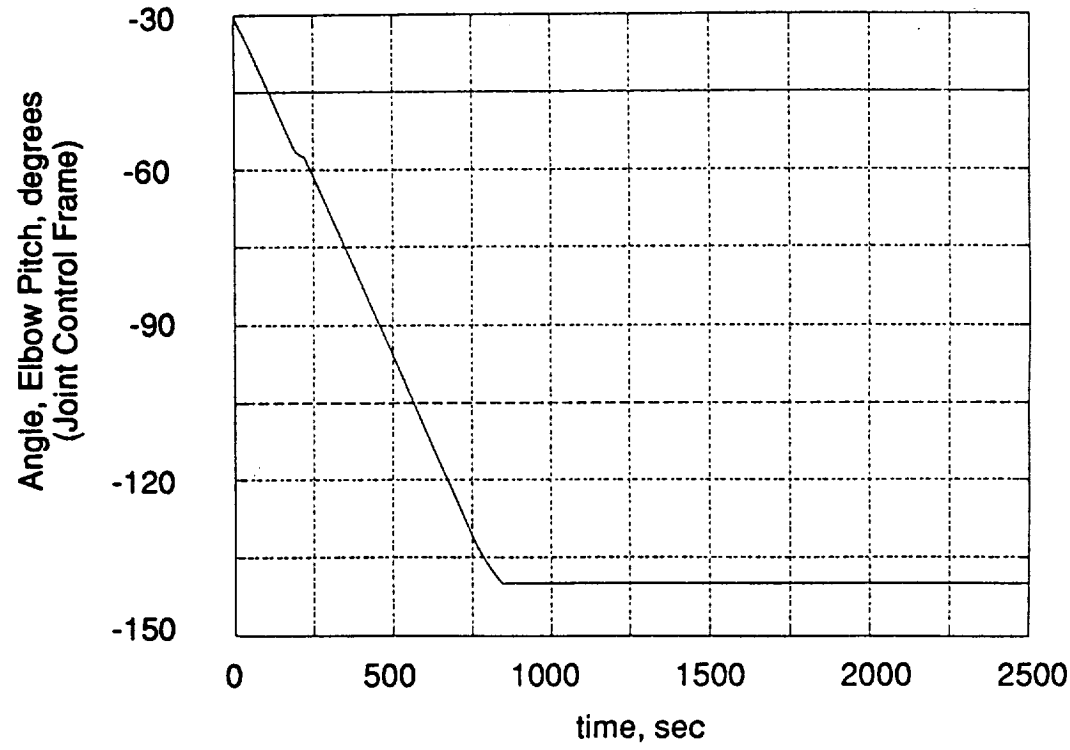

Figure 8-6.- Angle, elbow pitch.

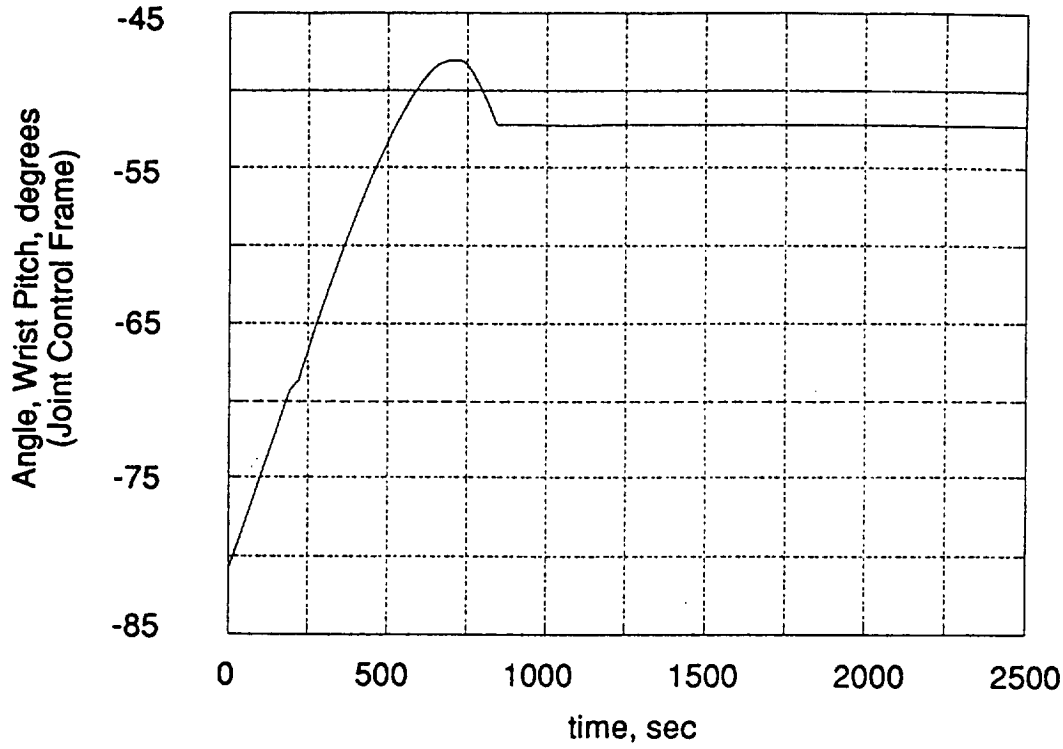

Figure 8-7.- Angle, wrist pitch.

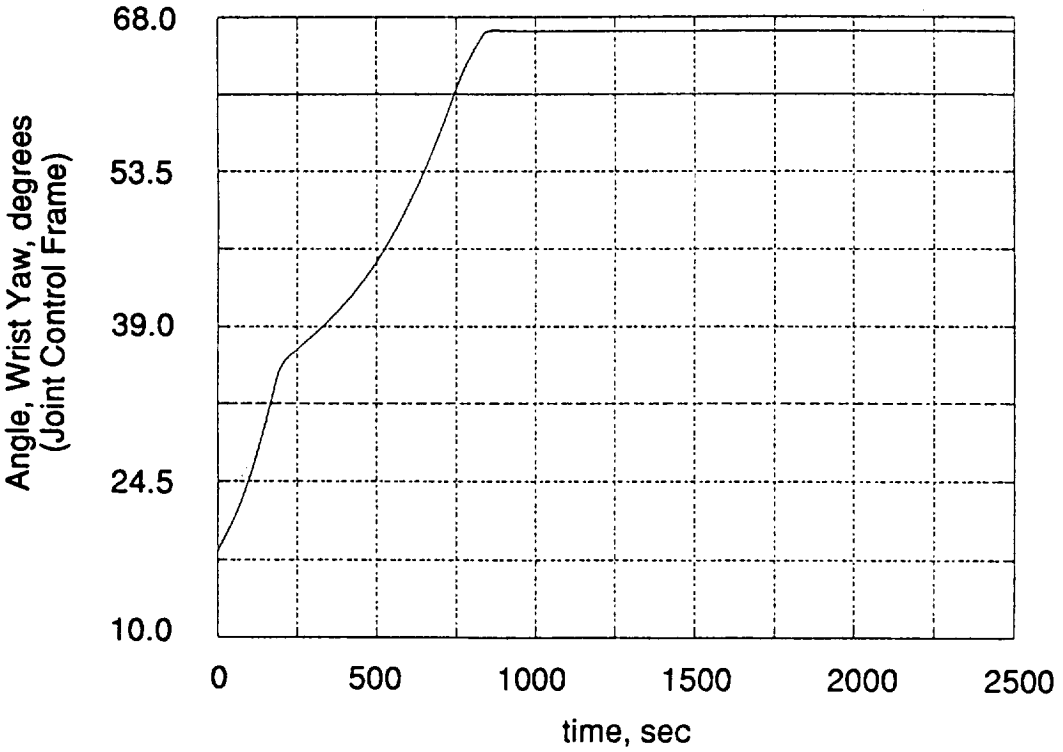

Figure 8-8.- Angle, wrist yaw.

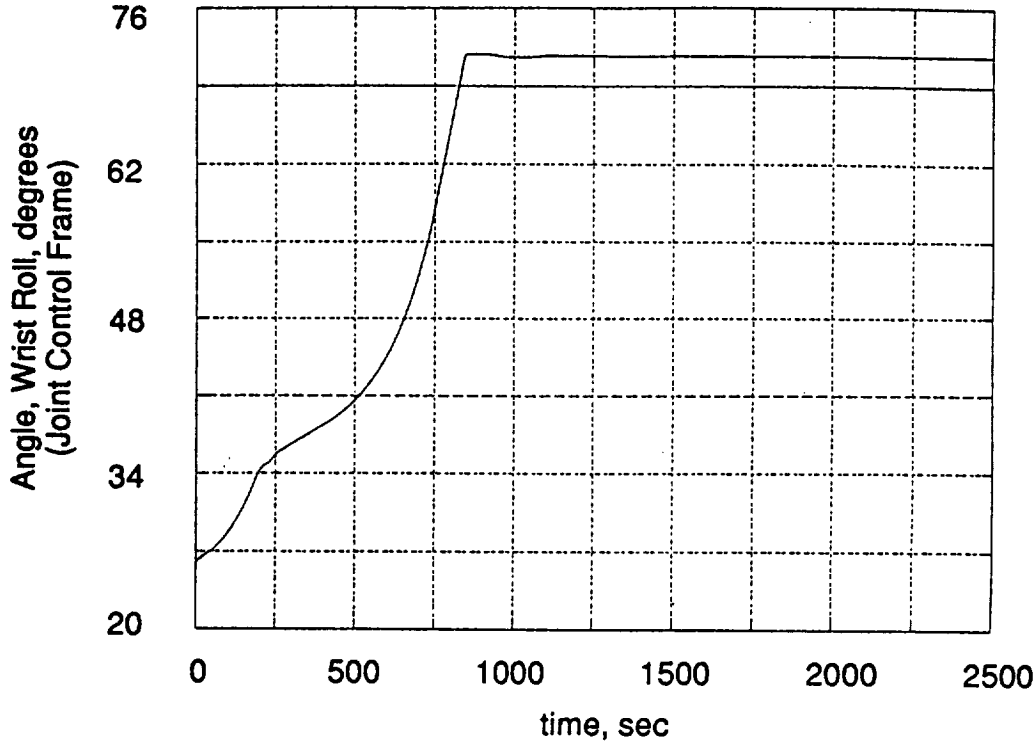

Figure 8-9.- Angle, wrist roll.

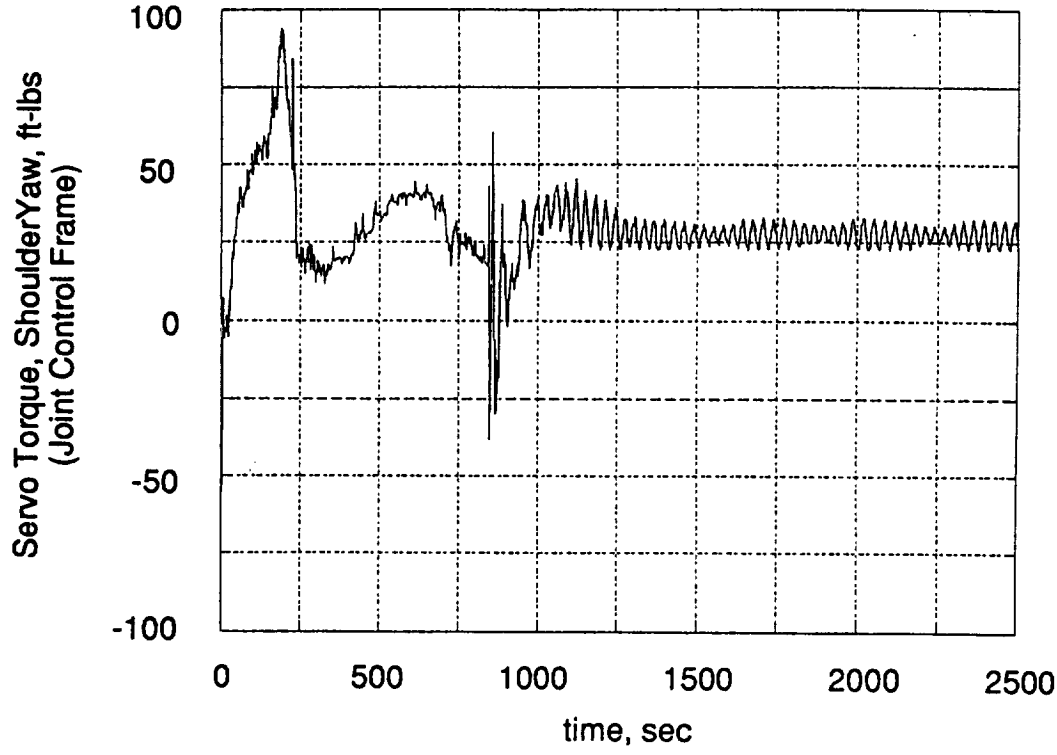

Figure 8-10.- Servo torque, shoulder yaw.

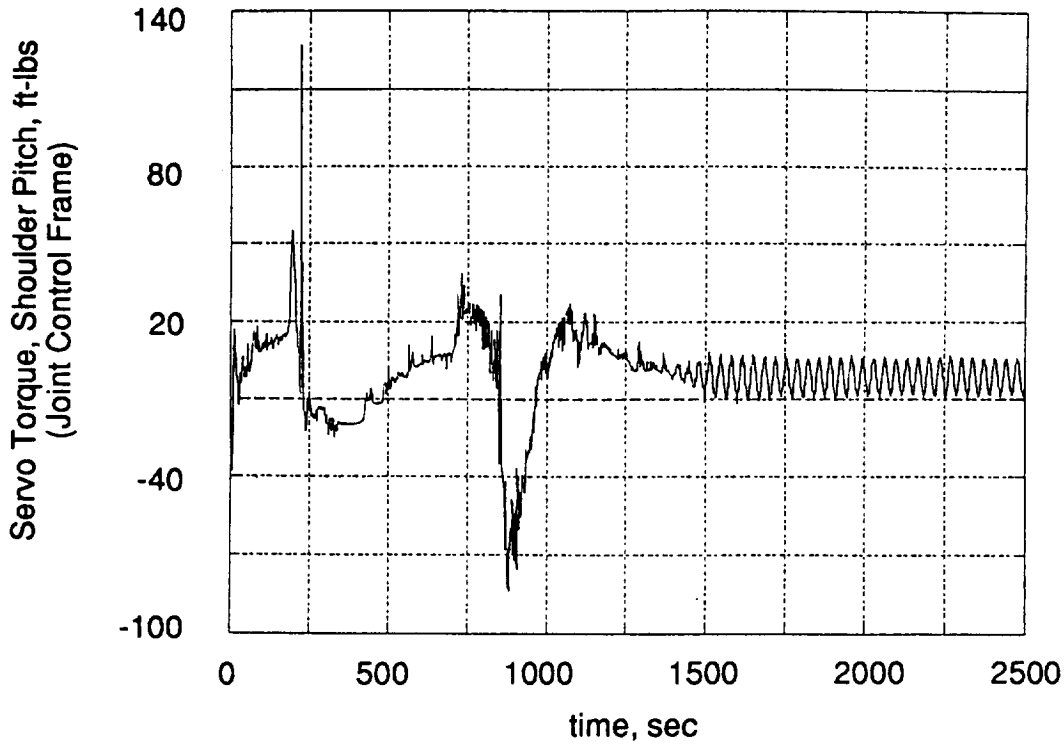

Figure 8-11.- Servo torque, shoulder pitch.

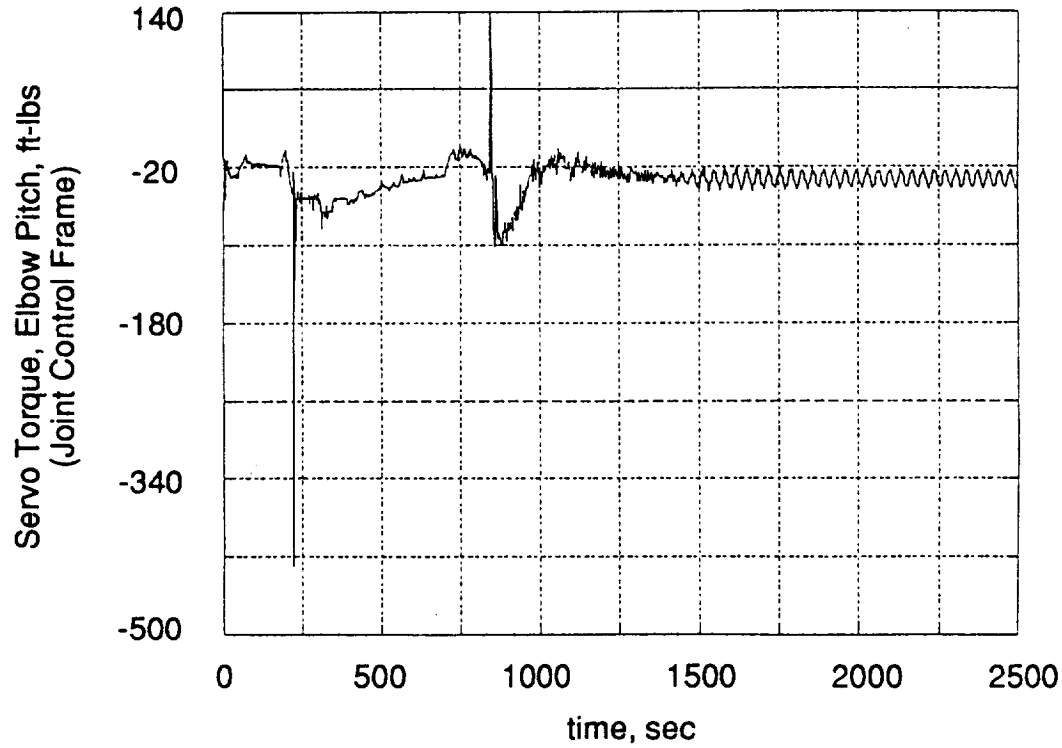

Figure 8-12.- Servo torque, elbow pitch.

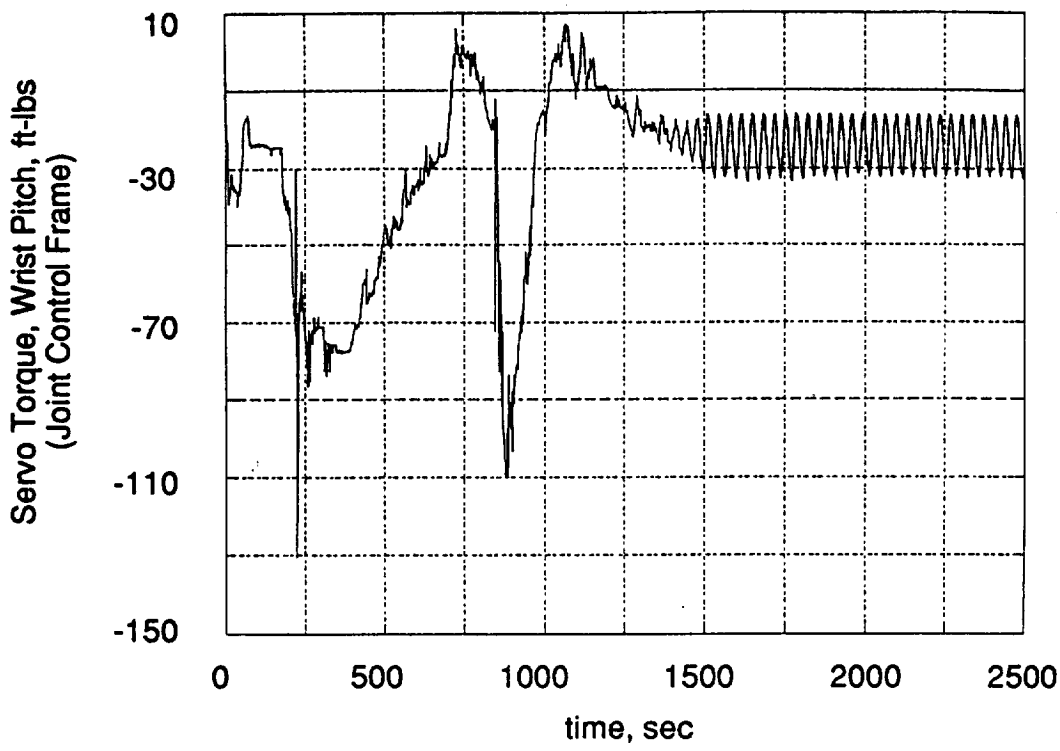

Figure 8-13.- Servo torque, wrist pitch.

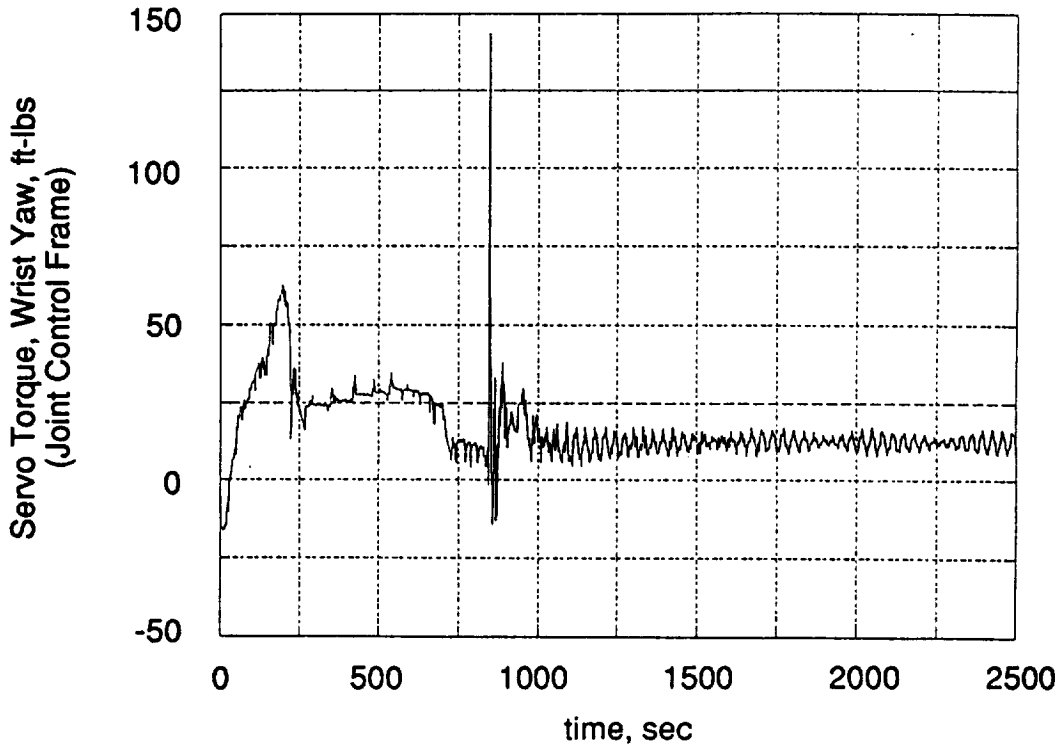

Figure 8-14.- Servo torque, wrist yaw.

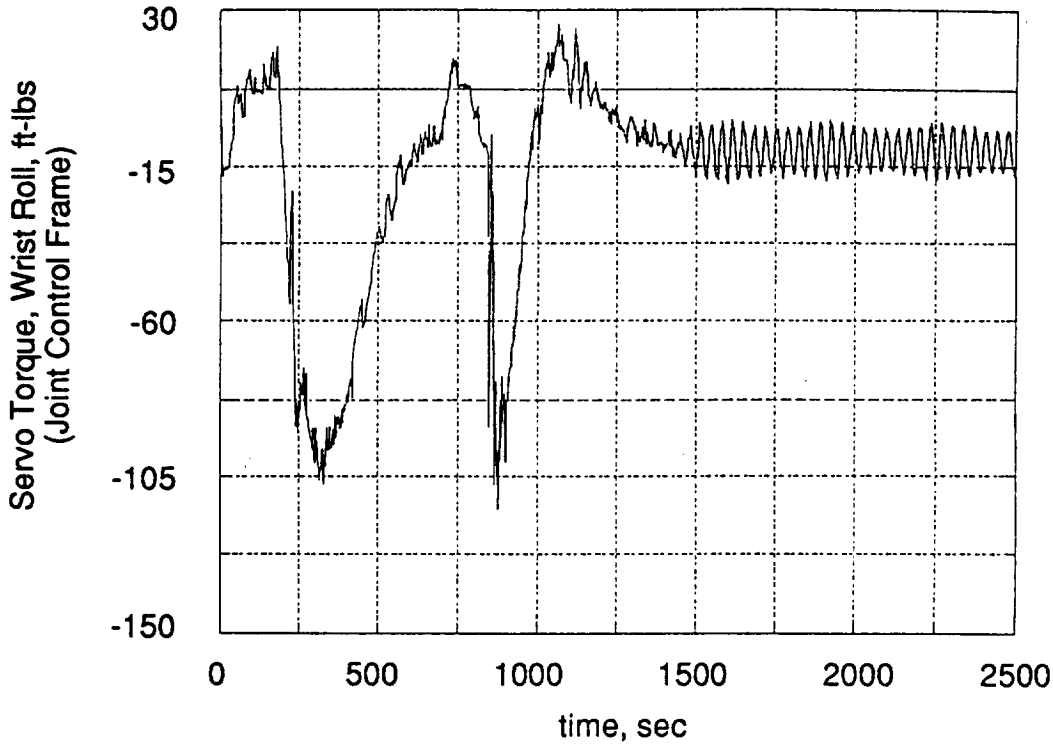

Figure 8-15.- Servo torque, wrist roll.

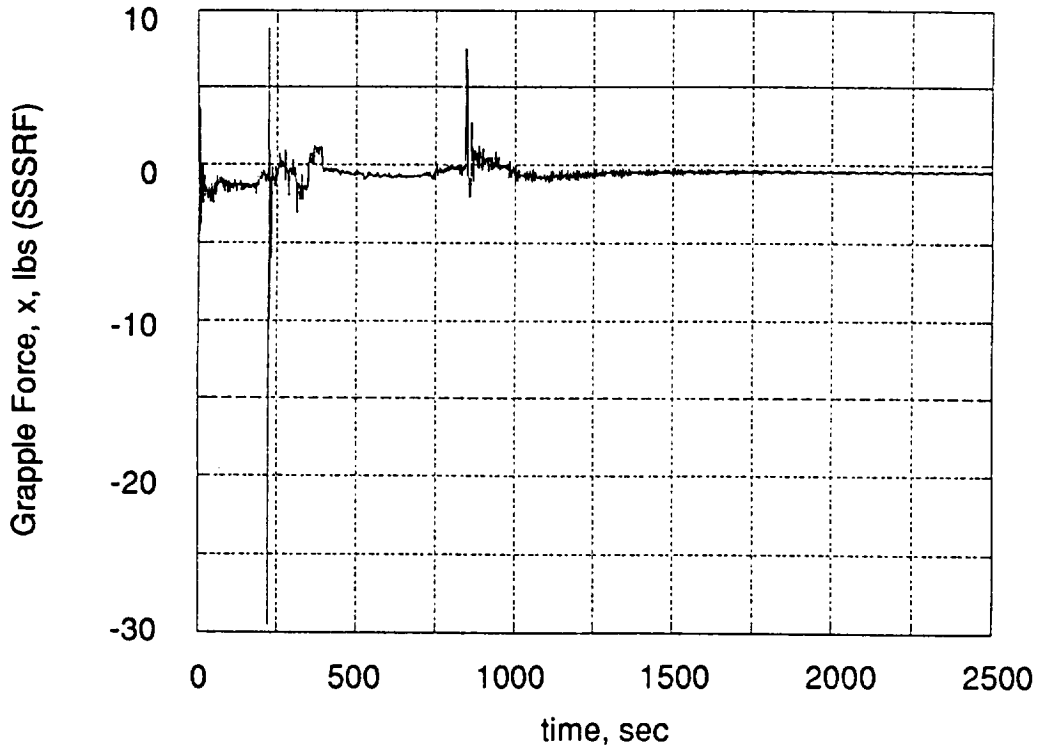

Figure 8-16.- Force at grapple point, x.

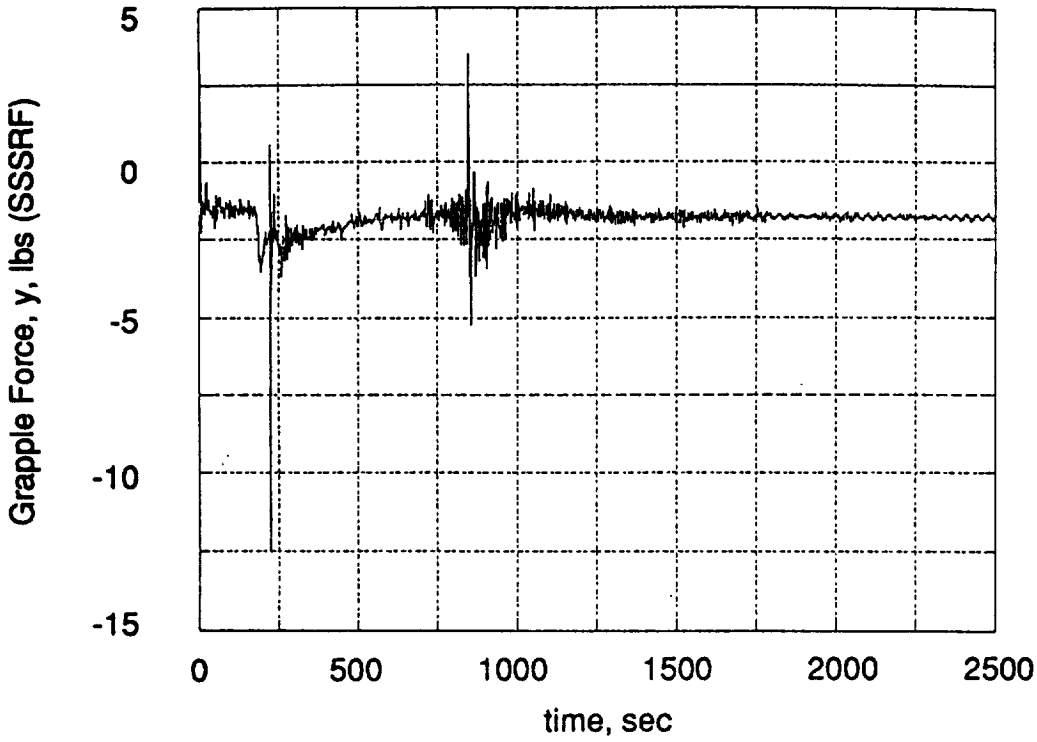

Figure 8-17.- Force at grapple point, y.

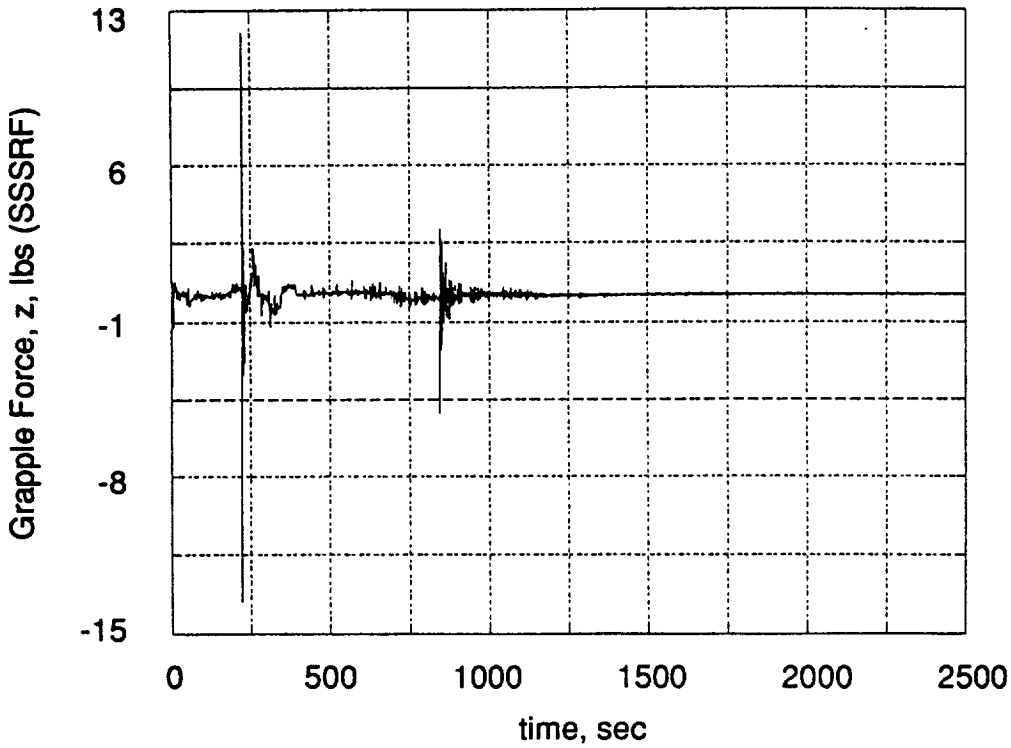

Figure 8-18.- Force at grapple point, z.

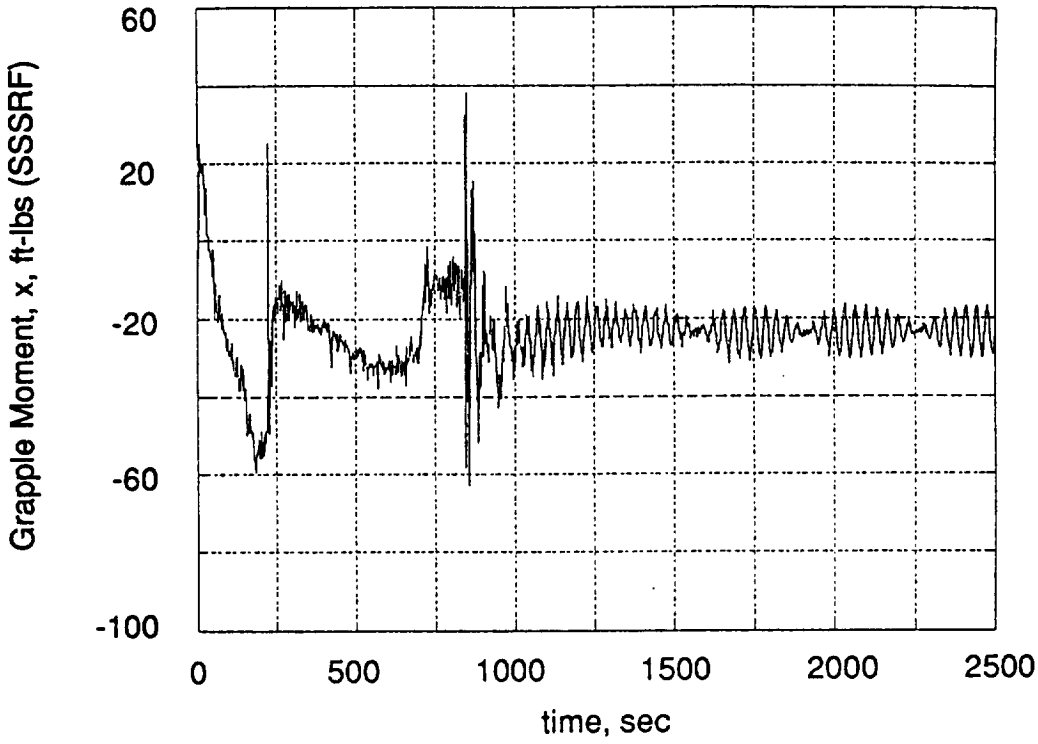

Figure 8-19.- Moment at grapple point, x.

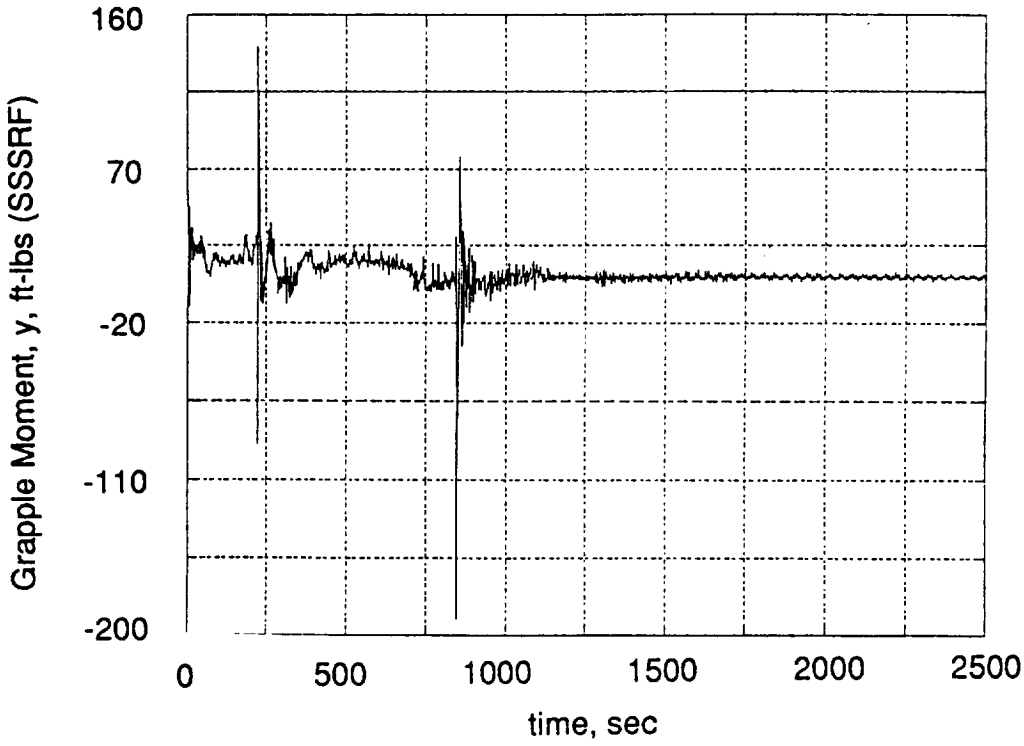

Figure 8-20.- Moment at grapple point, y.

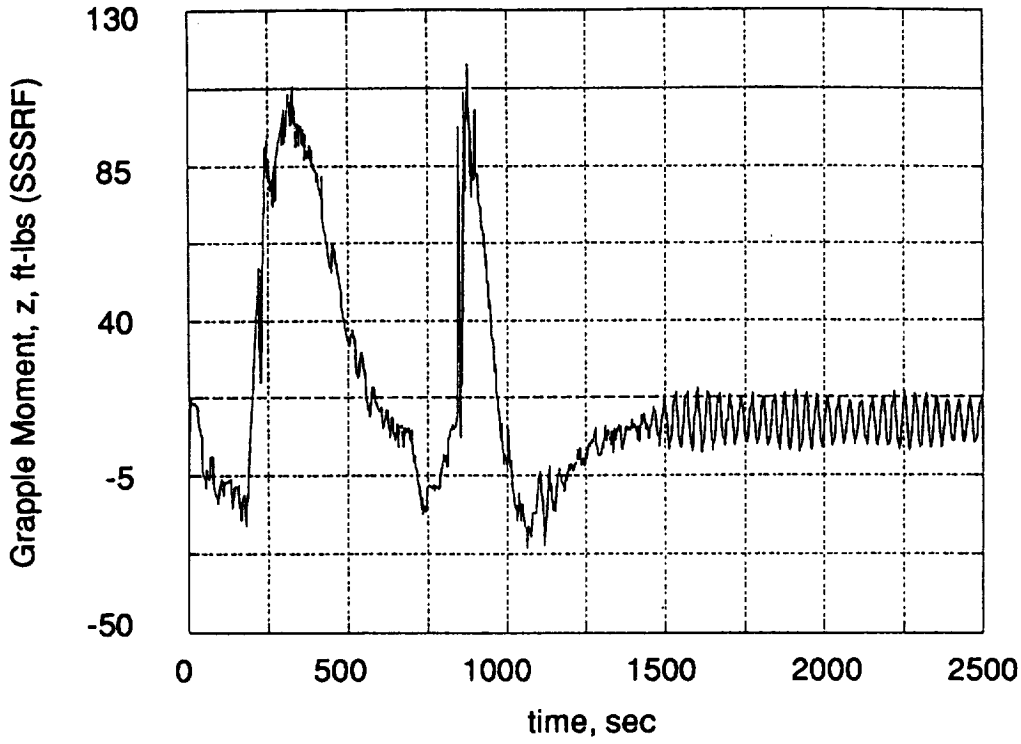

Figure 8-21.- Moment at grapple point, z.

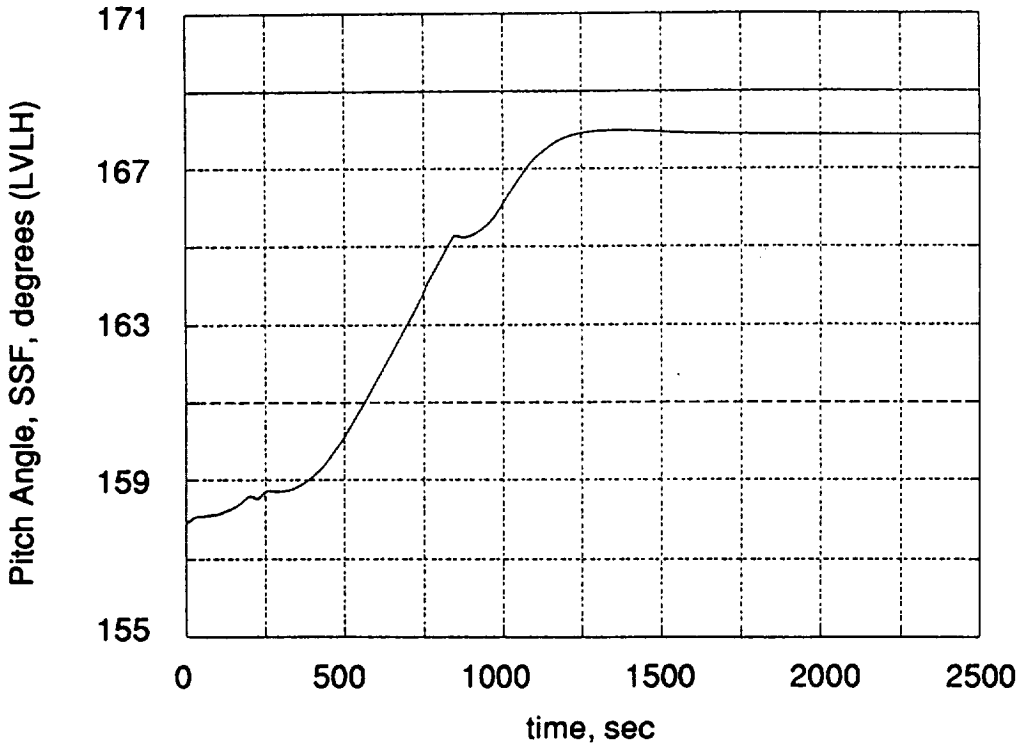

Figure 8-22.- Pitch angle, SSF.

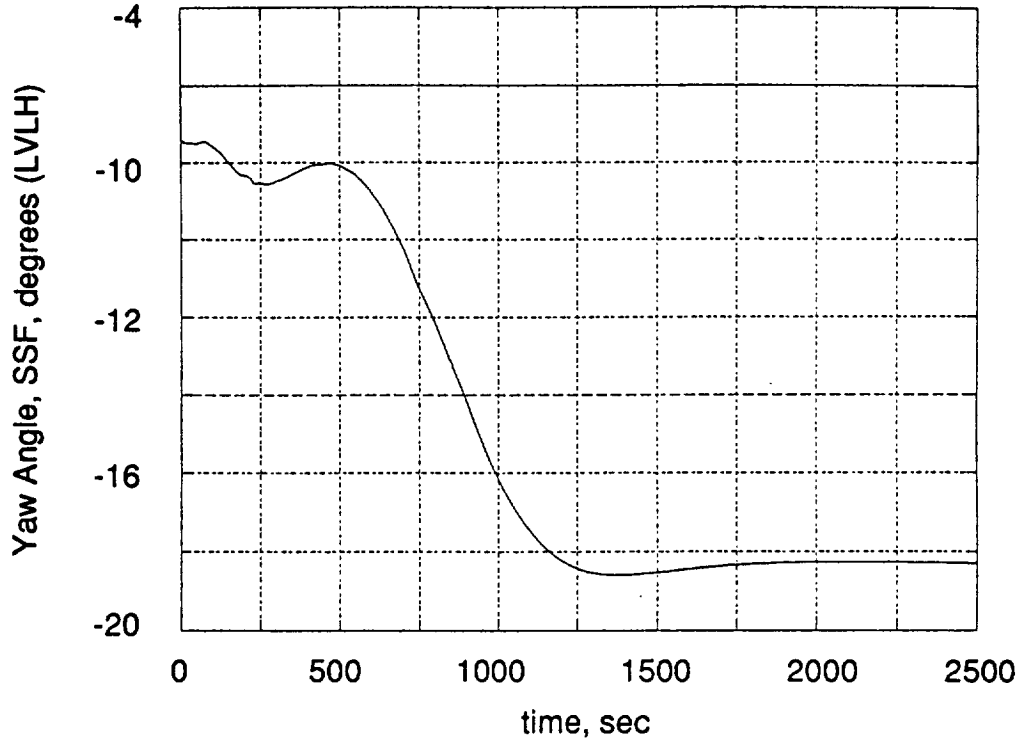

Figure 8-23.- Yaw angle, SSF.

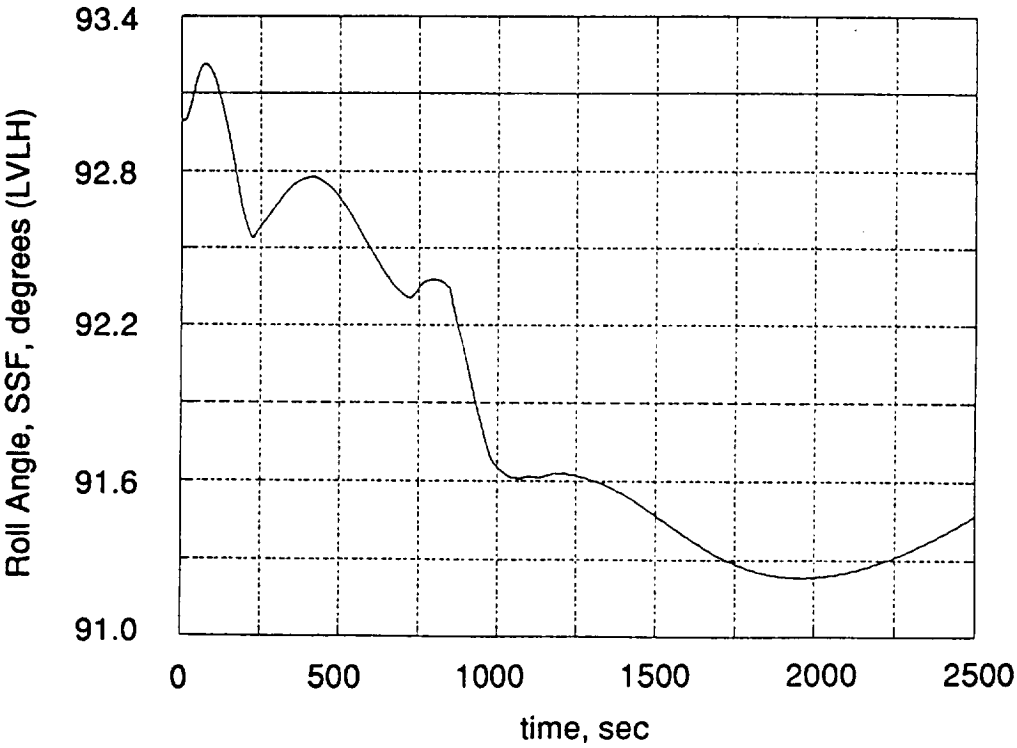

Figure 8-24.- Roll angle, SSF.

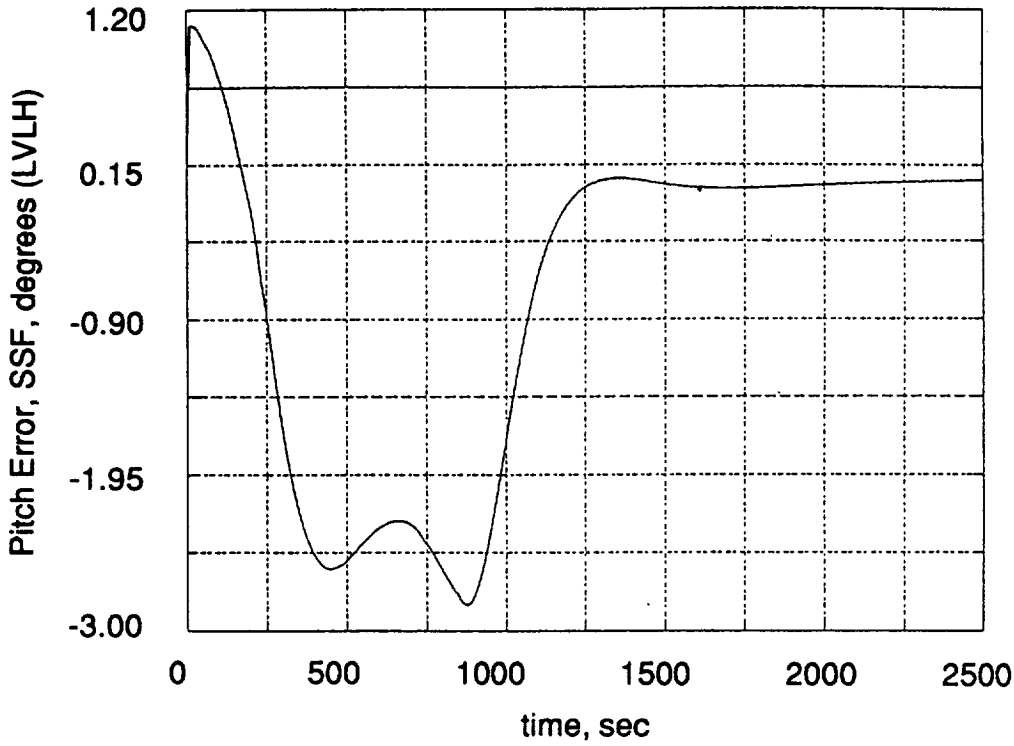

Figure 8-25.- Pitch error.

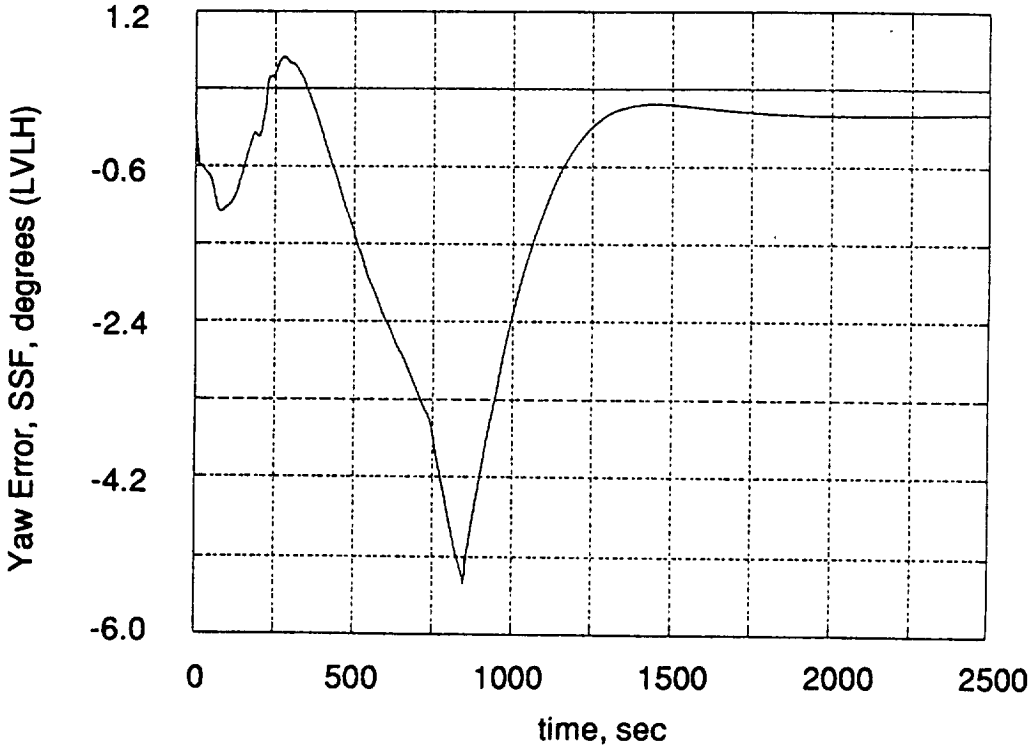

Figure 8-26.- Yaw error.

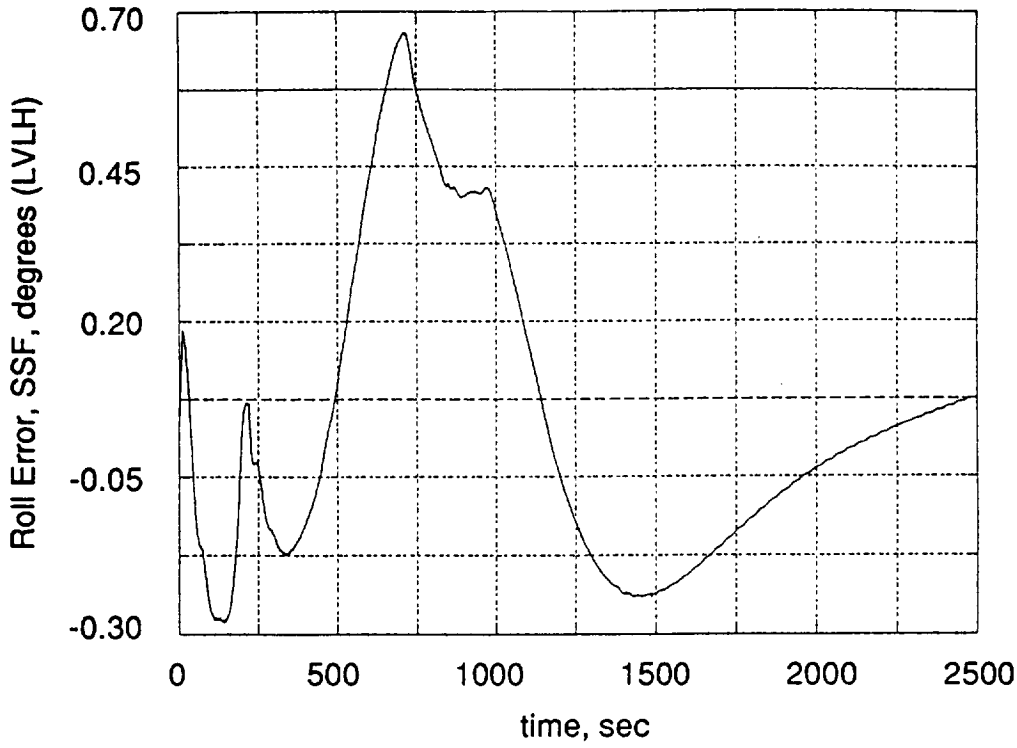

Figure 8-27.- Roll error.

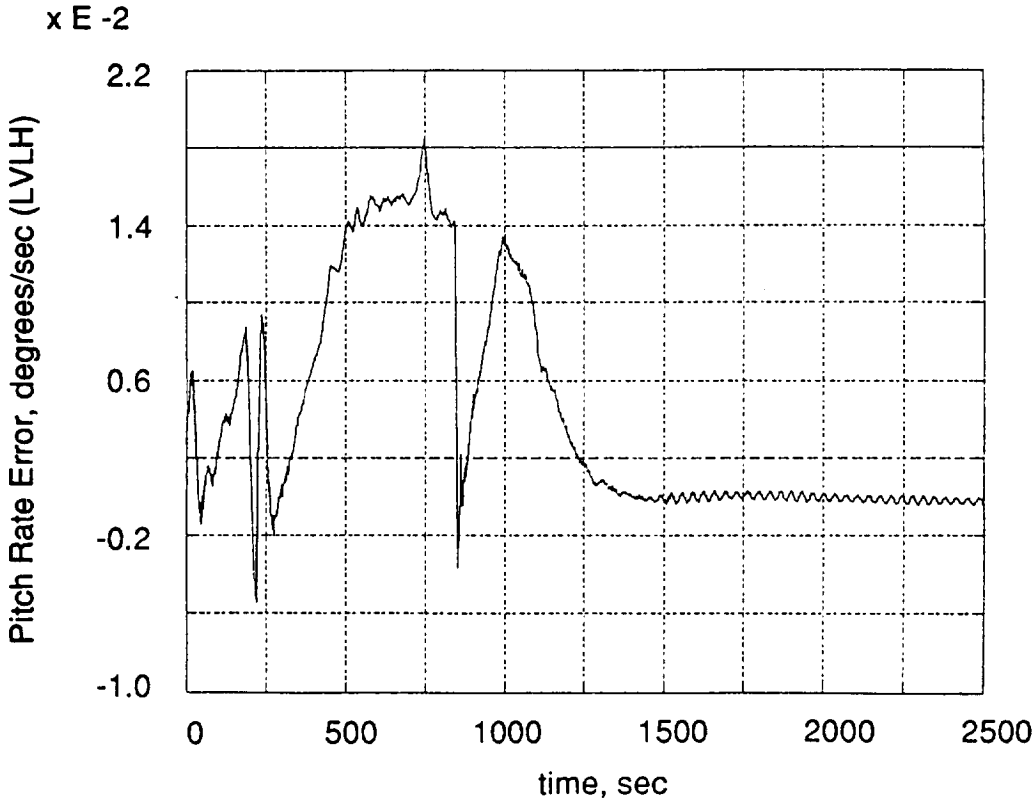

Figure 8-28.- Pitch rate error.

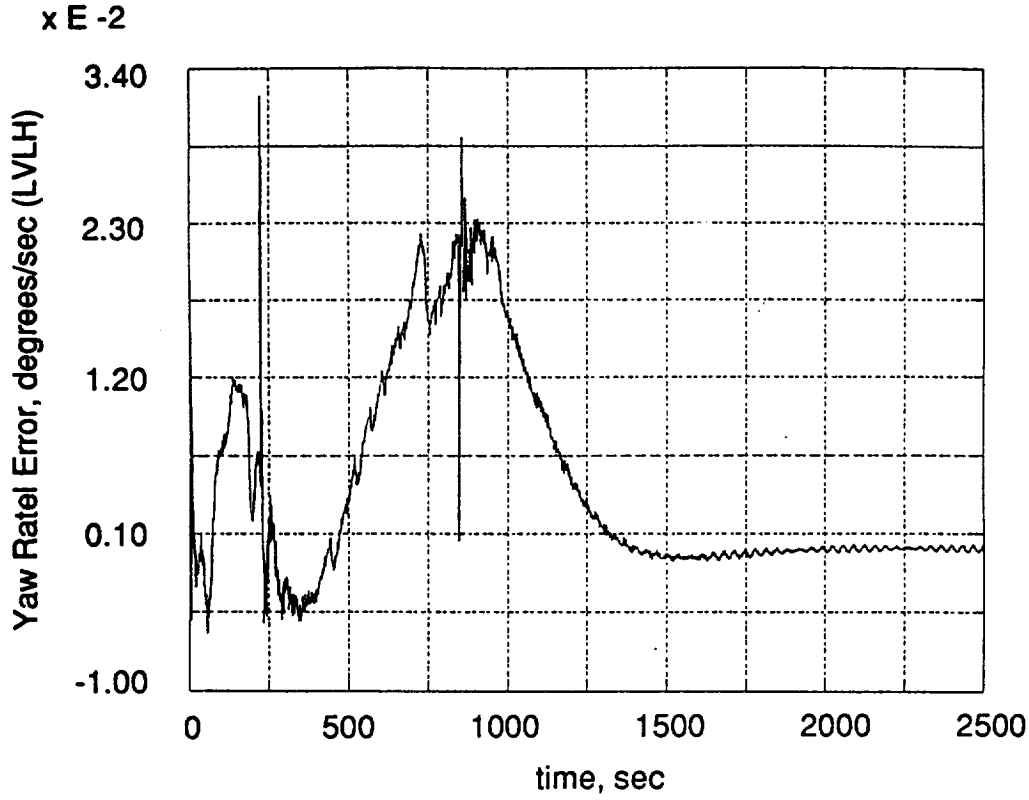

Figure 8-29.- Yaw rate error.

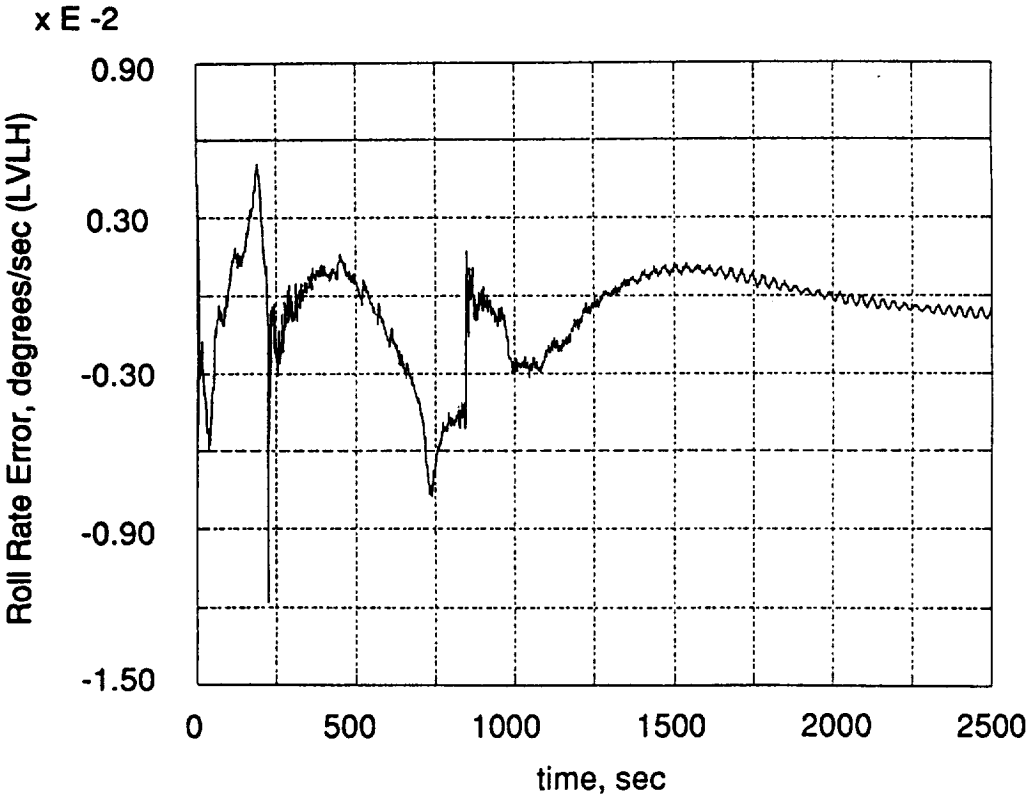

Figure 8-30.- Roll rate error.

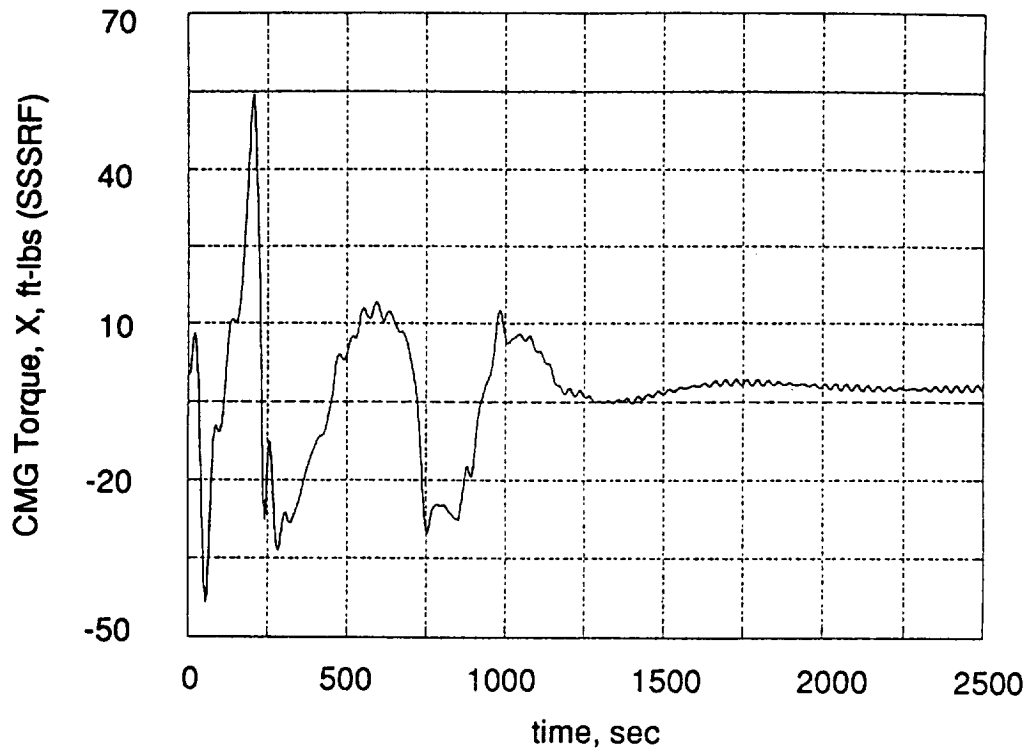

Figure 8-31.- Commanded torque, CMG, x.

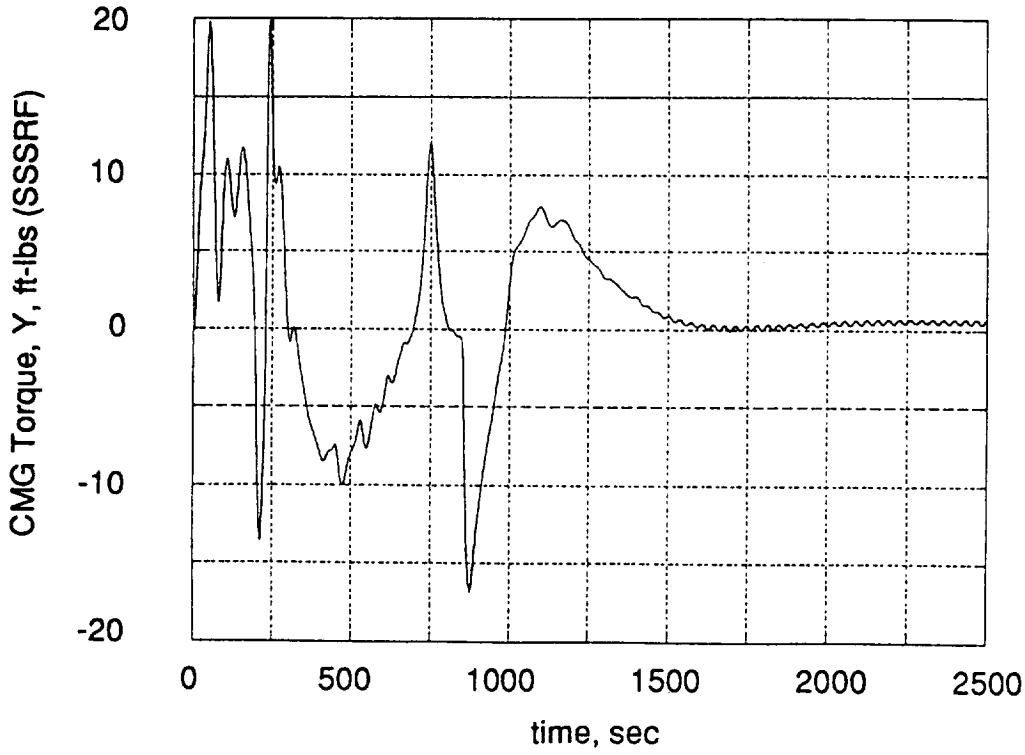

Figure 8-32.- Commanded torque, CMG, y.

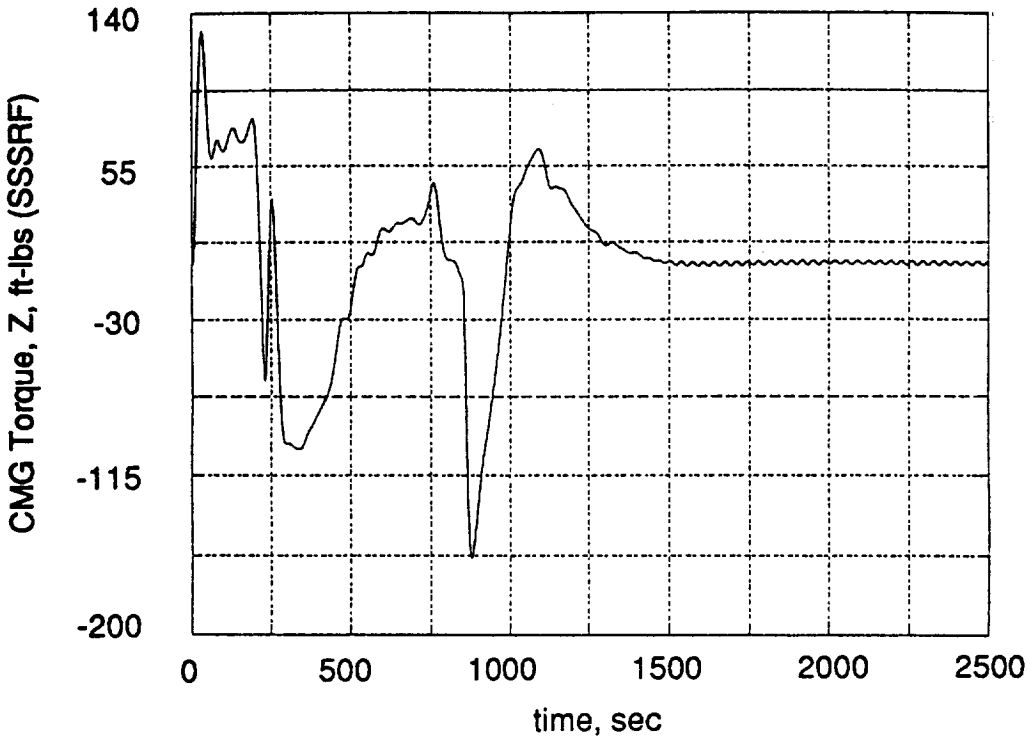

Figure 8-33.- Commanded torque, CMG, z.

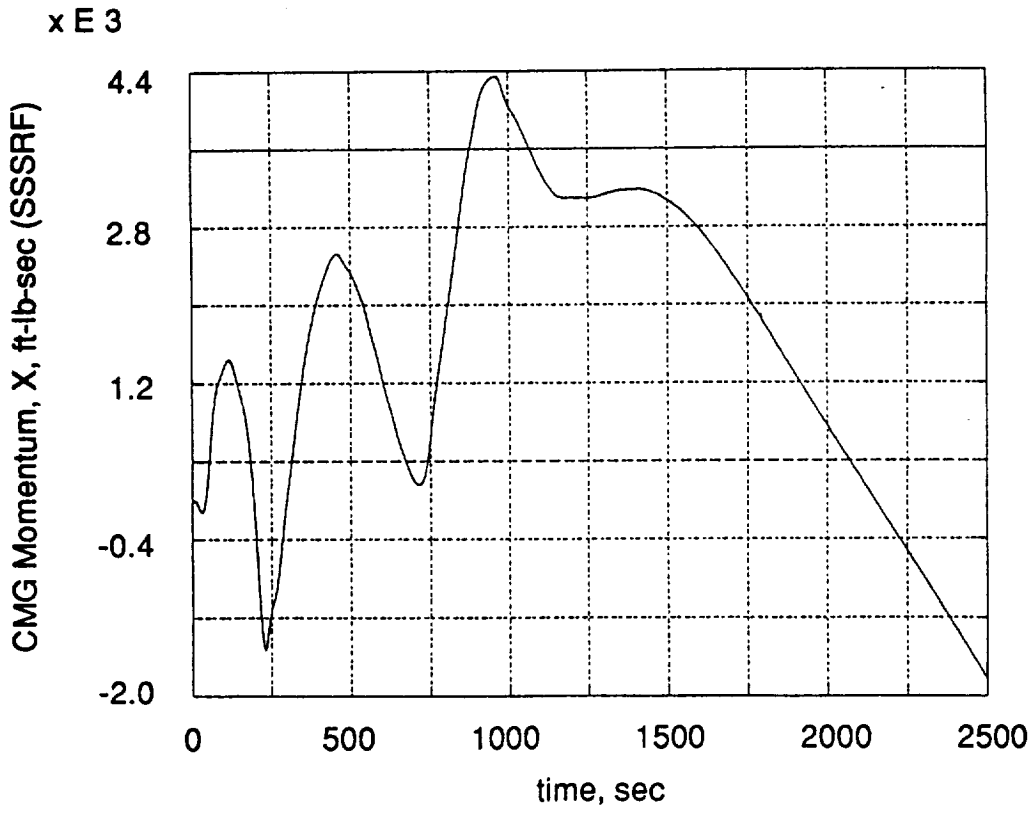

Figure 8-34.- CMG momentum, x.

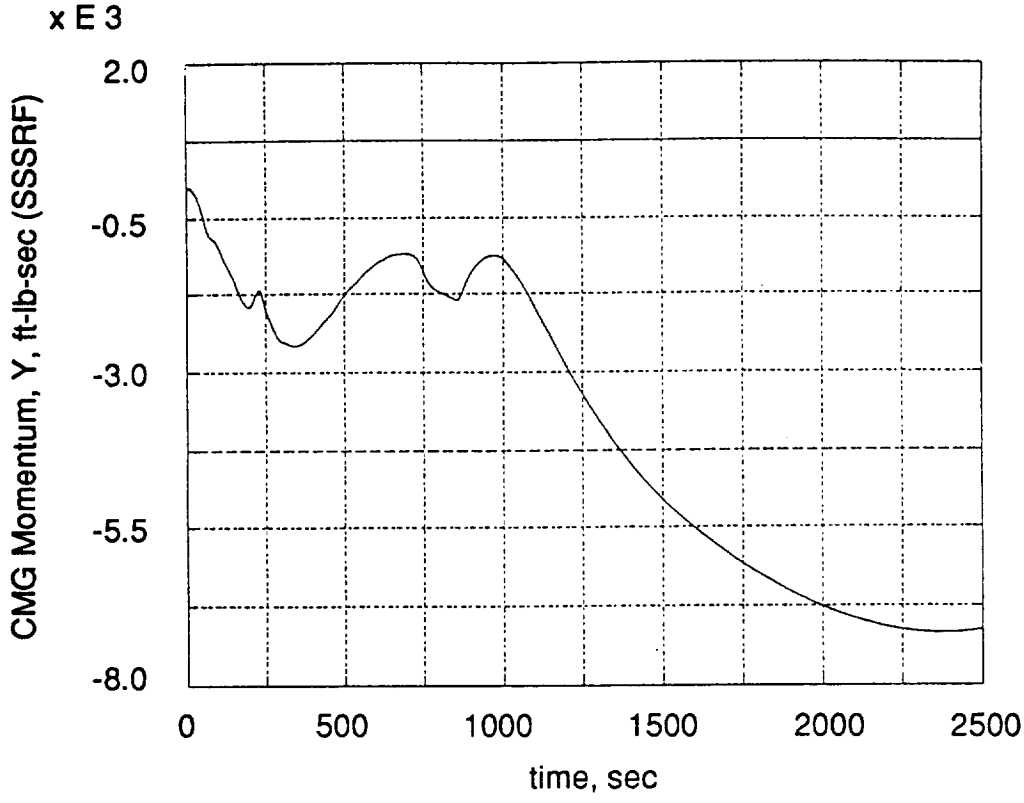

Figure 8-35.- CMG momentum, y.

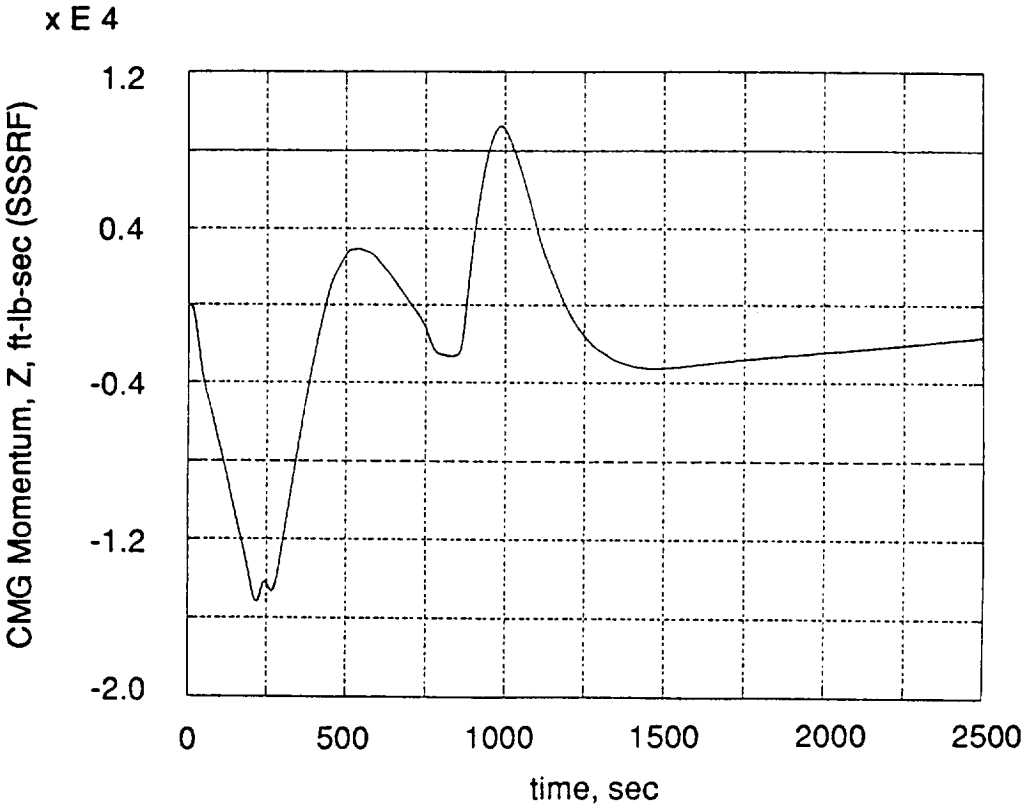

Figure 8-36.- CMG momentum, z.

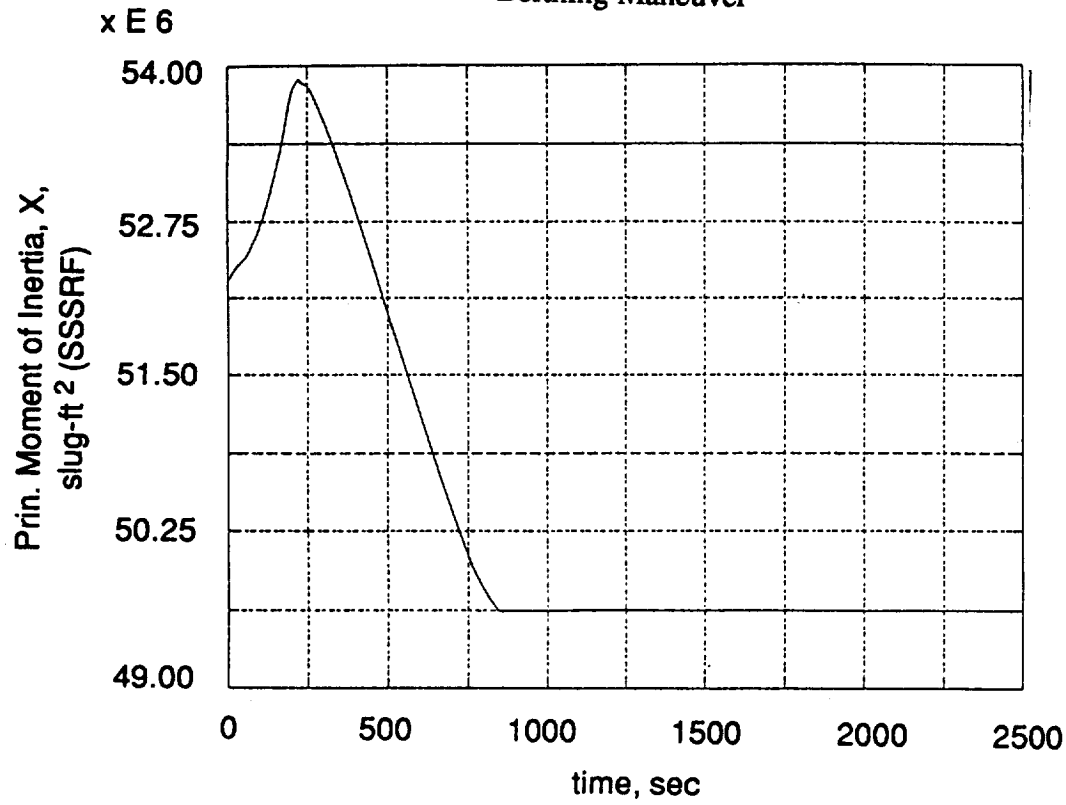

Figure 8-37.- Principal moment of inertia, x.

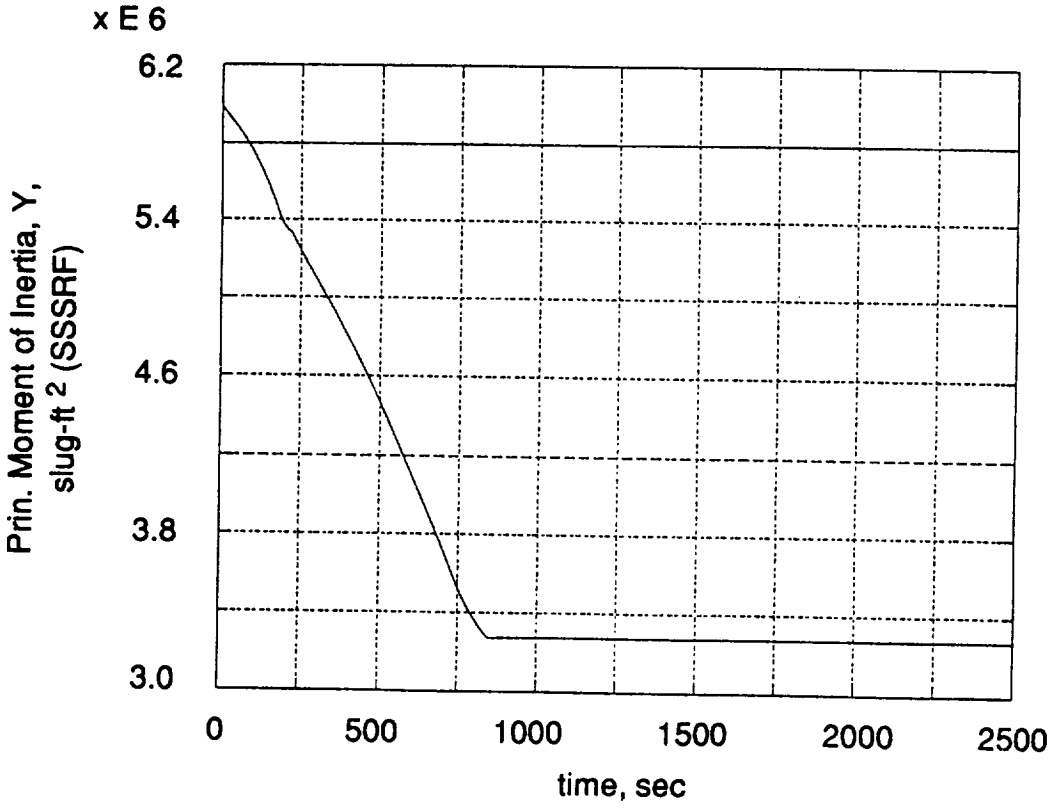

Figure 8-38.- Principal moment of inertia, y.

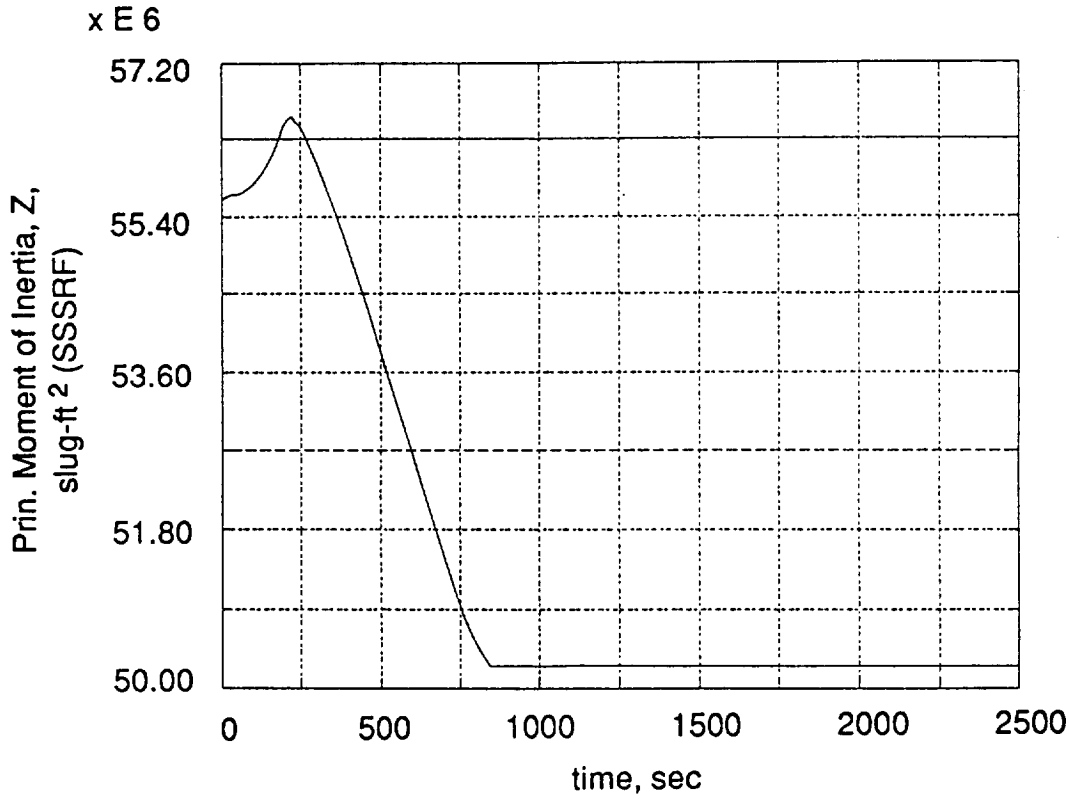

Figure 8-39.- Principal moment of inertia, z.

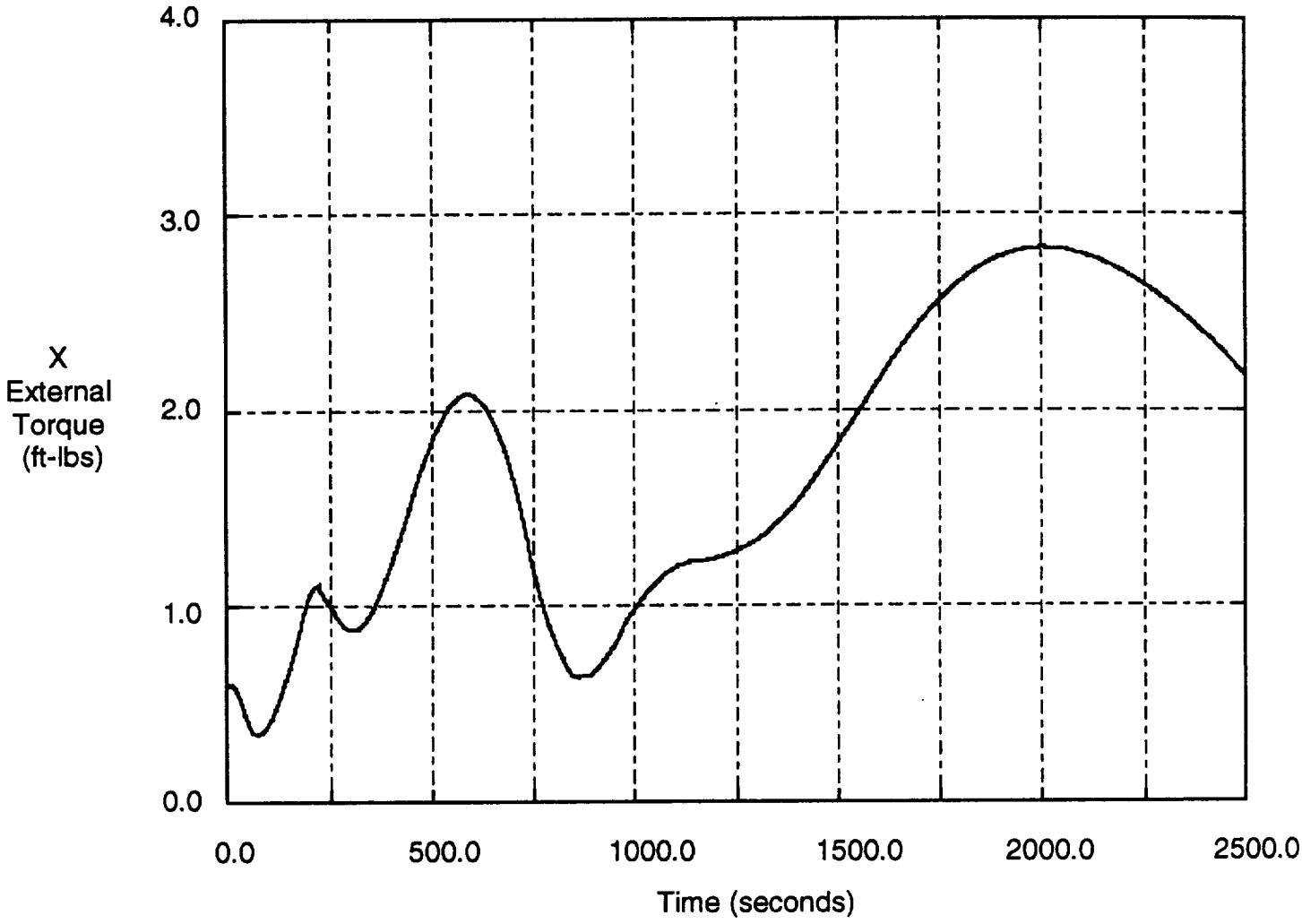

Figure 8-40. External disturbance torque, X component in SSSRF coordinates.

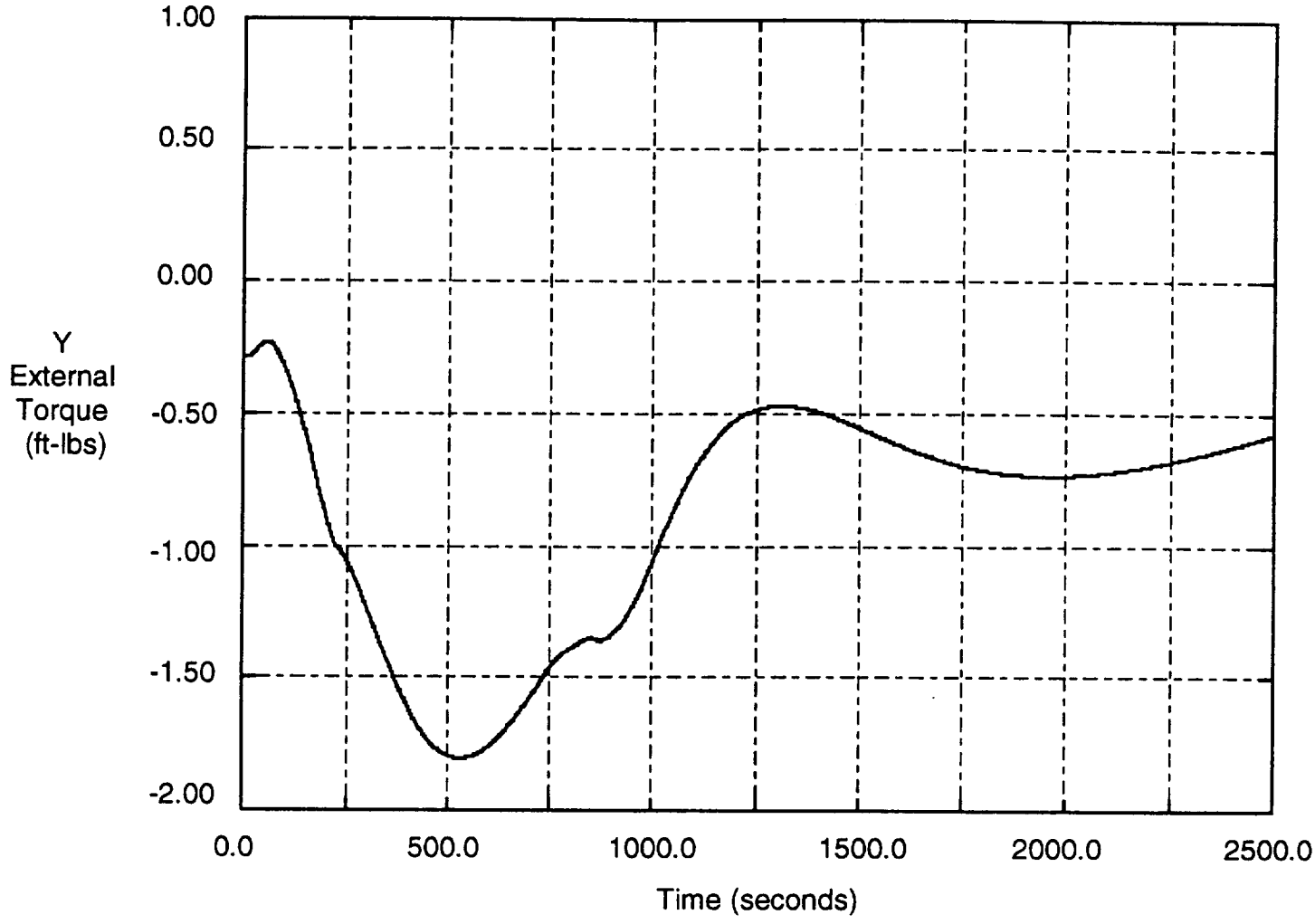

Figure 8-41. External disturbance torque, Y component in SSSRF coordinates.

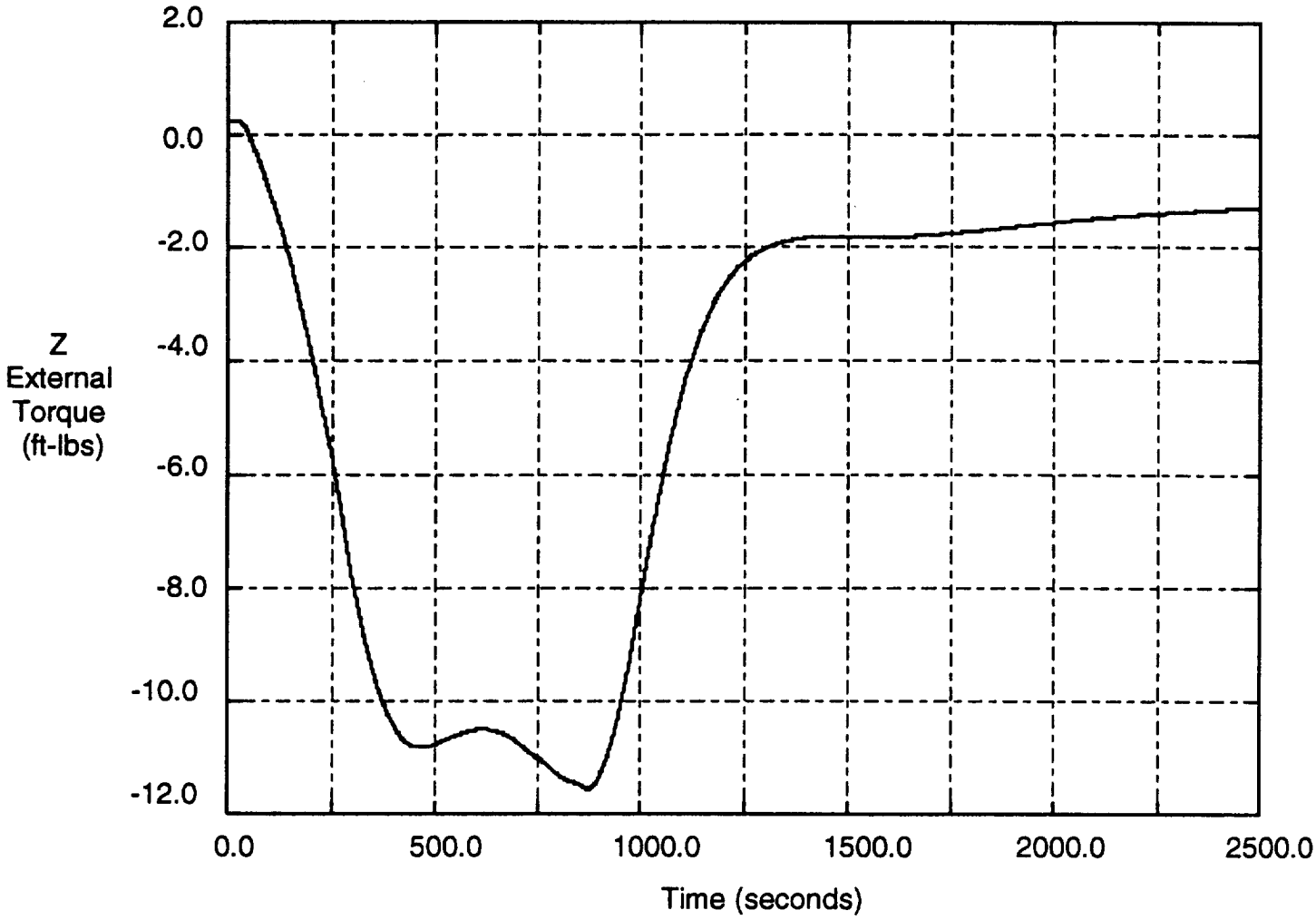

Figure 8-42. External disturbance torque, Z component in SSSRF coordinates.

9.0 CONCLUDING REMARKS

A large-angle, flexible, multi-body, dynamic modeling capability was developed to help validate numerical simulations of the dynamic motion and control forces which occur during berthing of early build configurations of SSF to the Shuttle Orbiter. The paper describes the dynamics and control of the station, the attached SRMS, and the Shuttle Orbiter during two maneuvers. The first is a maneuver from a gravity-gradient configuration to a torque equilibrium configuration using station reaction control jets, and the second is the subsequent berthing of the station to the Orbiter with the station CMGs actively maintaining attitude.

The SSF RCS successfully established a torque equilibrium attitude for the station/arm/Orbiter stack with only a small amount of brake slip. During the berthing maneuver, the CMGs were able to track the required changing TEA given a small initial bias. The elastic behavior of the station and of the SRMS during the maneuvers was investigated and found to have only a minor influence on the attitude control of the system stack during the maneuvers. The control loads did not cause excessive internal structural loads and dynamic response.

10.0 REFERENCES

1-1. Kilby, Mark; Lin, Yeong-Ching; and Jalal Mapar: "Station Orbiter Multibody Berthing Analysis (Preliminary Results)", DYNACS-92-HR1, Dynacs Engineering Company, Inc., Houston, Texas, February 14, 1992.

1-2. Hua, T.; Kubiak, E.; Lin, Yeong-Ching; Kilby, M.; and J. Mapar: "Control/Structure Interaction During Space Station Freedom-Orbiter Berthing", NASA Conference Publication 3177, Fifth NASA/DoD Controls-Structures Interaction Technology Conference, Lake Tahoe, Nevada, March 3-5, 1992.

1-3. SSFP PDR Loads Data Book, Volume II: On Orbit Loads, SSJ 10450, NASA Johnson Space Center, September 15, 1991.

1-4. Cooper, Paul A.; Stockwell, Alan E.; and Shih-Chin Wu: "Space Station/Orbiter Berthing Dynamics During an Assembly Flight", NASA TM 109049, December 1993.

1-5. Honeywell Space and Strategic Systems Operation, Clearwater, Florida, "MDSSC Space Station Program Interim Design Review #6", May 1991.

1-6. Garrison, James L.; and Raymond C. Montgomery: "Space Station Freedom Attitude Control During Orbiter Berthing", Ninth VPI&SU Symposium on Dynamics and Control of Large Structures, Virginia Polytechnic Institute and State University, Blacksburg, Virginia, May 10-12, 1993.

1-7. JSC-25134, "Payload Deployment and Retrieval System Simulation Database", Version 1.0, Flight Support Equipment, RMS Operations, NASA Johnson Space Center, Houston, TX, July 1, 1991.

1-8. Gray, C.; et. al.: "Validation of the Draper RMS Simulation (DRS) Against Flight Data", CSDL-R-1755, Volume 1-2, The Charles Stark Draper Laboratory, Cambridge, Massachusetts, April, 1985.

1-9. Cooper, Paul A.; and Martha E. Demeo: "Berthing of the Space Station Freedom Using the Shuttle Remote Manipulator System" Presented at *Selected Topics in Robotics for Space Exploration Workshop,* NASA Langley Research Center, Hampton, Virginia, March 17, 1993.

1-10. Space Station Freedom Program IDEAS**2 Users Guide, Version SSP 2.0, SSE-E-88-R24 Grumman Space Systems, October 31, 1988.

1-11. DADS User's Manual, Revision 6.5, Computer Aided Design Software, Inc., Oakdale, Iowa, March 1991.

2-1. SSFP PDR Loads Data Book, Volume II: On Orbit Loads, SSJ 10450, NASA Johnson Space Center, September 15, 1991.

2-2. MSC/NASTRAN User's Manual, Version 67, The MacNeal-Schwendler Corporation, August 1991.

2-3. JSC-25134, "Payload Deployment and Retrieval System Simulation Database", Version 1.0, Flight Support Equipment, RMS Operations, NASA Johnson Space Center, Houston, TX, July 1, 1991.

3-1. JSC-12770, "Shuttle Flight Operations Manual: Volume 16 - Payload Deployment and Retrieval System", Flight Operations Directorate, NASA Johnson Space Center, Houston, TX, June 1, 1981.

3-2. STS-87-0017D, "Space Shuttle Operation Level C Functional Subsystem Software Requirements Document Remote Manipulator System (RMS)", OI20, Revision D, March 15, 1991, The Charles Stark Draper Laboratory, Inc., Cambridge, MA 02139.

3-3. JSC-25134, "Payload Deployment and Retrieval System Simulation Database", Version 1.0, Flight Support Equipment, RMS Operations, NASA Johnson Space Center, Houston, TX, July 1, 1991.

3-4. Keene, Donald, "An Improved Joint Friction Model for the Space Shuttle Remote Manipulator Simulation", RMS MEMO 80-4, The Charles Stark Draper Laboratory, Inc., Cambridge, MA, April 7, 1980.

4-1. Jacchia, L. G.: Revised Static Models of the Thermosphere and Exosphere with Empirical Temperature Profiles. Smithsonial Astrophysical Observatory Special Report No. 332, 1971. as referenced in Space Station Freedom IDEAS-squared Users Guide, Grumman Space Systems, October 31, 1988.

4-2. Space Station Freedom Program IDEAS**2 Users Guide, Version SSP 2.0, SSE-E-88-R24 Grumman Space Systems, October 31, 1988.

5-1. MDSSC Space Station Program Interim Design Review, Honeywell Space and Strategic Systems Operation, May 29-31, 1991, Clearwater, FL.

5-2. Guidance, Navigation and Control/Propulsion System Software Flight System Software Requirements Document, Volume 1, Space System Freedom Program, SSJ 10550, NASA Johnson Space Center, February 27, 1992.

5-3. Space Station Freedom Guidance, Navigation and Control System Detailed Design Review Summary Presentation Package, McDonnell Douglas Space Systems Company and Honeywell Space and Strategic Systems Operation, November 2-6, 1992.

5-4. Montgomery, Raymond C.; and Shih-Chin Wu: Simulation of the Attitude Determination System for Space Station Berthing Dynamics Research. Presented at the Symposium on Dynamics and Control of Large Structures, Virginia Polytechnic Institute and State University, Blacksburg, Virginia, May 10-12, 1993.

6-1. DADS User's Manual, Revision 6.5, Computer Aided Design Software, Inc., Oakdale, Iowa, March 1991.

6-2. MSC/NASTRAN User's Manual, Version 67, The MacNeal-Schwendler Corporation, August 1991.

APPENDIX A - COORDINATE SYSTEM DEFINITIONS

A-1 Inertial

This coordinate system, in which the system dynamic equations are integrated, is defined with the origin located at the combined stack center of mass at the initial time of the simulation. The Z_0 axis is defined along nadir, the vector from the center of mass of the system to the geometric center of the Earth. The Y_0 axis is defined along the vector perpendicular to the orbit plane in a direction opposite to that of the orbital angular momentum vector. The X_0 axis is defined such as to complete a right handed triad. If a circular orbit is assumed, X_0 would also be parallel to the initial spacecraft velocity vector. It is assumed that this coordinate system is a true inertial reference frame, i.e., it does not rotate with respect to the fixed stars.

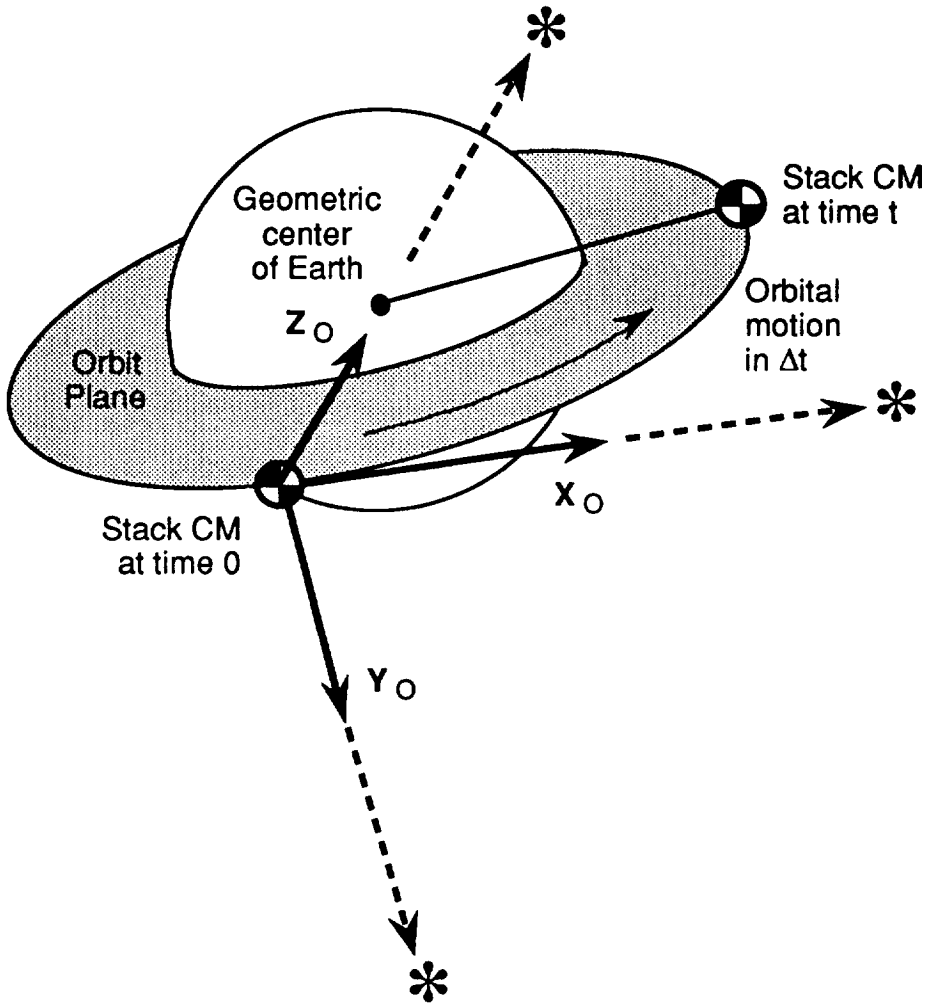

A-2 Local Vertical Local Horizontal (LVLH)

This coordinate system is defined with the origin located at the instantaneous center of mass of the stack configuration. The Z axis is defined along the instantaneous nadir, the vector from the spacecraft center of mass to the geometric center of the Earth. The Y axis is defined from the spacecraft center of mass along a direction perpendicular to the orbital plane in the opposite direction to the orbital angular momentum vector. The X axis is defined so as to complete a right handed triad. If a circular orbit is assumed, X would be parallel to the spacecraft's instantaneous velocity vector.

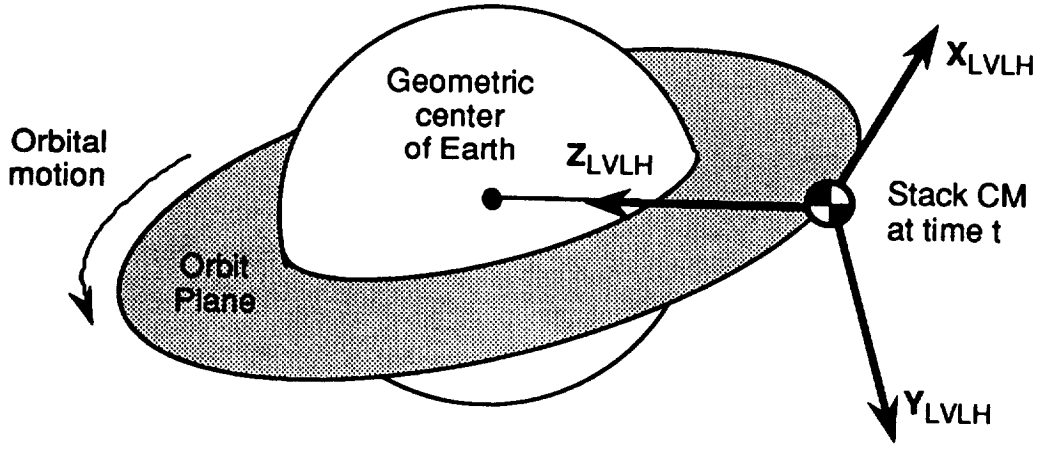

A-3 Space Station Structural Reference Frame (SSSRF)

This coordinate system, also identified as the Space Station Analysis Coordinate System, is a spacecraft body-fixed reference frame. Its origin is defined at the geometric center of the M1 pre-integrated truss segment. The X axis is defined parallel to the longitudinal axis of the modules. The Y axis is defined along the rotation axis of the alpha joint with positive in the direction of the starboard PV arrays. The Z axis is defined so as to complete a right handed triad.

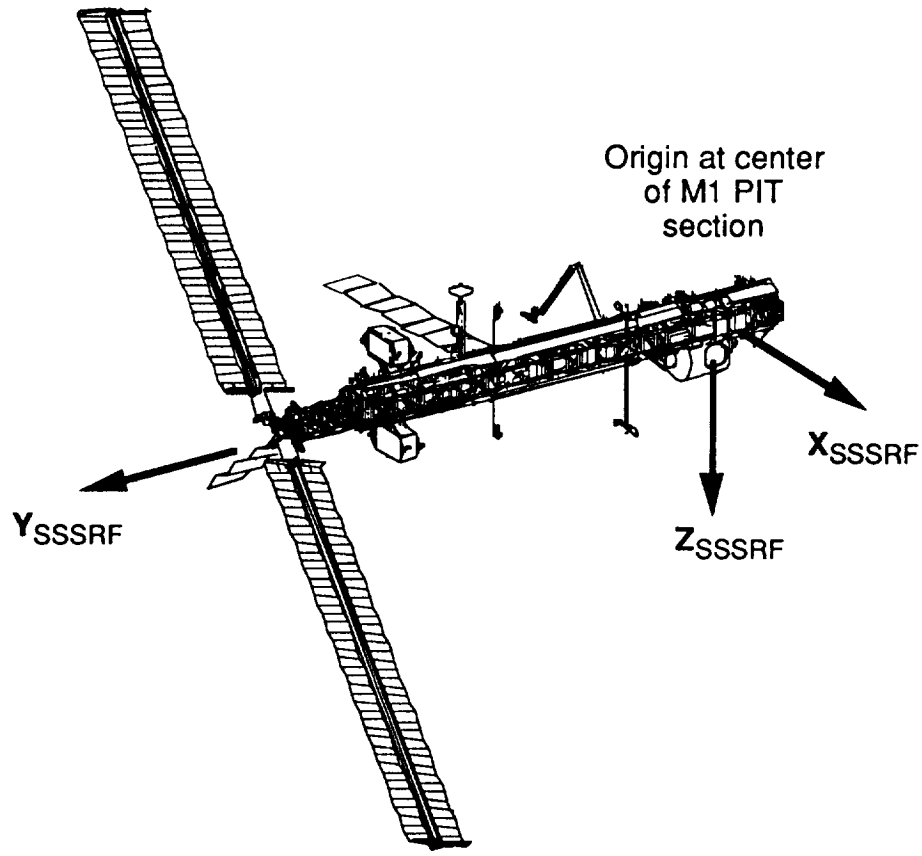

A-4 Space Station Body

This coordinate system is defined with the X, Y, and Z axis parallel to and in the same direction as those in the SSSRF, but with the origin located at the instantaneous center of mass of the combined stack configuration.

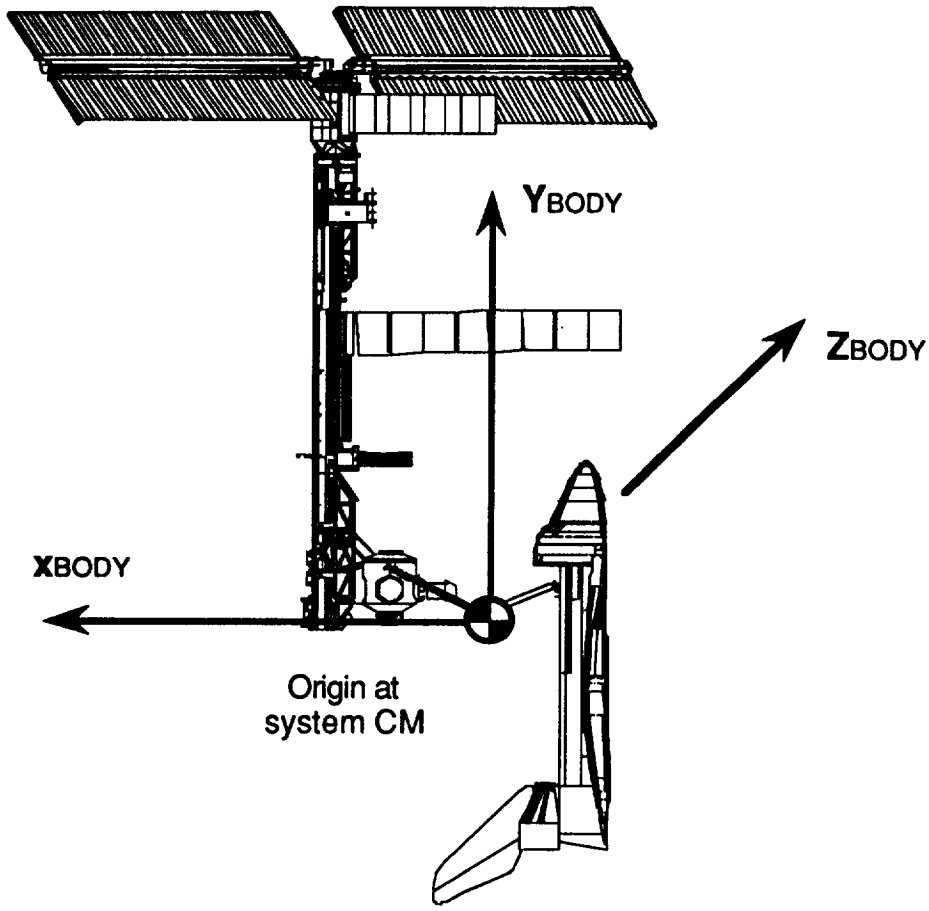

A-5 Orbiting Spacecraft Body

This coordinate system is a spacecraft body-fixed reference frame with its origin defined at the instantaneous center of mass of the combined stack configuration. At the initial time of the RCS simulation, when the stage 5 station is in a gravity gradient orientation, the X, Y, and Z axes are defined to be parallel to the LVLH axes, but spacecraft body-fixed. The Z axis is nadir, Y is perpendicular to the orbit plane, and X is defined to complete the right handed triad. This coordinate system is used inside of the orbital mechanics calculations.

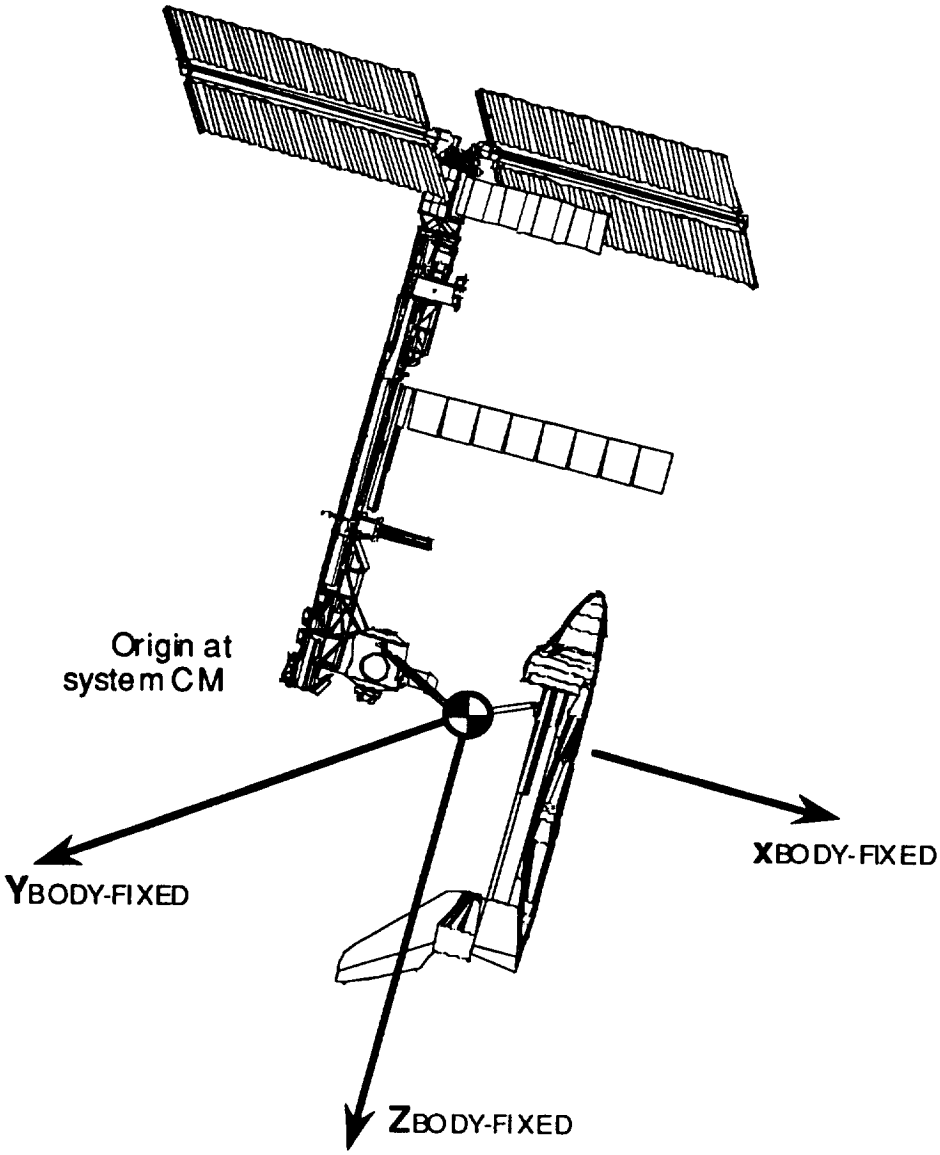

A-6 Orbiter Structural Reference (OSR)

This coordinate system is an Orbiter body fixed reference frame in which the X and Z axes lie in the Orbiter plane of symmetry. The origin is located 236 inches forward of the nose of the Orbiter and 400 inches below the centerline of the payload bay. X is defined parallel to the longitudinal axis of the payload bay, with positive towards the tail. The Z axis is defined to lie in the Orbiter plane of symmetry and be perpendicular to X with positive defined in the outward direction from the payload bay. The Y axis completes the right handed triad and thus is positive in the Orbiter port direction.

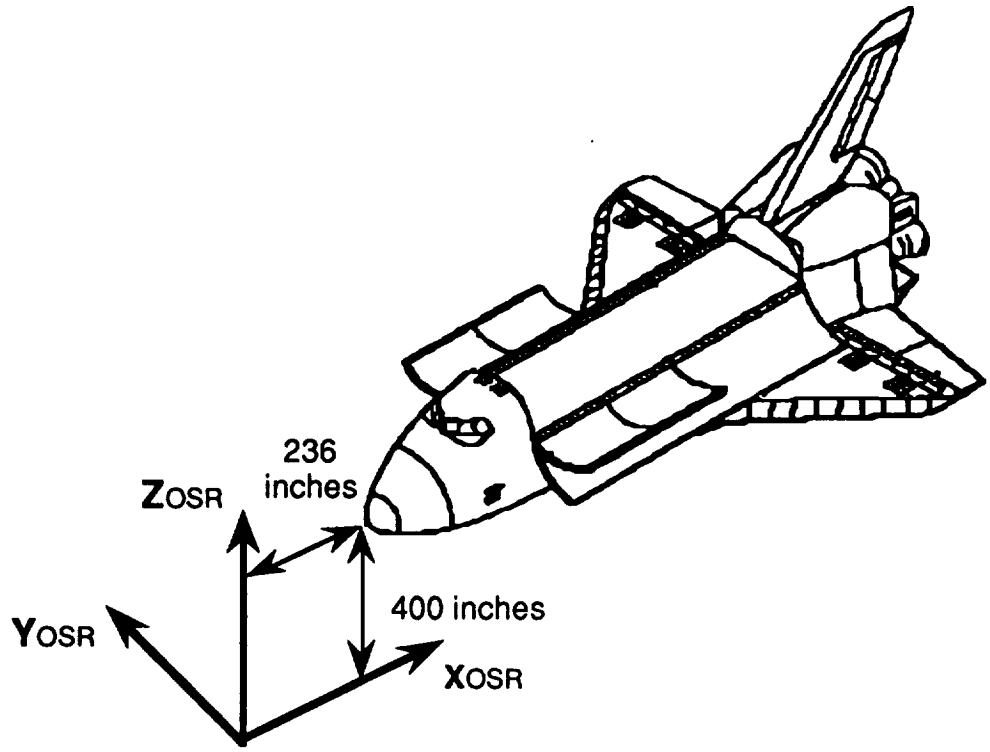

A-7 Orbiter Body Axis System (OBAS)

This coordinate system is an Orbiter body fixed reference frame in which the X and Z axes lie in the plane of symmetry. The origin is located 236 inches forward of the nose of the Orbiter and 400 inches below the centerline of the payload bay. The X, Y and Z axes are defined parallel to those in the OSR coordinate system, but with the direction of the X axis in the direction of the Orbiter's flight path and the direction of the Z axis such that negative is in the outward direction from the payload bay.

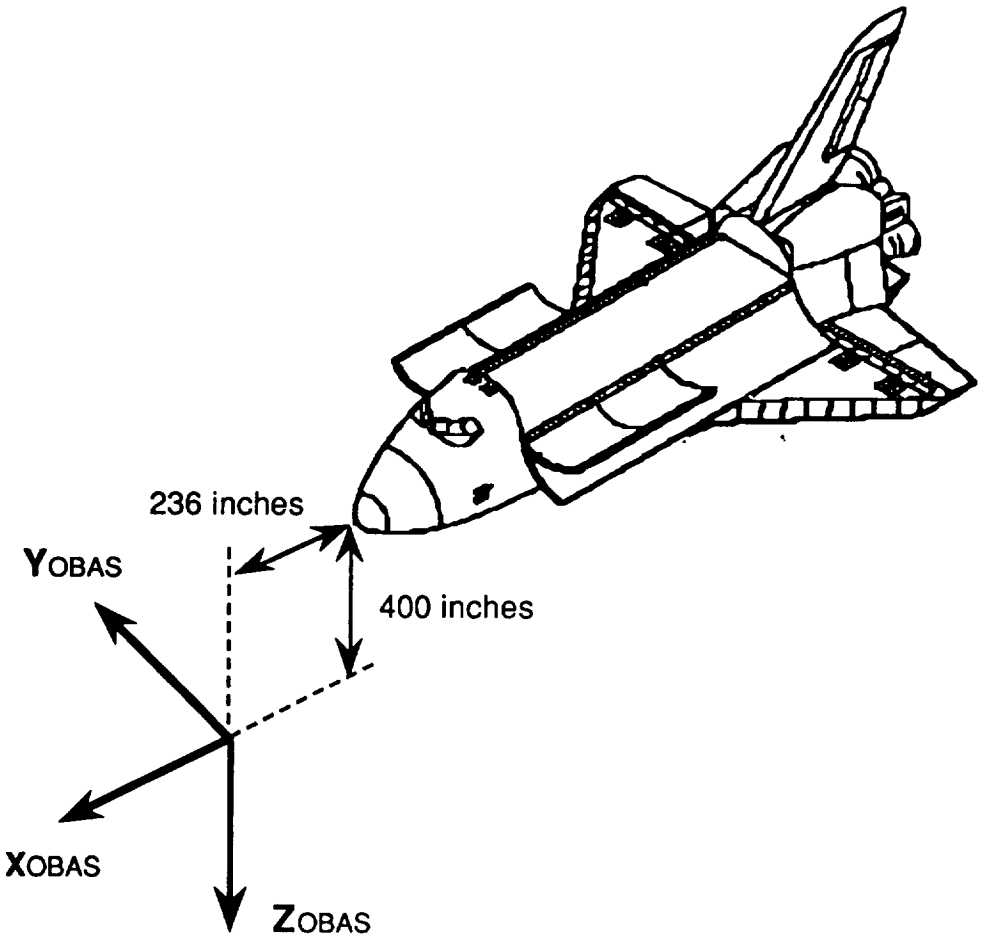

APPENDIX B - SELECTED SSF FLEXIBLE MODE PLOTS

Figure B-1.- Mode 1, f=0.0099 Hz (Model fixed at Grapple Fixture)

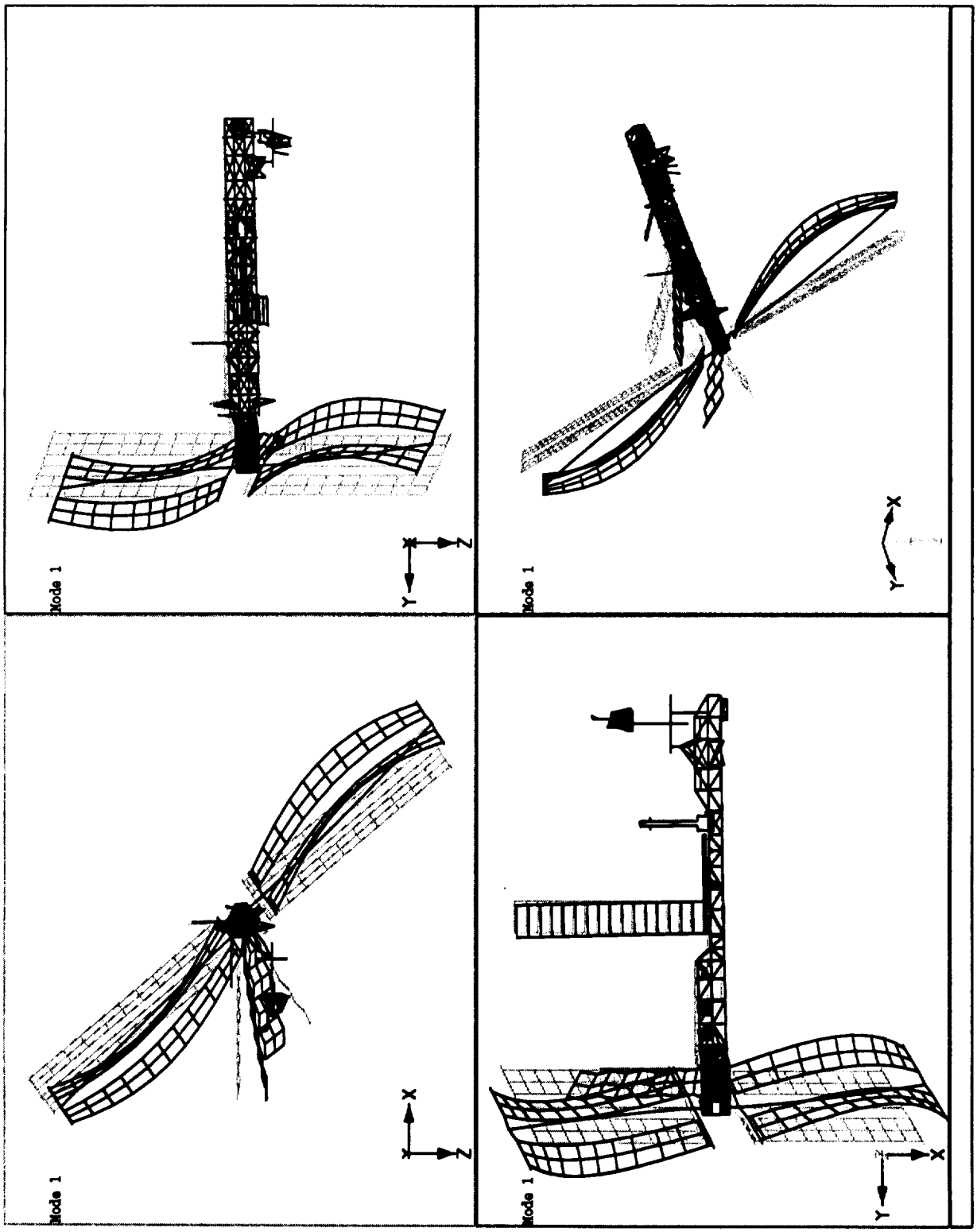

Figure B-1.- Mode 1, f = 0.099 Hz (Model fixed at Grapple Fixture).

Figure B-2.- Mode 2, f=0.109 Hz (Model fixed at Grapple Fixture)

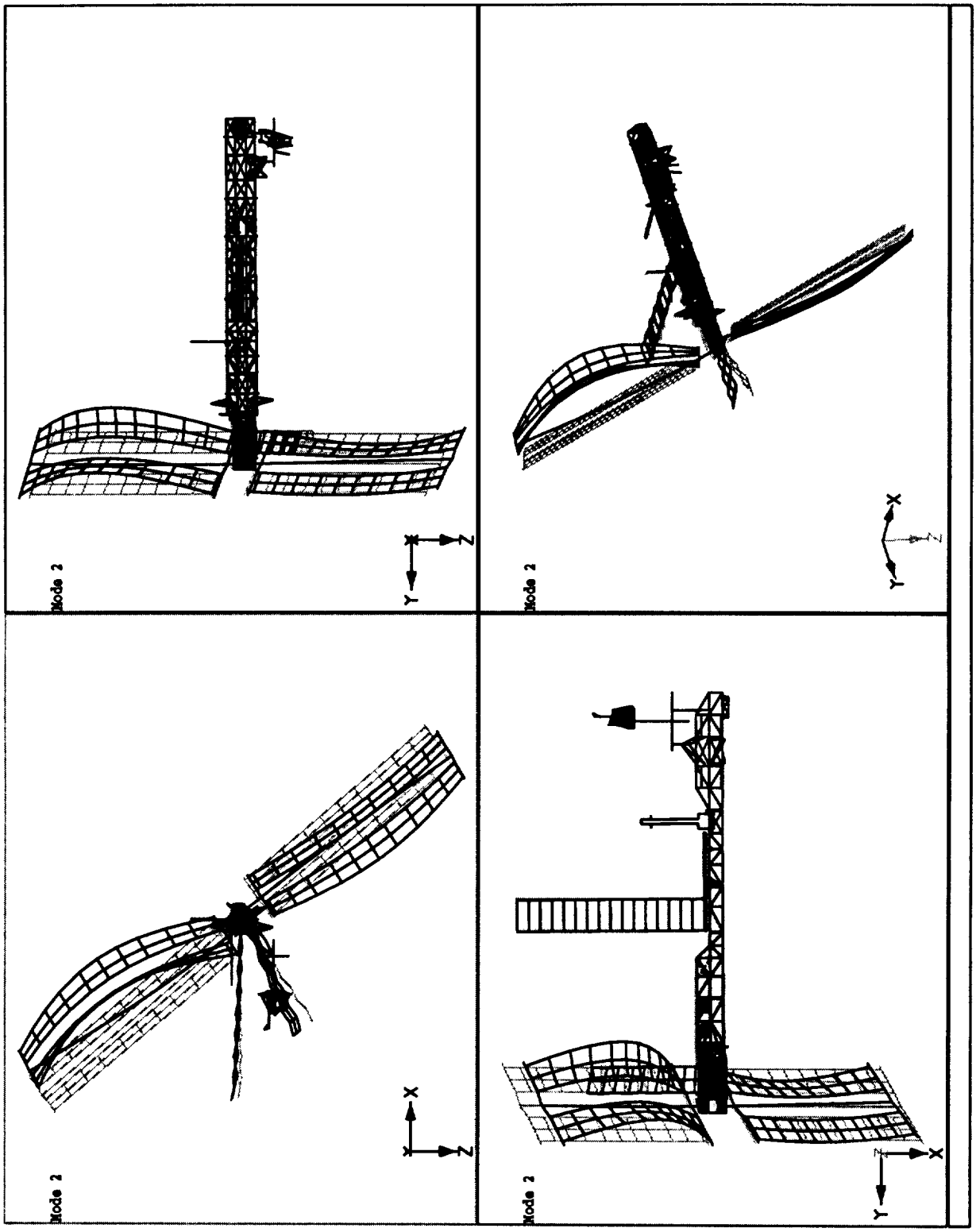

Figure B-2.- Mode 2, f = 0.109 Hz (Model fixed at Grapple Fixture).

Figure B-3.- Mode 9, f=0.142 Hz (Model fixed at Grapple Fixture)

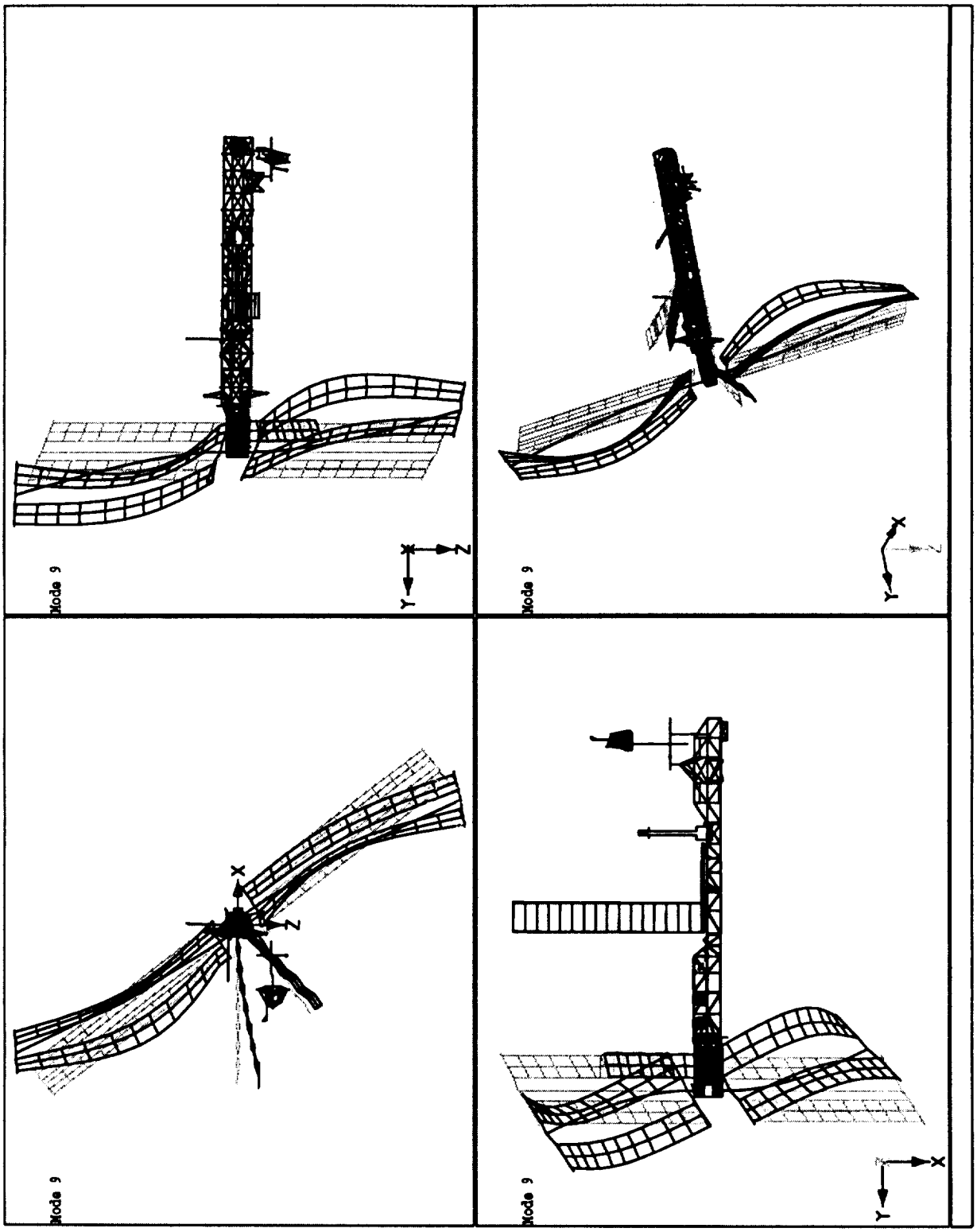

Figure B-3.- Mode 9, f = 0.142 Hz (Model fixed at Grapple Fixture).

Figure B-4.- Mode 11, f=0.180 Hz (Model fixed at Grapple Fixture)

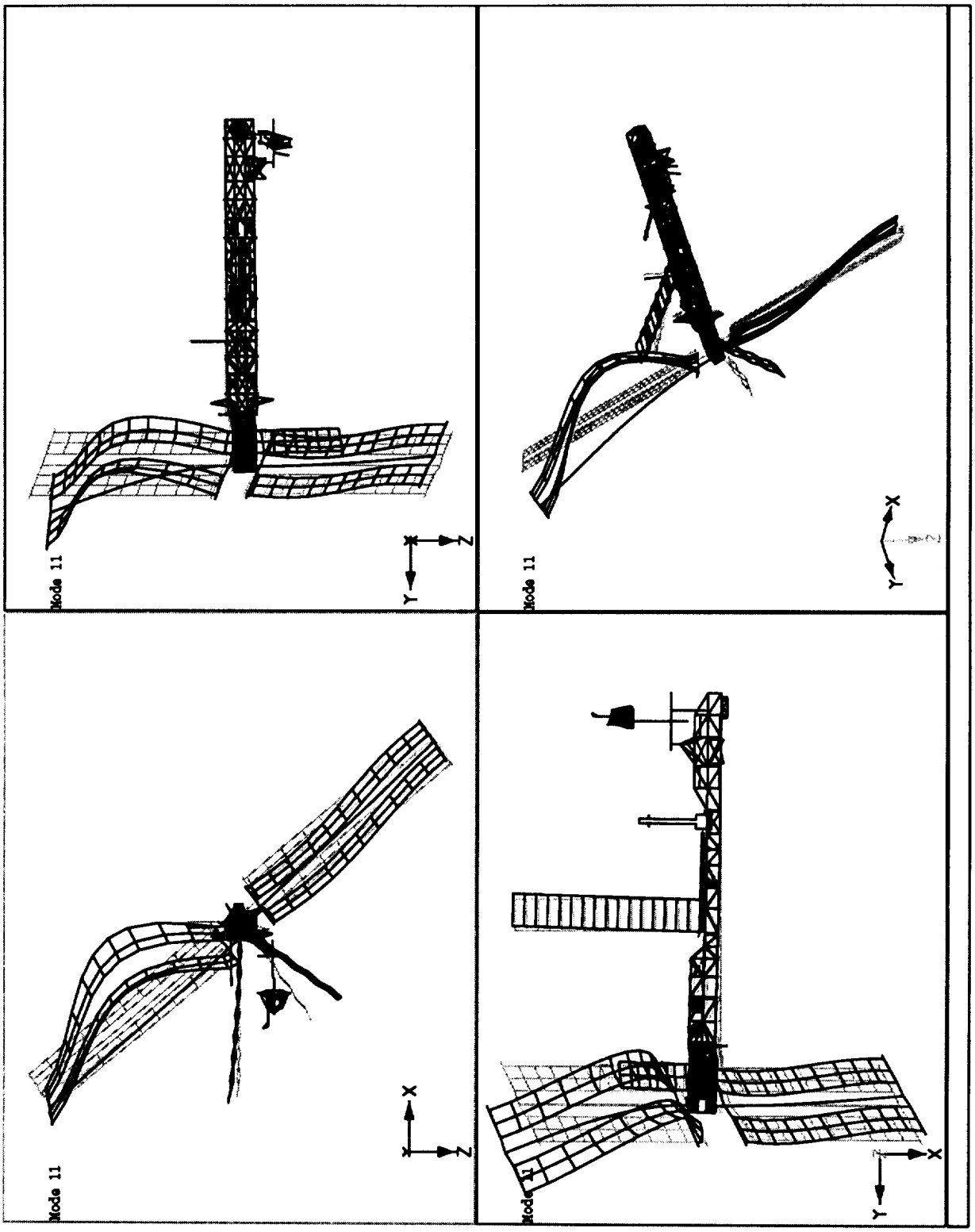

Figure B-4.- Mode 11, f = 0.180 Hz (Model fixed at Grapple Fixture).

Figure B-5.- Mode 12, f=0.184 Hz (Model fixed at Grapple Fixture)

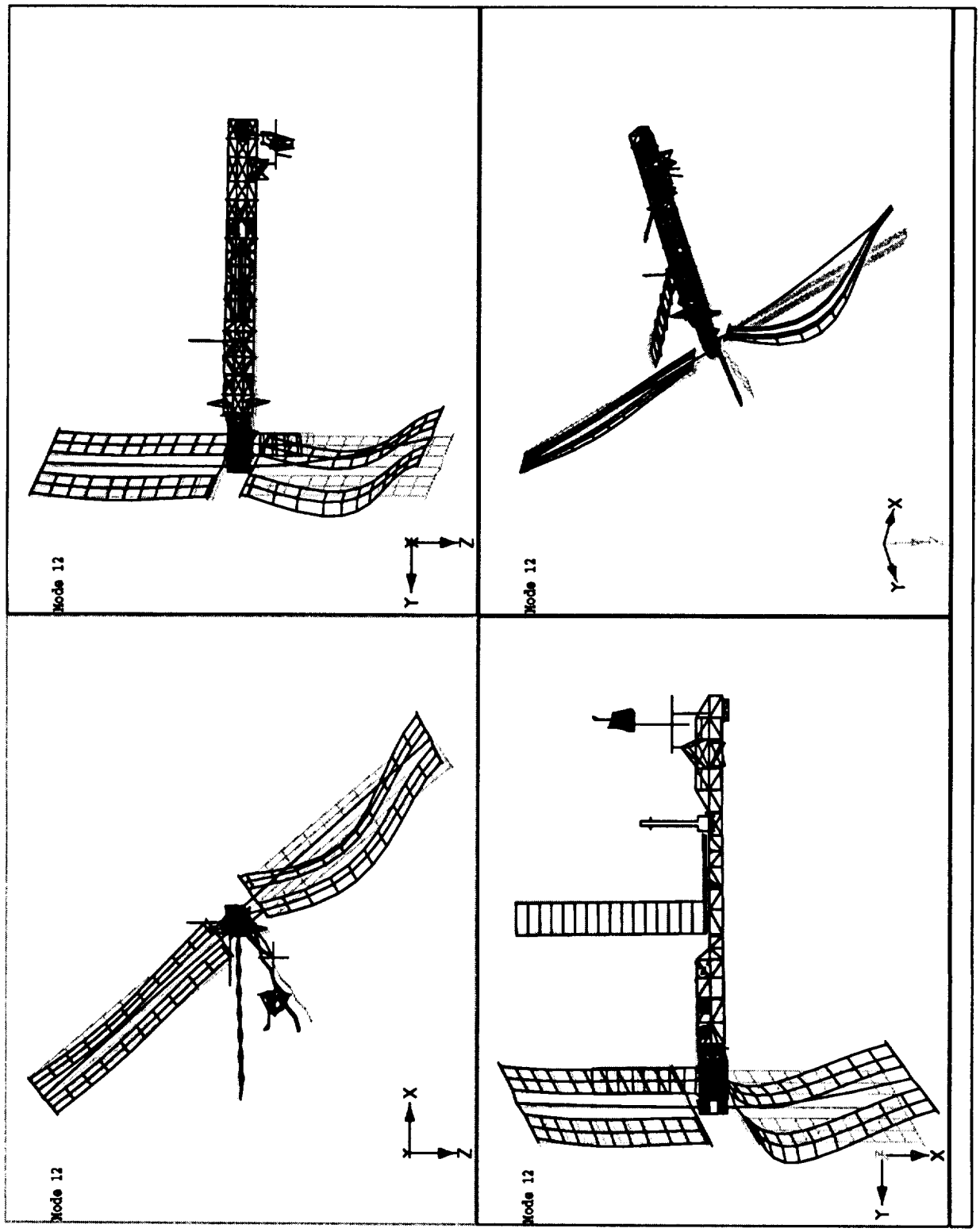

Figure B-5.- Mode 12, f = 0.184 Hz (Model fixed at Grapple Fixture).

Figure B-6.- Mode 32, f=0.491 Hz (Model fixed at Grapple Fixture)

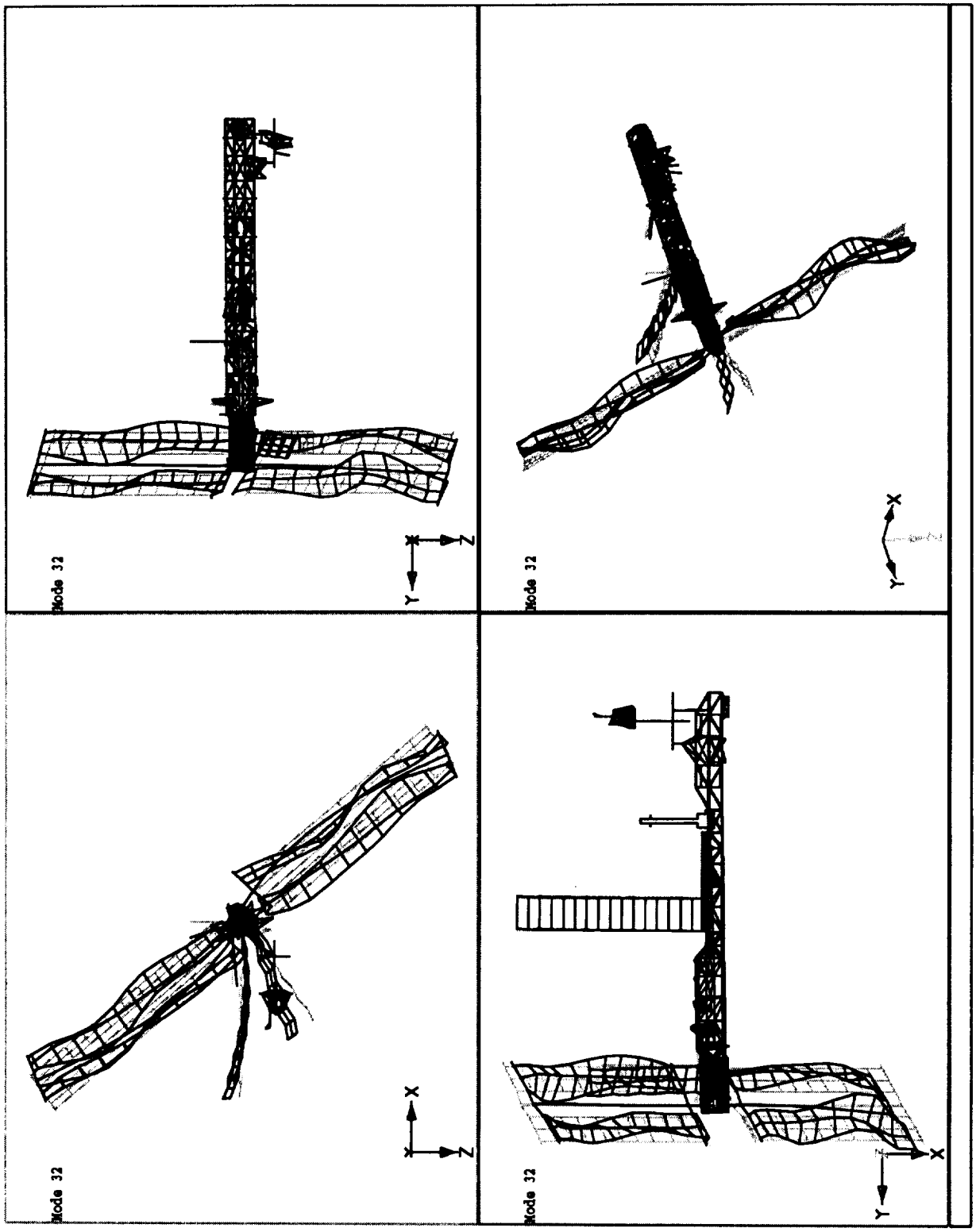

Figure B-6.- Mode 32, f = 0.491 Hz (Model fixed at Grapple Fixture).

Figure B-7.- Mode 36, f=0.657 Hz (Model fixed at Grapple Fixture)

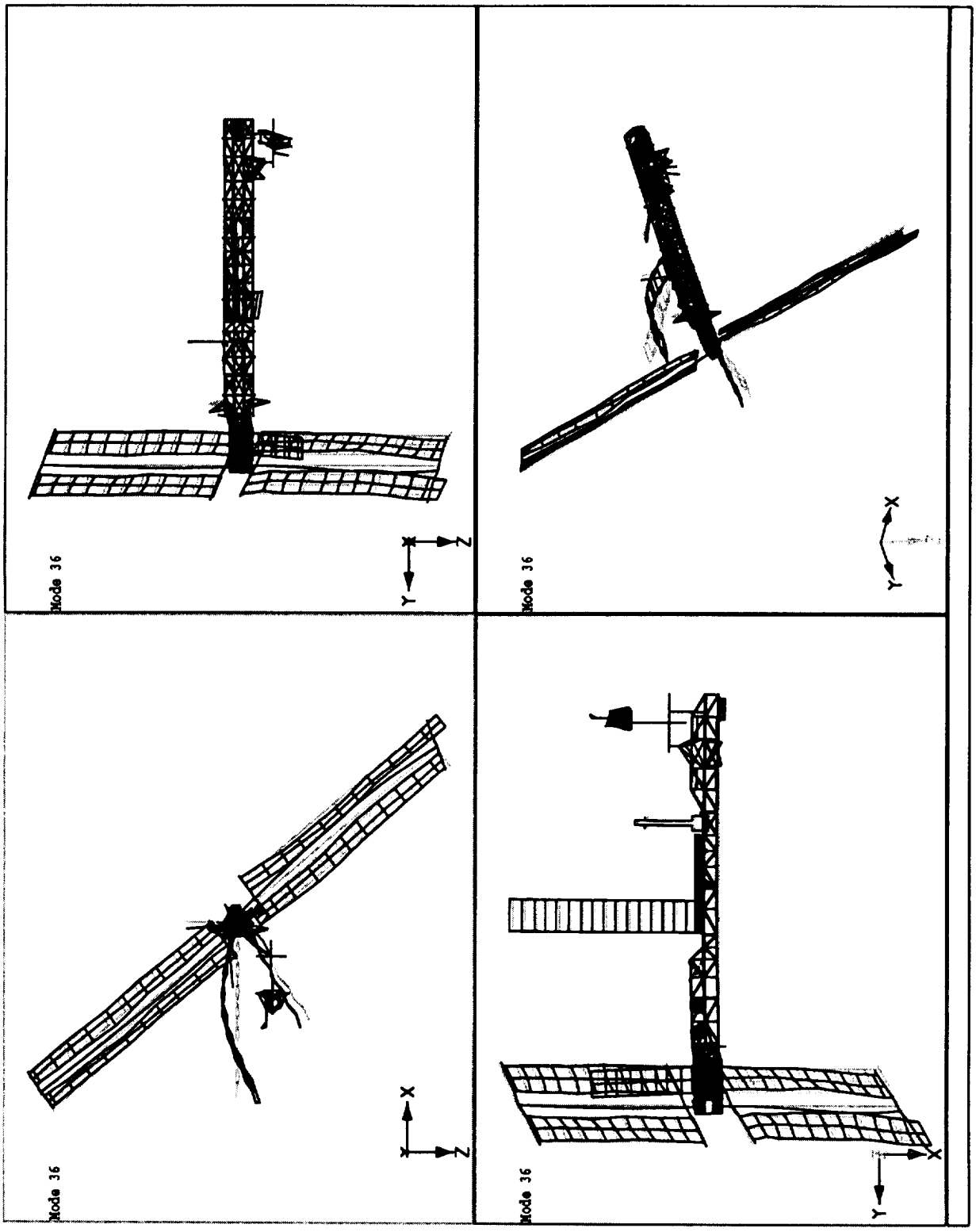

Figure B-7.- Mode 36, f = 0.657 Hz (Model fixed at Grapple Fixture).

Figure B-8.- Mode 43, f=0.813 Hz (Model fixed at Grapple Fixture)

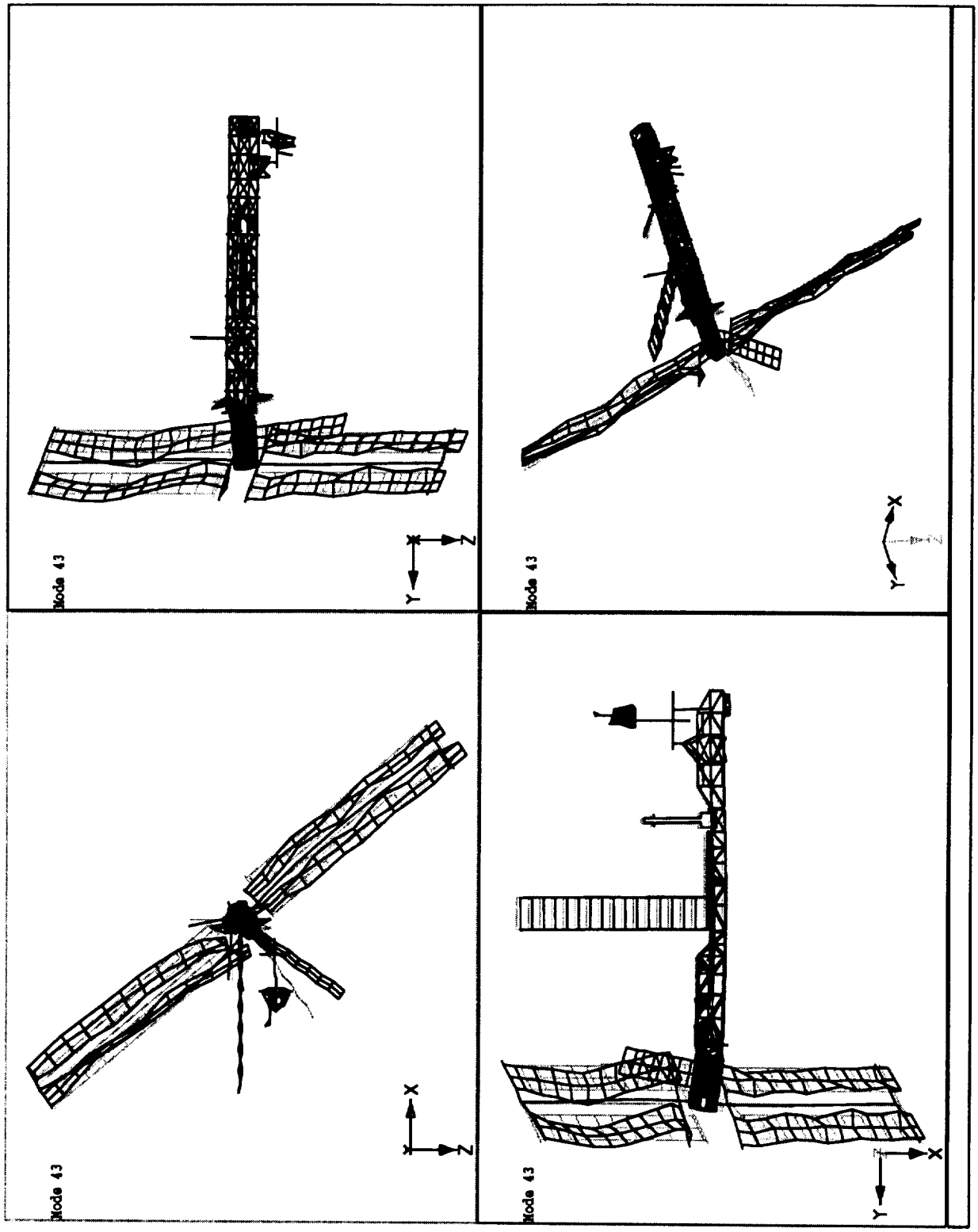

Figure B-8.- Mode 43, f = 0.813 Hz (Model fixed at Grapple Fixture).

Figure B-9.- Mode 48, f=1.031 Hz (Model fixed at Grapple Fixture)

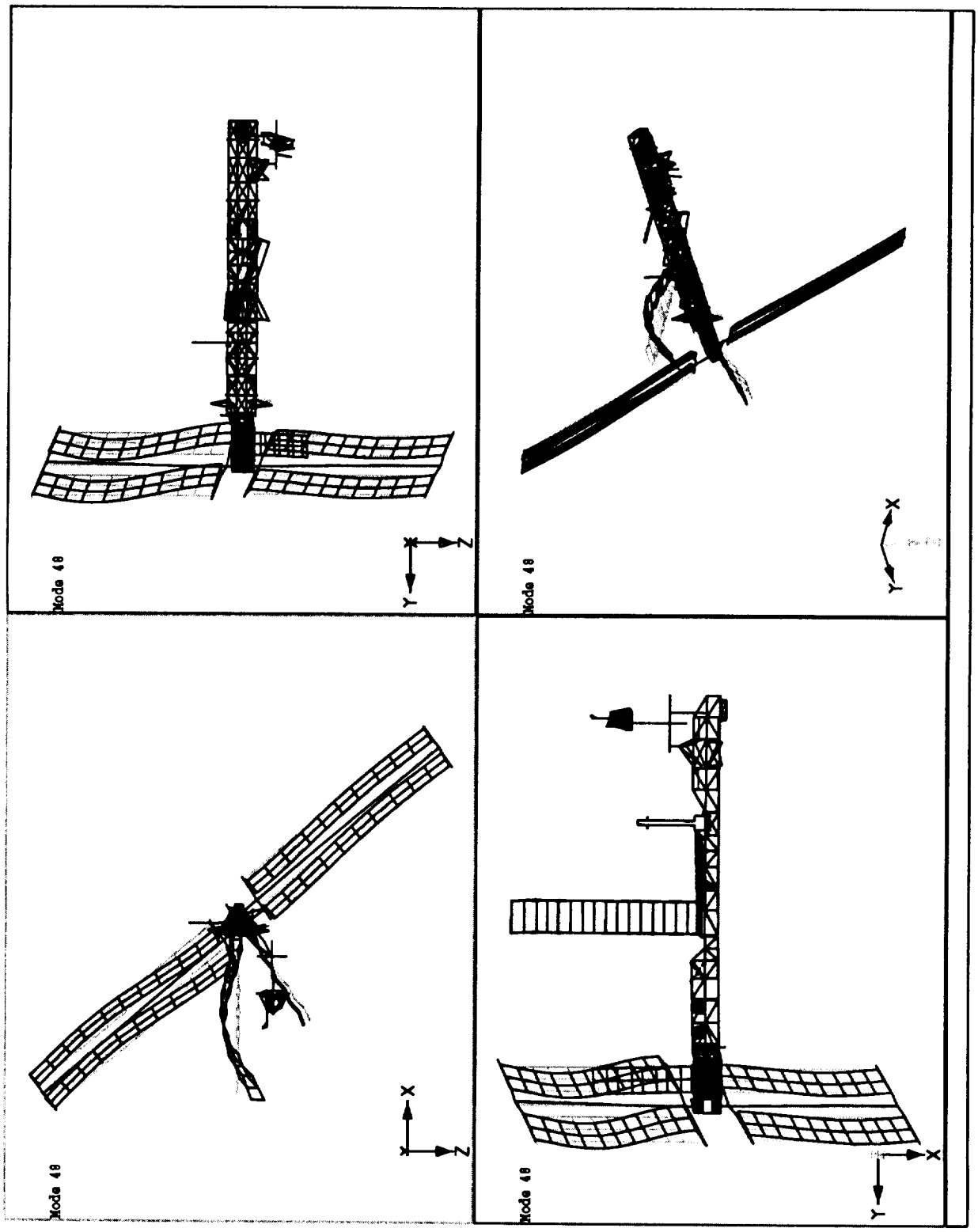

Figure B-9.- Mode 48, f = 1.031 Hz (Model fixed at Grapple Fixture).

Figure B-10.- Mode 49, f=1.094 Hz (Model fixed at Grapple Fixture)

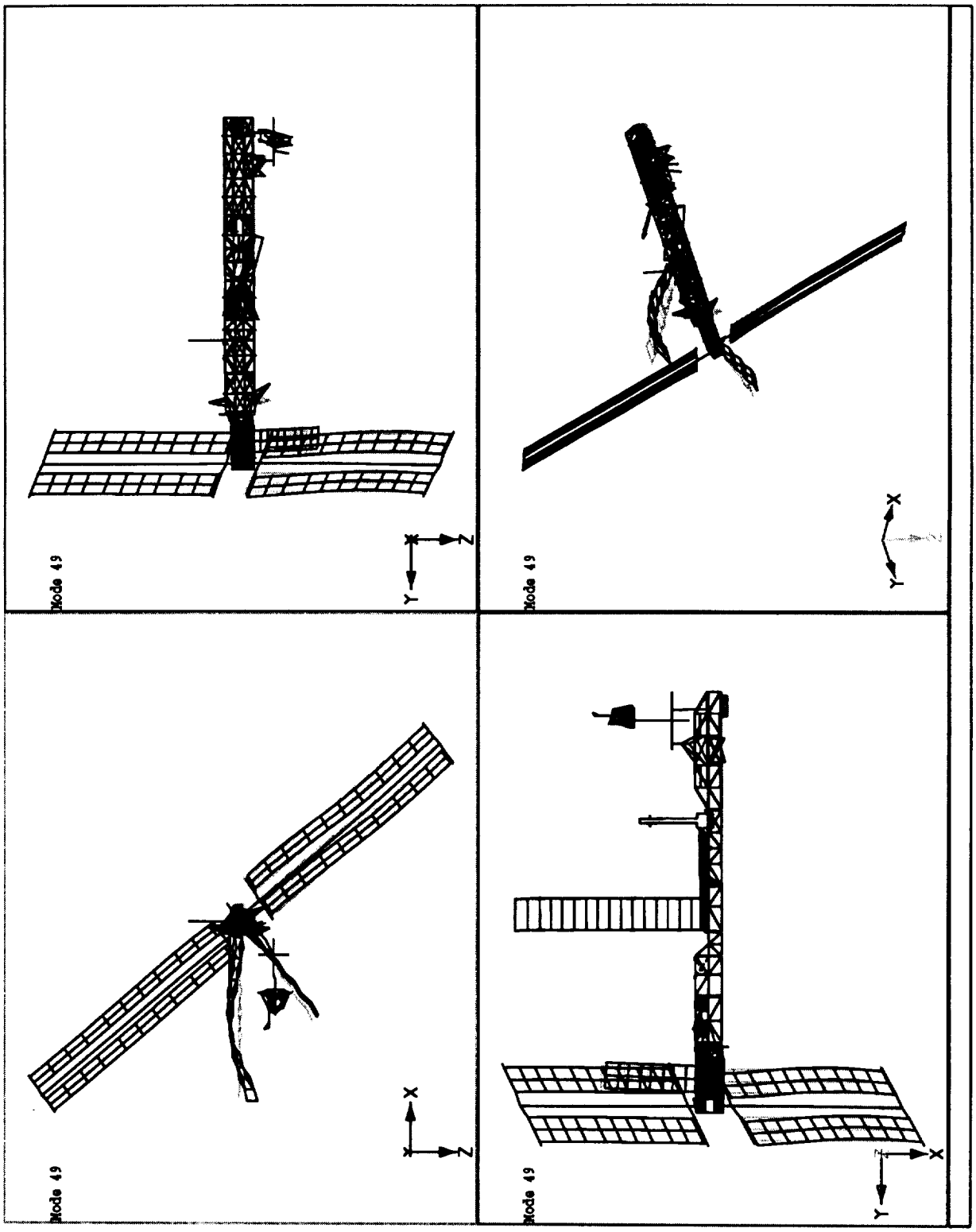

Figure B-10.- Mode 49, f = 1.094 Hz (Model fixed at Grapple Fixture).

APPENDIX C - CONFIGURATION DATA

C-1 Orbiter Mass Properties

Mass

units	value
slugs	7668.8
lbs	246,935.36

Center of Mass (CM) in Orbiter Structural Reference (OSR) frame

units	X	Y	Z
inches	1116.0	1.6	351.3
feet	93.0	0.133	29.275

Inertia tensor about CM with respect to a OSR frame

units	value		
slug-ft^2	967,252.2	-13,766.7	-285,269.8
	-13,766.7	7,313,913.2	1,179.8
	-285,269.8	1,179.8	7,637,149.1

C-2 SRMS Mass Properties

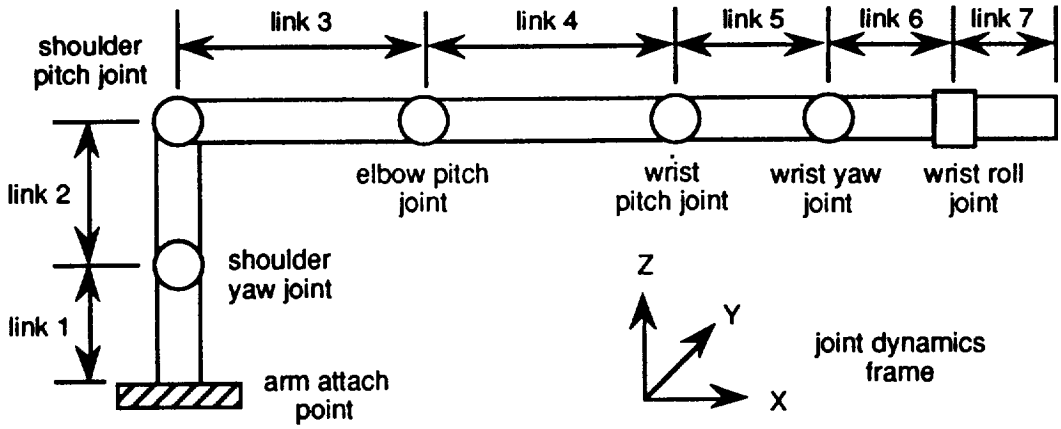

Link No.	Mass (slugs)	Center of Mass (inches)		
		X	Y	Z
1	4.3333	0.0	0.0	11.245
2	2.201	0.0	0.0	6.0
3	9.5485	125.525	0.0	-1.11
4	5.9902	138.975	0.0	0.26
5	0.5809	9.0	0.0	0.0
6	3.1479	15.0	0.0	0.0
7	3.098	13.0	0.0	0.0

Link No.	Units	Inertia tensor
1	slug-ft^2	I_{XX} = 2.70253 I_{YY} = 2.80506 I_{ZZ} = 5.0636 (*) I_{XY} = -0.00324 I_{XZ} = -0.00345 I_{YZ} = 0.37340
2	slug-ft^2	I_{XX} = 8.2213 (*) I_{YY} = 10.4531 (*) I_{ZZ} = 4.3880 (*) I_{XY} = 0.01425 I_{XZ} = 0.05871 I_{YZ} = -0.02698

Link No.	Units	Inertia tensor
3	slug-ft^2	I_{XX} = 2.8025 I_{YY} = 358.3754 I_{ZZ} = 358.2576 I_{XY} = 0.0 I_{XZ} = 2.5919 I_{YZ} = 0.0
4	slug-ft^2	I_{XX} = 1.7594 I_{YY} = 277.5304 I_{ZZ} = 277.4941 I_{XY} = 0.0 I_{XZ} = -0.85694 I_{YZ} = 0.0
5	slug-ft^2	I_{XX} = 6.583 (*) I_{YY} = 2.9678 (*) I_{ZZ} = 2.9635 (*) I_{XY} = 0.0 I_{XZ} = 0.0 I_{YZ} = 0.0
6	slug-ft^2	I_{XX} = 3.0110 (*) I_{YY} = 3.45171 I_{ZZ} = 3.45042 I_{XY} = 0.00108 I_{XZ} = -0.00540 I_{YZ} = -0.00022
7	slug-ft^2	I_{XX} = 1.40361 I_{YY} = 2.81477 I_{ZZ} = 2.08199 I_{XY} = -0.28426 I_{XZ} = -0.71249 I_{YZ} = 0.26052

Notes:

1. Center of mass assumed to be located at geometric center of link.
2. Moment of inertia for links 3 and 4 assume that the links are thin walled cylindrical beams with circular cross section and uniform mass.
3. Products of inertia are negative integrals.
4. Small inertias (*) are boosted to be greater than 1.0 (as done in the DRS)
5. Mass and inertia tensors for links 3 and 4 are consistent with FEM model definition described in Part 2.

C-3 SC-5 Mass Properties

Mass

units	value
slugs	4520.40
lbs	145,439.35

Center of Mass (CM) in Space Station Structural Reference Frame (SSSRF)

units	X	Y	Z
inches	-51.43158	547.4320	35.73118
feet	-4.285965	45.61933	2.977598

Inertia matrix about CM with respect to a SSSRF frame
(products of inertia are negative integrals)

units	value		
slug-ft^2	13,431,739.22	-835,411.012	-36,892.58
	-835,411.012	1,388,776.005	1,005,845.17
	-36,892.58	1,005,845.17	13,381,808.90

C-4 SC-5 Sensor Locations

Sensor Location in SSSRF (Inches)

X	Y	Z
-37.58	970.47	-34.88

C-5 SC-5 Jet Locations

Jet Locations in SSSRF (inches)

Jet	X	Y	Z
Upper	-39.7	1242.11	-174.88
Lower	-39.7	1224.61	174.88

C-6 SC-5 CMG Locations

CMG Locations in SSSRF (Inches)

CMG	X	Y	Z
1	**-12.5**	**831.65**	**51.5**
2	-12.5	831.65	-51.5
3	-12.5	879.6	26.34
4	-12.5	879.6	-26.34

Note: SSF ACS commanded torque applied to CMG location (1).

C-7 Point of Resolution Location Definition

Vector from origin of Payload Axis System (PAS) to Point of Resolution (POR) (origin of Payload Operating (PLOP) frame) in PAS frame: (inches)

VPASOP	-178.8	-66.95	277.95

Vector from End Effector to POR in PLOP frame: (inches)

VEFPOR	0.0	0.0	0.0

Transformation matrix from PAS frame to PLOP frame:

PAS2PL	0.0	0.0	-1.0
	-0.00907559	-0.99995882	0.0
	-0.99995882	0.00907559	0.0

Transformation matrix from PLOP frame to End Effector Operating (EEOP) frame:

PLEFOP	1.0	0.0	0.0
	0.0	1.0	0.0
	0.0	0.0	1.0

Assumptions:

1. Payload Axis System (PAS) aligned with Space Station Structural Reference Frame (SSSRF).
2. Point of Resolution (POR) at End Effector and aligned with End Effector Operating Frame (EEOP).

C-8 Stack Mass Properties at Capture

Mass

units	value
slugs	12,189.20
lbs	392,492.24

Center of Mass (CM) in Space Station Structural Reference Frame (SSSRF)

units	X	Y	Z
inches	613.54	-712.76	-61.58
feet	51.13	-59.40	-5.13

Inertia matrix about CM with respect to a SSSRF frame
(products of inertia are negative integrals)

units	value		
slug-ft^2	4.530 E+07	-1.650 E+07	2.324 E+06
	-1.650 E+07	1.352 E+07	4.522 E+06
	2.324 E+06	4.522 E+06	5.505 E+07

C-9 Stack Mass Properties at Berth

Mass

units	value
slugs	12,189.20
lbs	392,492.24

Center of Mass (CM) in Space Station Structural Reference Frame (SSSRF)

units	X	Y	Z
inches	482.24	-691.44	-62.23
feet	40.19	-57.62	-5.19

Inertia matrix about CM with respect to a SSSRF frame
(products of inertia are negative integrals)

units	value		
slug-ft^2	4.799 E+07	-9.582 E+06	1.231 E+06
	-9.582 E+06	5.967 E+06	4.704 E+06
	1.231 E+06	4.704 E+06	5.019 E+07

APPENDIX D - SRMS INPUTS

Symbol	Description	Units	Joint					
			Shoulder Yaw	Shoulder Pitch	Elbow Pitch	Wrist Pitch	Wrist Yaw	Wrist Roll
η_B	gearbox backdrive efficiency	%	78.0	78.5	76.5	77.3	77.3	77.3
η_f	gearbox forward drive efficiency	%	84.5	79.0	83.5	82.5	82.5	82.5
Δ	gearbox transition angle†	rad	1.3	1.55	0.7	0.6	0.55	0.6
J_M	motor inertia	slug-ft^2	2.71E-4	2.71E-4	2.905E-4	2.563E-4	2.563E-4	2.563E-4
K_A	MDA gain	volts/volt	1.92	1.92	1.92	1.92	1.92	1.92
K_B	motor back EMF gain	volts/rad/sec	0.235	0.235	0.235	0.235	0.235	0.235
K_D	digital tach gain	counts/rad/sec	11.37778	11.37778	11.37778	11.37778	11.37778	11.37778
K_{DA}	D/A converter gain	volts/count	0.1615	0.1615	0.1615	0.1615	0.1615	0.1615
K_G	gearbox linear stiffness†	ft-lbs/rad	0.483	0.620	1.322	1.205	1.203	1.205
K_I	analog tach processing gain	volts/rad/sec	0.12	0.12	0.12	0.12	0.12	0.12
K_T	motor torquing gain	ft-lbs/amp	0.17	0.17	0.17	0.17	0.17	0.17
K_{TR}	integral trim gain	sec^{-1}	0.05	0.05	0.05	0.05	0.05	0.05
L_A	MDA saturation voltage	volts	± 20	± 20	± 20	± 20	± 20	± 20

† Flight derived "1983" values (from DRS).

APPENDIX D-1.- SRMS Servo Parameters

Symbol	Description	Units	Joint					
			Shoulder Yaw	Shoulder Pitch	Elbow Pitch	Wrist Pitch	Wrist Yaw	Wrist Roll
L_D	D/A converter input limit	counts	± 63	± 63	± 63	± 63	± 63	± 63
L_I	analog tach processing saturation voltage	volts	± 13	± 13	± 13	± 13	± 13	± 13
L_T	integral trim limit voltage	volts	1.5	1.5	1.5	1.5	1.5	1.5
N	gear ratio	none	1841.953	1842.953	1260.284	737.7409	738.7409	737.7409
R_L	motor resistance	ohms	4.12	4.12	4.12	4.12	4.12	4.12
T_2	digital tach processing update period	msec	8.75	8.75	8.75	8.75	8.75	8.75
τ_1	analog tach processing time constant for 1st stage filter	sec	0.1	0.1	0.1	0.1	0.1	0.1
τ_2	analog tach processing time constant for 2nd stage filter	sec	0.1	0.1	0.1	0.1	0.1	0.1
τ_f	rate loop filter time constant	sec	0.1	0.1	0.1	0.1	0.1	0.1
τ_M	motor electrical time constant	msec	1.0	1.0	1.0	1.0	1.0	1.0
T_B	back drive motor current (15/15) limit	amps	2.57	2.57	2.57	1.95	1.95	1.95
T_{BIAS}	tach bias	counts	-1	-1	-1	-1	-1	-1

† Flight derived "1983" values (from DRS).

APPENDIX D-1.- SRMS Servo Parameters (continued)

Symbol	Description	Units	Joint					
			Shoulder Yaw	Shoulder Pitch	Elbow Pitch	Wrist Pitch	Wrist Yaw	Wrist Roll
T_{BC}	brake coulomb friction torque	ft-lbs	0.3268	0.3268	0.3268	0.2656	0.2656	0.2656
T_{BR}	brake stiction torque	ft-lbs	0.3268	0.3268	0.3268	0.2656	0.2656	0.2656
T_D	gearbox transition torque†	ft-lbs	0.0868	0.0651	0.0635	0.0813	0.0812	0.0813
T_f	forward drive motor current (15/15) limit	amps	4.53	4.53	4.53	3.43	3.43	3.43
T_{LC}	joint coulomb friction torque	ft-lbs	40.53	37.92	27.40	15.86	15.88	15.86
T_{LS}	joint stiction torque	ft-lbs	40.53	37.92	27.40	15.86	15.88	15.86
T_{MC}	motor coulomb friction torque	ft-lbs	0.0208	0.0208	0.0208	0.0208	0.0208	0.0208
T_{MS}	motor stiction torque	ft-lbs	0.0208	0.0208	0.0208	0.0208	0.0208	0.0208

† Flight derived "1983" values (from DRS).

APPENDIX D-1.- SRMS Servo Parameters (concluded)

D-2 SRMS Rate Limits

Joint Rate Limits (deg/sec)						
Mode	**Shoulder Yaw**	**Shoulder Pitch**	**Elbow Pitch**	**Wrist Pitch**	**Wrist Yaw**	**Wrist Roll**
Coarse	0.14	0.14	0.14	0.14	0.14	0.14
Vernier[1]	0.042	0.042	0.042	0.042	0.042	0.042

End Effector Rate Limits			
Limit	**Unit**	**Coarse**	**Vernier[1]**
Translational Rate Resultant:	ft/sec	0.14	0.042
Translational Rate Component:	ft/sec	0.14	0.042
Rotational Rate Resultant:	deg/sec	0.14	0.042
Rotational Rate Component:	deg/sec	0.14	0.042
Auto Translation Vernier:	ft/sec	N/A	1.2157
Auto Rotation Vernier:	deg/sec	N/A	0.4899

Notes:

1. Vernier limits are equal to 30% of coarse.

APPENDIX E - ORBITAL MECHANICS AND AERODYNAMICS DATA

E-1 Orbital Data

Parameter	Value	Units
Altitude	220.0	nmi.
Inclination	28.5	deg.
Right ascension of ascending node	0.0	deg.
Argument or perigee	0.0	deg.
True anomaly (@ time = 0)	0.0	deg.
Day of the year	80.0	days

E-2 Atmospheric Data

Parameter	Value	Units
Drag coefficient	2.0	
Solar flux (10.7 cm)	100.0	10^{22} W/m^2/cycle/sec
Geomagnetic index	16.9	

E-3 Geometric Data

Projected areas	**Value (SSSRF coordinates)**	**Units**
Area normal to x	.10624	ft^2
Area normal to y	5634	ft^2
Area normal to z	8159	ft^2

Center of pressure to center of mass offset vectors	**Value (SSSRF coordinates)**	**Units**
Area normal to x	(0.00, 61.88, -4.84)	ft.
Area normal to y	(32.18, 0.00, -6.405)	ft.
Area normal to z	(21.51, 76.25, 0.00)	ft.

APPENDIX F - SPACE STATION FREEDOM ATTITUDE CONTROL SYSTEM DATA

F-1 RCS Initialization Parameters

Parameter	Value	Units
Maneuver rate limit	0.1	deg/sec
Torque output limit	400	ft-lb
ACS bandwidth	7.0]	rad/sec
ACS damping	0.7	---
RCS jet command period	33	sec
Burn time command deadzone	0.2	sec
Burn time quantization offset	50	%
Burn time quantization interval	0.2	sec
RCS execution period	1.0	sec
Position vector from SSF body center of mass to 'capture' configuration center of mass (SSSRF coordinates): x	-35.22	ft
y	-54.52	ft
z	7.93	ft.
Bending filter break frequency	140 ω_0	rad/sec
Bending filter damping	0.7	---
Rate feedback filter break frequency	140 ω_0	rad/sec

NOTE: ω_0 is the SSF orbital frequency

F-2 RCS Jet Locations and Thruster Directions

Jet No.	Location, ft (SSSRF)			Thrust Direction (SSSRF)		
	x	y	z	x	y	z
1	-3.308	103.51	-14.57	1	0	0
2	-3.308	103.51	-14.57	-1	0	0
3	-3.308	103.51	-14.57	0	0	1
4	-3.308	102.05	14.57	1	0	0
5	-3.308	102.05	14.57	-1	0	0
6	-3.308	102.05	14.57	0	0	-1

F-3 CMG Initialization Parameters

Parameter	Value	Units
Torque output limit	400.0	ft-lb
ACS bandwidth	7.0 $\dot{\omega}_0$	rad/sec
ACS damping	0.7	---
Maneuver rate limit	0.1	deg/sec
CMG execution period	1.0	sec
Number of CMGs	4	---
CMG outer gimbal redistribution rate limit	0.005	rad/sec
CMG inner gimbal proportional rate limit	0.02	rad/sec
Torque output filter break frequency	140 ω_0	rad/sec
Torque output filter damping (ζ_n)	0.7	---
Rate feedback filter break frequency (ζ_n)	140 ω_0	rad/sec

NOTE: ω_0 is the SSF orbital frequency

APPENDIX G - BERTHING TRAJECTORY

MB-6	SRMS Joint Angles (deg)					
Point	Shoulder Yaw	Shoulder Pitch	Elbow Pitch	Wrist Pitch	Wrist Yaw	Wrist Roll
1	-109.24	90.60	-30.35	-80.79	18.10	26.12
2	-129.18	101.92	-57.71	-68.74	36.55	34.68
3	-165.07	137.29	-139.84	-51.38	65.64	70.84

MB-6	End Effector Position (inches) (OSR)			End Effector Attitude (deg) (ORAS)		
Point	X	Y	Z	Pitch	Yaw	Roll
1	629.10	-78.96	954.0	0.0	270.0	0.0
2	574.98	-77.0	900.0	0.0	270.0	359.99
3	575.01	-77.01	599.03	0.0	270.0	0.01

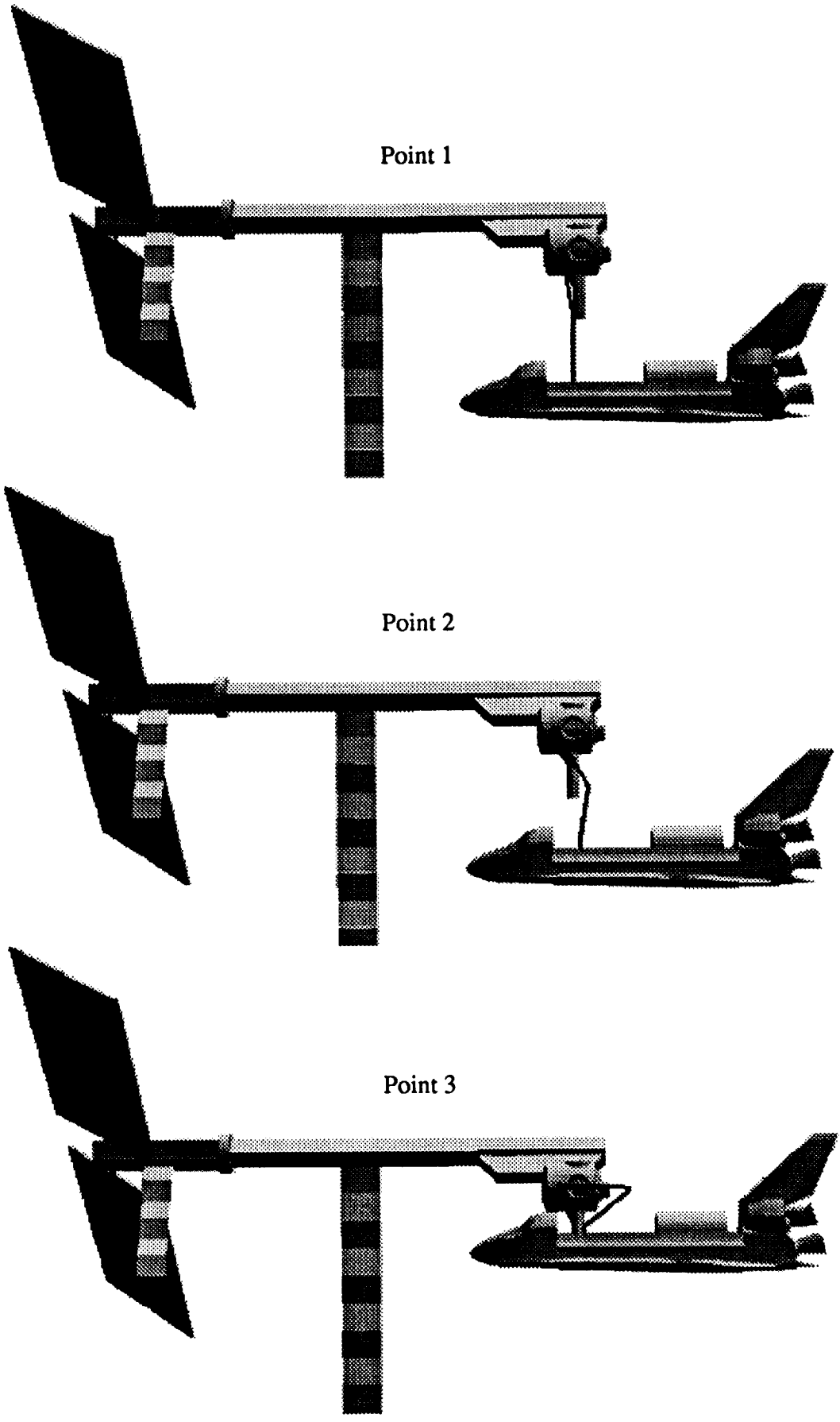

Figure G-1.- MB6 berthing trajectory

REPORT DOCUMENTATION PAGE

Form Approved
OMB No. 0704-0188

1. AGENCY USE ONLY (*Leave blank*)	2. REPORT DATE	3. REPORT TYPE AND DATES COVERED
	August 1994	Technical Memorandum

4. TITLE AND SUBTITLE
Modelling and Simulation of Space Station Freedom Berthing Dynamics and Control

5. FUNDING NUMBERS
233-01-01-01

6. AUTHOR(S)
Paul A. Cooper, James L. Garrison, Jr., Raymond C. Montgomery, Shih-Chin Wu, Alan E. Stockwell, and Martha E. Demeo

7. PERFORMING ORGANIZATION NAME(S) AND ADDRESS(ES)
National Aeronautics and Space Administration
Langley Research Center
Hampton, VA 23681-0001

8. PERFORMING ORGANIZATION REPORT NUMBER

9. SPONSORING / MONITORING AGENCY NAME(S) AND ADDRESS(ES)
National Aeronautics and Space Administration
Washington, DC 20546-0001

10. SPONSORING / MONITORING AGENCY REPORT NUMBER
NASA TM-109151

11. SUPPLEMENTARY NOTES
Cooper, Garrison, and Montgomery: Langley Research Center, Hampton, VA
Wu and Stockwell: Lockheed Engineering & Sciences Company, Hampton, VA
Demeo: ViGYAN, Inc., Hampton, VA

12a. DISTRIBUTION / AVAILABILITY STATEMENT
Unclassified-unlimited
Subject Category-18

12b. DISTRIBUTION CODE

13. ABSTRACT (*Maximum 200 words*)

A large-angle, flexible, multi-body, dynamic modelling capability has been developed to help validate numerical simulations of the dynamic motion and control forces which occur during berthing of Space Station Freedom to the Shuttle Orbiter in the early assembly flights. This paper outlines the dynamics and control of the Station, the attached Shuttle Remote Manipulator System, and the Orbiter. The simulation tool developed for the analysis is described and the results of two simulations are presented. The first is a simulated manuever from a gravity-gradient attitude to a torque equilibrium attitude using the Station reaction control jets. The second simulation is the berthing of the Station to the Orbiter with the Station control moment gyros actively maintaining an estimated torque equilibrium attitude. The influence of the elastic dynamic behavior of the Station and of the Remote Manipulator System on the attitude control of the Station/Orbiter system during each maneuver was investigated. The flexibility of the Station and the arm were found to have only a minor influence on the attitude control of the system during the maneuvers.

14. SUBJECT TERMS
Berthing; Space Station; Shuttle; Orbital Mechanics; Multi-Body Dynamics

15. NUMBER OF PAGES
168

16. PRICE CODE
A08

17. SECURITY CLASSIFICATION OF REPORT	18. SECURITY CLASSIFICATION OF THIS PAGE	19. SECURITY CLASSIFICATION OF ABSTRACT	20. LIMITATION OF ABSTRACT
Unclassified	Unclassified		